AD-A119 381 HONEYWELL POWER SOURCES CENTER HORSHAM PA F/G 10/3
LITHIUM-SULFUR DIOXIDE (LI/SO2) BATTERY SAFETY HAZARDS - THERMA--ETC(U)
MAR 82 W B EBNER, K Y KIM, H V VENKATASETTY N60921-81-C-0085
UNCLASSIFIED NL

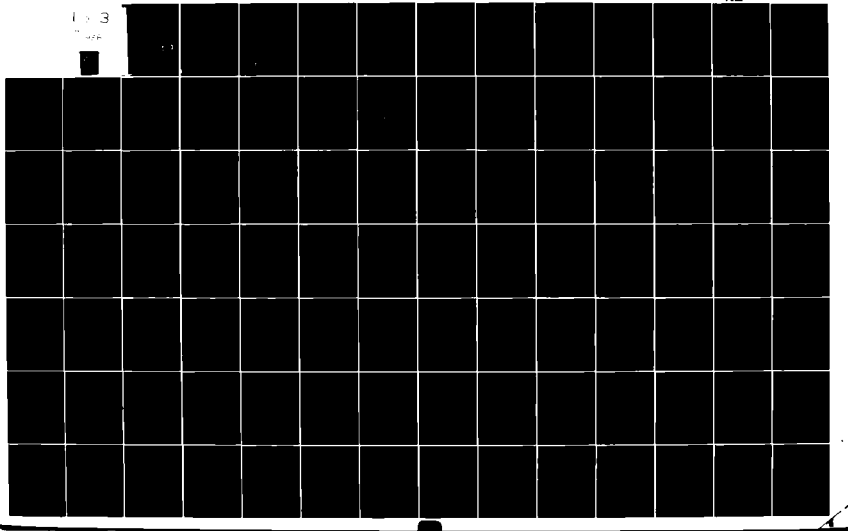

(12)

LITHIUM-SULFUR DIOXIDE (Li/SO_2) BATTERY SAFETY HAZARDS

THERMAL STUDIES

NAVAL SURFACE WEAPONS CENTER
WHITE OAK LABORATORY
SILVER SPRING, MD

AUTHORS

W. B. EBNER
DR. H. V. VENKATASETTY
DR. KWANG Y. KIM

HONEYWELL INC.

CONTRACT NO. N60921-81-C-0085

FINAL REPORT
24 DEC 80 - 5 MAR 1982

SECURITY CLASSIFICATION OF THIS PAGE (When Data Entered) Unclassified

REPORT DOCUMENTATION PAGE	READ INSTRUCTIONS BEFORE COMPLETING FORM
1. REPORT NUMBER	2. GOVT ACCESSION NO. AD-A119381	3. RECIPIENT'S CATALOG NUMBER
4. TITLE (and Subtitle) LITHIUM-SULFUR DIOXIDE (Li/SO_2) BATTERY SAFETY HAZARDS - THERMAL STUDIES	5. TYPE OF REPORT & PERIOD COVERED Final Report 24 Dec 80 - 5 Mar 82
	6. PERFORMING ORG. REPORT NUMBER
7. AUTHOR(s) Walter B. Ebner, Dr. Kwang Y. Kim, Dr. H. V. Venkatasetty	8. CONTRACT OR GRANT NUMBER(s) N60921-81-C-0085
9. PERFORMING ORGANIZATION NAME AND ADDRESS Honeywell Power Sources Center 104 Rock Road Horsham, Pa. 19044	10. PROGRAM ELEMENT, PROJECT, TASK AREA & WORK UNIT NUMBERS
11. CONTROLLING OFFICE NAME AND ADDRESS Naval Surface Weapons Center White Oak, Silver Spring, MD 20910 Attn: Code R-33	12. REPORT DATE March 1982
	13. NUMBER OF PAGES 234
14. MONITORING AGENCY NAME & ADDRESS(if different from Controlling Office) DCAS-MA Philadelphia P.O. Box 7699 Philadelphia, PA 19101	15. SECURITY CLASS. (of this report) Unclassified
	15a. DECLASSIFICATION/DOWNGRADING SCHEDULE N/A

16. DISTRIBUTION STATEMENT (of this Report)

Approved for Public Release; distribution unlimited

17. DISTRIBUTION STATEMENT (of the abstract entered in Block 20, if different from Report)

18. SUPPLEMENTARY NOTES

19. KEY WORDS (Continue on reverse side if necessary and identify by block number)

20. ABSTRACT (Continue on reverse side if necessary and identify by block number)

In this program, the Accelerating Rate Calorimeter (ARC) has been employed to study the thermal and pressure behavior of exothermic reactions occurring in Li/SO_2 cells under the conditions of (1) forced overdischarge at ambient temperature, (2) resistive overdischarge at ambient temperature, (3) forced overdischarge at -35°C, and (4) discharge at -35°C. Detected reactions have been characterized in terms of self-heating rate, rate of pressure generation, magnitude of overall heat generation, magnitude of overall

DD FORM 1 JAN 73 1473 EDITION OF 1 NOV 65 IS OBSOLETE Unclassified

SECURITY CLASSIFICATION OF THIS PAGE (When Data Entered)

pressure rise, and kinetic parameters including activation energy and reaction order.

Micro-calorimeter studies determined the heat of reaction for the lithium/acetonitrile reaction to be -54.6 ± 1.0 kcal/mole-Li. Lithium/aluminum alloy was found to be unreactive with acetonitrile at ambient temperature.

Preliminary investigations were also carried out using FTIR spectroscopy to study the products of electrolyte oxidation on nickel and stainless steel electrodes.

TABLE OF CONTENTS

LIST OF FIGURES

LIST OF FIGURES - CONT'D

LIST OF FIGURES - CONT'D

LIST OF FIGURES - CONT'D

LIST OF FIGURES - CONT'D

LIST OF TABLES

LIST OF TABLES - CONT'D

LIST OF TABLES - CONT'D

LIST OF TABLES - CONT'D

Introduction

In recent years, the excellent performance capabilities of the Li/SO_2 electrochemical technology have been clearly demonstrated. Production facilities have emerged and Li/SO_2 cells are now employed in large numbers throughout the Department of Defense (DoD).

The extensive field testing to which the Li/SO_2 system has been subjected, however, has brought to light some safety problems. Because of the importance of this technology to the overall DoD strategy, it is imperative that these safety problems be resolved as rapidly as possible.

The safety problems associated with the Li/SO_2 system arise under the following conditions of use and abuse:

- Forced discharge into reversal
- Short circuit
- Charging
- Resistive discharge to low cell potentials

The problem is intensified by the fact that many Li/SO_2 cells are incorporated into battery packs with series-connected or series-parallel connected arrays such that forced discharge into reversal and charging are possible during normal battery operation.

Much work has already been done concerning the safety of Li/SO_2 cells and although much information has been obtained, neither the cell behavior nor the chemical reactions leading to instability have been completely defined. Accelerating rate calorimetry is a new technique developed in the chemical industry specifically to study thermal runaway reactions. Because this method includes the effects of self-heating, obtains pressure data, and can closely simulate actual end-use conditions, it is ideally suited for thermal hazard evaluation of electrochemical systems. The ability to obtain pressure data is particularly important since it is the pressure behavior that ultimately defines the magnitude of a hazard.

We believe the unique capabilities of the ARC technique can provide the detailed understanding necessary to resolve the safety problems associated with the Li/SO_2 system. This program represents the first systematic application of the ARC technique to the study of safety problems in an electrochemical system. By characterizing exothermic reactions with respect to both thermal and pressure behavior, a much greater insight has been obtained regarding the hazards associated with the Li/SO_2 system. The results obtained have identified key areas where future work should be focused.

Acknowledgement

We acknowledge the helpful suggestions of Dr. Donald Ernst, the Contract Monitor, throughout the course of this program and the support of the Electrochemical Technology Block Program at NSWC.

Summary

In this program, the Accelerating Rate Calorimeter (ARC) has been employed to study the thermal and pressure behavior of exothermic reactions occurring as a result of the following test modes.

- Forced overdischarge at ambient temperature
- Resistive overdischarge at ambient temperature
- Forced overdischarge at -35°C
- Discharge at -35°C

Originally, it had been intended to also study the effects of charging on Li/SO_2 cell safety, but subsequently these tests were replaced with the discharge and forced overdischarge tests at -35°C. This substitution was made primarily because of the greater concern of the Li/SO_2 battery user to the hazards associated with forced overdischarge and because of the reported cell explosions following forced overdischarge at low temperatures[1].

The ARC studies employed a wrap Li/SO_2 cell (approx. 1.4 Ah capacity) housed in a stainless steel container as a test vehicle. The ambient temperature tests employed four different cell designs, each representing a different materials balance in order to study the effects of cell design on safety. Forced overdischarge was conducted to 200% of the original cell capacity (based on SO_2) while resistive overdischarge was carried out until the cell potential dropped below 0.1 volts. Thermal stability was evaluated periodically during the discharge and overdischarge testing. Any exothermic reactions detected were monitored continuously by the ARC instrument. At the completion of the electrical testing, the thermal stability of the cells was evaluated at elevated temperatures. In most instances, these tests were conducted up to a cutoff temperature of 350°C.

Any exotherms detected during an experiment were resolved into their individual reactions and each reaction then characterized with respect to its kinetic parameters (activation energy and reaction order), rates of temperature and pressure increase and overall temperature and pressure rise. The magnitude

the hazard represented by a given reaction (or exotherm) was assessed from its maximum pressure rate and overall pressure rise. The reaction intiation temperatures were used to speculate on the actual reactions occurring.

All cells were found to be thermally stable following discharge to a two-volt cutoff. Overdischarge often initiated an exothermic reaction, believed to be the lithium/acetonitrile reaction. In the forced overdischarge tests, this reaction was observed not only in cells having excess lithium by design but also in those where significant amounts of lithium remained at end of life because of rate induced inefficiencies. In the resistive overdischarge tests, only the cell having excess lithium by design gave an exothermic reaction during overdischarge and this reaction was found to have different kinetic characteristics than the reactions observed in the force overdischarge tests. In general, the reactions observed during overdischarge were characterized by low activation energies, low temperature and pressure rates but often led to substantial pressure and temperature increases.

Many reactions were observed during the elevated temperature evaluations of the cells following completion of the electrical testing. In the cells tested at ambient temperature, the resistive overdischarged cells were found to exhibit reactions having significantly higher pressure rates than those from the forced overdischarged cells. In all cases, however, the observed pressure rates were low enough to make explosion unlikely in cells incorporating safety vents, although venting was a distinct possibility because of the magnitude of the overall pressure and temperature increases.

The results obtained with the cells tested at -35°C were very dramatic. The cell force overdischarged demonstrated an explosive reaction initiating at 108°C. This reaction was characterized by temperature and pressure rates approaching 200°C/min and 2000 psig/min., respectively. The cell evaluated following discharge to 2.0 volts also produced temperature and pressure rates that characterized it as an explosion hazard but not nearly of the magnitude of the cell force overdischarged. Low temperature testing appears to significantly increase the hazards associated with Li/SO_2 cells and is an area where further investigation is critically needed.

To support the ARC work, micro-calorimeter studies were carried out to determine the heats of reaction for the lithium acetonitrile and the lithium/aluminum alloy - acetonitrile reactions. A value of -54.6 $\pm$ 1.0 KCal/mole - Li was found for the lithium/acetonitrile reaction while the lithium/aluminum alloy was found to be unreactive with acetonitrile at ambient temperature.

Preliminary investigations were also carried out using FTIR spectroscopy to study the products of electrolyte oxidation on nickel and stainless steel electrodes. During forced overdischarge of cells in which the lithium has been depleted, oxidation of the electrolyte and/or anode grid and cell case material is going to occur. The products of these reactions could have a significant impact on cell safety. Very little work, however, has been done in this area to date. In this program, a spectroelectrochemical cell has been designed which allows the products of an electrochemical reaction to be monitored continuously in situ. This cell is sufficiently leak proof for use with SO_2 containing solutions, is inexpensive to fabricate, and readily allows the use of different electrode and window materials. This preliminary study has demonstrated the feasibility of using FTIR spectroscopy to study the oxidation reactions taking place in the Li/SO_2 system but more work is required before the reaction mechanisms can be elucidated.

This program represents a joint endeavor between Honeywell's Power Sources Center (PSC) in Horsham, PA and the Corporate Technology Center (CTC) in Bloomington, MN. The accelerating rate calorimetry studies were conducted at PSC by Mr. Walter B. Ebner while the micro-calorimeter and FTIR studies were carried out at CTC by Dr. K. Y. Kim and Dr. H. V. Venkatasetty, respectively.

TASK I

ACCELERATING RATE CALORIMETER STUDIES

WALTER B. EBNER
POWER SOURCES CENTER
HORSHAM, PA

Task I: Accelerating Rate Calorimeter Studies

The overall objective of this task was to quantitatively define the thermal behavior of the Li/SO_2 system under various conditions of use and abuse and to elucidate the chemical reactions associated with any observed instability. The abuse conditions evaluated include (1) resistive overdischarge at ambient temperature, (2) forced discharge into reversal at ambient temperature, and (3) forced discharge into reversal at -35°C. The test plan is shown in Table 1.

Instrument Operation

A detailed discussion of the general design and operating principles of the Accelerating Rate Calorimeter can be found in Appendix I. In this program, each experiment was broken into two distinct phases; electrical testing and elevated temperature testing. Thermal stability was evaluated during each phase.

Electrical testing refers to the process of discharging and overdischarging the cell, either galvanostatically or resistively. During this phase, thermal stability of each cell was evaluated periodically at its current temperature. This was accomplished by setting the step-heat increment to zero and initiating a heat-and-search operation of the ARC instrument. In this manner, the instrument would search for exothermic behavior but would not apply any step heating to the cell. While evaluating thermal stability in this way, the cell was put on open circuit so as to eliminate the effects of resistive heating.

Elevated temperature testing refers to the thermal stability testing conducted at the completion of the electrical testing. Here, the cell was put on open circuit and a heat-and-search operation initiated. Typical instrument parameters were as follows:

- Initial temperature: ambient
- Final temperature: 350°C
- Rate threshold: 0.02°C/min
- Step-heat increment: 15°C

Table 1. Test Plan for ARC Experiments

Test Group	Cell Design	Cell No.	Test Temp. °C	Current Density mA/cm²	Electrochemical Process(s) Studied
A	(I) Lithium Limited	I-1	25	1.0	Discharge + Forced Discharge to Reversal
	(II) Coulombically Balanced	II-1	25	1.0	" " " "
	(III) Excess Carbon	III-1	25	1.0	" " " "
	(IV) Excess Lithium	IV-1	25	1.0	" " " "
B	(I) Lithium Limited	I-2	25	5.0	Discharge + Forced Discharge to Reversal
	(II) Coulombically Balanced	II-2	25	5.0	" " " "
	(III) Excess Carbon	III-2	25	5.0	" " " "
	(IV) Excess Lithium	IV-2	25	5.0	" " " "
C	(I) Lithium Limited	I-3	25	(5 ohm load)	Resistive Discharge to Approx. 0.0 volts
	(II) Coulombically Balanced	II-3	25	"	" " " "
	(III) Excess Carbon	III-3	25	"	" " " "
	(IV) Excess Lithium	IV-3	25	"	" " " "
D	(II) Coulombically Balanced	II-5	-35	3.0	Discharge to 2.0 volts
	(II) Coulombically Balanced	II-6	-35	3.0	Discharge + Forced Discharge to Reversal

During an experiment, the ARC instrument prints out a listing of time, temperature, temperature rate, and pressure data. During an exotherm, this data is stored in memory for subsequent plotting and analysis. The instrument, however, is only capable of storing the data for a single experiment which means that all data reduction for one experiment must be completed, including all plotting, before another experiment can be started. This greatly slows down the experimental process and limits the flexibility one has in terms of data reduction. Also, the quality of the plots obtained with the ARC instrument are poor, unsuitable for reports or viewgraphs.

To overcome these shortcomings, software was developed for an HP-85 desk top computer to allow entering of data and plotting on a Model HP-7225A plotter. Time did not permit the development of the software needed for automatic data acquisition through the RS-232 interface, so the data were manually entered into the computer. Once entered, the data were stored on magnetic tape for future use. All of the graphs contained in this report were plotted with the HP-85 computer.

In the following sections dealing with the results of the individual cell tests, four different plots are presented for each exotherm. These plots are described in Table 2 along with a brief discussion of how each plot is used in interpretation of the ARC data.

The log temperature rate versus 1/T plot is particularly useful for identifying the number of reactions occurring during an exotherm and for determining the kinetic parameters for each reaction. In most instances, the activation energy for an observed reaction was estimated from the slope of the linear portion of the log temperature rate versus 1/T plot at the start of the reaction using the following equation.

$$E = \frac{RT_1T_2}{T_2-T_1} \ln \frac{M_2}{M_1} \qquad (1)$$

Table 2. Description of Four Data Plots Used in Interpretation of ARC Results

Plot No.	Independent Variable	Dependent Variable	Interpretation
1	Time, min.	Temperature, ^{o}C	Shows thermal response of cell during exotherm - exponential behavior denotes thermal runaway reaction.
2	Time, min.	Pressure, psig	Shows pressure behavior during exotherm - high values denote general hazard - exponential behavior denotes explosion hazard.
3	Reciprocal Absolute Temp., $1/^{o}K$	Log Temperature Rate, ^{o}C/min	Arrhenius-type plot - each exothermic reaction gives distinct peak from which kinetic information can be extracted.
4	Reciprocal Absolute Temp., $1/^{o}K$	Log Pressure, psig	Used to identify changes in reaction mechanism - vapor pressure of pure liquid gives linear behavior

where, E = Activation Energy, kcal/mole

R = Universal gas constant, 1.987 cal/mole - ^{o}K

T_1 and T_2 = Temperatures on linear portion of log temperature rate versus 1/T plot, ^{o}K ($T_2 > T_1$)

M_1 = Temperature rate at T_1, $^{o}C/min$

M_2 = Temperature rate at T_2, $^{o}C/min$

This approach assumes pseudo-zero order kinetics in the early stages of a reaction before significant concentration changes have occurred.

The reaction order is then calculated using the following equation:

$$N = \frac{E(T_F - T_M)}{RT_M^2} \qquad (2)$$

where, N = Reaction order

E = Activation energy, kcal/mole

T_F = *Final temperature of observed reaction*, ^{o}K

T_M = Temperature at which the maximum temperature rate has occurred in the observed reaction, ^{o}K

R = Universal gas constant, 1.987 cal/mole - ^{o}K

Because of the complexity of most of the exotherms detected in this program, many of the peaks were not fully resolved making it difficult to obtain an accurate value of T_F. As a result, the reaction orders calculated from Equation (2) are only approximations and could be subject to significant error in some cases.

In some experiments, low activation energy reactions were observed where the rate did not change significantly with temperature. Here, Equation (1) was not applicable and a curve fitting procedure was employed to determine the kinetic parameters using the following plotting equation.

$$M_T = Mo\left(\frac{T_F - T}{T_F - To}\right)^N \exp\left[\frac{E}{R}\left(\frac{1}{To} - \frac{1}{T}\right)\right] \qquad (3)$$

where, M_T = Temperature rate at temperature (T), $^{o}C/min$

Mo = Temperature rate at initiation temperature of reaction, $^{o}C/min$

T_F = Final temperature of reaction, ^{o}K

To = Initiation temperature of reaction, ^{o}K

E = Activation energy, kcal/mole

R = Universal gas constant, 1.987 cal/mole - ^{o}K

N = Reaction order

The values of N and E were varied until a good fit with the experimental data was obtained.

Figure 1 illustrates the effects of activation energy on the thermal response of an exothermic reaction. The adiabatic temperature rise is determined by concentration (i.e., total quantity of materials undergoing reaction) while the activation energy influences the rate of the reaction at any given temperature. The higher the activation energy, the more the reaction rate will be accelerated by temperature. High activation energy reactions, therefore, constitute the greatest threat in terms of a thermal runaway hazard. Such reactions would appear as sharp peaks on the log temperature rate versus 1/T plot while low activation energy reactions are characterized by flat, broad peaks.

In designing an ARC experiment, one of the most important considerations is the value of thermal inertia (ϕ). This value indicates the fraction of heat that goes to heat the bomb as compared to that which is used to heat the sample during an exothermic reaction and is given by

$$\phi = 1 + \frac{Mb\bar{C}vb}{Ms\bar{C}vs}$$

where, ϕ = Thermal inertia

Mb = Mass of bomb, gm

Ms = Mass of sample, gm

$\bar{C}vb$ = Average heat capacity of bomb, cal/gm - ^{o}K

$\bar{C}vs$ = Average heat capacity of sample, cal/gm - ^{o}K

The higher the value of ϕ, the greater the thermal diluting effect of the bomb.

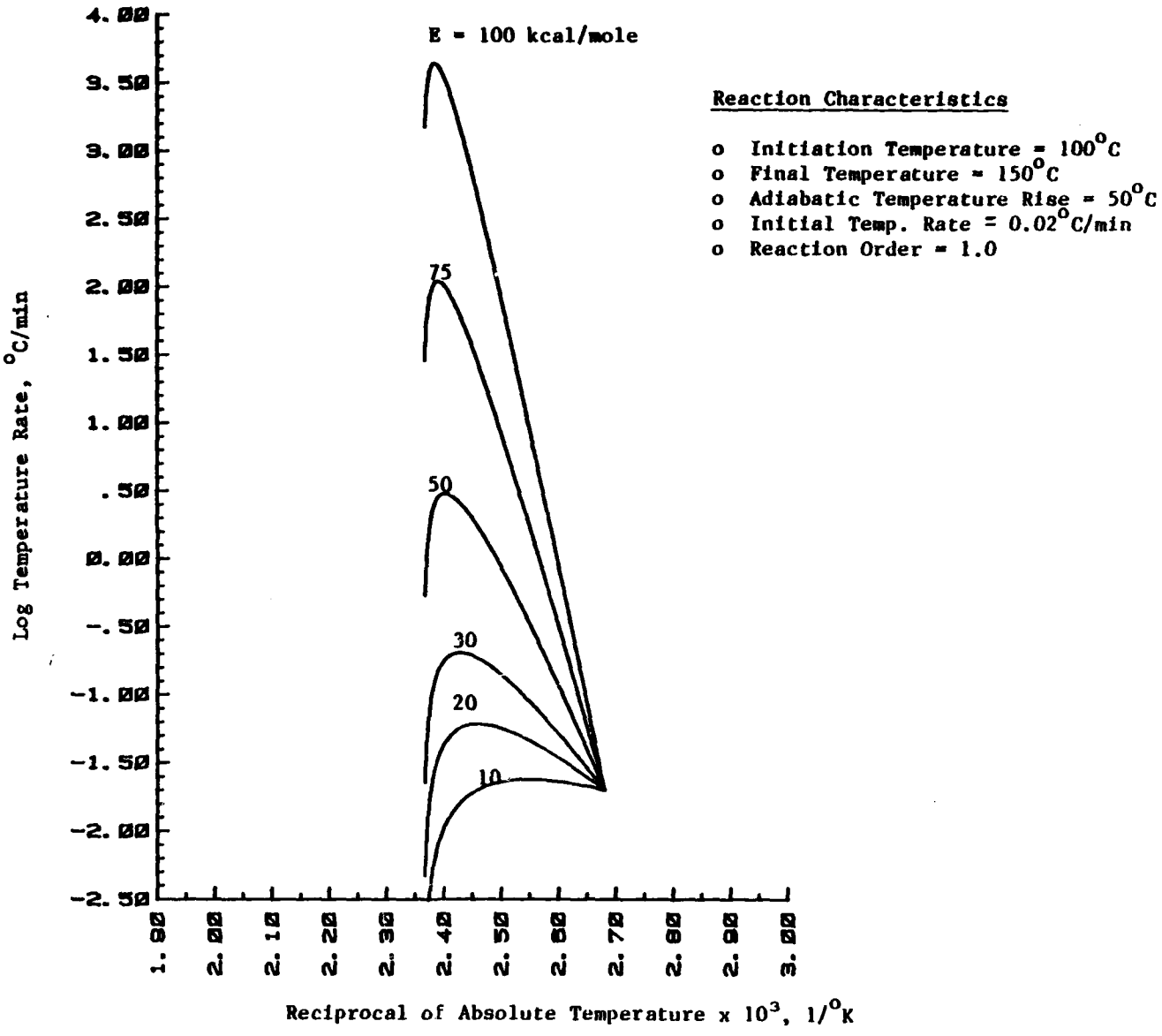

Figure 1. Log Temperature Rate Versus 1/T Plot for Hypothetical Exothermic Reaction Illustrating the Effect of Activation Energy on the Thermal Response Under Adiabatic Conditions

One of the major advantages of the ARC technique is the ability to accurately scale the results up from the experimental sample to the end use application, be it a larger battery or a tank car of chemicals. The basic premise on which the scaling is based is that the thermal behavior of a chemical system does not change with size for a constant value of thermal inertia (ϕ). That is, for a given value of thermal inertia, the thermal behavior of a system will be the same regardless of the size of the system. Furthermore, the thermal behavior of a configuration having a different ϕ-value can be easily determined using the following equations.

$$T_{F_2} = To + \frac{\phi_1}{\phi_2} (T_{F_1} - To) \qquad (4)$$

$$M_{T_2} = \frac{\phi_1}{\phi_2} M_{T_1} \qquad (5)$$

where,

T_{F_2} = Predicted final temperature for configuration having thermal inertia ϕ_2, ^{o}C

To = Initial temperature of exotherm, ^{o}C

T_{F_1} = Observed final temperature for experimental configuration having thermal inertia ϕ_1, ^{o}C

ϕ_1 = Thermal inertia of experimental system

ϕ_2 = Thermal inertia of system for which predictions are being made

M_{T_2} = Predicted temperature rate at temperature (T) for configuration having thermal inertia ϕ_2, $^{o}C/min$

M_{T_1} = Observed temperature rate at temperature (T) for experimental configuration having thermal inertia ϕ_1, $^{o}C/min$.

In general, the closer the two ϕ values, the more accurate the prediction.

This ability to accurately scale the results from an experiment involving a few grams of material to an end use application involving many pounds or tons of material without having any knowledge of the reactions involved is really the strength of the ARC technique. In the following discussions involving our experimental results, predictions have been made regarding the thermal behavior of "D" size Li/SO_2 cells. These predictions have been made using Equation (4). Knowing their ϕ-values, predictions can be easily made for Li/SO_2 cells of any size.

Cell Design and Construction

This program employed four cell designs to evaluate the effects of different component ratios on Li/SO_2 safety. These designs are summarized in Table 3 . As can be seen, each design has all three active components specified; i.e., lithium, sulfur dioxide, and carbon, where the carbon capacity is based on 1.44 Ah per gram of cathode mix. Therefore, a design methodology had to be developed to achieve the desired materials balance while, at the same time, obtaining good packaging efficiency within the given case dimensions. The latter are given by the inside dimensions of the ARC bombs which are 0.75 in. diameter x 1.17 in.

The designs were formulated based on a reverse wrap (i.e., the cathode as the outermost electrode), a separator thickness of 0.007 in. (actually two layers of 0.0035 in. material), and a cathode thickness of 0.032 in. The desired materials balance for the different configurations was achieved by varying the lithium thickness and the electrolyte quantity. Initial electrode and separator lengths were estimated using a calculator program for spiral-wrap cells and then adjusted through an empirical process to achieve the optimum packaging efficiency.

Because the test plan given in the proposal did not list the Li/C ratio, the first step in the design process was to calculate this value. The Li/C ratio is given by the product of the Li/SO_2 and SO_2/C ratios; i.e.,

$$Li/C = Li/SO_2 \times SO_2/C \qquad (6)$$

Next, the anode thickness is estimated using Equation (7) (derivation of this equation is given in Appendix II). This equation assumes equal lengths for the anode and cathode. Therefore, the result must be adjusted later on to take into account the greater length of the cathode in the spiral-wrap configuration.

$$Ta = \frac{(Tc)(Cc)(R_3)}{2.062} \qquad (7)$$

where, Ta = Anode thickness, cm
Cc = Specific cathode capacity, Ah/cc
Tc = Cathode thickness, cm
R_3 = Li/C ratio

Table 3. Cell Design Description

Design No.	Li/SO_2 Ratio	SO_2/C Ratio	Li/C Ratio	Design Description
I	0.5	1.25	0.625	Lithium Limited
II	1.0	1.25	1.25	Coulombically Balanced (Baseline)
III	1.0	0.5	0.5	Excess Carbon
IV	1.5	1.25	1.875	Excess Lithium

The cathodes employed in this program had a density of 0.36 g/cc. Therefore,

$$Cc = 1.44 \text{ Ah/g} \times 0.36 \text{ g/cc} = 0.518 \text{ Ah/cc}$$

The anode and cathode lengths are estimated by evaluating Equation (8) between the limits of n_1 and n_2, the latter being defined by Equations (9) and (10), respectively. A complete derivation of these equations is given in Appendix III.

$$S = t\left[\frac{n}{2}\sqrt{4\pi^2n^2+1} + \frac{1}{2\pi}\ln\left(2\pi n + \sqrt{4\pi^2n^2+1}\right)\right]\Bigg|_{n_1}^{n_2} \quad (8)$$

$$n_2 = \frac{1}{t}\left[\frac{d}{2} + E - 0.75t\right] \quad (9)$$

$$n_1 = \frac{r+E}{t} \quad (10)$$

where,

S = Electrode length, cm
t = Total thickness of cell stack including separators, cm
E = Edge thickness of component whose length is being determined, cm
(See Appendix III for a more complete definition of this term).
d = Desired final wrap thickness, cm
r = Radius of wrap mandrel, cm

Since the inside diameter of an ARC bomb is 0.75 in., a value of 0.73 in. was selected for the desired final wrap diameter to ensure that the completed cell assembly would fit into the bomb. Also, it was assumed that the mandrel radius would include the thickness of one turn of separator which is normally employed to initiate the wrapping process.

The ratio of the calculated anode length to cathode length is determined and the anode thickness recalculated using Equation

$$Ta = \frac{(Cc)(Tc)(R_3)}{2.062K} \qquad (11)$$

where,

Ta = Anode thickness, cm
Cc = Specific cathode capacity, Ah/cc
Tc = Cathode thickness, cm
R_3 = Li/C ratio
K = Calculated anode length/cathode length ratio

The result is the anode thickness needed to achieve the required materials balance taking into account the difference in length between the anode and cathode. This approach is based on the assumption that the anode to cathode length is independent of small changes in component thicknesses and analysis has shown this assumption to be valid for the range of thickness variations encountered in these cell designs.

Next, the lengths of the electrodes and separators are calculated using equations (8) through (10) and the recalculated anode thickness. A cell is then built using these component lengths and minor adjustments made as needed to achieve the proper component overlap and good packaging efficiency. For the four cell configurations involved in this program, it was found that no significant changes in the anode or cathode lengths were required. All separator lengths, however, had to be increased somewhat to ensure proper insulation of the electrodes. Also, the final layer of separator was lengthened so that it could be given one complete turn around the cell and then heat sealed to prevent the cell assembly from becoming unraveled.

Table 4 lists the component dimensions for each of the four cell configurations along with the quantity of electrolyte solution required to achieve the desired materials balance. This latter quantity was calculated from Equation (12), which is derived in Appendix II.

Table 4 . Component Dimensions and Electrolyte Quantities for the Four Cell Designs

Design No.	Anode* Dimensions, in.			Cathode* Dimensions, in.			Top Separator Dimensions, in.			Bottom Separator Dimensions, in.			Electrolyte Quantity, gm
	L	W	T	L	W	T	L	W	T	L	W	T	
I	6.27	0.80	0.006	7.44	0.80	0.032	7.40 7.70	1.00 1.00	0.0035 0.0035	9.95 10.20	1.00 1.00	0.0035 0.0035	7.14
II	5.62	0.80	0.012	6.65	0.80	0.032	6.60 6.90	1.00 1.00	0.0035 0.0035	8.90 9.10	1.00 1.00	0.0035 0.0035	6.40
III	6.40	0.80	0.005	7.61	0.80	0.032	6.85 7.15	1.00 1.00	0.0035 0.0035	9.00 10.40	1.00 1.00	0.0035 0.0035	3.04
IV	5.09	0.80	0.018	6.02	0.80	0.032	6.00 6.25	1.00 1.00	0.0035 0.0035	8.00 8.25	1.00 1.00	0.0035 0.0035	5.80

* REPORTED LENGTH IS FOR ACTIVE MATERIAL ONLY AND DOES NOT INCLUDE LEAD CONNECTION.

$$El = \frac{13.56W}{R_1} \qquad (12)$$

where,

El = Required quantity of electrolyte solution, gm
W = Weight of lithium metal in anode, gm
R_1 = Li/SO_2 ratio

Table 5 gives a description of each component used to construct the cells. All four cell designs incorporated anode grids to ensure efficient utilization of the lithium metal during discharge.

The cell wrap is housed in a 316 stainless steel case incorporating an internal o-ring seal. The case acts as the negative terminal while the positive terminal is brought out through a Teflon compression seal. This is the same electrical configuration employed in hardware Li/SO_2 cells where cathodic protection of the case is required to prevent corrosion. Swagelok fittings are used to connect the cell to the calorimeter. Figure 2 shows a schematic drawing of the cell hardware.

The cathode manufacturing process is summarized in the flow diagram shown in Figure 3. The actual electrode is made by a roll forming process in which the dry, micronized cathode mix is rolled onto the aluminum grid.

In the remaining sections of this report, cells will be referenced by their cell number. The numbering system employed consists of a two-part designation. The Roman numeral represents the design type (i.e., lithium limited, coulombically balanced, etc.) as given in Table 3. The Arabic numerals represent the manufacturing serial number for that specific cell design. Thus, I-3 would designate the third lithium limited cell manufactured. The test plan shown in Table 1 includes the cell numbers for easy reference as to which cell was tested under each condition.

Table 5. Summary of Cell Components

Component	Material	Description
Anode	Lithium	Foil
Separator	Polypropylene	Webril E-1488 Non-Woven Fabric
Cathode	Carbon (95 wt. %)	Shawinigan Acetylene Black (100 percent compressed)
	Teflon (5 wt. %)	Added as Teflon-30 Dispersion
Anode Collector	Nickel	Delker 3Ni5-125
Anode Lead	Nickel	Ribbon
Cathode Collector	Aluminum	Delker 5AL8-077
Cathode Lead	Aluminum	Wire (0.040 in. dia.)
Bottom Insulator	Polypropylene	Film
Top Insulator	Polypropylene	Film
Electrolyte Solution	LiBr (6.40 wt. %)	
	Acetonitrile (25.6 wt.%)	
	Sulfur Dioxide (68.0 wt.%)	
Bomb (Body & Lid)	316 Stainless Steel	
O-Ring (for bomb seal)	Viton	Part Number 568-019

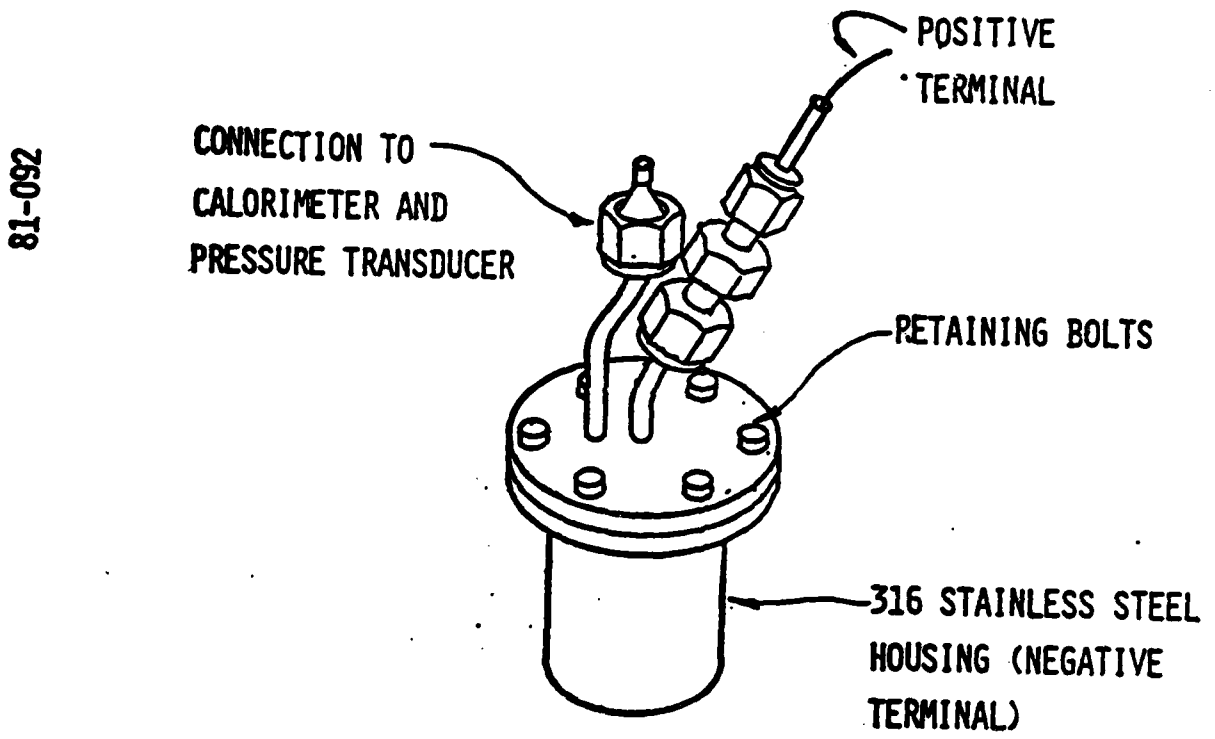

Figure 2. ARC Li/SO_2 Cell Hardware

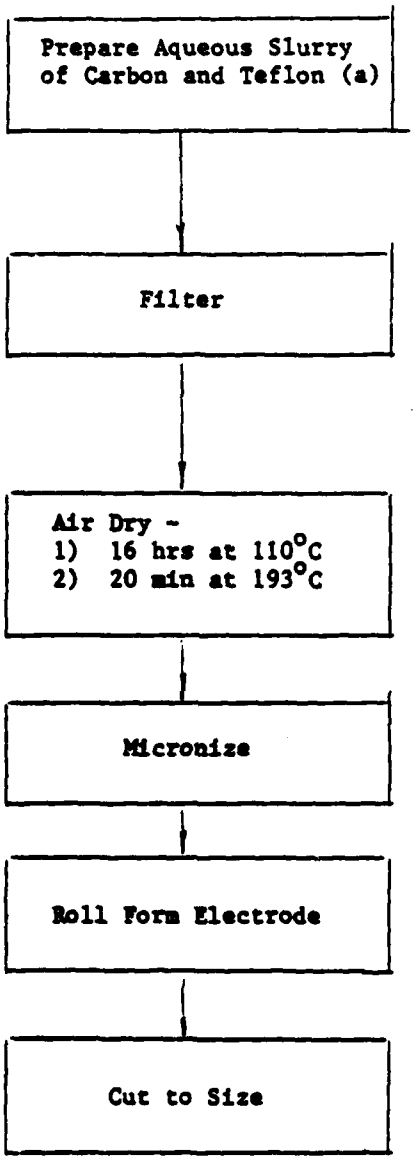

(a) Teflon added as Teflon-30 dispersion.

Figure 3. Flow Diagram of Cathode Fabrication Process

Experimental Problem Areas

The desire to obtain high temperature data (up to 350°C) in the ARC studies put great demands on the test cell in terms of it remaining hermetic over this temperature range. During the course of experimentation, an occasional leakage problem was identified with the compression seal used for the positive lead. In the cell design employed, the positive lead, consisting of Teflon-jacketed aluminum wire (0.040" dia.) is brought out through a Teflon bushing housed in a 1/16" Swagelok fitting. The seal is made by tightening the fitting, compressing the bushing against the wire. Because of the intrinsic softness of aluminum metal, however, even slight overtightening can cause the bushing to cut right through the wire. Too little tightening, on the other hand, can result in the seal failing at elevated temperatures and pressures. This problem makes it very difficult to obtain a reproducible seal. Even so, the general quality of the seal is good as evidenced by the fact that no leakage was observed at temperatures up to 100°C, well above the normal operating and storage temperatures of Li/SO_2 cells.

It was found that by optimizing the tightness of the compression seal fitting, the leakage problem was resolved satisfactorily as evidenced by the fact that no leakage problems were encountered below 290°C for the last 5 cells tested. Between 290 and 350°C, however, seal failure often occurred. This is believed to be due to thermal degradation of the Teflon bushing at these temperatures and probably represents the upper operating limit for this cell design.

Cell leakage at elevated temperatures also resulted in instrumentation problems. Following such leakage, the inside of the calorimeter would become covered with an electrically conductive, blue-black film (believed to be a metallic sulfide film) which would short out the calorimeter thermocouples and, sometimes, the radiant heater. For proper operation of the instrument, it is very important that the thermocouples be electrically isolated from the calorimeter. A cleaning procedure was developed that, in most cases, gave good results. Occasionally however, an instrument malfunction would occur. The problem was found to be intermittent and is believed to be due to chemical corrosion of the Type N thermocouples.

Group A Tests

Forced Overdischarge at 1.0 mA/cm^2 ($25^{\circ}C$)

Group A Tests

Objective

The objective of the Group A tests was to evaluate the thermal behavior of Li/SO_2 cells during ambient temperature discharge and reverse discharge at a moderate current density (1.0 mA/cm^2).

Experimental

The discharge tests were performed galvanostatically. Because of the long run times, a test station was employed to monitor the cell voltage and automatically remove the load when the cell potential dropped below 2.0 volts. The reverse discharge tests were conducted in the same manner except that a chart recorder was employed to record the cell voltage data because the data-logger used in the test station cannot sense negative voltages in its present configuration. Throughout the cell tests, the time, temperature, and pressure data were continuously recorded by the ARC instrument.

The construction features of the four Group A cells are shown in Table 6. Due to the tolerances associated with cell manufacture, the actual component ratios differ somewhat from those planned. In all cases, however, the basic features are preserved; i.e., lithium-limited, excess lithium, etc.

Discharge Performance

The discharge behavior of the four cells to a 2.0 volt cutoff is summarized in Table 7. The low lithium and SO_2 utilization obtained in Cell No. III-1 is believed to be the result of the cell drying out during discharge because of the reduced electrolyte quantity employed in the excess carbon design. The reported average voltages are estimated to be approximately 0.19 volts low because of an error introduced by the test circuit. The test station design is such that the same set of leads must be used to carry the discharge current and sense the cell voltage. The resulting IR drop through the leads is therefore included in the potential measurements. The component ratios present at the 2.0 volt cutoff are summarized in Table 8.

Table 6 . Construction Features of Group A Cells

Cell No.	Li/SO_2 Ratio	SO_2/C Ratio	Li/C Ratio	Electrolyte Qty, gm	Cathode Surface Area, cm^2	Thermal[1] Intertia Value, ϕ
I-1[2]	0.52	1.11	0.58	6.70	76.9	2.23
II-1	0.85	1.18	1.01	6.35	68.6	2.26
III-1	0.76	0.64	0.49	4.20	78.4	2.69
IV-1	1.48	1.09	1.62	5.22	61.9	2.45

(1) For comparison, the ϕ value for a "D" Li/SO_2 cell is approximately 1.15.

(2) Lithium weight for this cell is estimated on basis of 91% discharge efficiency to 2.0 volts.

Table 7. Discharge Performance to 2.0 Volts for Group A Cells

Cell No.	Current, mA	Run Time, Hr.	Capacity Delivered, Ah	Average Voltage, V	Discharge Efficiency, %		
					Anode	Carbon	SO_2
I-1	76.9	11.7	0.900	2.62	91.0*	52.5	47.2
II-1	68.6	20.6	1.41	2.62	91.4	92.5	78.1
III-1	78.4	7.96	0.624	2.59	68.7	33.4	52.2
IV-1	61.9	21.4	1.32	2.66	60.0	97.2	89.0

* Estimated anode efficiency

Table 8. Component Ratios Present at End of Discharge to a 2.0 Volt Cutoff for Group A Cells.

Cell No.	Cell Design	SO_2/Li	SO_2/Li Area, mg/cm^2
I-1	Lithium Limited	11.3	31.3
II-1	Coulombically Balanced	3.0	13.8
III-1	Excess Carbon	2.0	17.4
IV-1	Excess Lithium	0.19	6.44

Each cell was reverse discharged for a minimum of 200 percent based on the original SO_2 capacity. The actual degree of reverse discharge for each cell is summarized in Table 9. Figure 4 shows the temperature versus time profiles for each cell during the initial stages of reverse discharge.

Figure 5 shows the cell potential, temperature, and pressure versus time data for Cell No. II-1 which is typical of the data obtained for these cells. This figure also includes the results during the final heat and search operation (i.e., elevated temperature testing).

Thermal Behavior

Table 10 summarizes the thermal behavior of the Group A cells. Only Cell No. IV-1, containing excess lithium, exhibited exothermic behavior.

Because it was intended to postmortem these cells at the completion of the experiments, the upper temperature limit of the heat and search operation (in the absence of any exothermic reactions) was limited to about 135°C so as to remain below the melting point of the polypropylene separator material (168-170°C). When the cells were disassembled, however, it was discovered that the internal components had expanded to such an extent that it was impossible to remove them intact. In fact, they had to literally be chiseled out of the bomb making postmortem investigation of the cell components impossible.

Cell No. IV-1

Immediately upon going into voltage reversal, the temperature of this cell began to rise. After 23 minutes, the cell temperature reached 40°C at which time the current was interrupted and the cell tested for exothermic behavior. An exotherm was detected and monitored by the ARC. Once the exotherm was complete, the cell was cooled to approximately 40°C and reverse discharge continued. No unusual thermal behavior was observed during the remainder of the reverse discharge testing.

The initial exotherm detected while the cell was in voltage reversal is postulated to be due to the Li/AN reaction. The data plots for this reaction are shown in

Table 9. Summary of Reverse Discharge Testing Performed on Group A Cells.

Cell No.	Cell Design	Time in Reverse, hr	Degree of[1] Reverse Discharge, %
I-1	Lithium Limited	58.0	234
II-1	Coulombically Balanced	56.1	213
III-1	Excess Carbon	38.0	249
IV-1	Excess Lithium	58.7	244

(1) Based on original SO_2 capacity

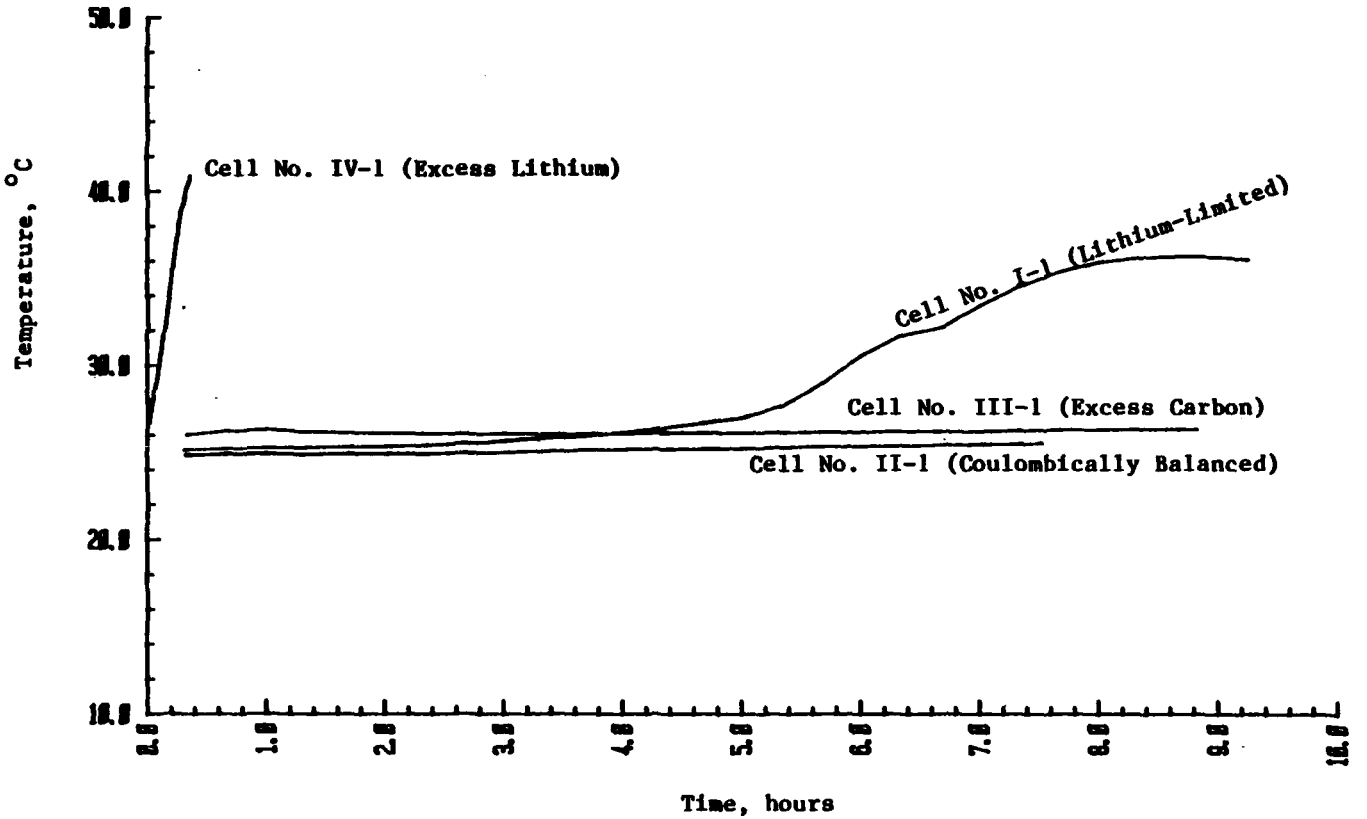

Figure 4. Time/Temperature Behavior During Initial Forced Overdischarge Testing of Group A Cells

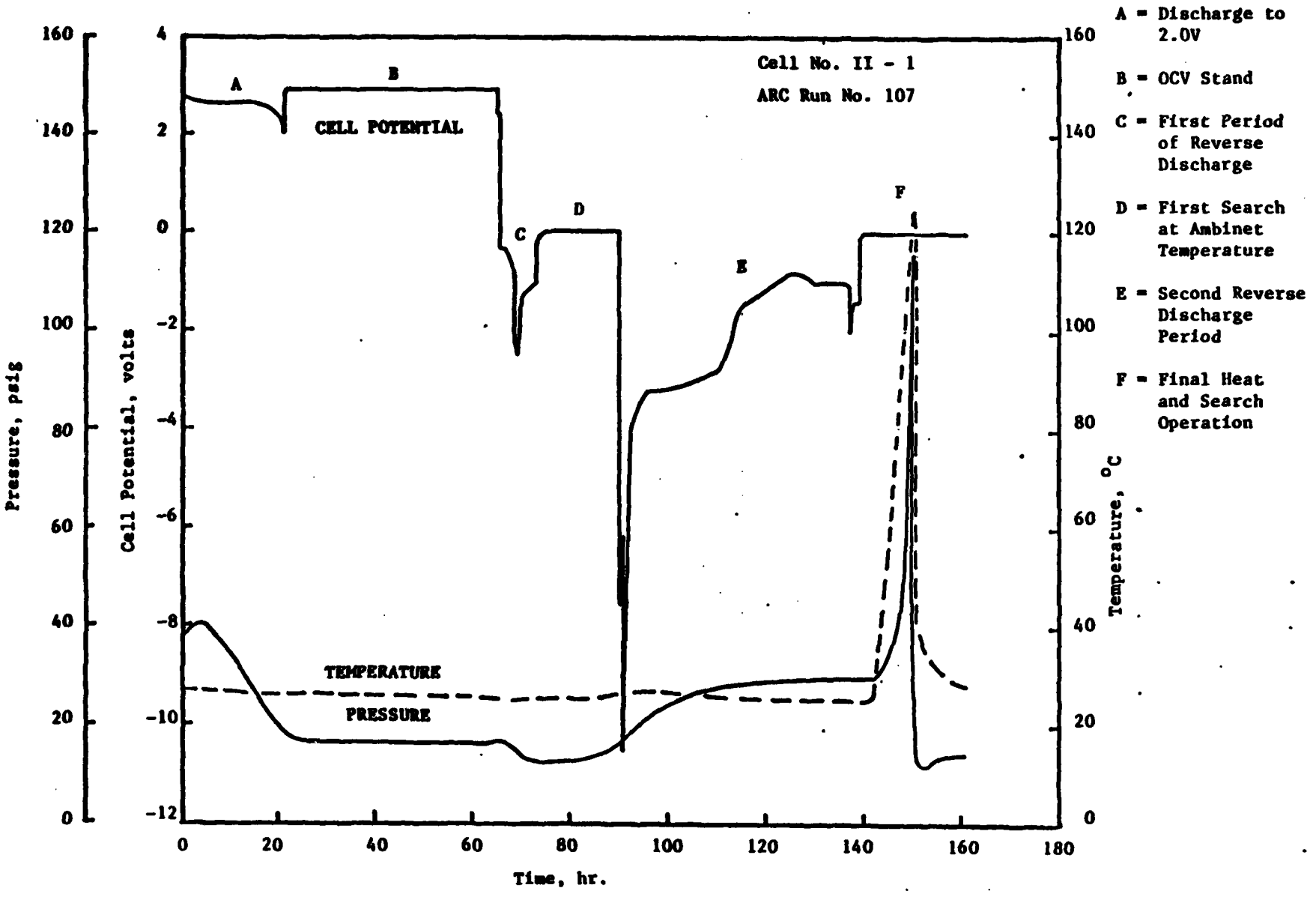

Figure 5. Voltage, Pressure, and Temperature Versus Time for Cell No. II-1 Under Discharge and Reverse Discharge Test Conditions of 1.0 mA/cm2 at 25°C.

Table 10. Summary of the Thermal Behavior of the Group A Cells

Cell No.	Cell Design	Exotherms			Final Temp. During Heat and Search, °C
		During Discharge to 2.0V Cutoff	During Reverse Discharge	During Heat and Search	
I-1	Lithium Limited	No	No	No	130
II-1	Coulombically Balanced	No	No	No	124
III-1	Excess Carbon	No	No	No	135
IV-1	Excess Lithium	No	Yes	Yes	345

Figures 6 through 9 while Table 11 summarizes the general characteristics of this exotherm including the apparent kinetic parameters and the behavior predicted for a Li/SO_2 "D" cell ($\phi = 1.15$). As can be seen, this is a significant exotherm resulting in a 46°C rise in temperature. In agreement with Dey's results[2] this was found to be a low activation energy reaction. Such a reaction is characterized by a time/temperature profile that levels off with time (Figure 6) and a flat log temperature rate versus 1/T plot with very little acceleration of the reaction rate with increasing temperature (Figure 7). The discontinuity observed in the data plots near the beginning of the exotherm is due to an inadvertent 2.8°C cooling of the cell during the exotherm.

As would be expected for the Li/AN reaction, this reaction was found to lead to a substantial pressure increase. Here, the pressure rise would be the combined result of methane generation from the Li/AN reaction and increased vapor pressure of the electrolyte solution at the elevated temperatures.

During the elevated temperature phase of testing (i.e., final heat and search operation) the experiment was initially terminated at 200°C. However, because exothermic reactions were still taking place, the sample was reheated and the experiment continued to 340°C at which point the cell leaked. A total of seven exotherms were detected up to the final temperature of 340°C. These are summarized in Table 12. The first four exotherms are relatively small but the fifth and sixth exotherms are significant. In fact, it is quite possible that exotherms 5, 6, and 7 are, in reality, a single exotherm separated in this experiment because of the initial cooling at 200°C and the cell leaking problems encountered above 300°C.

The data plots for the fifth and sixth exotherms are shown in Figures 10 through 13. The log temperature rate versus 1/T plot (Figure 11) indicates that these two exotherms actually consist of seven distinct reactions, as labeled in Figure 11. Table 13 summarizes the data for each of these peaks including the apparent kinetic parameters as derived through an analysis of the data. Insufficient data were available for the first peak for a kinetic evaluation since only the last stages of the reaction were detected.

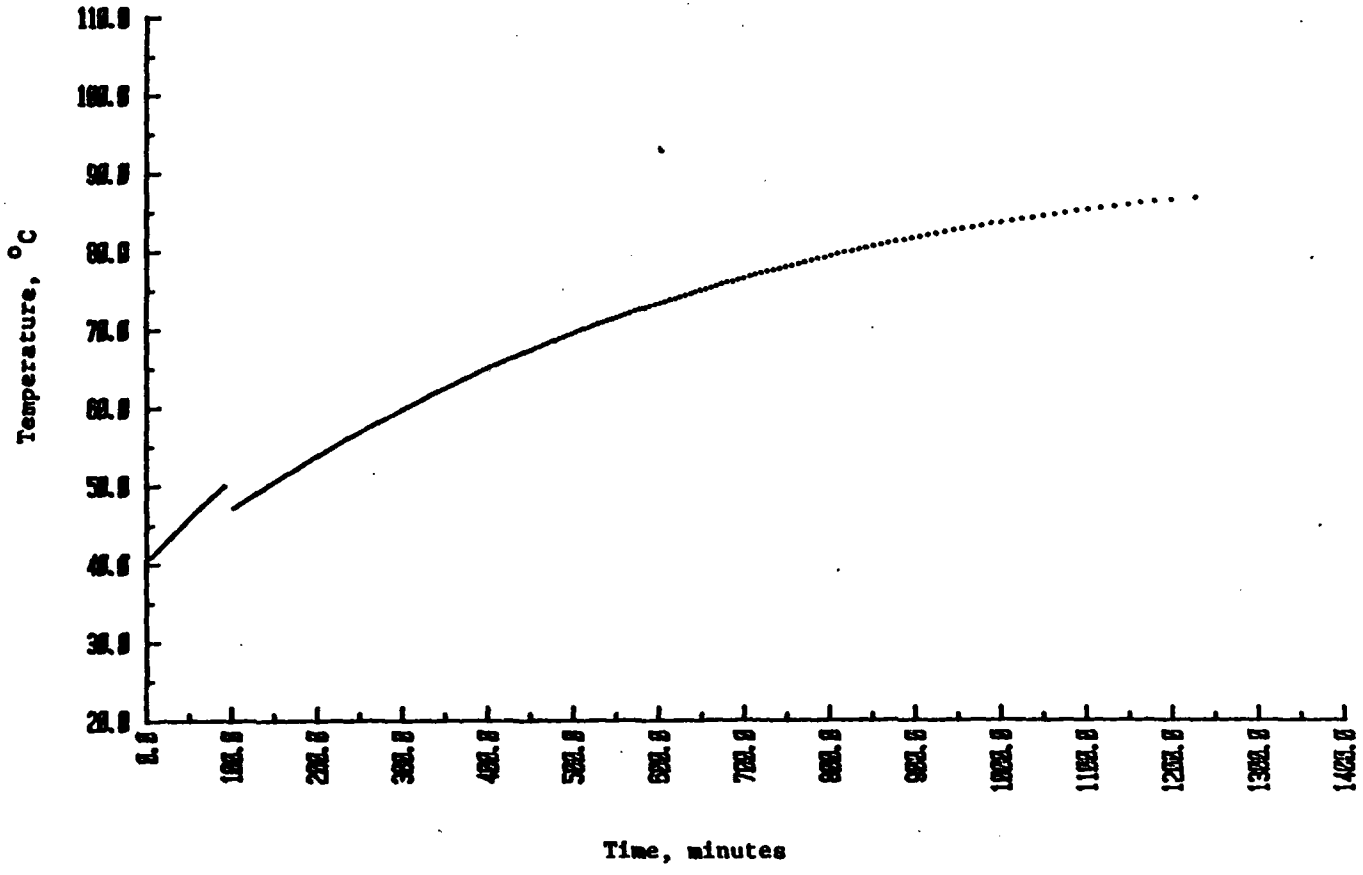

Figure 6. Temperature Versus Time Plot for the Exotherm Detected During Forced Overdischarge Testing of Cell No. IV-1 (Excess Lithium)

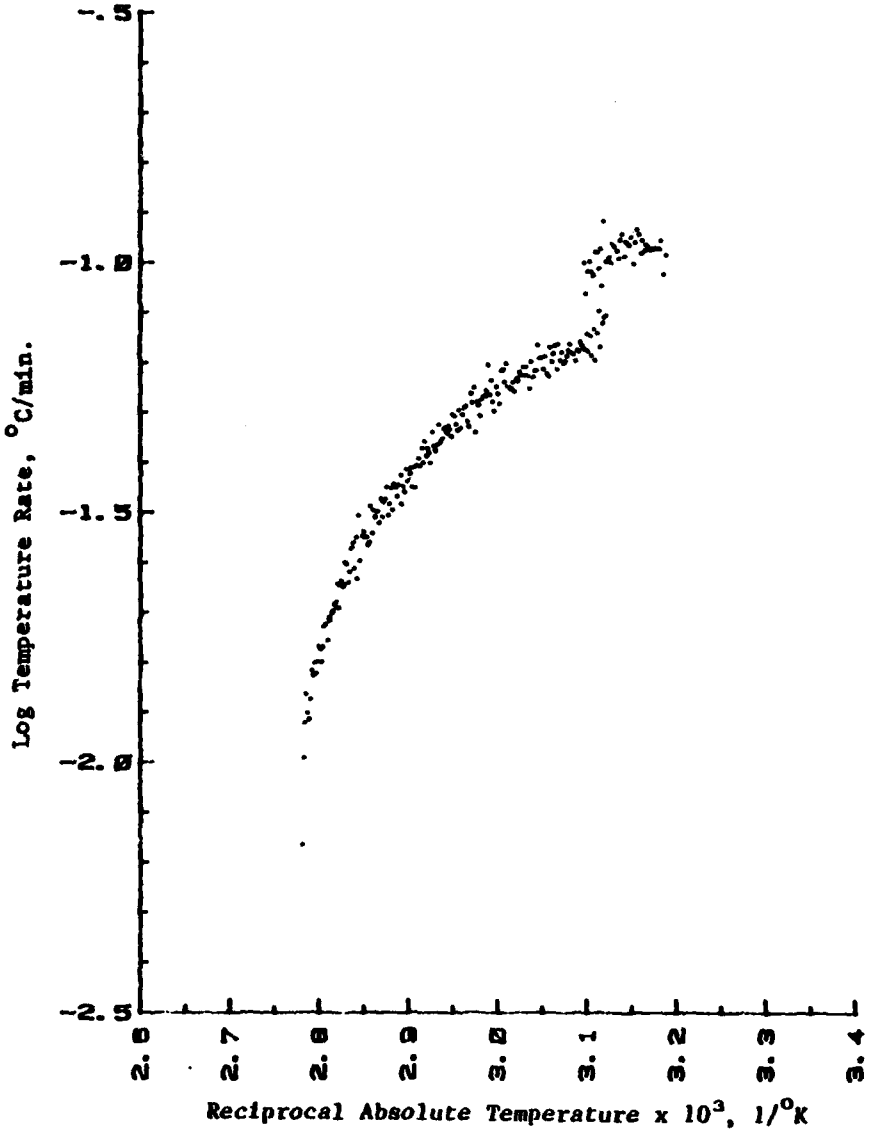

Figure 7. Log Temperature Rate Versus 1/T Plot for the Exotherm Detected During Forced Overdischarge Testing of Cell No. IV-1 (Excess Lithium)

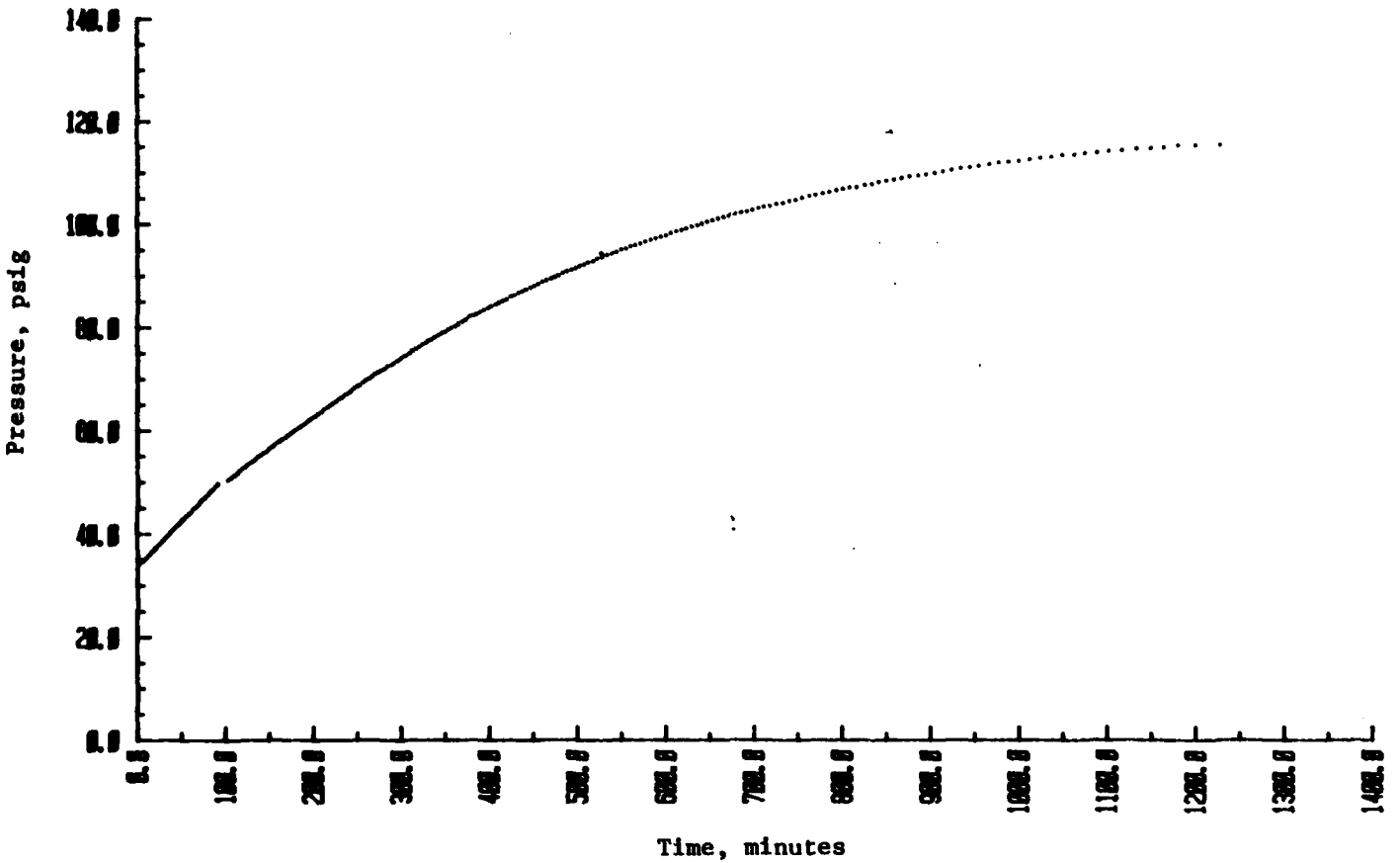

Figure 8. Pressure Versus Time Plot for the Exotherm Detected During Forced Overdischarge Testing of Cell No. IV-1 (Excess Lithium)

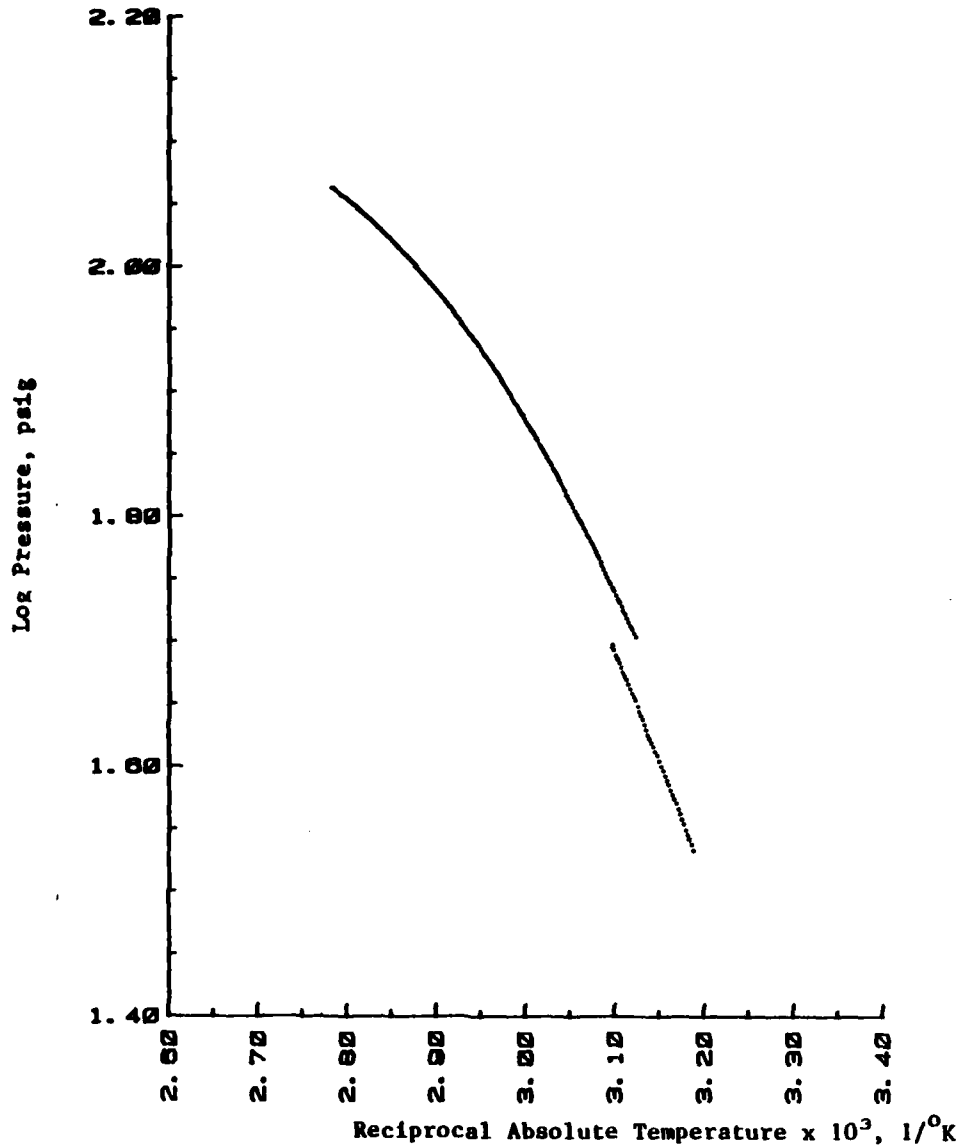

Figure 9. Log Pressure Versus 1/T Plot for the Exotherm Detected During Forced Overdischarge Testing of Cell No. IV-1 (Excess Lithium)

Table 11. Summary of Characteristics of Reverse Exotherm for Cell No. IV-1 (Excess Lithium)

Initial Temperature, ^{o}C	40.5
Initial Pressure, psig	33.8
Initial Temp. Rate, $^{o}C/min$	0.100
Final Temperature, ^{o}C	86.5
Final Pressure, psig	115.6
Maximum Temp. Rate, $^{o}C/min$	0.116
Maximum Pressure Rate, psig/min	0.25
Adiabatic Temp. Rise, ^{o}C	46.0
ΔH, cal	541
Pressure Change, psig	81.8
Time Duration of Exotherm, min	1228
Activation Energy, kcal/mole	5.9
Reaction Order	1.0
Projected Final Temp. for Li/SO_2 "D" Cell, ^{o}C	138.5
Projected Temp. Rise for Li/SO_2 "D" Cell, ^{o}C	98.0

Table 12. Summary of Exotherms Detected During the Heat and Search Operation for Cell No. IV-1.

	Exotherm Number						
	1	2	3	4	5[a]	6[b]	7
Initial Temperature, °C	102.9	109.1	115.9	123.0	131.3	202.0	334.7
Initial Pressure, psig	115.9	118.8	122.9	127.7	131.4	93.9	435.9
Initial Temperature Rate, °C/min	0.013	0.017	0.016	0.018	0.015	0.138	0.182
Final Temperature, °C	103.7	110.5	117.5	125.9	200.0	327.3	(c)
Final Pressure, psig	116.5	120.3	124.8	129.2	220.5	524.2	-
Maximum Temperature Rate, °C/min	0.013	0.017	0.016	0.020	0.289	0.338	-
Maximum Pressure Rate, psig/min	-	-	-	-	1.14	1.35	-
Temperature Rise, °C	0.8	1.4	1.6	2.9	68.7	125.3	-
ΔH, cal	9.4	16.5	18.8	34.1	808	1473	-
Pressure Change, psig	0.6	1.5	1.9	1.5	89.1	430.3	-
Projected Final Temperature for Li/SO_2 "D" Cell	104.6	112.1	119.3	129.2	277.7	468.9	-
Projected Temperature Rise for Li/SO_2 "D" Cell	1.7	3.0	3.4	6.2	146.4	266.9	-

(a) By experimental design, the run was terminated at 200°C and the sample cooled to ambient temperature. Because exothermic reactions were still occurring when the run was terminated, the actual final temperature would be expected to be significantly greater than 200°C.

(b) Exotherms 6 and 7 were detected after the sample was reheated.

(c) The cell leaked at approximately 342 °C.

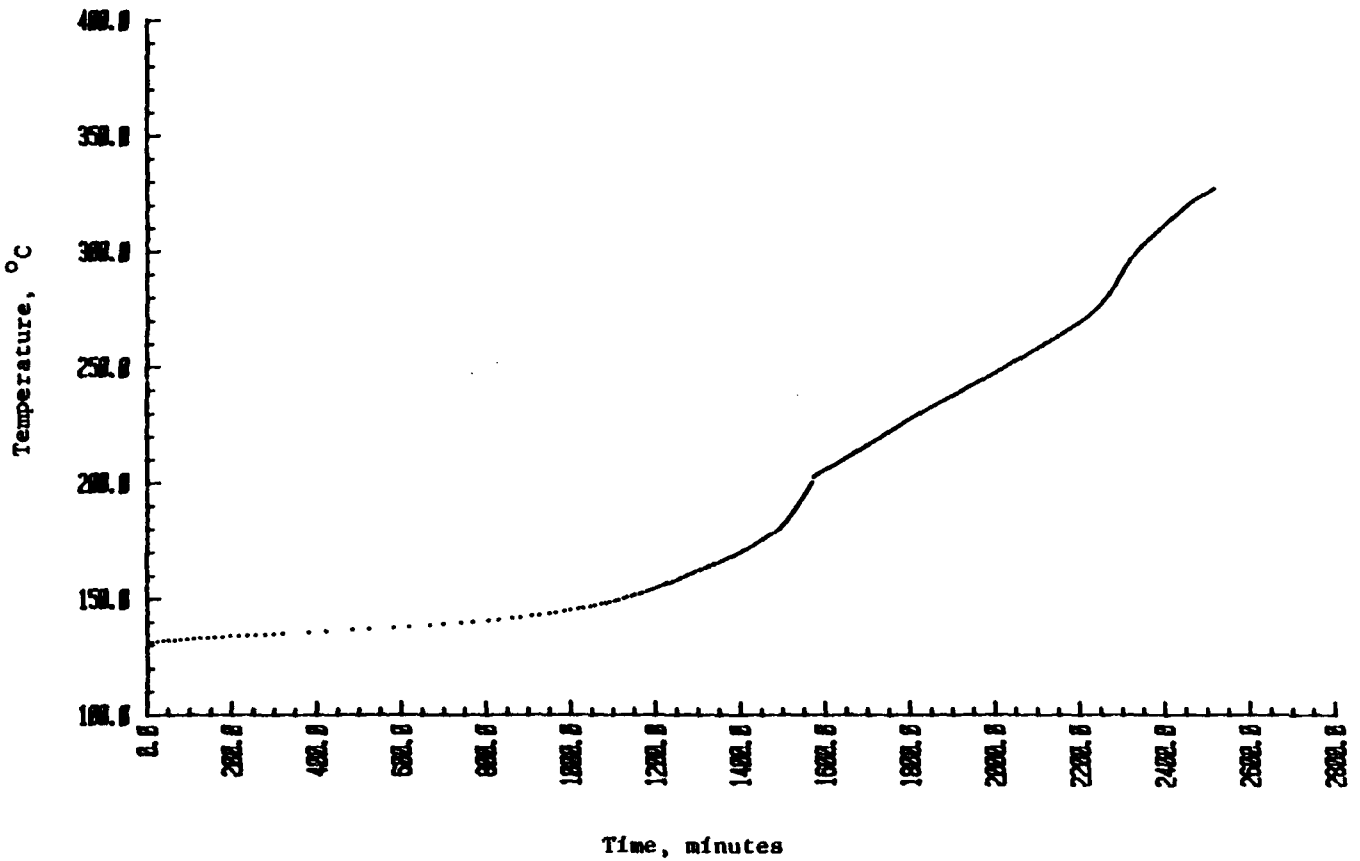

Figure 10. Temperature Versus Time Plot for the Fifth and Sixth Exotherms Detected During the Heat and Search Test of Cell No. IV-1 (Excess Lithium)

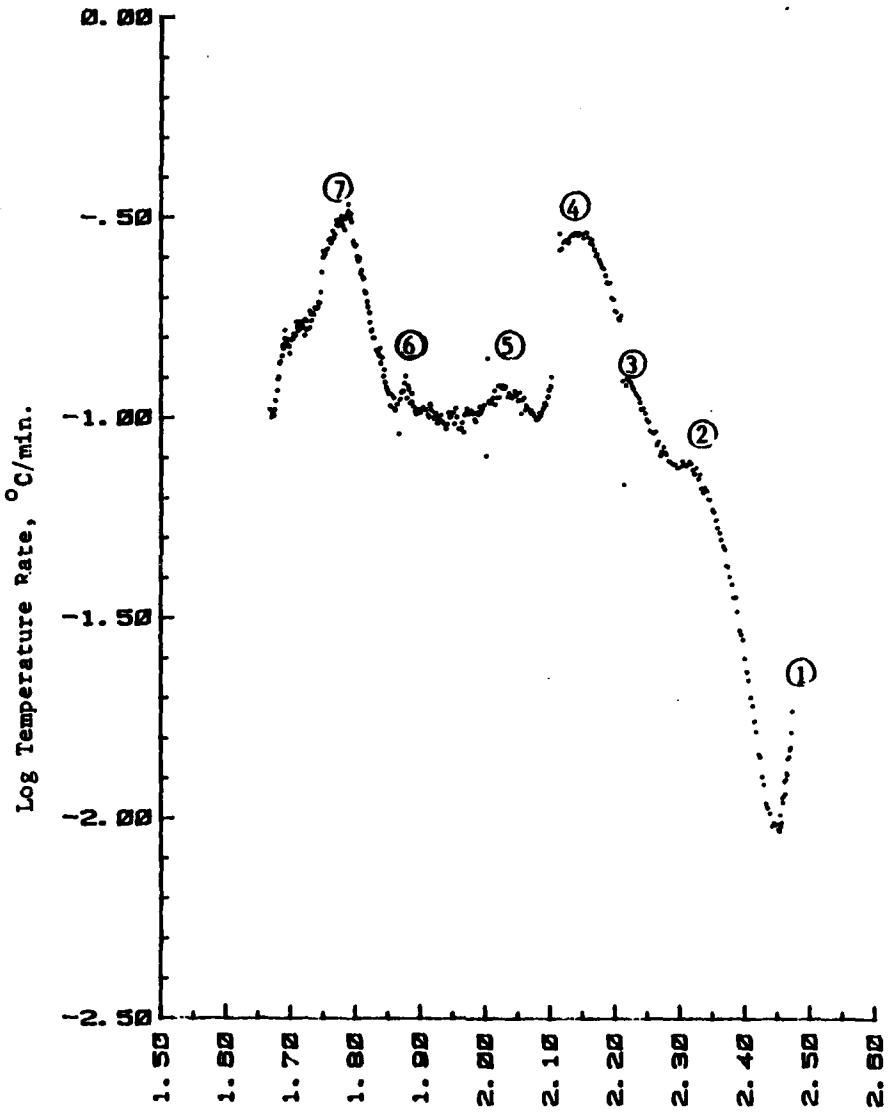

Figure 11. Log Temperature Rate Versus 1/T Plot for the Fifth and Sixth Exotherms Detected During the Heat and Search Test of Cell No. IV- (Excess Lithium)

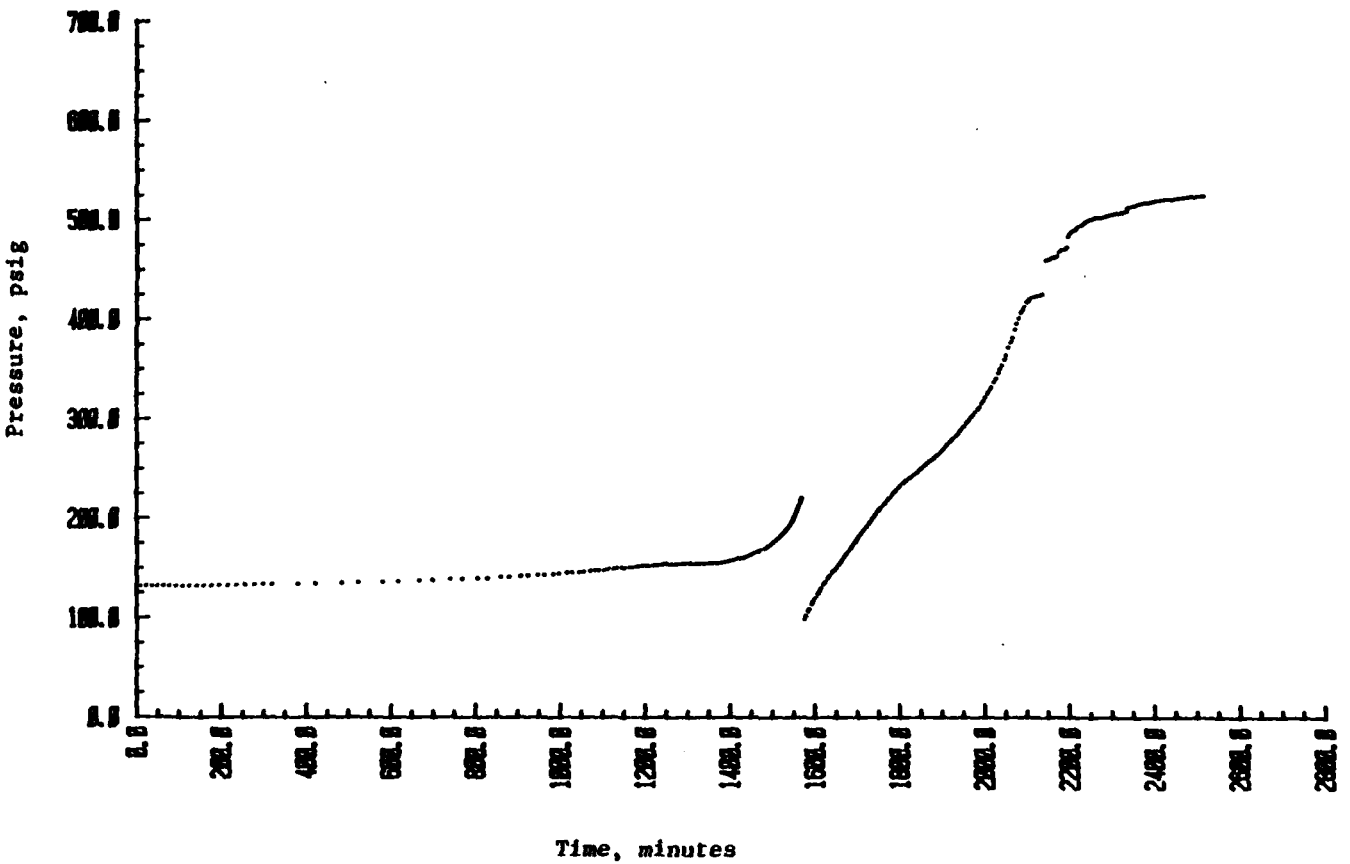

Figure 12. Pressure Versus Time Plot for the Fifth and Sixth Exotherms Detected During the Heat and Search Test of Cell No. IV-1 (Excess Lithium)

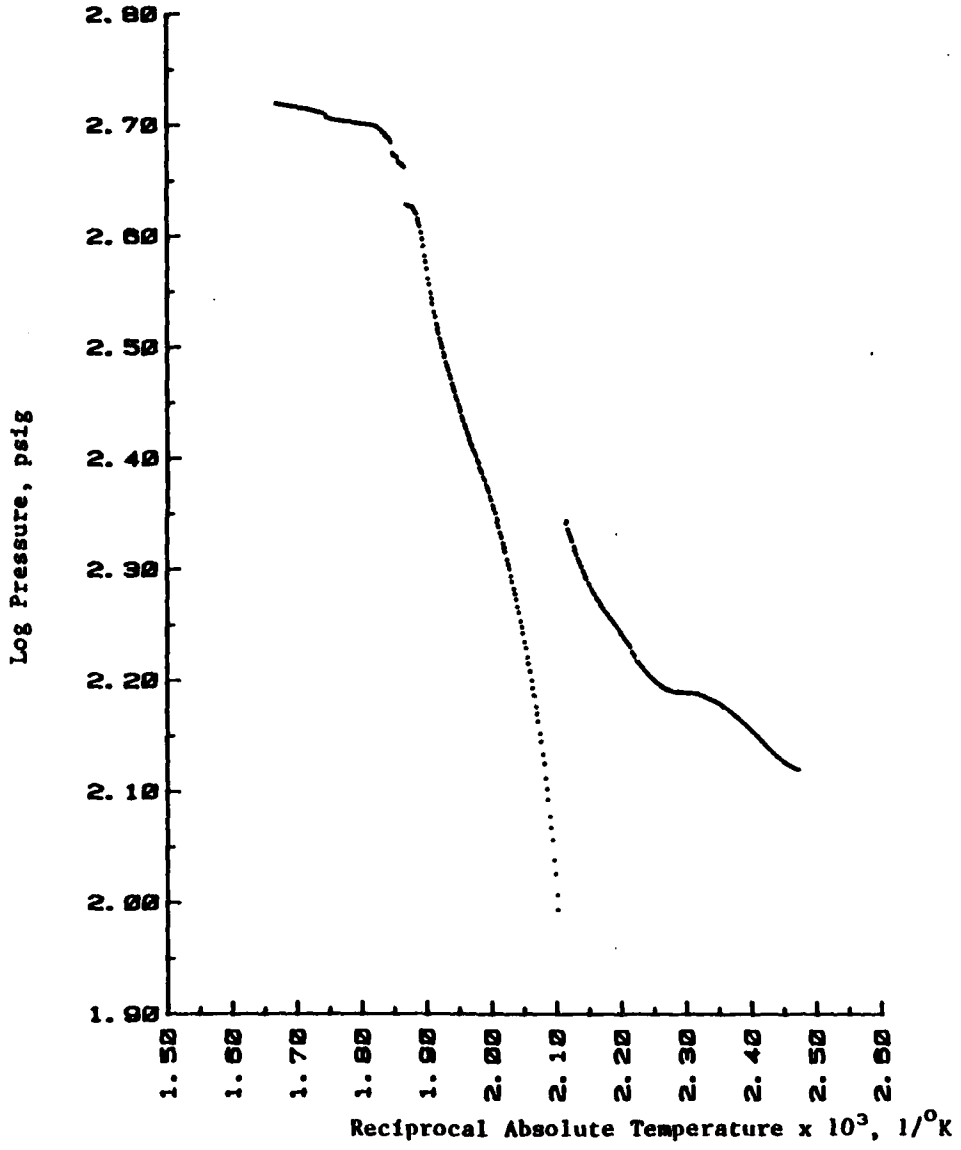

Figure 13. Log Pressure Versus 1/T Plot for the Fifth and Sixth Exotherms Detected During the Heat and Search Test of Cell No. IV-1 (Excess Lithium)

Table 13. Summary of the Seven Peaks Observed in the Fifth and Sixth Exotherms Detected During the Heat and Search Test of Cell No. IV-1 (Excess Lithium)

	Peak Numbers						
	1	2	3	4	5	6	7
Initial Temperature, ^{o}C	131.3	134.7	162.6	180.1	208.0	255.3	264.2
Initial Pressure, psig	131.4	133.5	154.6	172.3	136.0	400.5	461.7
Initial Temperature Rate, ^{o}C/min	0.015	0.009	0.076	0.175	0.098	0.102	0.104
Final Temperature, ^{o}C	134.7	162.6	178.6	199.9	229.8	264.2	301.4
Final Pressure, psig	133.5	154.6	169.8	220.3	239.7	461.7	513.7
Maximum Temperature Rate, ^{o}C/min	0.018	0.077	0.126	0.290	0.120	0.127	0.339
Maximum Pressure Rate, psig/min	0.03	0.06	0.24	1.1	0.69	1.4	0.73
Adiabatic Temperature Rise, ^{o}C	3.40	27.9	16.0	19.8	21.8	8.9	37.2
ΔH, cal	40.0	328	188	233	256	105	437
Pressure Change, psig	2.1	21.1	15.2	48.0	103.7	61.2	52.0
Activation Energy, kcal/mole	(1)	60.0	18.3	25.5	10.1	21.8	28.7
Reaction Order	(1)	1.0	0.2	0.4	0.2	0.2	0.7
Projected Temperature Rise for Li/SO_2 "D" Cell, ^{o}C	7.2	59.4	34.1	42.2	46.4	19.0	79.2

(1) insufficient data were obtained to perform a kinetic analysis for this peak.

Group B Cells

Forced Overdischarge at 5.0 mA/cm^2 (25^{o}C)

Group B Tests

Objective

The objective of the Group B tests was to evaluate the thermal behavior of Li/SO_2 cells during ambient temperature discharge and reverse discharge at a high current density (5.0 mA/cm^2).

Experimental

The discharge tests were performed galvanostatically. In these tests, the test station was not employed so that the voltage could be sensed directly at the cell, thus avoiding the error introduced by IR losses in the sensing leads. Because of the shorter run times of the Group B cells, manual removal of the load at the 2.0 volt cutoff was easily accomplished.

The construction features of the four Group B cells are shown in Table 14 .

Discharge Performance

The discharge performance of the four Group B cells is summarized in Table 15 . The component ratios present at the 2.0 volt cutoff are summarized in Table 16 .

Table 17 summarizes the reverse discharge testing that was conducted on each cell while Figure 14 shows the time/temperature behavior of the cells during the initial stages of reverse discharge. This last figure shows the effects of ohmic heating during forced overdischarge. In all cases, a substantial temperature rise occurred but, in general, the temperature tended to level off after approximately one-half hour. Since these tests were not conducted adiabatically, the leveling-off effect indicated that the rate of heat generation became less than or equal to the rate of heat dissipation by the cell. The exception was Cell No. III-2 (excess carbon) which showed a very rapid and continuous rate of temperature rise. By design, this cell contained a much lower electrolyte quantity than the other cells. As a result, this cell would be expected to be relatively dry at end of life which could result in a high internal impedance and the excess heating observed. If the load had not been removed, the internal temperature of this

Table 14. Construction Features of Group B Cells

Cell No.	Li/SO_2 Ratio	SO_2/C Ratio	Li/C Ratio	Electrolyte Quantity, gm	Cathode Surface Area, cm^2	Thermal Inertia Value, ϕ [1]
I-2	0.46	1.25	0.58	7.01	71.74	2.16
II-2	0.98	1.19	1.16	6.42	68.64	2.23
III-2	0.73	0.69	0.50	4.45	78.45	2.67
IV-2	1.49	1.18	1.77	5.78	61.94	2.34

(1) For comparison, the ϕ value for a "D" Li/SO_2 cell is approximately 1.15.

Table 15. Discharge Performance to 2.0 Volts for Group B Cells

Cell No.	Current, mA	Run Time, hr	Capacity Delivered, Ah	Average Voltage, V	Discharge Efficiency, %		
					Anode	Carbon	SO_2
I-2	359	2.09	0.750	2.67	80.9	47.0	37.6
II-2	343	3.41	1.17	2.62	65.5	76.1	63.9
III-2	392	1.09	0.427	2.62	46.0	23.1	33.7
IV-2	310	3.20	0.993	2.60	40.3	71.4	60.3

Table 16. Component Ratios Present at End of Discharge to a 2.0 Volt Cutoff for Group B Cells

Cell No.	Cell Design	SO_2/Li	SO_2/Li Area, mg/cm^2
I-2	Lithium Limited	7.0	41.5
II-2	Coulombically Balanced	1.1	23.0
III-2	Excess Carbon	1.7	25.5
IV-2	Excess Lithium	0.44	25.2

Table 17. Summary of Reverse Discharge Testing Performed on the Group B Cells

Cell No.	Cell Design	Time in Reverse, hr	Degree of Reverse Discharge, %[1]
I-2	Lithium Limited	12.8	231
II-2	Coulombically Balanced	12.9	242
III-2	Excess Carbon	0.20	6.2
IV-2	Excess Lithium	12.6	237

(1) Based on original SO_2 capacity

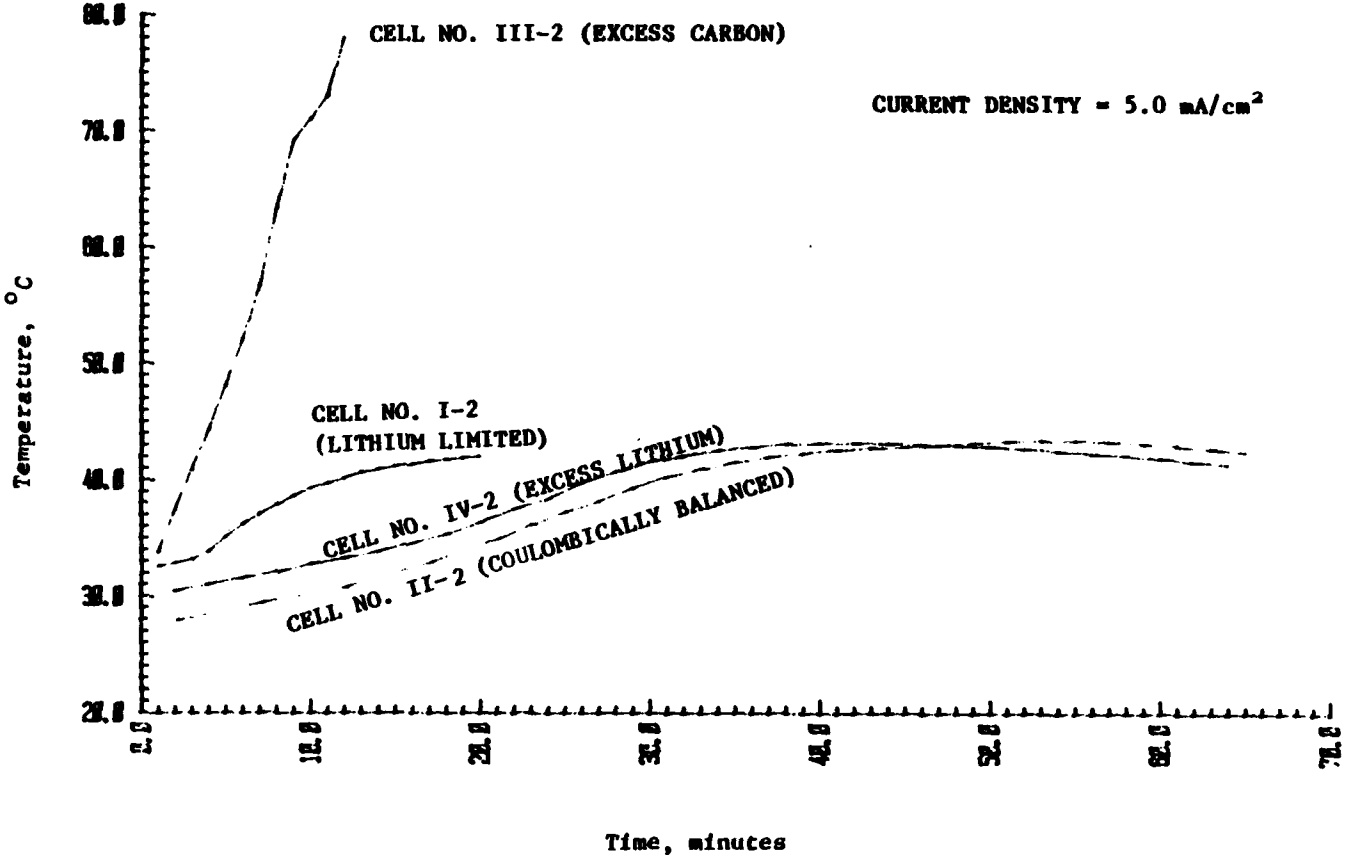

Figure 14. Time/Temperature Behavior During Initial Forced Overdischarge Testing of Group B Cells.

cell could quite possibly have reached the melting point of lithium leading to catastrophic results.

Thermal Behavior

Table 18 summarizes the thermal behavior of the Group B cells. All the cells except the lithium-limited design gave an exotherm during voltage reversal. Since this exotherm is attributed to the lithium/acetonitrile reaction, these results demonstrate that even coulombically balanced cells can exhibit exothermic behavior when excess lithium is present at end of life due to rate induced inefficiencies, in spite of the higher SO_2 concentrations also present.

In order to gain more information on the high temperature stability of these cells, the upper temperature limit of the final heat and search mode was extended to 350°C. In some instances, however, this temperature could not be attained because of cell leakage problems.

Cell No. I-2 (Lithium-Limited)

This cell gave no exotherms during the electrical phase of testing. During the initial heat and search operation, the cell leaked at 106°C. No exotherms were detected to this point. The cell was then cooled to ambient temperature and a second heat and search operation initiated. This heat and search operation was successfully completed to the cutoff temperature of 350°C, during which a total of four exotherms were detected. Table 19 summarizes the data for the four exotherms.

The data plots are shown in Figures 15 through 18. In these figures, the first small exotherm has not been included. Because of the leakage problems encountered with this cell, a detailed interpretation of the data is not possible. A sharp peak is indicated at approximately 236°C (See Figure 16), but an apparent slight leaking at about 240°C caused the cell to cool enough to stop the exotherm momentarily. This caused the break in the curve when the instrument was going through another heat and search step.

Although a quantitative evaluation is not possible, some general observation can be made. First, these results show that lithium-limited cells are capable of

Table 18. Summary of the Thermal Behavior of the Group B Cells

Cell No.	Cell Design	Exotherms During Discharge to 2.0 Volt Cutoff	Exotherms During Reverse Discharge	Exotherms During Final Heat & Search	Final Temp. During Heat & Search, °C
I-2	Lithium Limited	No	No	Yes	328
II-2	Coulombically Balanced	No	Yes	Yes	256
III-2	Excess Carbon	No	Yes	N/A	N/A
IV-2	Excess Lithium	No	Yes	Yes	350

Table 19. Summary of Exotherms Detected During the Heat and Search Operation of Cell No. I-2.

	Exotherm Number			
	1	2	3	4
Initial Temp., °C	146.82	163.06	256.17	315.11
Initial Pressure, psig	60.1	54.6	36.1	38.8
Initial Temp. Rate, °C/min.	0.058	0.042	0.074	0.240
Final Temp., °C	147.36	240.65	298.11	328.54
Final Pressure, psig	56.7	27.2	39.2	39.7
Max. Temp. Rate, °C/min.	0.058	0.076	0.156	0.333
ΔH, cal	6.8	978	529	169
Temperature Rise, °C	0.54	77.59	41.94	13.43
Pressure Change, psig	-3.4	-27.4	3.1	0.9
Time Duration of Exotherm, min	22.3	1940	443	51.9
Projected Final Temperature for Li/SO_2 "D" Cell, °C	147.8	308.8	335.0	340.3
Projected Temperature Rise for Li/SO_2 "D" Cell	1.0	145.7	78.8	25.2

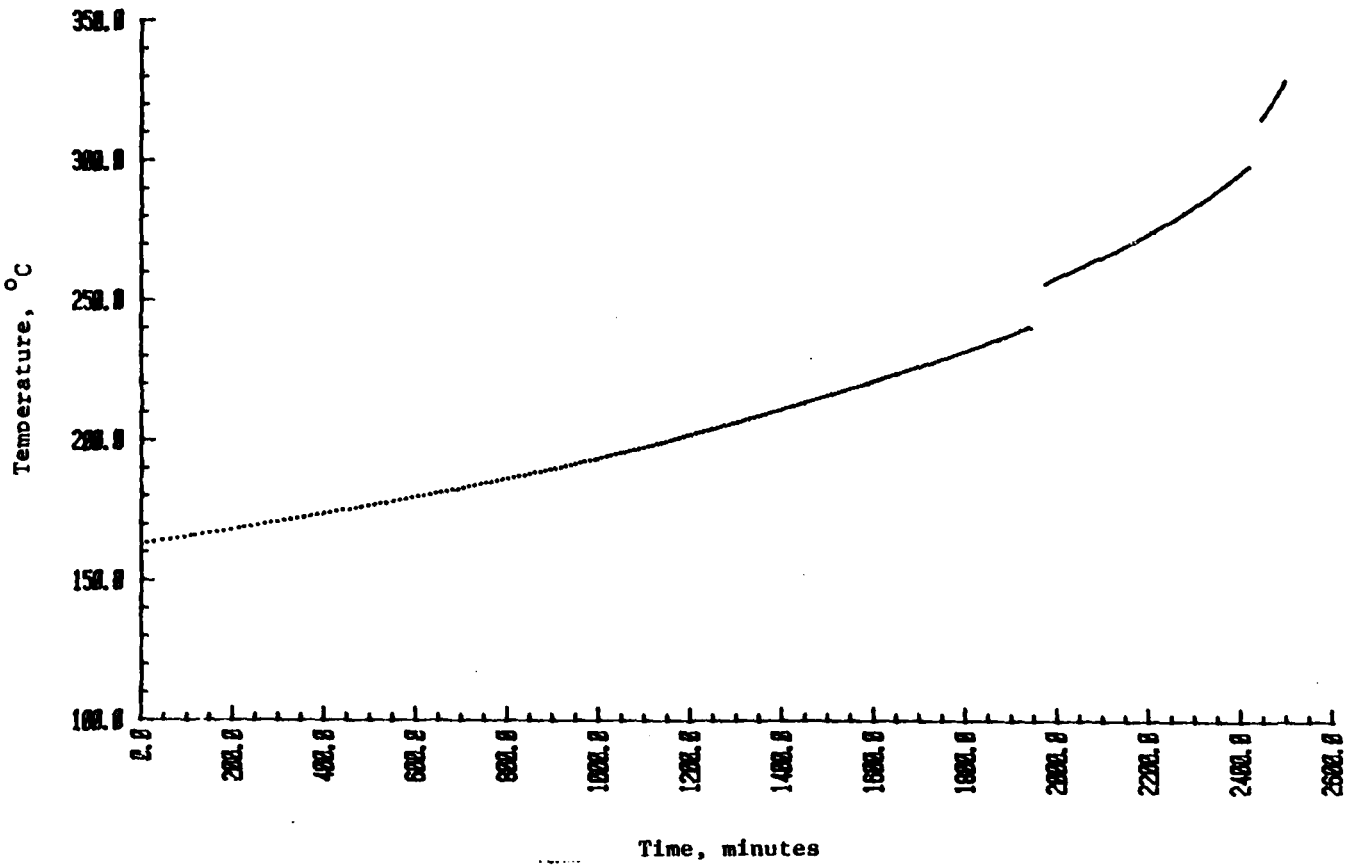

Figure 15. Temperature Versus Time Plot for Elevated Temperature Exotherms Detected During ARC Analysis of Cell No. I-2 (Lithium Limited)

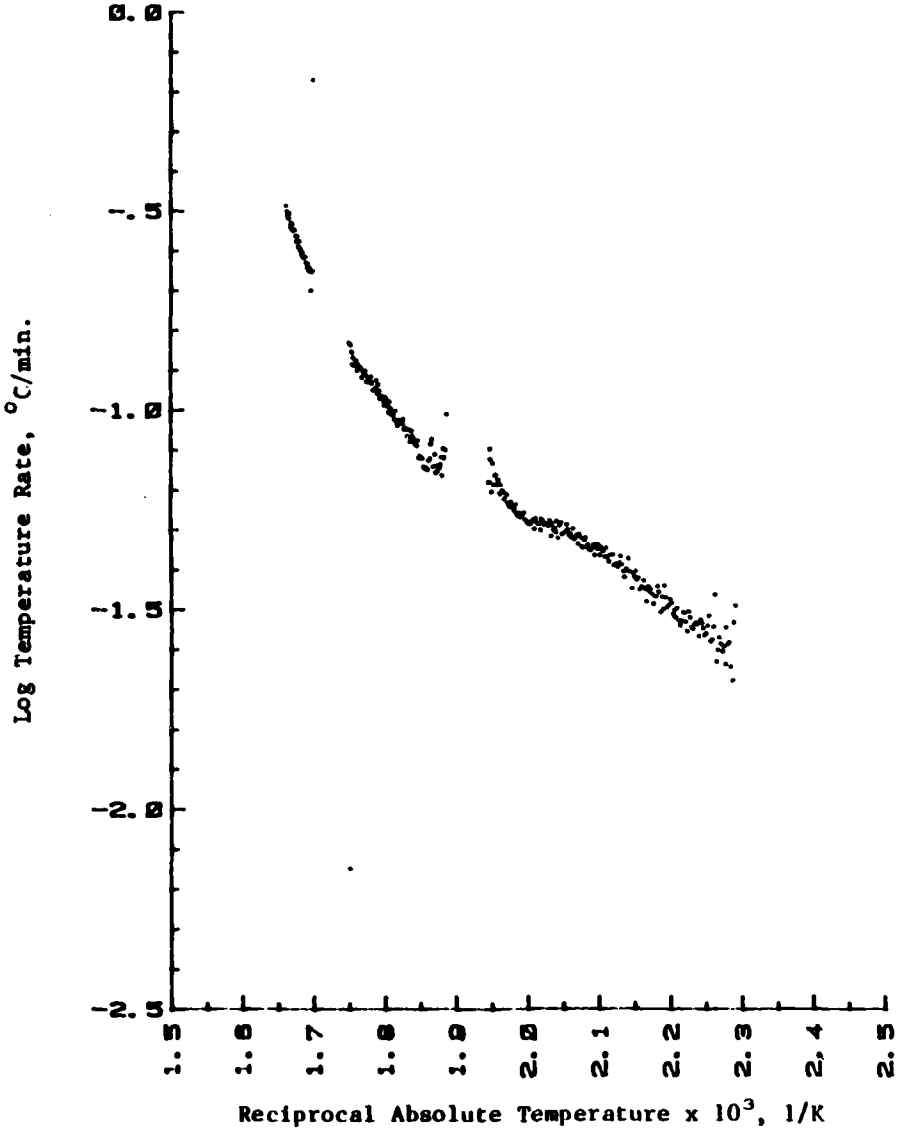

Figure 16. Log Temperature Rate Versus 1/T Plot for Elevated Temperature Exotherms Detected During ARC Analysis of Cell No. I-2 (Lithium Limited).

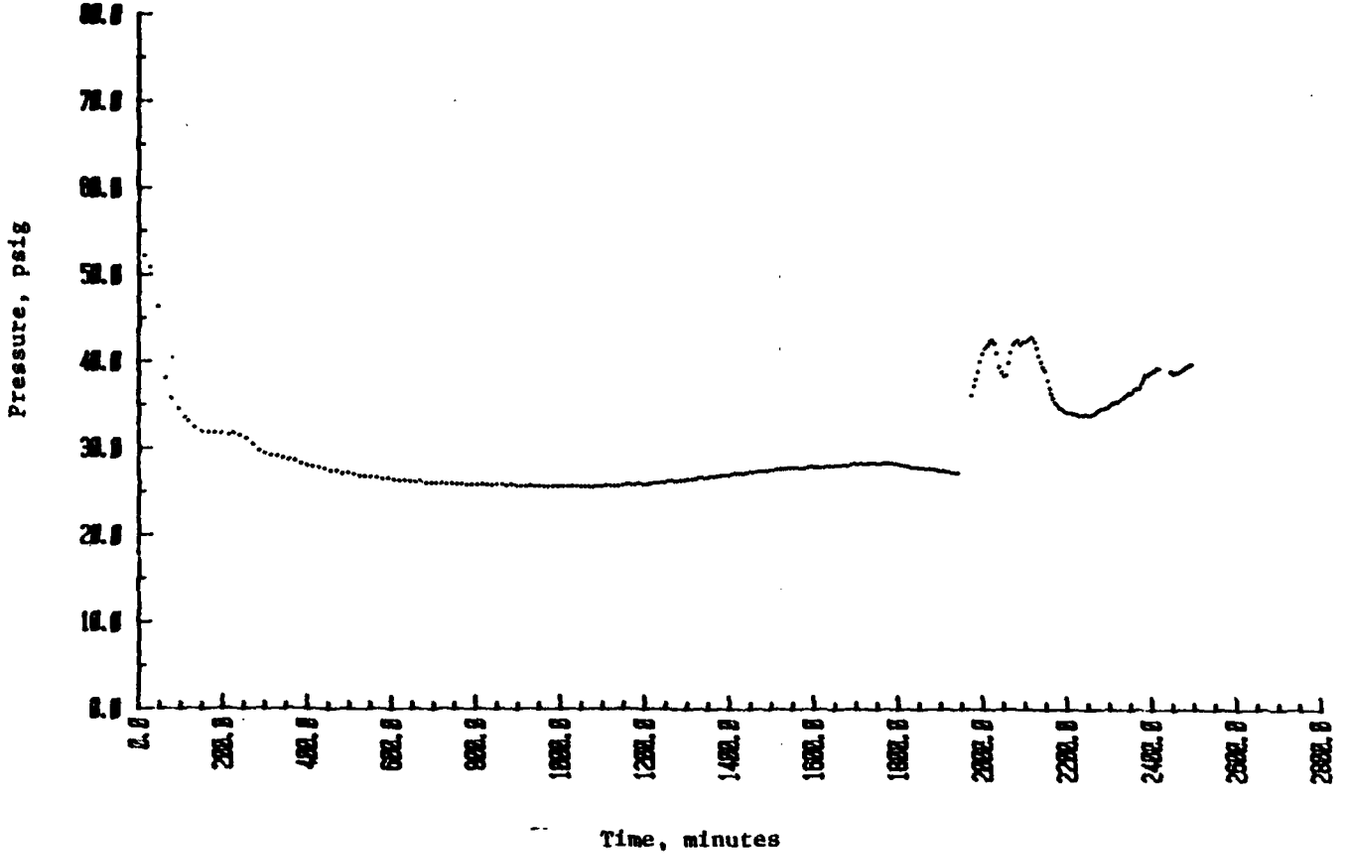

Figure 17. Pressure Versus Time Plot for Elevated Temperature Exotherms Detected During ARC Analysis of Cell No. I-2 (Lithium Limited)

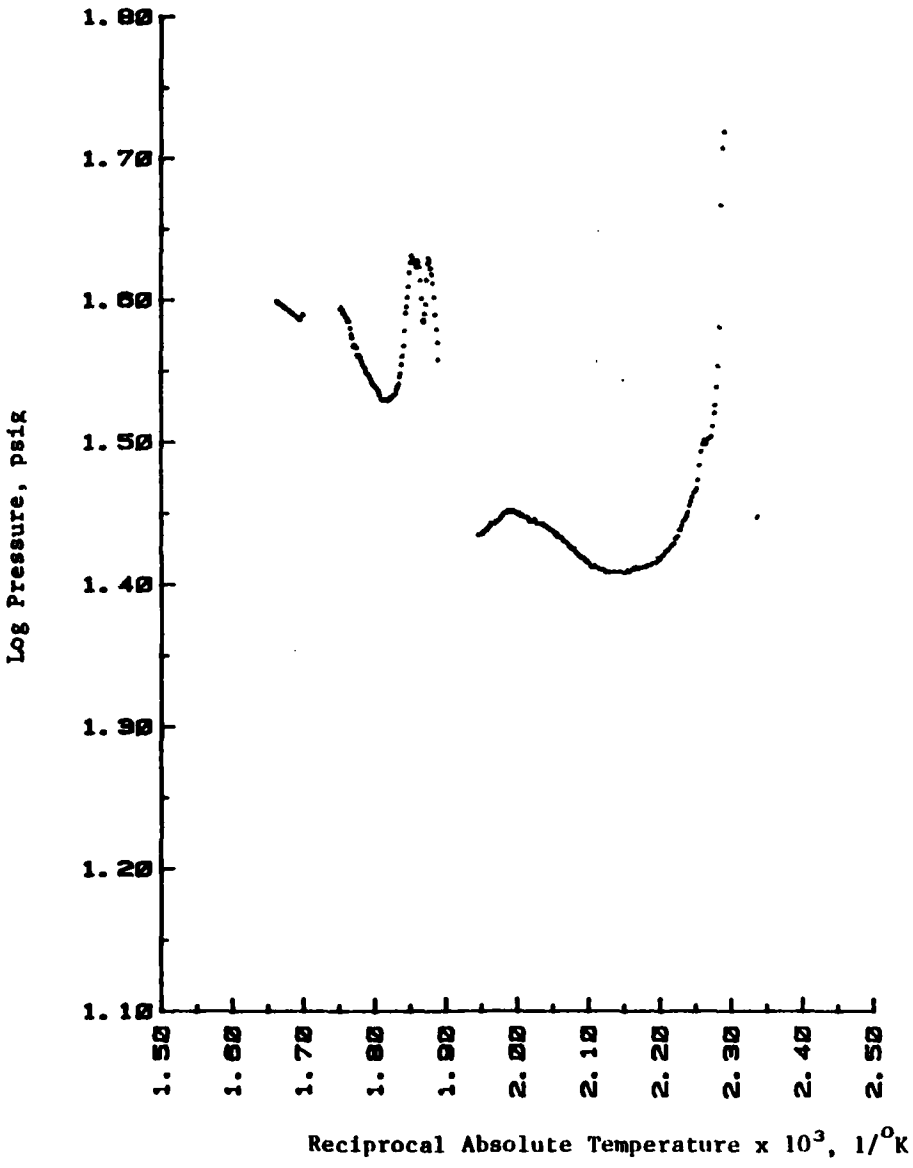

Figure 18. Log Pressure Versus 1/T Plot for Elevated Temperature Exotherms Detected During ARC Analysis of Cell No. I-2 (Lithium Limited)

undergoing exothermic reactions at elevated temperatures. Secondly, these reactions can occur even in partially vented cells. Finally, the reaction initiating at 163°C appears to involve a gaseous component, possibly SO_2, as evidenced by the sharp decrease in pressure at the start of the reaction (See Figure 17).

Cell No. II-2 (Coulombically Balanced)

This cell gave an exothermic reaction during reverse discharge testing. Table 20 summarizes the characteristics of this exotherm while the data plots are shown in Figures 19 through 22 . In general, this reaction was similar to the reverse exotherm detected in Cell No. IV-1 in that, overall, a low activation energy reaction is indicated. This reaction was somewhat unusual, however, in that two peaks were observed during the course of the reaction (See Figure 20). Whether these peaks represent actual separate reactions or are due to abrupt changes in the kinetics of the Li/AN reaction, such as might occur from sudden disruptions of the surface film characteristics, etc., is not known at this time.

The final heat and search operation was conducted on this cell up to 256°C at which point the cell leaked and the test terminated. In total, 13 exotherms were detected as summarized in Table 21 . The results for this cell were unusual in that all of the exotherms were very small; the maximum temperature rise for a single exotherm was 2.4°C.

Although the exotherms are small in terms of the amount of energy released, significant changes in pressure were sometimes observed. Exotherms 8, 9, and 10 all resulted in significant pressure reduction indicating consumption of a gaseous

Table 20. Summary of Characteristics of Reverse Exotherm for Cell No. II-2 (Coulombically Balanced)

Initial Temperature, ^{o}C	45.68
Initial Pressure, psig	19.2
Initial Temp. Rate, $^{o}C/min$	0.082
Final Temperature, ^{o}C	102.19
Final Pressure, psig	79.5
Maximum Temp. Rate, $^{o}C/min$	0.121
Maximum Pressure Rate, psig/min	0.24
Adiabatic Temperature Rise, ^{o}C	56.51
ΔH, cal	704
Pressure Change, psig	60.3
Time Duration of Exotherm, min.	1610
Activation Energy, kcal/mole	4.5
Reaction Order	1.0
Projected Final Temp. for Li/SO_2 "D" Cell, ^{o}C	171.7
Projected Temp. Rise for Li/SO_2 "D" Cell, ^{o}C	126.0

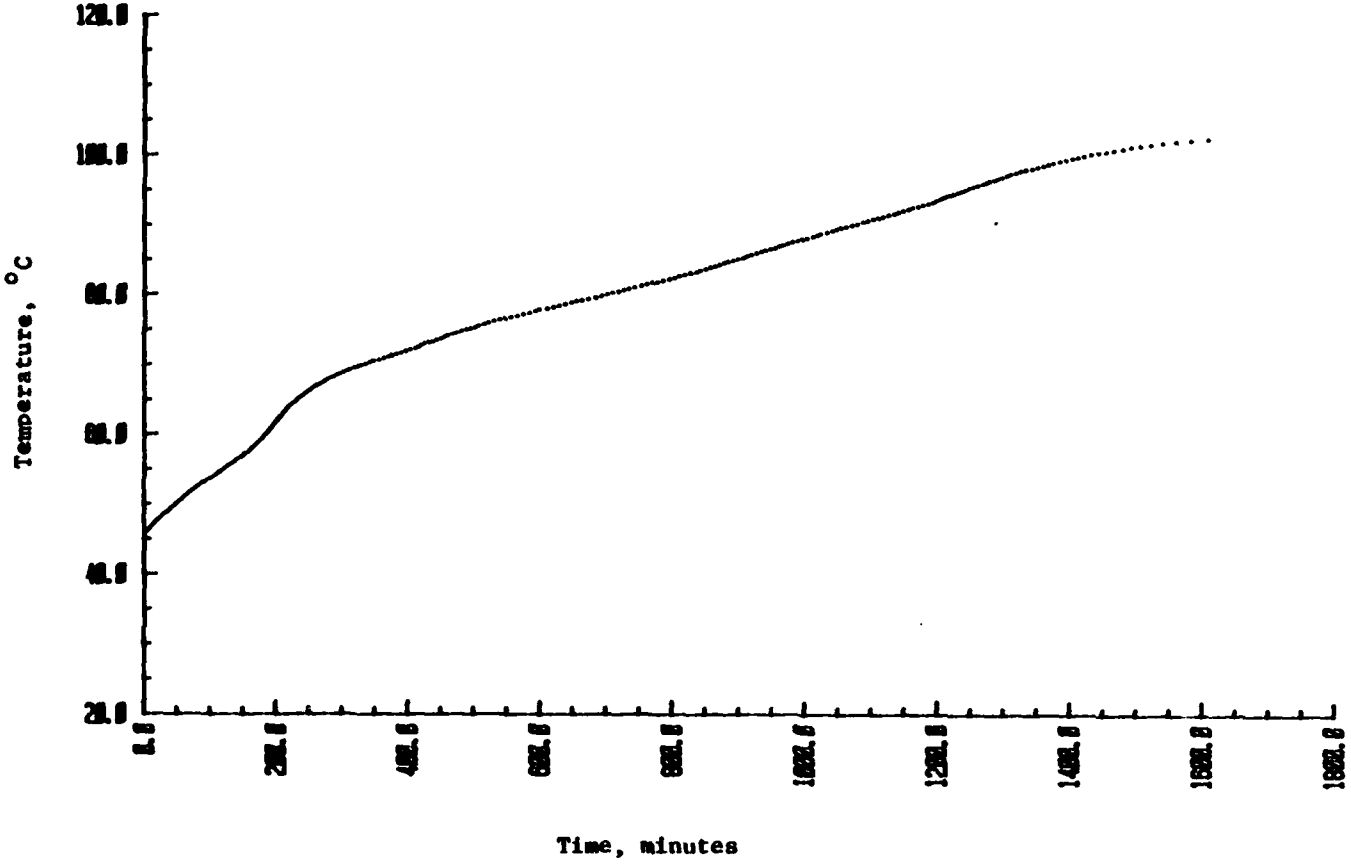

Figure 19. Temperature Versus Time Plot for the Exotherm Detected During Forced Overdischarge Testing of Cell No. II-2 (Coulombically Balanced)

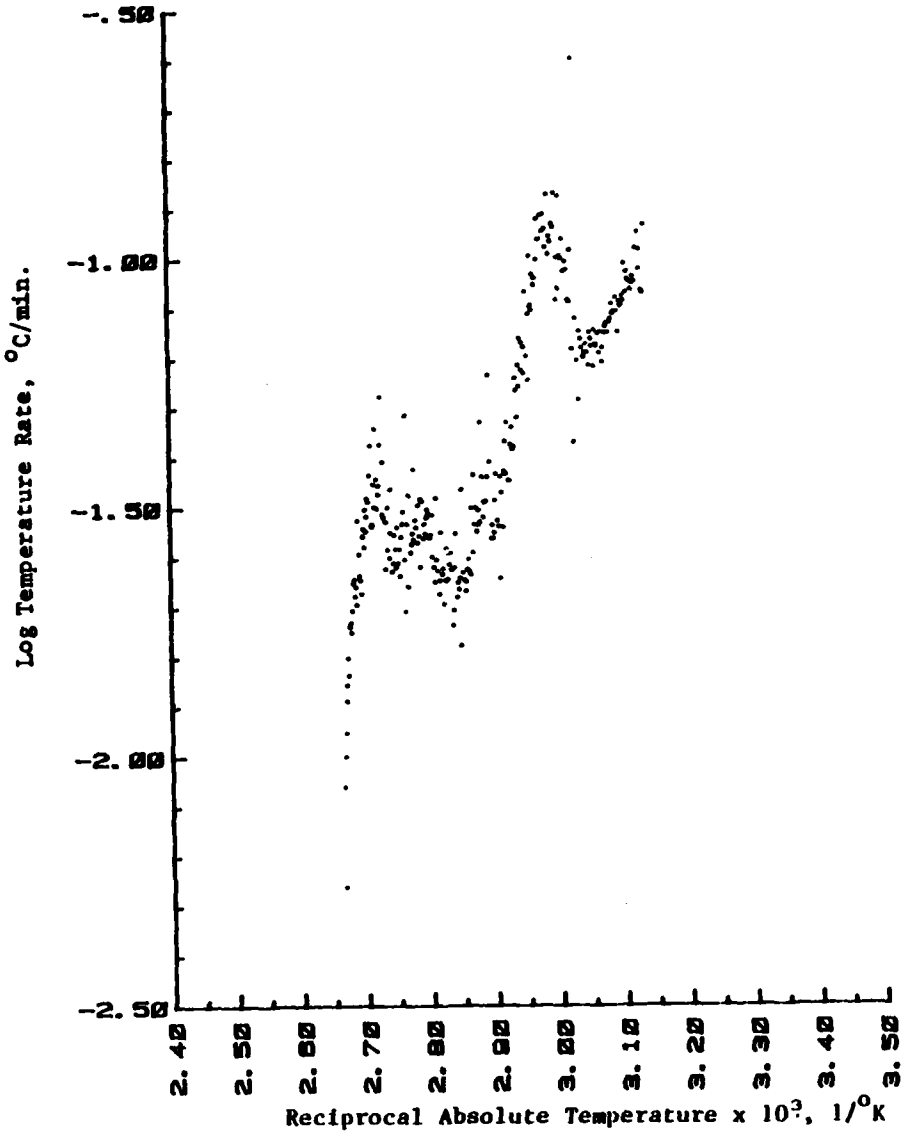

Figure 20. Log Temperature Rate Versus 1/T Plot for the Exotherm Detected During Forced Overdischarge Testing of Cell No. II-2 (Coulombically Balanced)

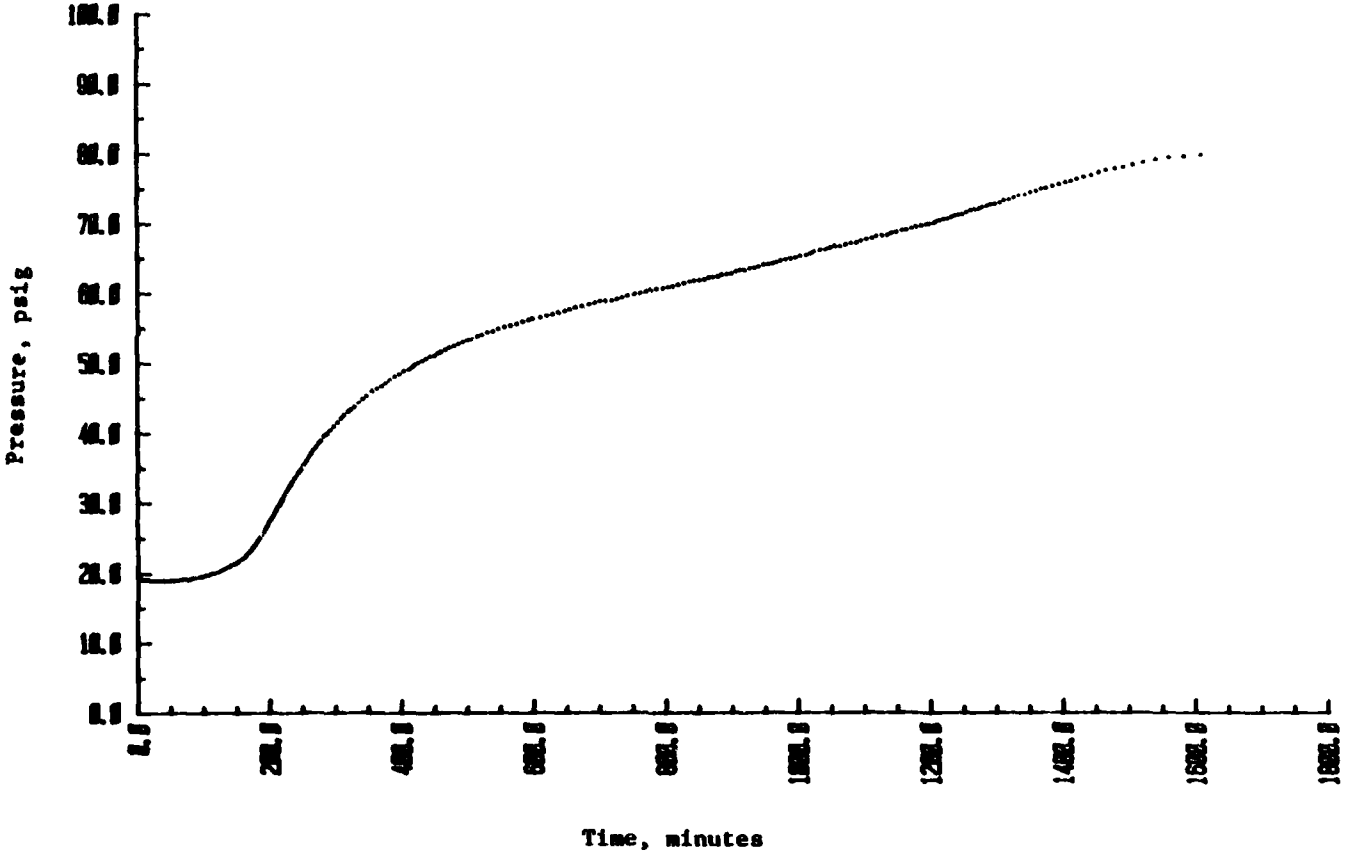

Figure 21. Pressure Versus Time Plot for Exotherm Detected During Forced Overdischarge Testing of Cell No. II-2 (Coulombically Balanced)

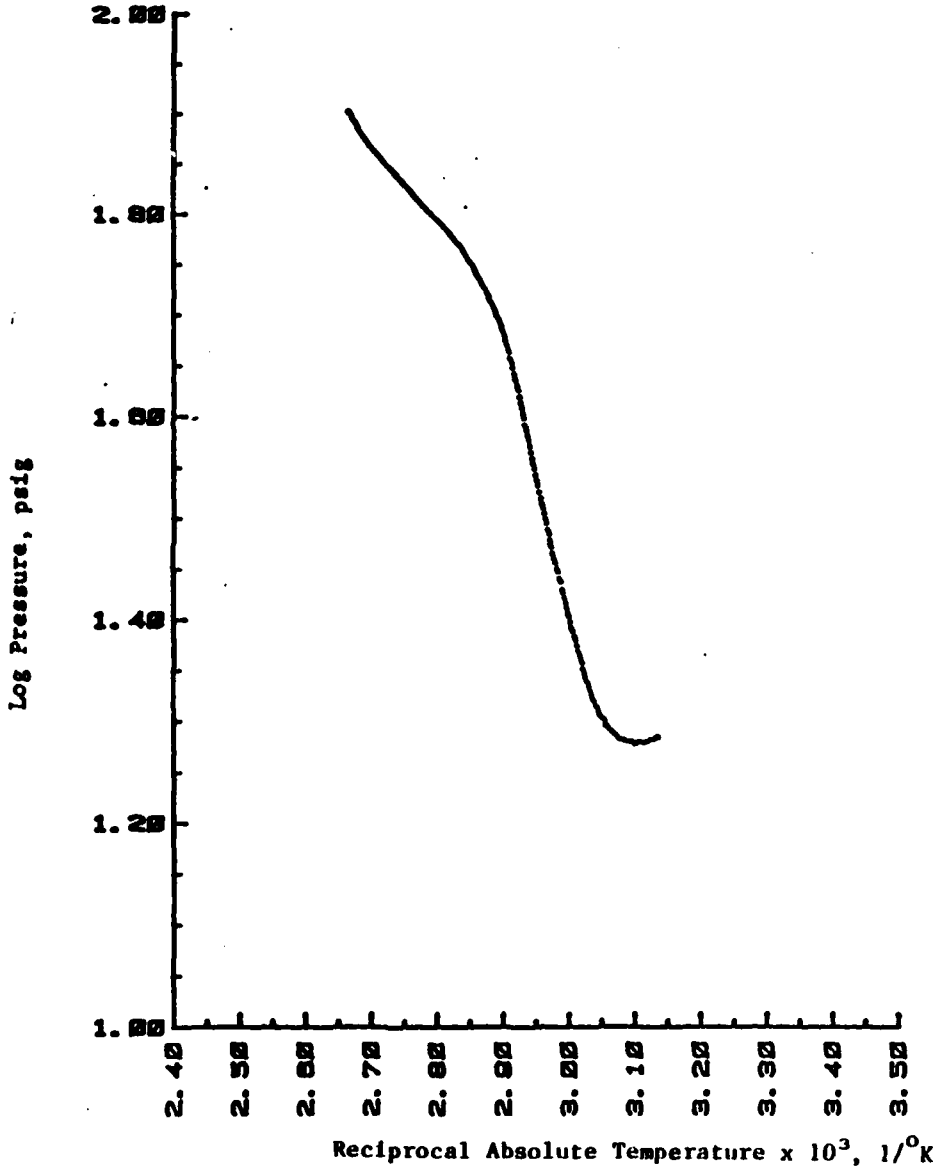

Figure 22. Log Pressure Versus 1/T Plot for Exotherm Detected During Forced Overdischarge Testing of Cell No. II-2 (Coulombically Balanced)

Table 21. Summary of Exotherms Detected During the Heat and Search Operation of Cell No. II-2 (Coulombically Balanced)

	Exotherm Number												
	1	2	3	4	5	6	7	8	9	10	11	12	13
Initial Temp., °C	119.77	125.53	133.25	139.97	146.48	152.55	157.97	178.31	184.18	190.65	221.93	248.73	255.00
Initial Pressure, psig	87.5	91.4	96.7	101.7	106.9	110.9	115.9	136.2	136.7	129.4	120.1	180.6	186.9
Initial Temp. Rate, °C/min.	0.010	0.021	0.020	0.016	0.018	0.013	0.012	0.010	0.018	0.018	0.017	0.012	0.025
Final Temp., °C	120.16	127.93	134.64	141.14	147.27	152.73	158.12	178.89	185.36	191.60	223.48	249.75	255.60
Final Pressure, psig	87.9	93.1	97.6	102.7	107.8	110.9	115.9	132.7	128.9	114.1	140.7	186.4	187.90
Max. Temp. Rate, °C/min.	0.010	0.021	0.020	0.018	0.018	0.013	0.012	0.010	0.018	0.018	0.017	0.019	0.025
Temperature Rise, °C	0.39	2.40	1.39	1.17	0.79	0.18	0.15	0.58	1.18	0.95	1.55	1.02	0.60
Pressure Change, psig	0.4	1.7	0.9	1.0	0.9	0.0	0.0	-3.5	-7.8	-15.3	20.6	5.8	1.0

component. The fact that these exotherms all occurred under 200°C is consistent with the results of Cell No. I-2 (lithium-limited). Exotherms 11 and 12 both led to substantial pressure increases, indicating pressure producing reactions.

Cell No. III-2 (Excess Carbon)

This cell gave an exotherm during reverse discharge. This exotherm was particularly significant in that it led to a temperature rise of 273°C, reaching the experimental cutoff temperature of 350°C. Because of the significant ohmic heating effects encountered with this cell, the initial exotherm, attributed to the lithium/acetonitrile reaction, was sufficient to raise the temperature to 116°C and trigger subsequent elevated temperature exotherms.

The characteristics of the initial portion of the exotherm attributed to the lithium/acetonitrile reaction are summarized in Table 22 while the data plots are shown in Figures 23 through 26. Once again, this is found to be a low activation energy reaction.

The portion of the exotherm following the lithium/acetonitrile reaction is summarized in Table 23 and the data plots shown in Figures 27 through 30. Because of the extensive nature of this exotherm, the memory capacity of the ARC microprocessor was exceeded and the data above 273°C were not stored. During the experiment, however, the data were being continuously plotted as the log temperature rate versus 1/T on an X-Y plotter and this information is available up to 350°C and has been included in Figure 28. No pressure data are available above 273°C, however.

The log temperature rate versus 1/T plot (Figure 28) shows the presence of six major peaks. These peaks are summarized in Table 24.

Cell No. IV-2 (Excess Lithium)

This cell gave an exotherm during reverse discharge. The characteristics of this exotherm are summarized in Table 25 while the data plots are shown in Figures 31 through 34. As with the reverse exotherms detected in the previous cells, this was found to be a low activation energy reaction.

Table 22. Summary of Characteristics of Reverse Exotherm for Cell No. III-2[1] (Excess Carbon)

Initial Temperature, °C	77.31
Initial Pressure, psig	59.4
Initial Temperature Rate, psig	0.103
Final Temperature, °C	116.41
Final Pressure, psig	68.1
Maximum Temperature Rate, °C/min	0.124
Maximum Pressure Rate, psig/min	0.07
Adiabatic Temperature Rise, °C	39.1
ΔH, cal	431
Pressure Change, psig	8.7
Time Duration of Exotherm, min	554
Activation Energy, kcal /mole	8.0
Reaction Order	0.9
Projected Final Temperature for Li/SO_2 "D" Cell, °C	168.1
Projected Temperature Rise for Li/SO_2 "D" Cell, °C	90.8

(1) These data actually refer to the initial portion of the reverse exotherm attributed to the lithium/acetonitrile reaction.

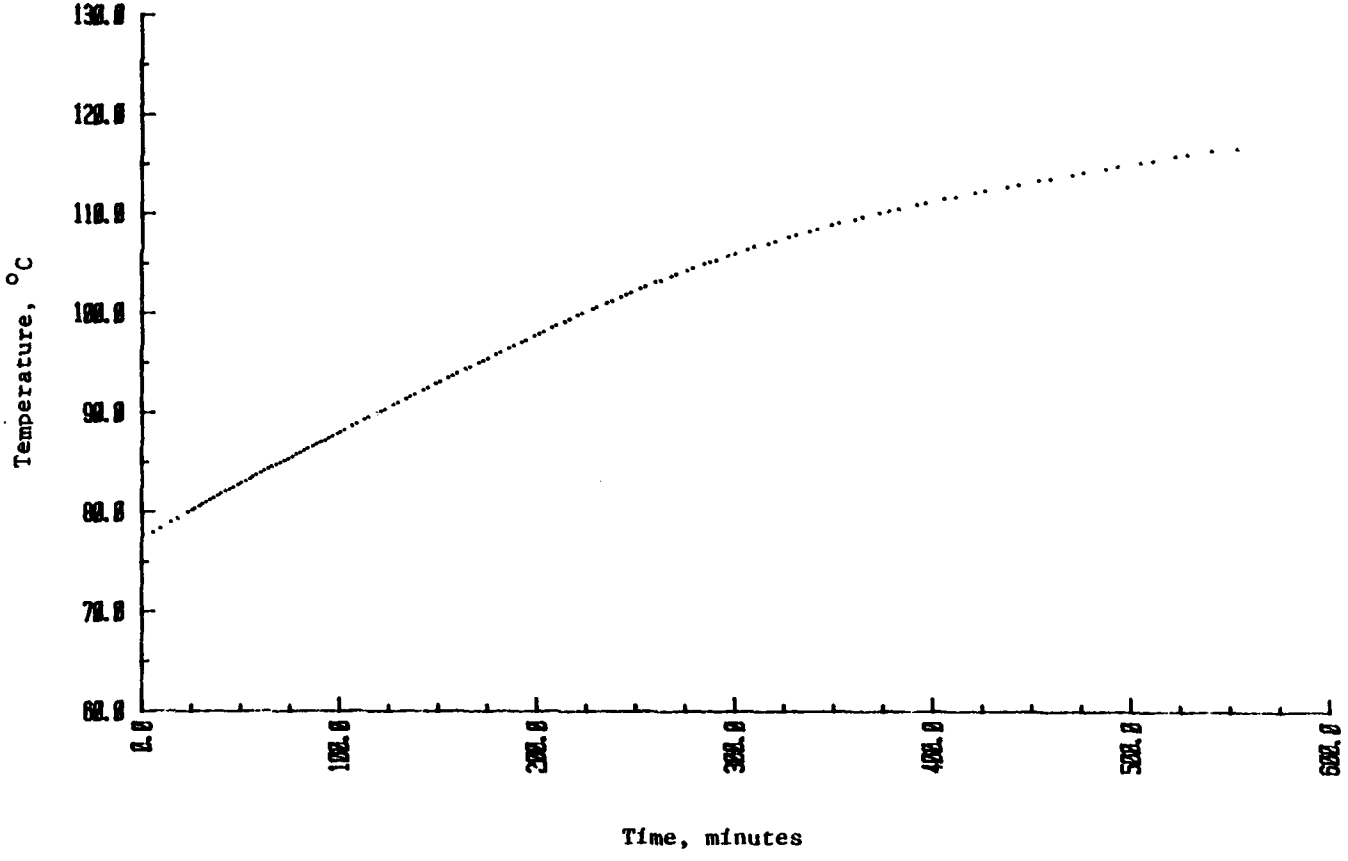

Figure 23. Temperature Versus Time Plot for the Exotherm Detected During Forced Overdischarge Testing of Cell No. III-2 (Excess Carbon)

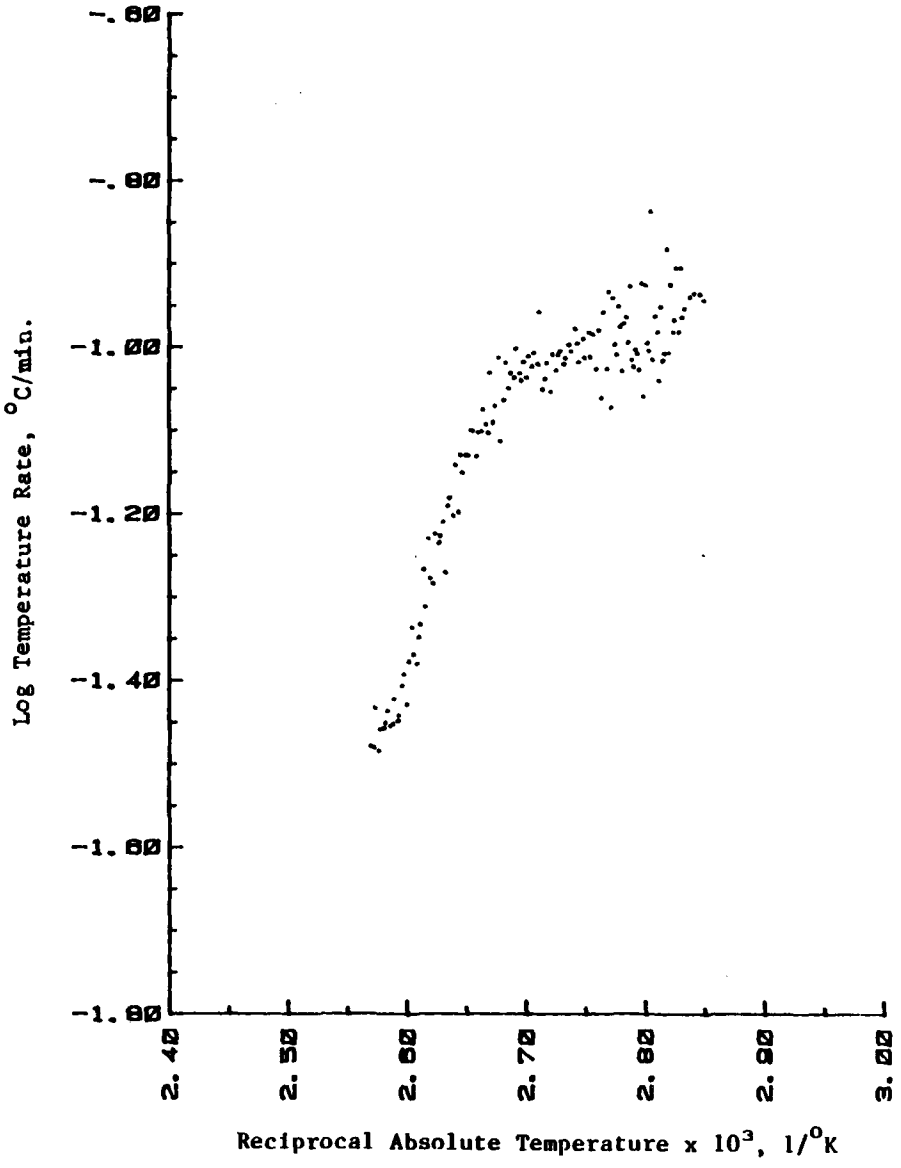

Figure 24. Log Temperature Rate Versus 1/T Plot for the Exotherm Detected During Forced Overdischarge Testing of Cell No. [illegible]-2 (Excess Carbon)

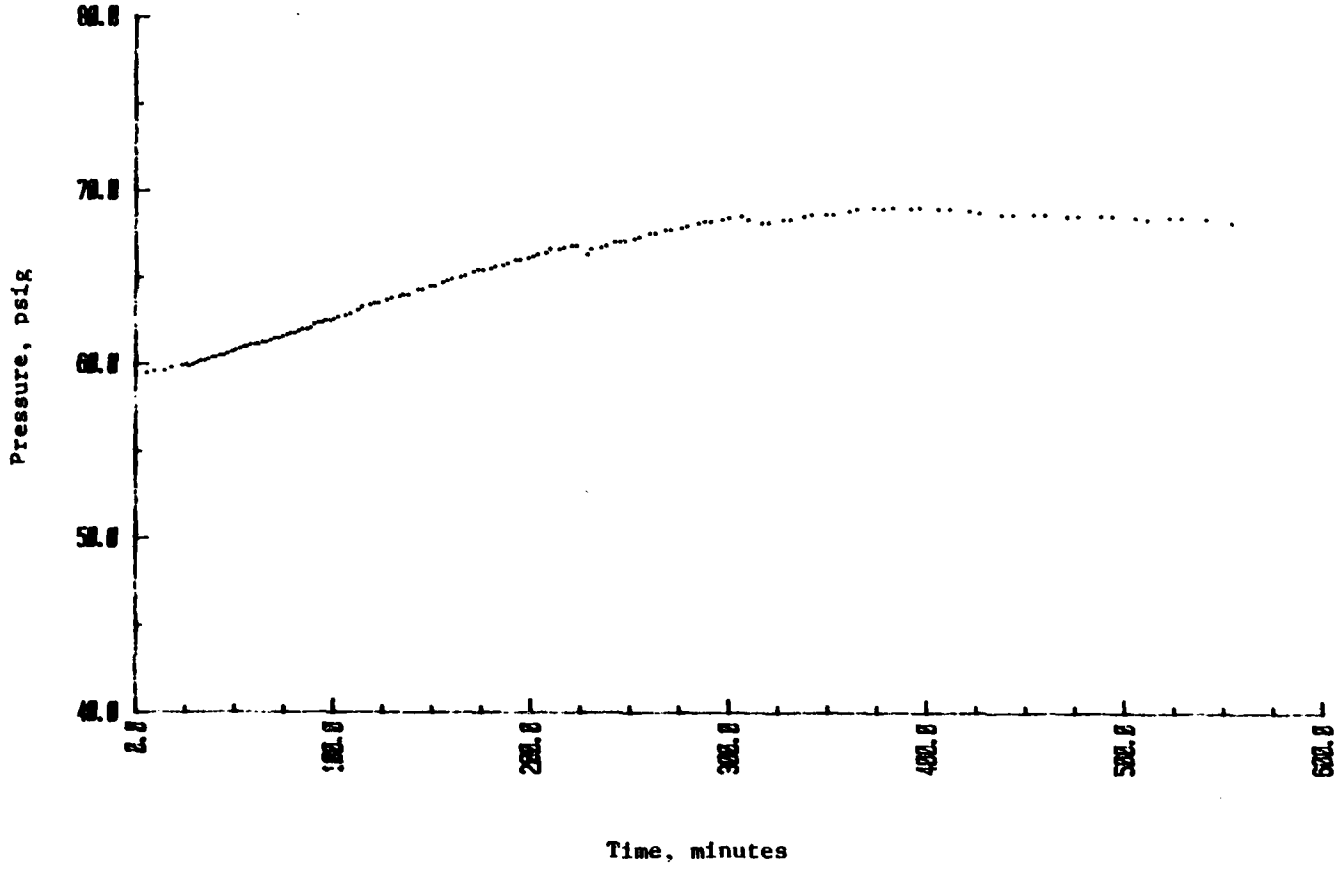

Figure 25. Pressure Versus Time Plot for Exotherm Detected During Forced Overdischarge of Cell No. III-2 (Excess Carbon)

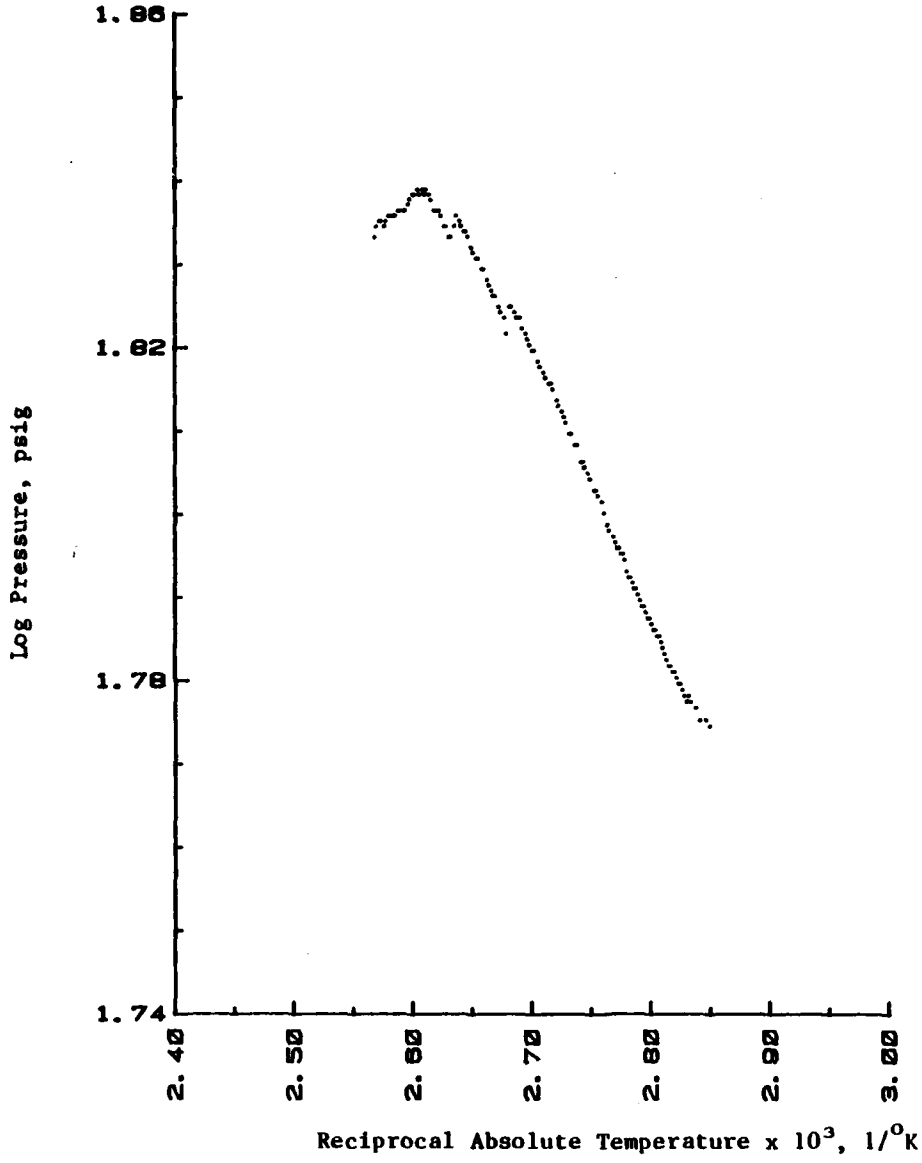

Figure 26. Log Pressure Versus 1/T Plot for Exotherm Detected During Forced Overdischarge Testing of Cell No. III-2 (Excess Carbon)

Table 23. Summary of Characteristics of Second Portion of Reverse Exotherm for Cell No. III-2(1)

Initial Temperature, °C	117.44
Initial Presure, psig	45.0
Initial Temperature Rate, °C/min	0.027
Final Temperature, °C	350.0
Final Pressure, psig	188.4 (at 273°C)
Maximum Temperature Rate, °C/min	0.560
Maximum Pressure Rate, psig/min	0.54 (to 273°C)
Adiabatic Temperature Rise, °C	232.6
ΔH, cal	2567
Pressure Change, psig	143.4 (at 273°C)
Projected Final Temperature for Li/SO_2 "D" Cell, °C	657.5
Projected Temperature Rise for Li/SO_2 "D" Cell, °C	540.0

(1) These data refer to the portion of the reverse exotherm following the lithium/acetonitrile reaction.

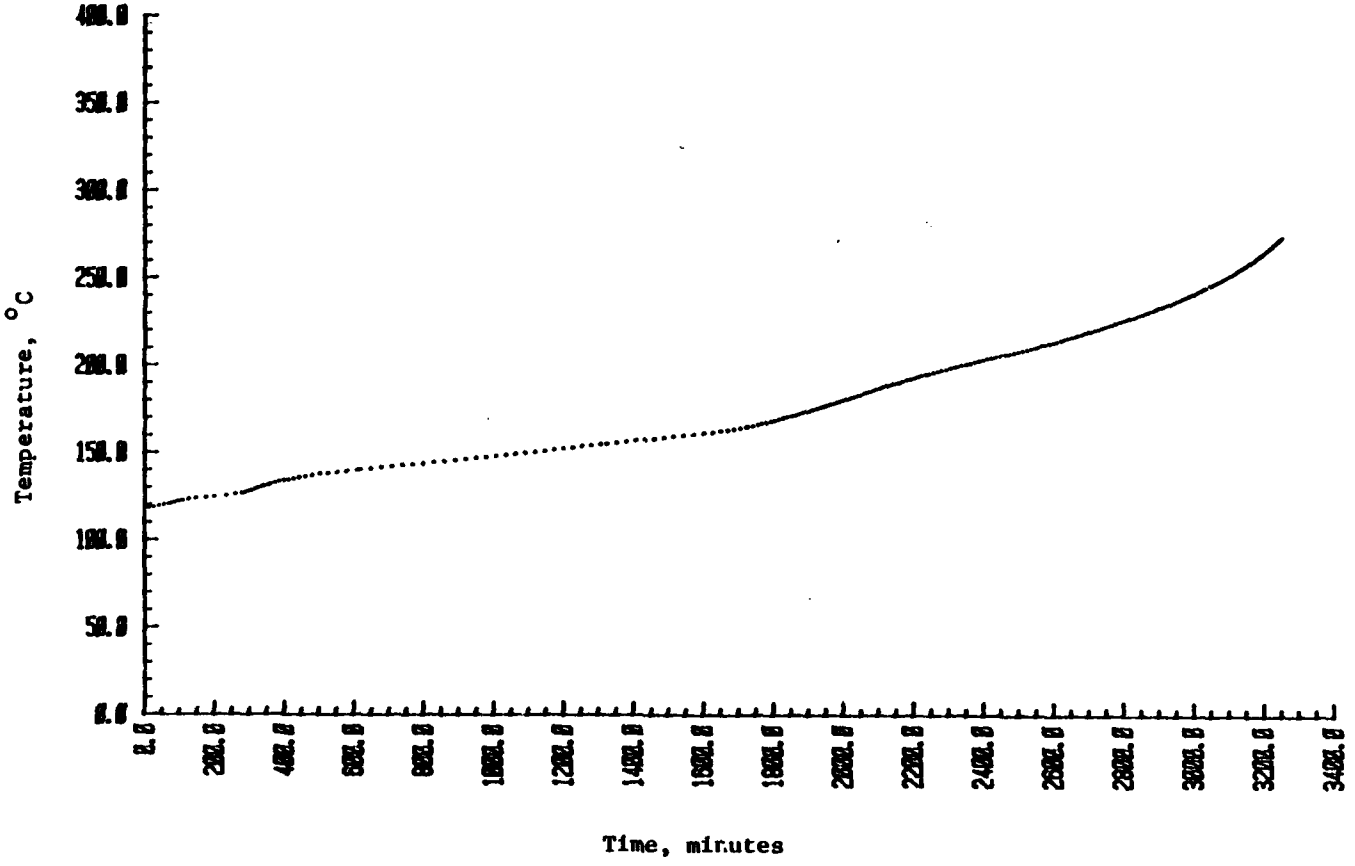

Figure 27. Temperature Versus Time Plot for Elevated Temperature Exotherm Detected in Cell No. III-2 (Excess Carbon)

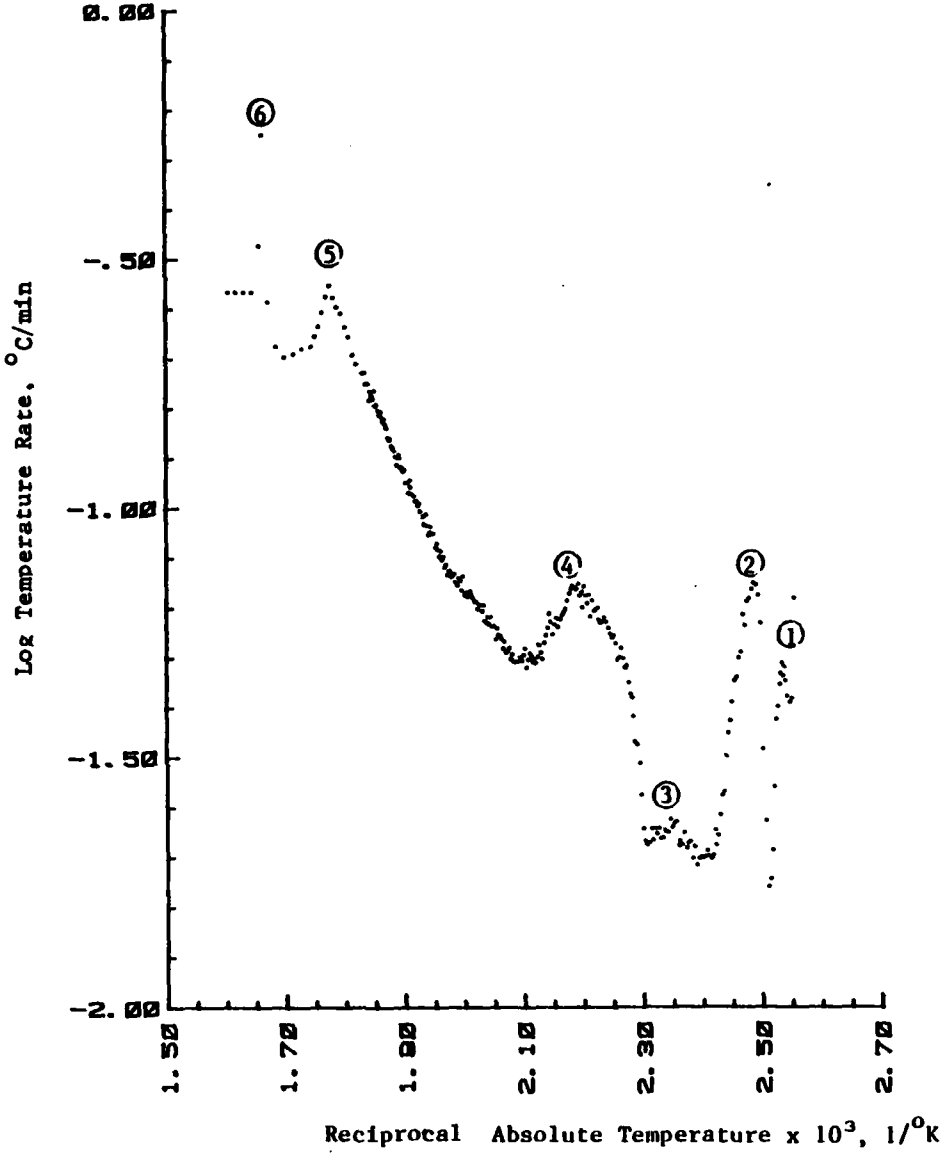

Figure 28. Log Temperature Rate Versus 1/T Plot for the Second Portion of the Reverse Exotherm Detected in Cell No. III-2 (Excess Carbon)

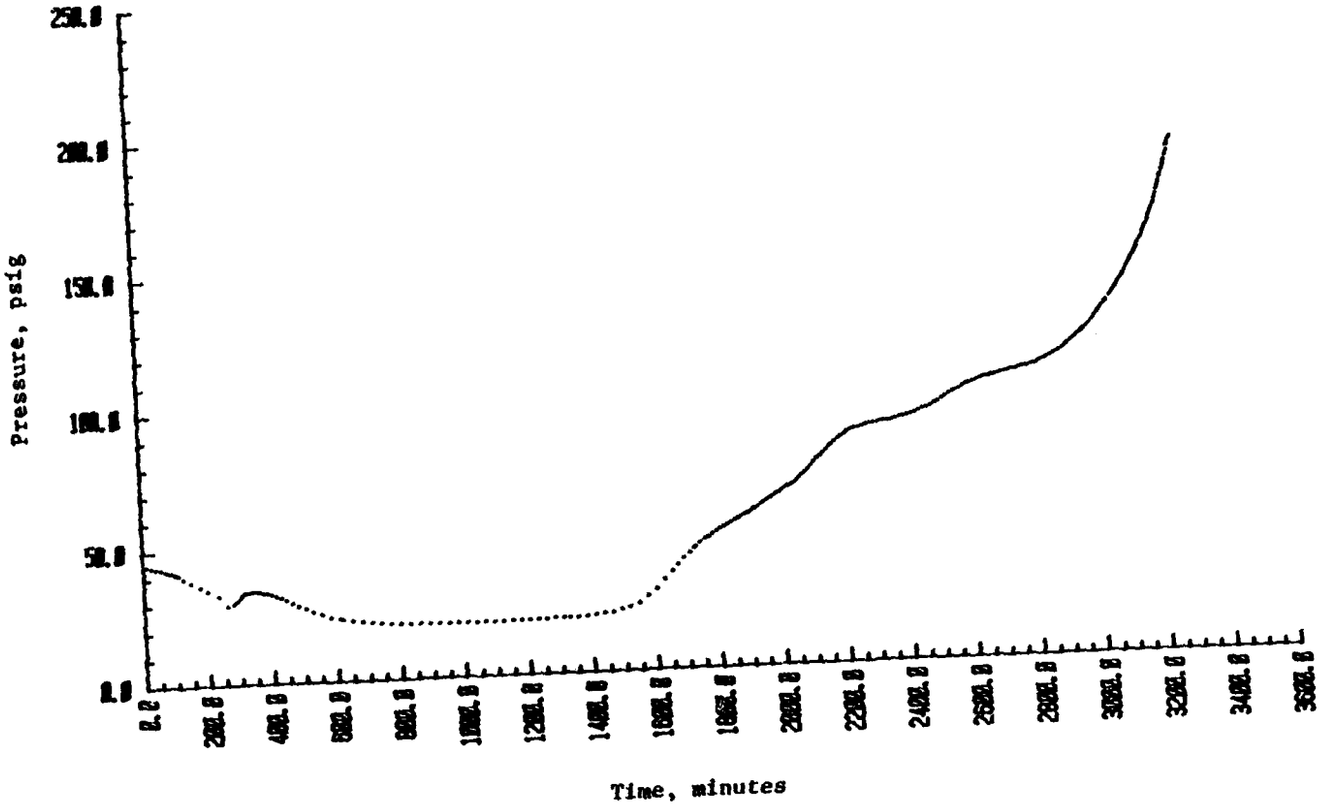

Figure 29. Pressure Versus Time Plot for Second Portion of Reverse Exotherm Detected in Cell No. III-2 (Excess Carbon)

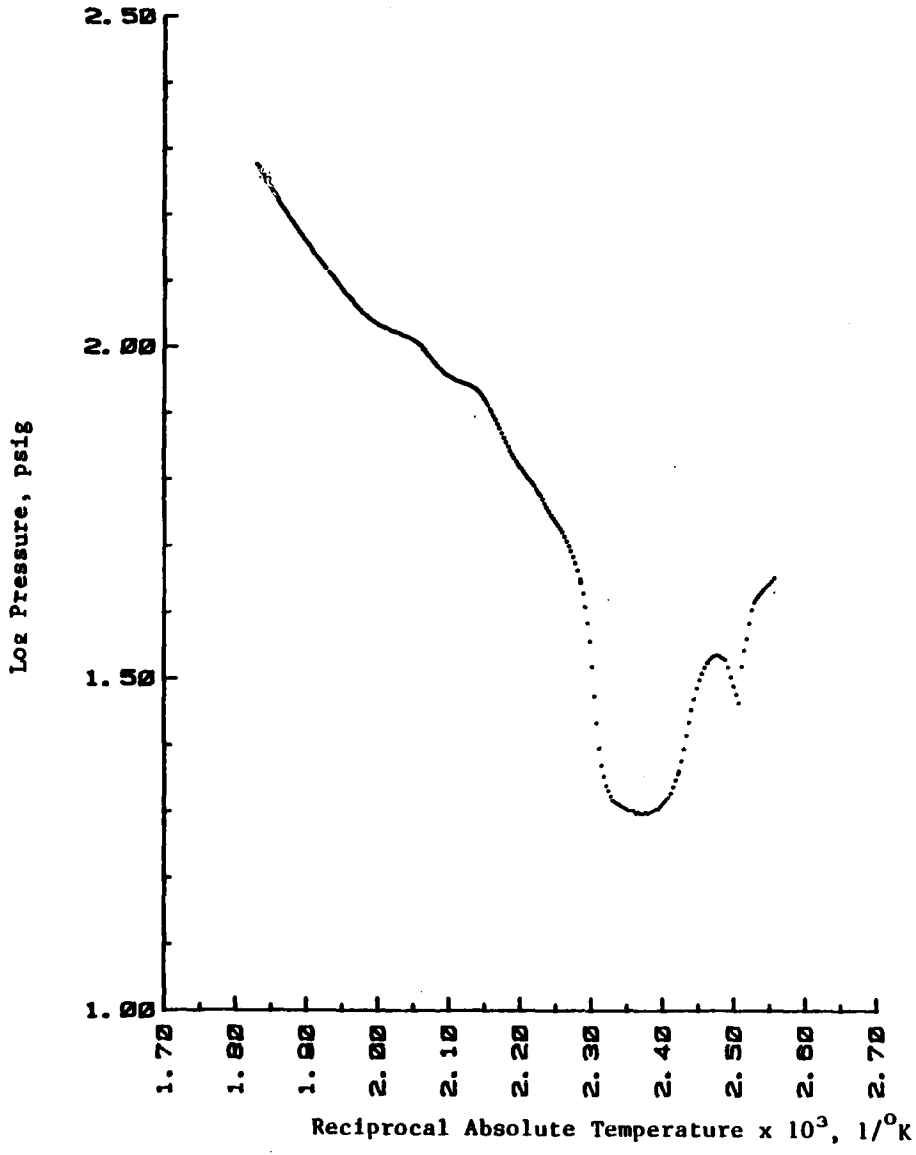

Figure 30. Log Pressure Versus 1/T Plot for Second Portion of Reverse Exotherm Detected in Cell No. III-2 (Excess Carbon)

Table 24. Summary of the Six Peaks Observed During the Second Portion of the Exotherm Initiated During Reverse Discharge Testing of Cell No. III-2 (Excess Carbon)

	Peak Numbers					
	1	2	3	4	5	6
Initial Temperature, °C	117.4	125.1	146.6	160.4	206.2	322.0
Initial Pressure, psig	45.0	33.4	19.9	27.1	92.7	-
Initial Temp. Rate, °C/min	0.027	0.017	0.020	0.021	0.049	0.210
Final Temperature, °C	125.1	141.1	156.1	199.2	302.0	332.0
Final Pressure, psig	33.4	21.8	20.7	88.0	-	-
Max. Temperature Rate, °C/min	0.049	0.071	0.024	0.070	0.278	0.560
Max. Pressure Rate, psig/min	< 0	0.13	0.01	0.014	-	-
Adiabatic Temp. Rise, °C	7.70	16.0	9.50	38.8	95.8	10.0
ΔH, cal	85.0	177	105	428	1057	110
Pressure Change, psig	-11.6	-11.6	0.8	60.9	-	-
Activation Energy, kcal/mole	18.0	196.2	8.3	87.2	16.2	236.9
Reaction Order	0.2	0.6	0.2	1.1	0.5	0.7
Projected Temperature Rise for Li/$SOCl_2$ "D" Cell, °C	17.9	37.1	22.0	90.0	222	23.2

Table 25. Summary of Characteristics of Reverse Exotherm for Cell No. IV-2 (Excess Lithium)

Initial Temperature, °C	44.05
Initial Pressure, psig	15.4
Initial Temperature Rate, °C/min	0.246
Final Temperature, °C	64.89
Final Pressure, psig	23.3
Maximum Temperature Rate, °C/min	0.246
Maximum Pressure Rate, psig/min	0.08
Adiabatic Temperature Rise, °C	20.84
Pressure Change, psig	7.9
Activation Energy, kcal/mole	8.0
Reaction Order	1.0
Projected Final Temperature for Li/SO_2 "D" Cell, °C	86.4
Projected Temperature Rise for Li/SO_2 "D" Cell, °C	42.4

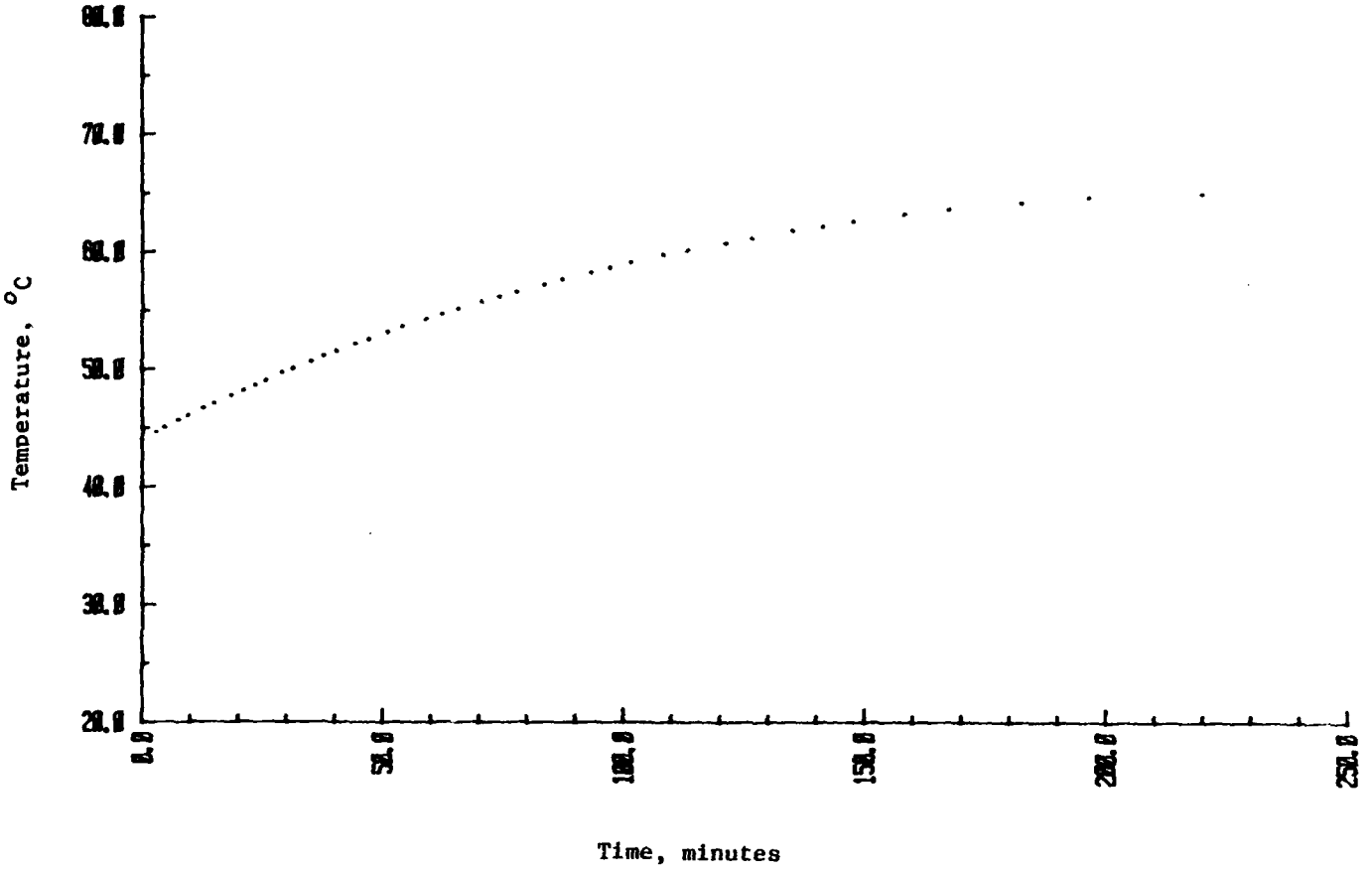

Figure 31. Temperature Versus Time Plot for the Exotherm Detected During Forced Overdischarge Testing of Cell No. IV-2 (Excess Lithium)

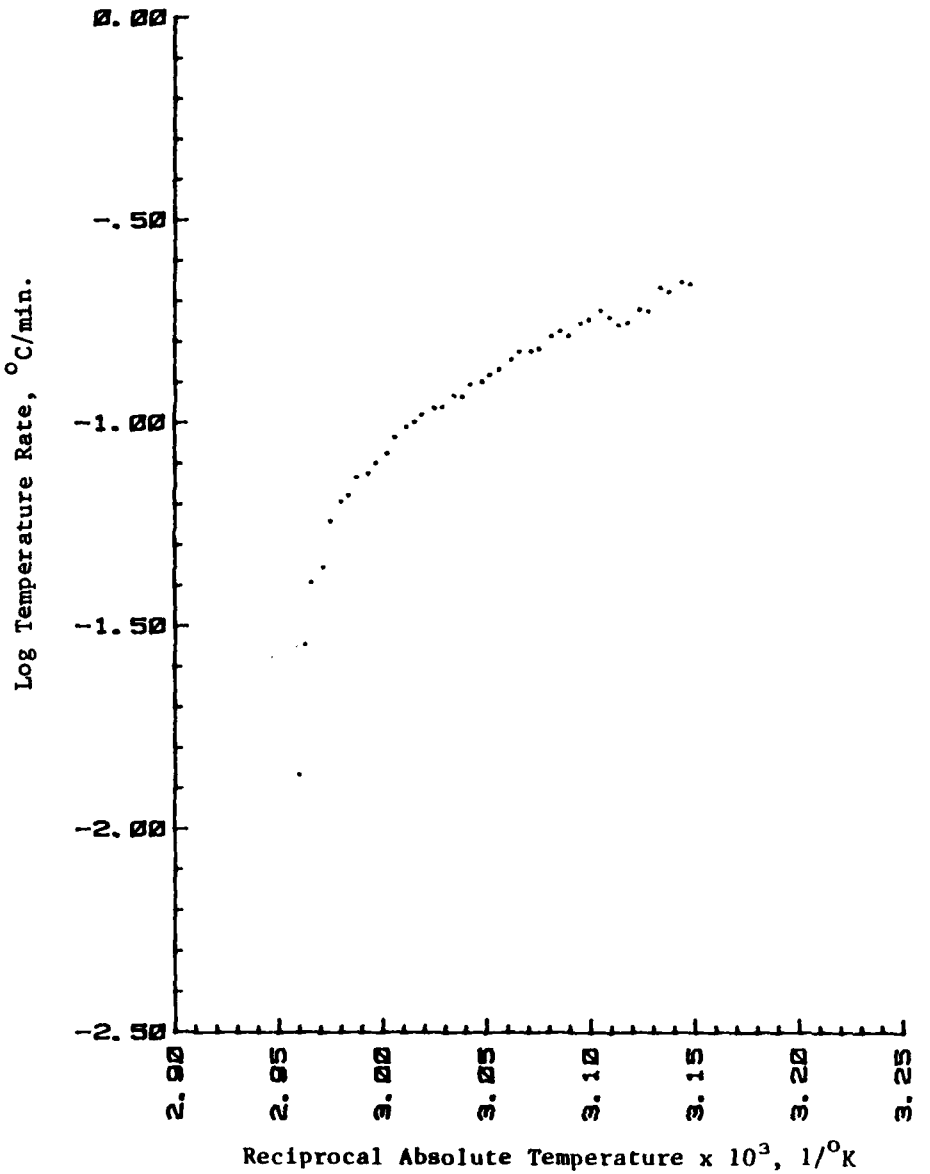

Figure 32. Log Temperature Rate Versus 1/T Plot for the Exotherm Detected During Forced Overdischarge Testing of Cell No. IV-2 (Excess Lithium)

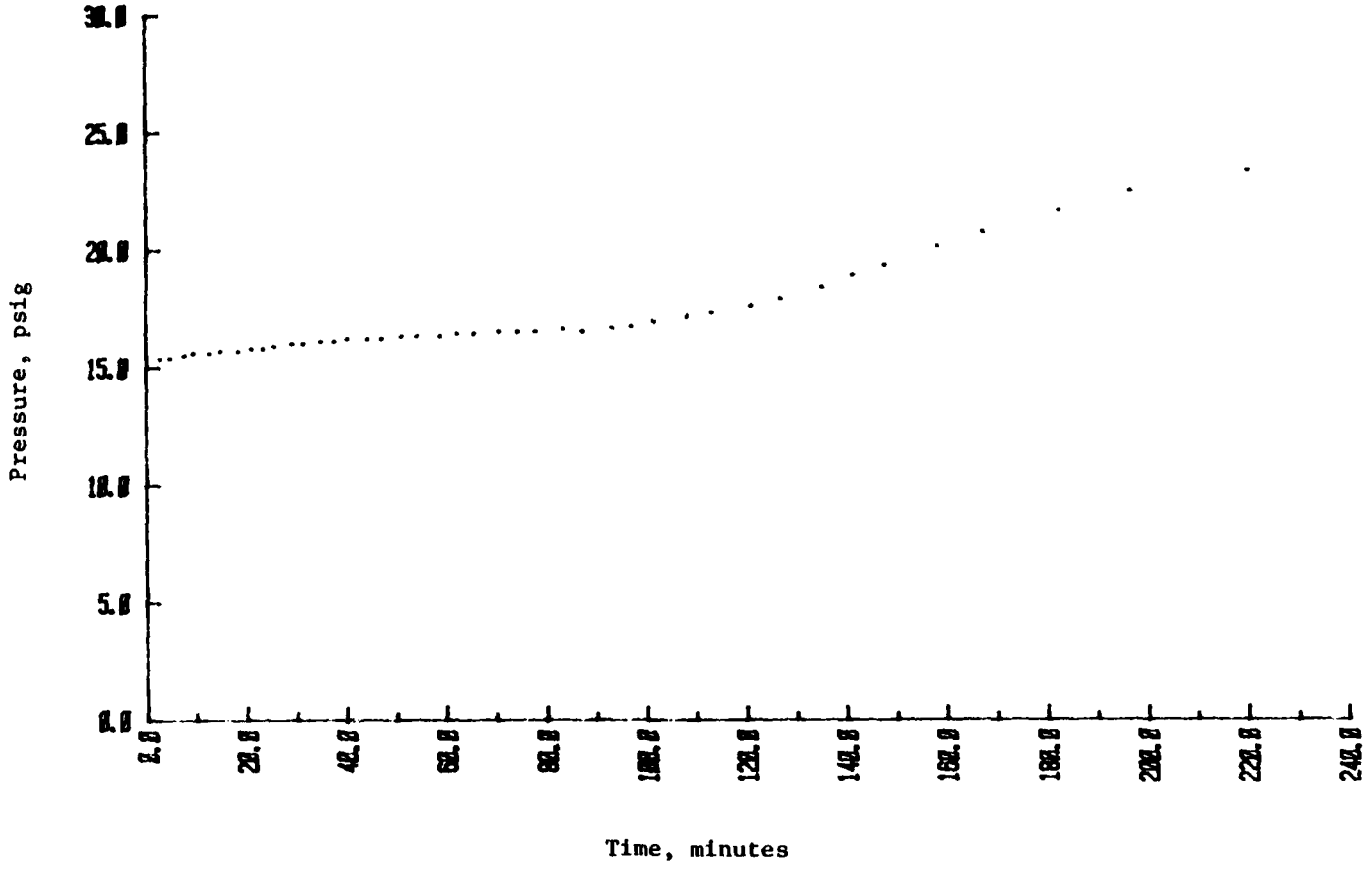

Figure 33. Pressure Versus Time Plot for Exotherm Detected During Forced Overdischarge Testing of Cell No. IV-2 (Excess Lithium)

AD-A119 381 HONEYWELL POWER SOURCES CENTER HORSHAM PA F/G 10/3
LITHIUM-SULFUR DIOXIDE (LI/SO2) BATTERY SAFETY HAZARDS - THERMA--ETC(U)
MAR 82 W B EBNER, K V KIM, H V VENKATASETTY N60921-81-C-0085
UNCLASSIFIED NL

2 3

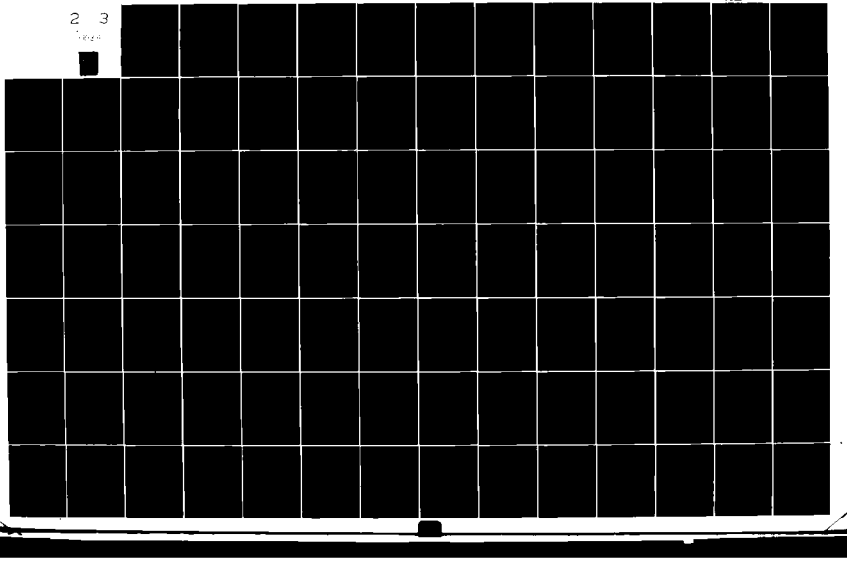

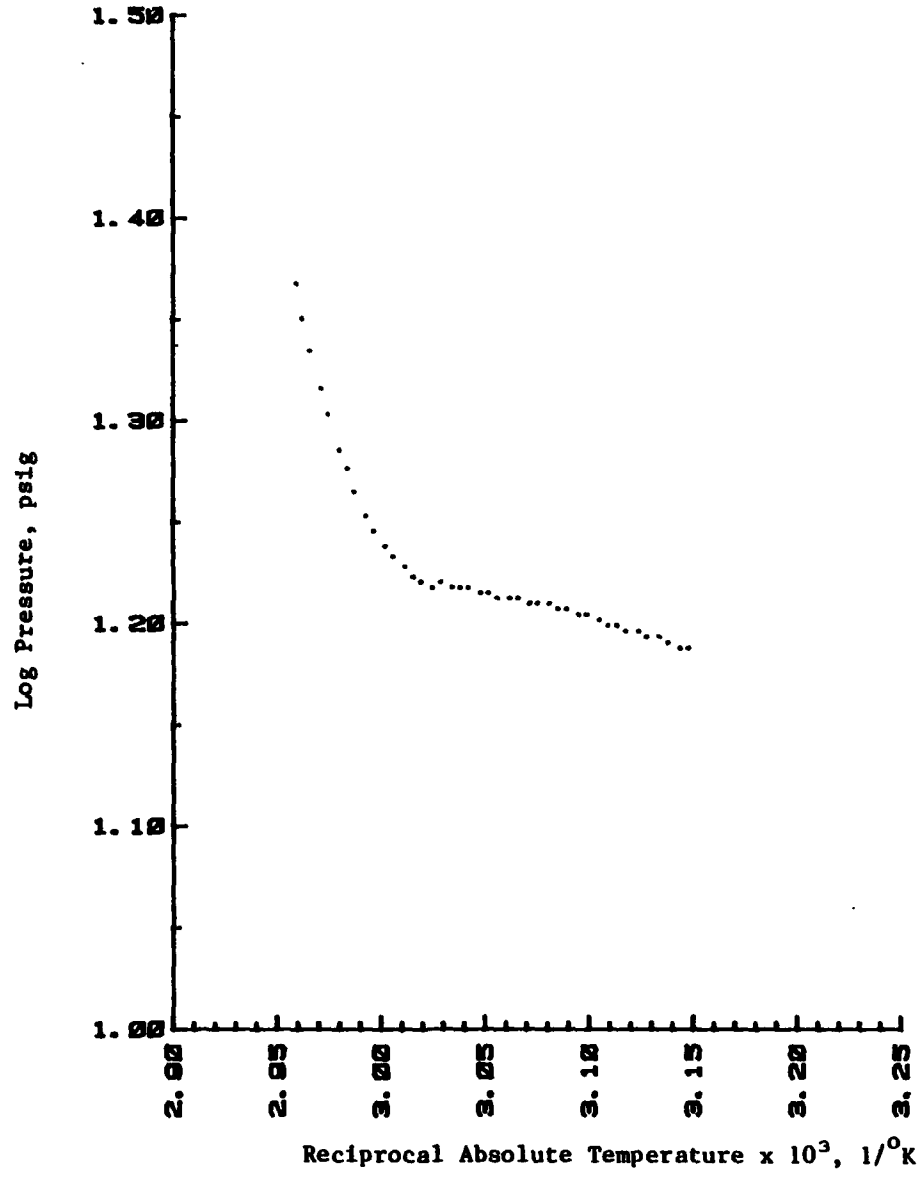

Figure 34. Log Pressure Versus 1/T Plot for Exotherm Detected During Forced Overdischarge Testing of Cell No. IV-2 (Excess Lithium)

The initial heat and search operation for this cell experienced an instrument malfunction at approximately 113°C. No exotherms were detected to this point. Although the test continued to about 230°C, the data above 113°C can not be considered reliable. The malfunction was related to problems resulting from deposited films and corrosion within the calorimeter due to cell leakage, as discussed earlier.

The cell was cooled to ambient temperature and attempts made to correct the problem. Because the malfunction only occurred intermittently, it was very difficult to troubleshoot the problem. Finally, a second heat and search analysis was initiated, during which the instrument performed well. A total of seven exotherms were detected above 230°C, as summarized in Table 26. The major exotherm initiated at approximately 242°C which is in the same temperature region where peaks had been observed in previous cells. The data plots for this exotherm, shown in Figures 35 through 38, indicate that this reaction is different than the others, however. This reaction has a much lower activation energy than the other reactions observed in this temperature region and is shown to be a pressure reducing reaction rather than a pressure generating reaction.

Table 26. Summary of Exotherms Detected During the Heat and Search Operation of Cell No. IV-2 (Excess Lithium)

	Exotherm Number						
	1	2	3	4	5	6	7
Initial Temp., °C	230.69	241.93	287.06	300.64	314.22	328.95	342.53
Initial Pressure, psig	178.9	186.0	179.0	179.8	182.1	184.1	187.8
Initial Temp. Rate, °C/min.	0.027	0.039	0.021	0.024	0.026	0.046	0.025
Final Temp., °C	231.04	276.32	289.85	303.44	318.01	331.75	349.82
Final Pressure, psig	183.4	178.6	179.2	180.9	183.5	186.2	89.3
Max. Temp. Rate, °C/min.	0.027	0.041	0.021	0.024	0.026	0.049	4.000
Max. Pressure Rate, psig/min	-	0.17	-	-	-	-	-
Temperature Rise, °C	0.35	34.39	2.79	2.80	3.79	2.80	7.29
ΔH, cal	4.3	421	34.1	34.2	46.4	34.2	89.2
Pressure Change, psig	4.5	-7.4	0.2	1.1	1.4	2.1	-98.5
Activation Energy, kcal/mole	-	8.0	-	-	-	-	-
Reaction Order	-	0.5	-	-	-	-	-
Projected Final Temperature for Li/SO_2 "D" Cell	231.4	311.9	292.7	306.3	321.9	334.6	357.4
Projected Temperature Rise for Li/SO_2 "D" Cell	0.71	70.0	5.7	5.7	7.7	5.7	14.8

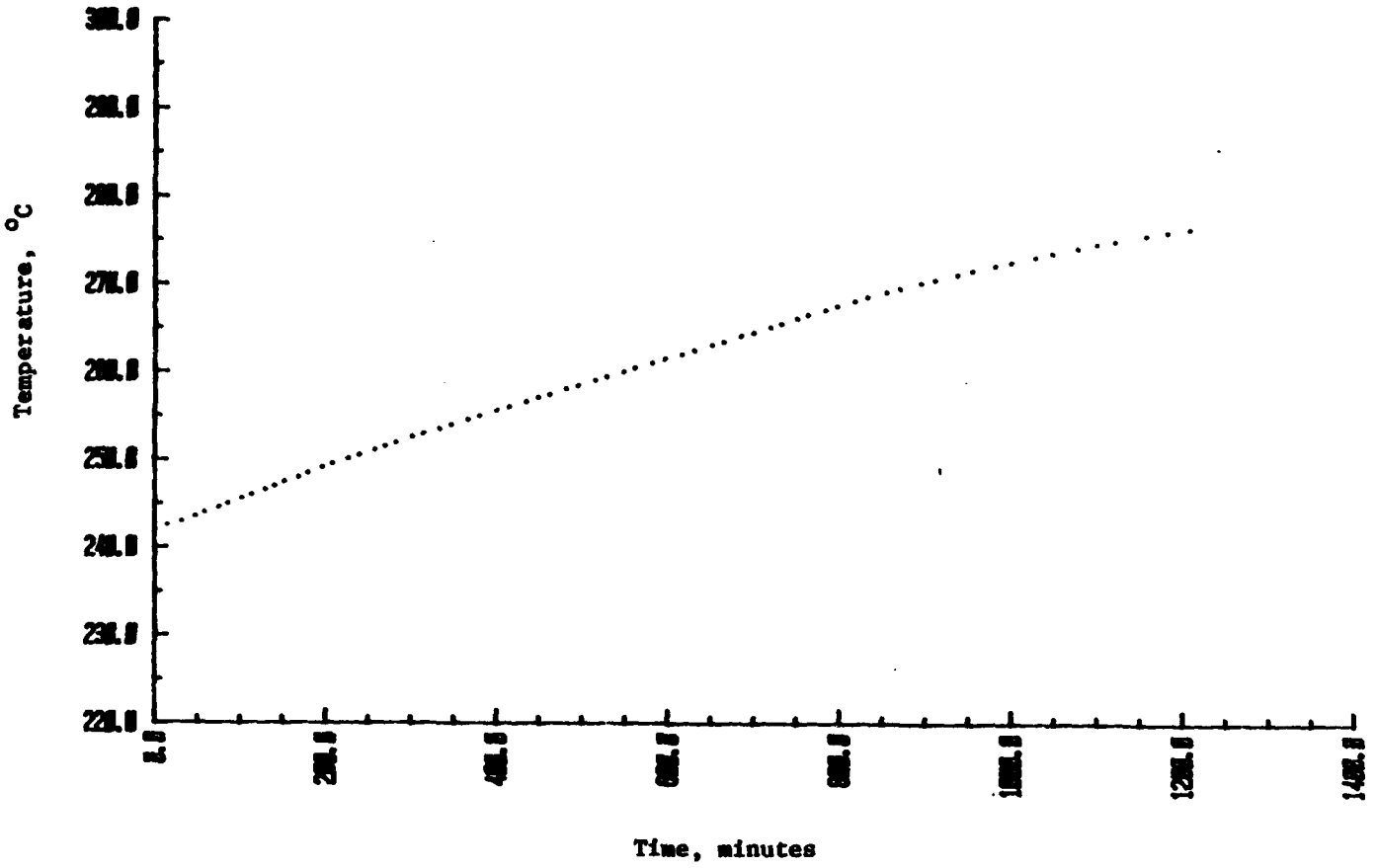

Figure 35. Temperature Versus Time Plot for Second Elevated Temperature Exotherm Detected During the ARC Analysis of Cell No. IV-2. (Excess Lithium)

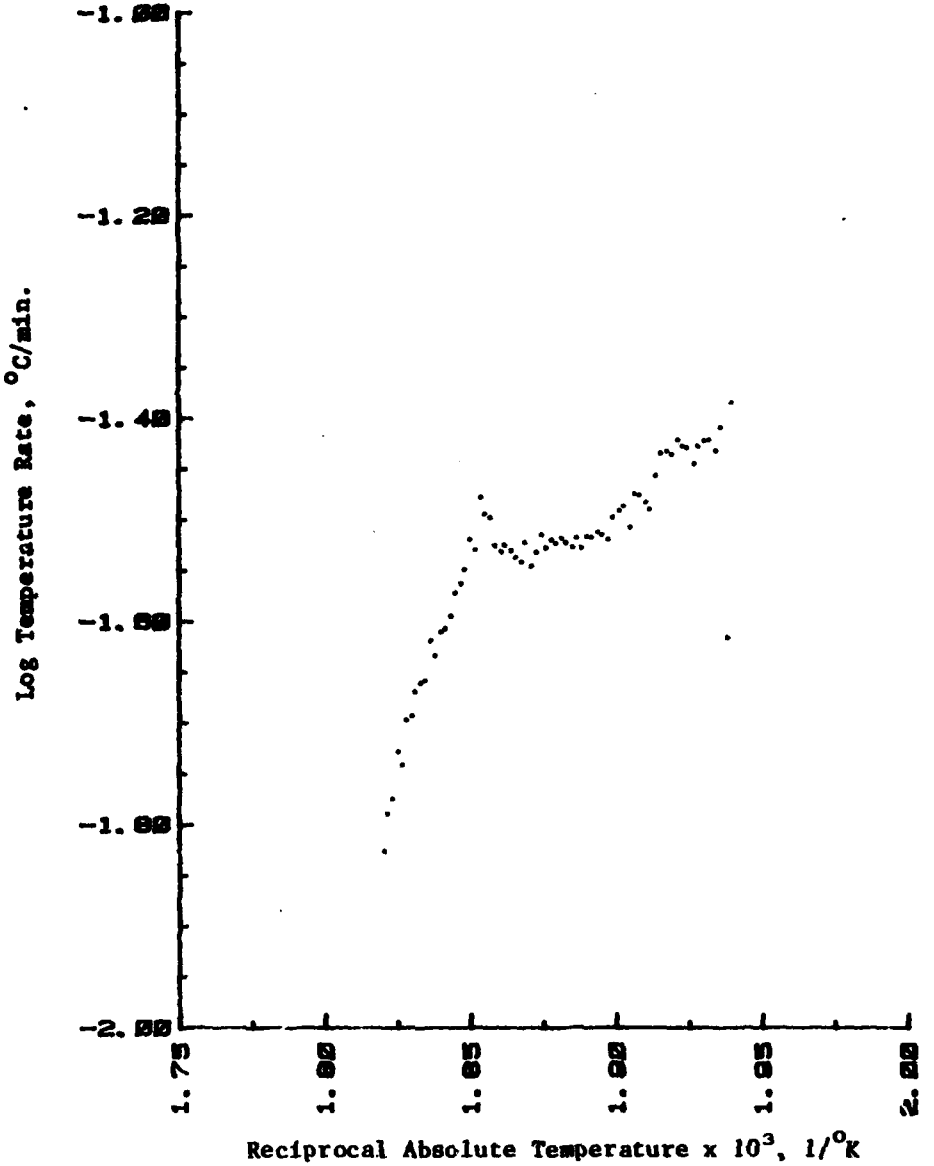

Figure 36. Log Temperature Rate Versus 1/T Plot for Second Elevated Temperature Exotherm Detected During the ARC Analysis of Cell No. TV-2 (Excess Lithium)

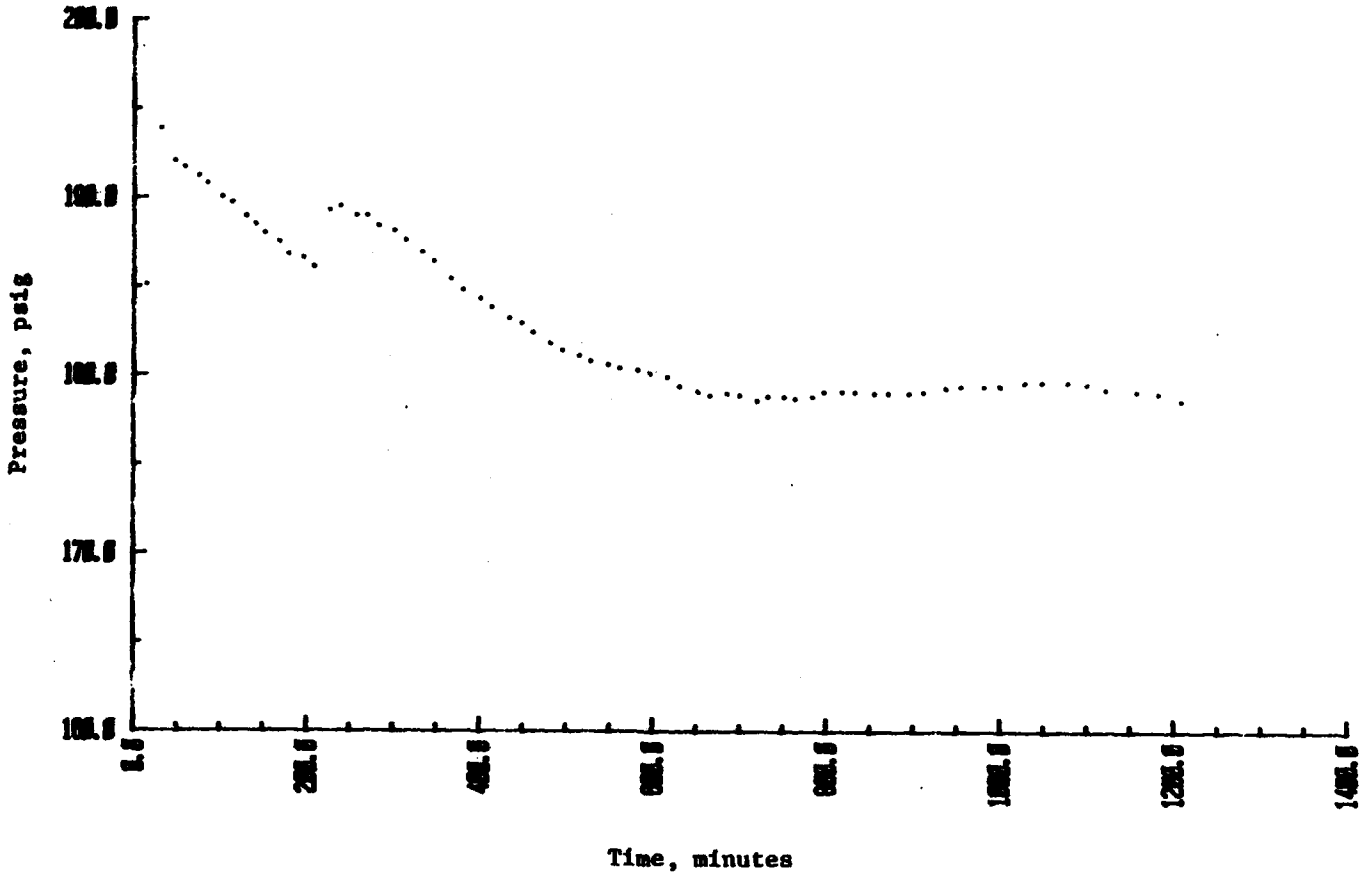

Figure 37. Pressure Versus Time Plot for the Second Elevated Temperature Exotherm Detected During the ARC Analysis of Cell No. IV-2. (Excess Lithium)

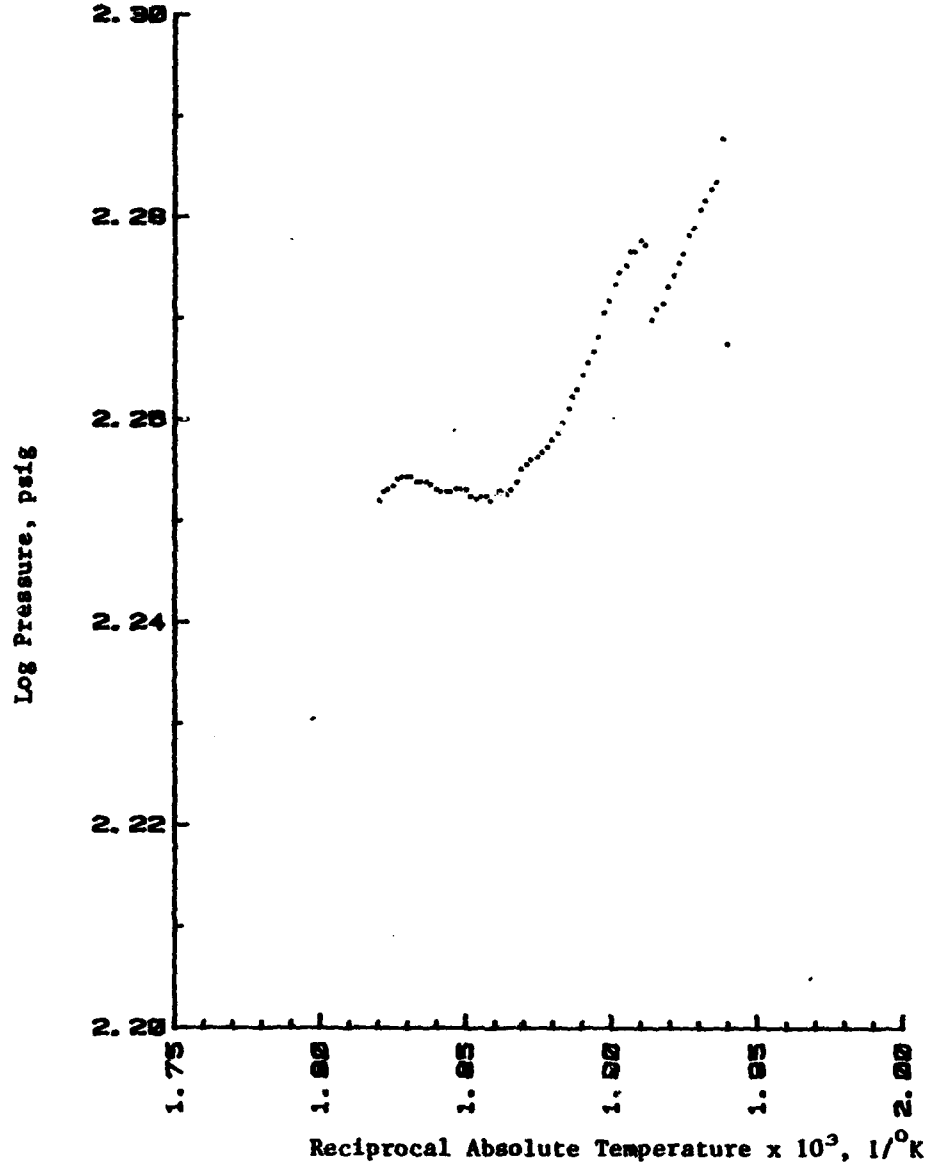

Figure 38. Log Pressure Versus 1/T Plot for the Second Elevated Temperature Exotherm Detected During the ARC Analysis of Cell No. IV-2 (Excess Lithium)

Group C Tests

Resistive Overdischarge (25°C)

Group C Tests

Objective

The objective of the Group C tests was to evaluate the thermal behavior of Li/SO_2 cells during ambient temperature discharge and overdischarge under a resistive load of 5 ohms.

Experimental

During these tests, the cell voltage was continuously recorded on a strip chart recorder. A second recorder was employed to record the voltage drop across the 5-ohm load resistor, thus providing a continuous monitor of the cell current.

The construction features of the four Group C cells are shown in Table 27.

Discharge Performance

The discharge performance of the four Group C cells is summaried in Table 28. The performance of these cells was similar to that of the Group B cells as expected from the similarity in discharge current densities. The component ratios present at the 2.0 volt cutoff are summarized in Table 29.

Table 30 summarizes the resistive overdischarge testing that was conducted on each cell. As can be seen, the cells were discharged down to very low potentials. Table 31 summarizes the status of each cell, including overall utilization efficiencies of the active components, at the completion of the resistive overdischarge.

Table 27. Construction Features of Group C Cells

Cell No.	Li/SO_2 Ratio	SO_2/C Ratio	Li/C Ratio	Electrolyte Qty., gm	Cathode Surface Area, cm^2	Thermal Inertia Value, ϕ
I-3	0.52	0.95	0.49	5.96	71.74	2.33
II-3	1.50	1.20	1.27	6.55	68.64	2.18
III-3	0.83	0.62	0.52	4.01	78.45	2.81
IV-3	1.46	1.18	1.73	5.87	61.94	2.25

Table 28. Discharge Performance to 2.0 Volts for Group C Cells

Cell No.	Run Time, hr	Average Voltage, V	Average Current, mA	Average Current Density, mA/cm^2	Capacity Delivered, Ah	Discharge Efficiency, %		
						Anode	Carbon	SO_2
I-3	2.31	2.66	332	4.63	0.769	87.5	42.9	45.3
II-3	3.33	2.60	363	5.29	1.21	61.6	78.0	64.9
III-3	0.99	2.62	347	4.42	0.343	36.0	18.7	30.0
IV-3	3.18	2.59	340	5.49	1.08	44.1	76.4	64.6

Table 29. Cell Status at End of Discharge to 2.0 Volt Cutoff for Group C Cells.

Cell No.	Cell Design	SO_2/Li	SO_2/Li Area, mg/cm^2
I-3	Lithium Limited	8.5	30.9
II-3	Coulombically Balanced	0.87	22.8
III-3	Excess Carbon	1.3	24.3
IV-3	Excess Lithium	0.43	22.8

Table 30. Performance Summary During Resistive Overdischarge of Group C Cells

Cell No.	Overdischarge Time, hr	Capacity Delivered During Overdischarge, Ah	Final Load Voltage, V
I-3	55.2	0.168	0.003
II-3	49.0	0.331	0.001
III-3	69.3	0.133	0.001
IV-3	7.9	0.380	0.06

Table 31. Cell Status at End of Resistive Overdischarge for Group C Cells

Cell No.	Total Capacity Delivered, Ah	SO_2/Li	SO_2/Li Area, mg/cm^2	Active Component Utilization, %		
				Anode	Carbon	SO_2
I-3	0.9375	-	-	106.7	52.4	55.3
II-3	1.5408	0.764	11.24	78.4	99.3	82.7
III-3	0.4760	1.399	20.27	50.0	26.0	41.7
IV-3	1.4599	0.214	8.16	59.6	103.2	87.3

Thermal Behavior

Table 32 summarizes the thermal behavior of the Group C cells. Only Cell No. IV-3 (excess lithium) gave an exotherm during resistive overdischarge while all four cells gave exotherms during the final evaluation at elevated temperatures. Because of leakage problems, Cell No. II-3 (coulombically balanced) could only be evaluated up to a temperature of 165°C.

Cell No. I-3 (lithium limited)

This cell gave no exotherms during the electrical phase of testing. During the final heat and search operation, three exotherms were detected to the cutoff limit of 350°C. The characteristics of these exotherms are summarized in Table 33.

The first exotherm was very small, but the other two exotherms were significant. Figures 39 through 42 show the data plots for the second exotherm while Table 34 gives the measured kinetic parameters. This exotherm appears to be composed of a single, low activation energy reaction. The pressure drop accompanying this reaction is significant indicating that a gaseous component, quite possibly SO_2, is involved.

Figures 43 through 46 show the data plots for the third exotherm. The log temperature rate versus 1/T plot (Figure 44) shows this exotherm to be composed of three distinct reactions (peaks) which are summarized in Table 35.

Table 32. Summary of the Thermal Behavior of the Group C Cells

Cell No.	Cell Design	Exotherms During Discharge to 2.0 Volt Cutoff	Exotherms During Resistive Overdischarge	Exotherms During Final Heat and Search	Final Temp. During Heat and Search, °C
I-3	Lithium Limited	No	No	Yes	350
II-3	Coulombically Balanced	No	No	Yes	165
III-3	Excess Carbon	No	No	Yes	338
IV-3	Excess Lithium	No	Yes	N/A	N/A

Table 33. Summary of Exotherms Detected During the Final Heat and Search Operation of Cell No. I-3 (Lithium Limited)

	Exotherm No.		
	1	2	3
Initial Temperature, °C	81.19	145.16	256.58
Initial Pressure, psig	64.9	189.4	174.9
Initial Temperature Rate, °C/min	0.041	0.181	0.133
Final Temperature, °C	81.91	164.92	292.81
Final Pressure, psig	64.9	111.1	233.2
Maximum Temp. Rate, °C/min	0.041	0.181	0.627
Maximum Pressure Rate, psig/min	-	<0	7.12
Temperature Rise, °C	0.72	19.76	36.23
Pressure Change, psig	0.0	-78.3	58.3
Time Duration of Exotherm, min	36.23	318.2	209.1
ΔH, cal	8.6	236	433
Projected Final Temperature for Li/SO_2 "D" Cell, °C	82.6	185.2	330.0
Projected Temperature Rise for Li/SO_2 "D" Cell	1.46	40.0	73.4

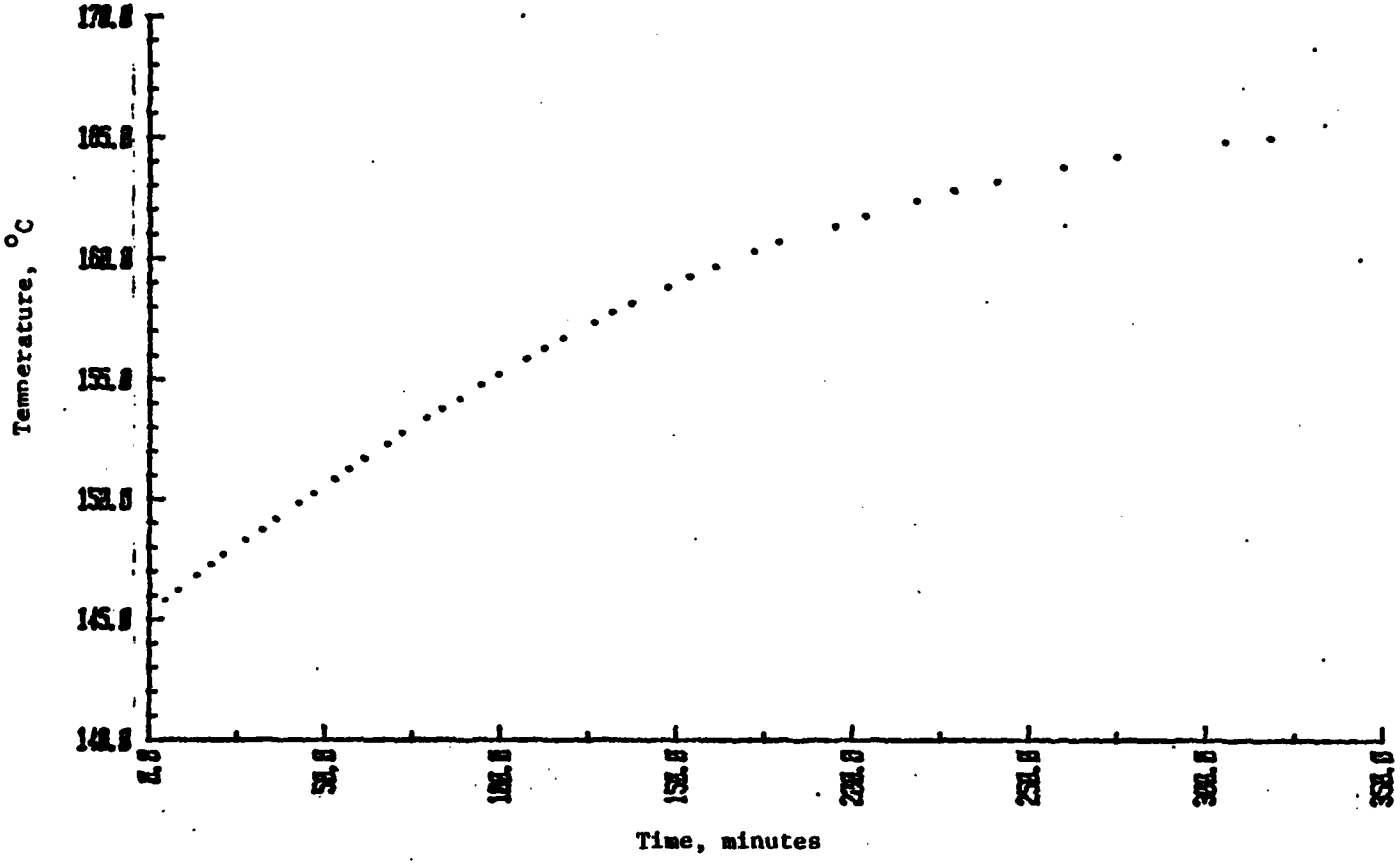

Figure 39. Temperature Versus Time Plot for the Second Elevated Temperature Exotherm Detected During the ARC Analysis of Cell No. I-3 (Lithium Limited)

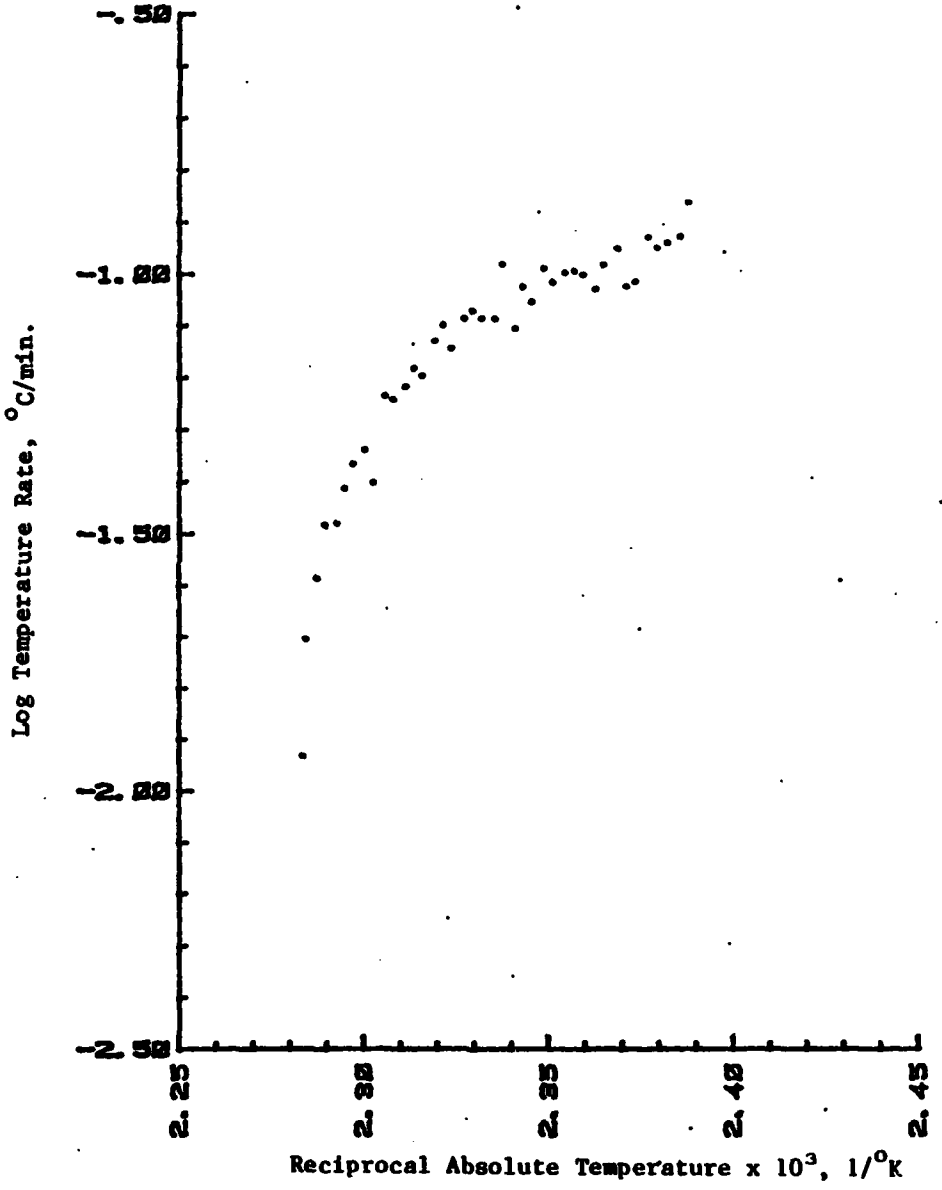

Figure 40. Log Temperature Rate Versus 1/T Plot for the Second Elevated Temperature Exotherm Detected During the ARC Analysis of Cell No. I-3 (Lithium Limited)

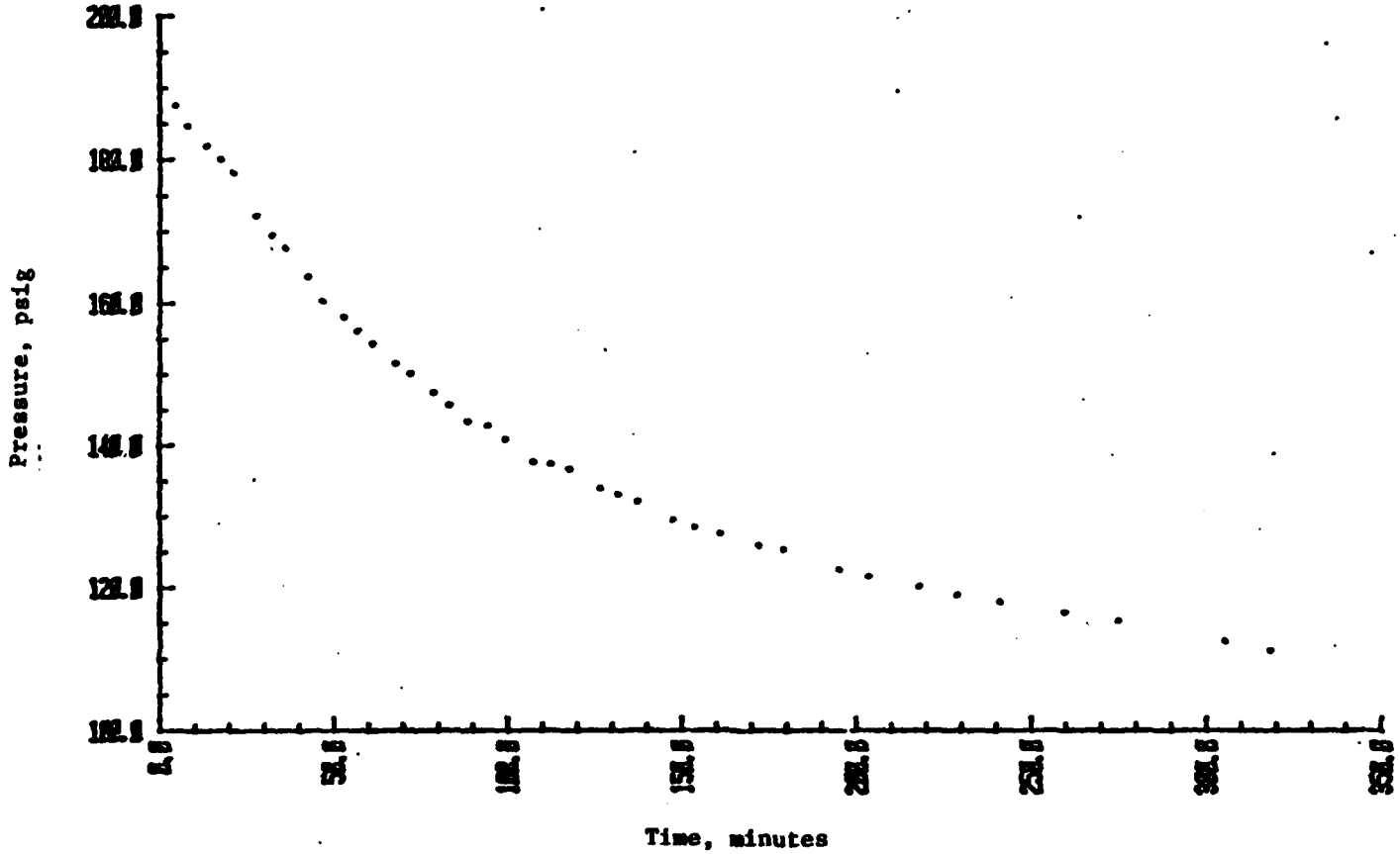

Figure 41. Pressure Versus Time Plot for the Second Elevated Temperature Exotherm Detected During the ARC Analysis of Cell No. I-3 (Lithium Limited)

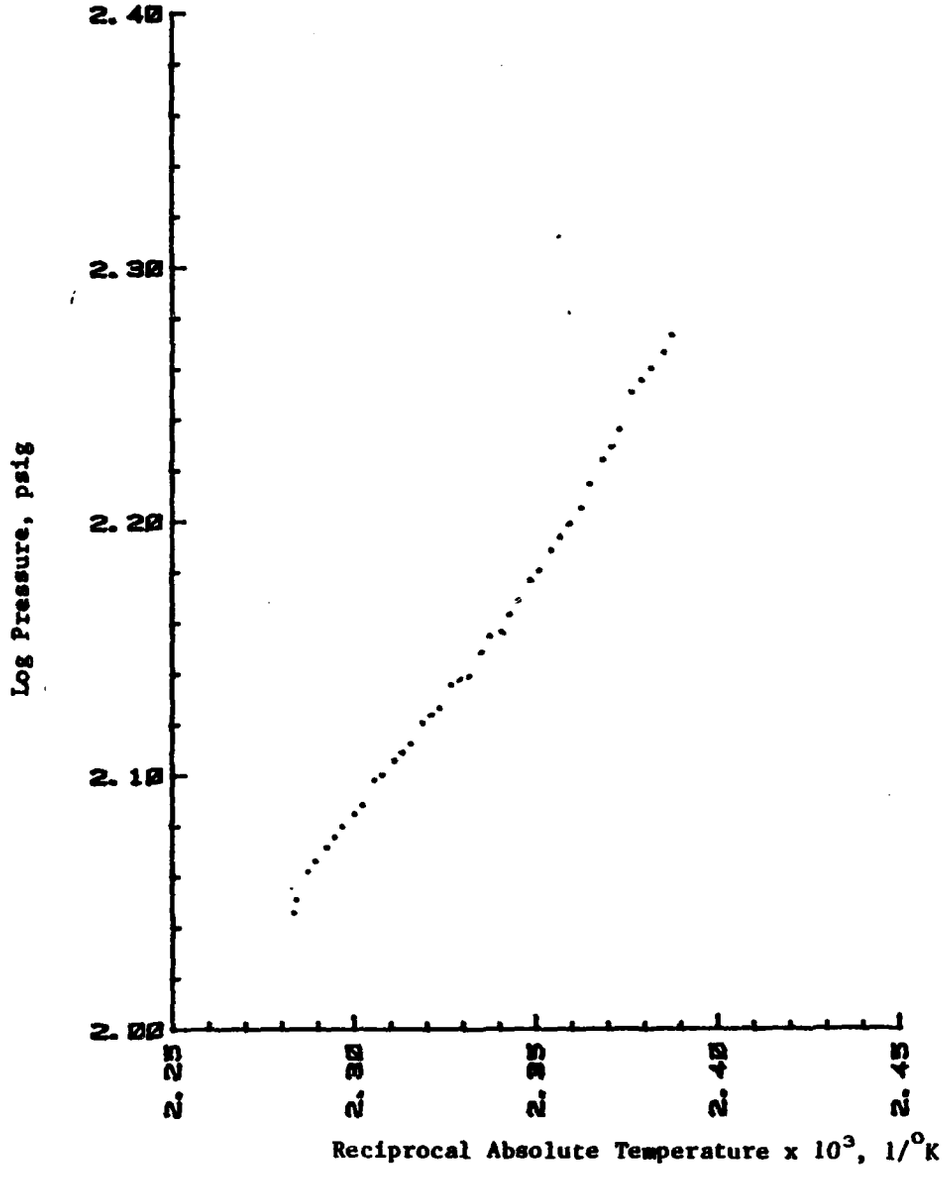

Figure 42. Log Pressure Versus 1/T for the Second Elevated Temperature Exotherm Detected During the ARC Analysis of Cell No. I-3 (Lithium Limited)

Table 34. Measured Kinetic Parameters for the Second Heat and Search Exotherm of Cell No. I-3 (Lithium Limited)

Activation Energy, kcal/mole	12.0
Reaction Order	0.9

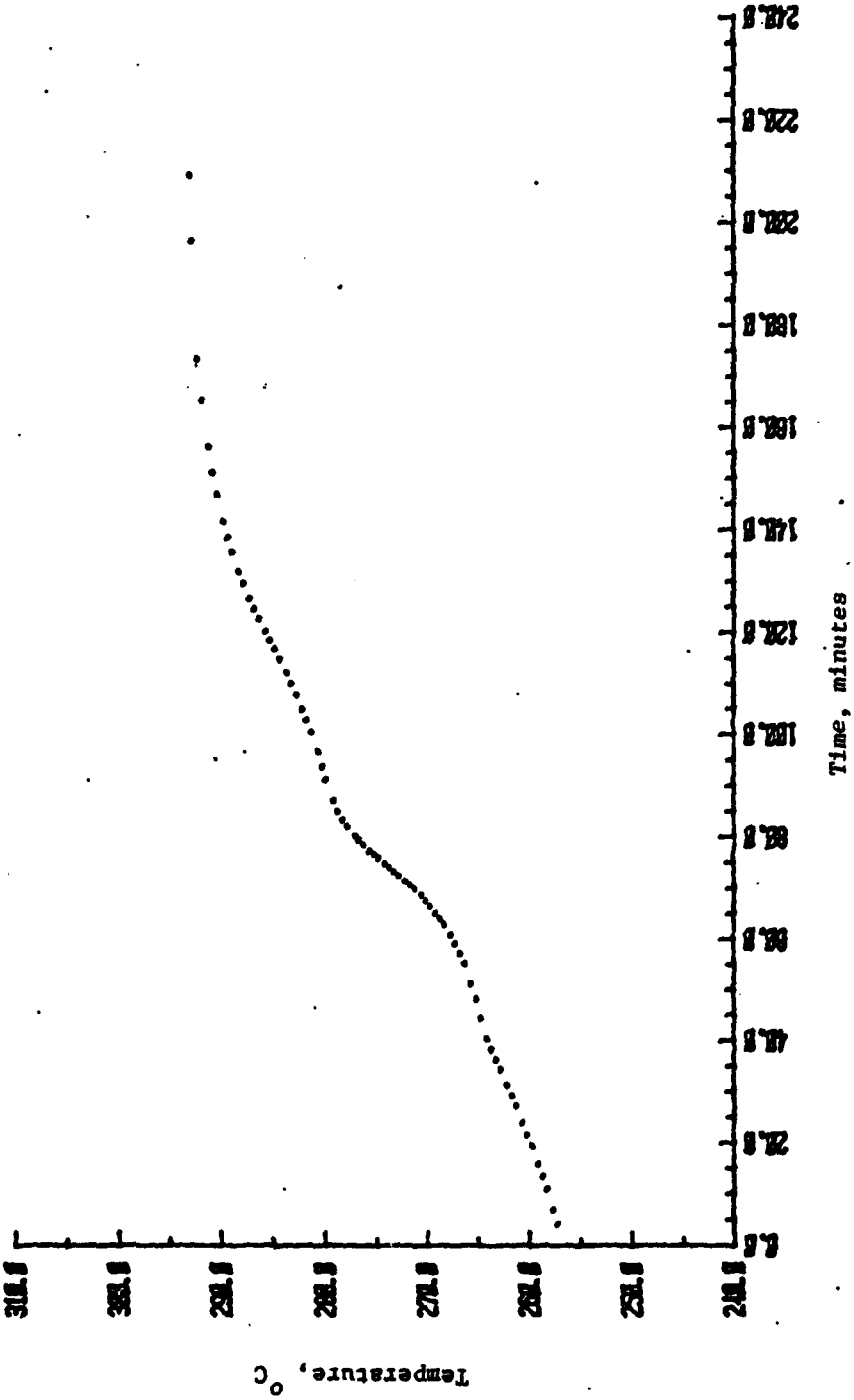

Figure 43. Temperature Versus Time Plot for the Third Elevated Temperature Exotherm Detected During the ARC Analysis of Cell No. I-3 (Lithium Limited)

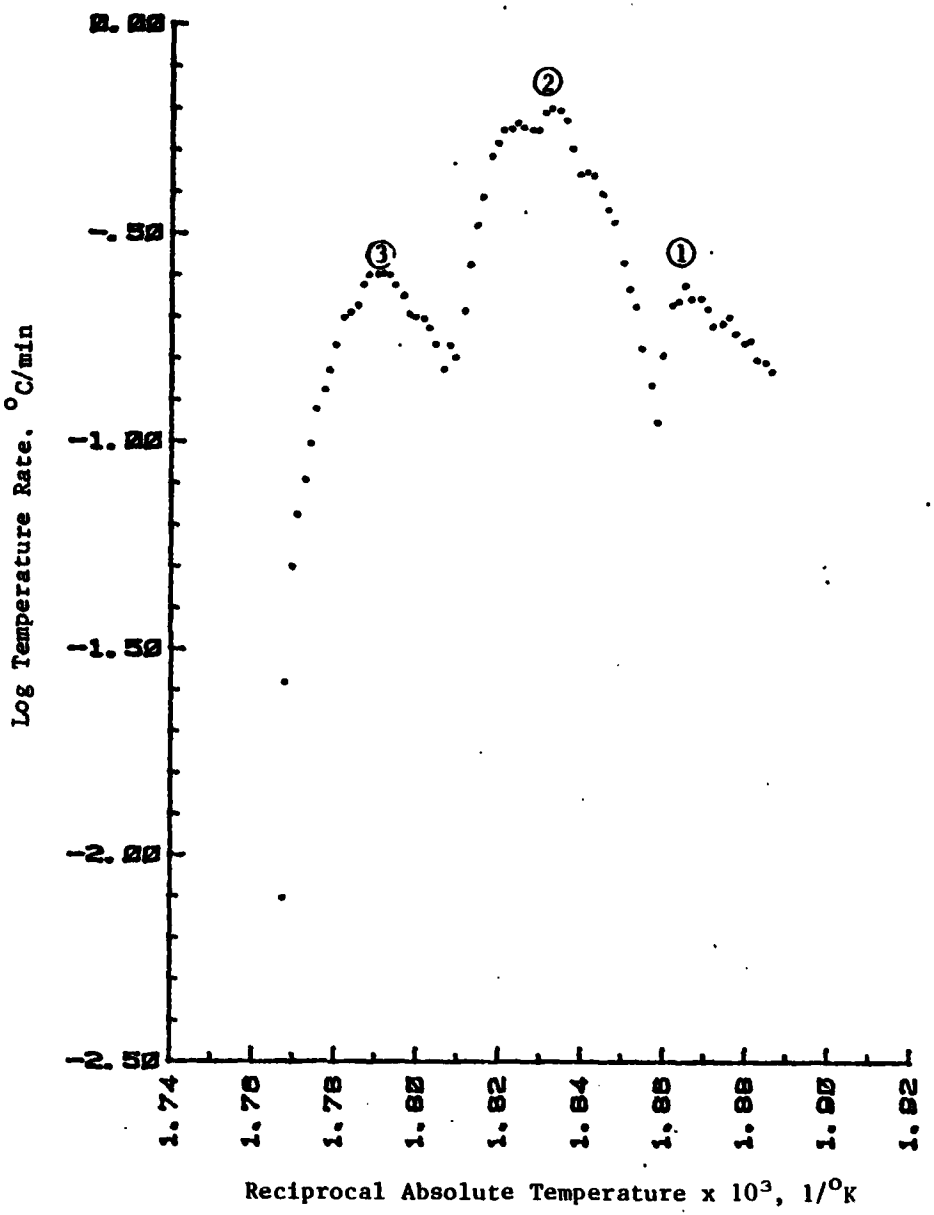

Figure 44. Log Temperature Rate Versus 1/T Plot for the Third Elevated Temperature Exotherm Detected During the ARC Analysis of Cell No. I-3 (Lithium Limited)

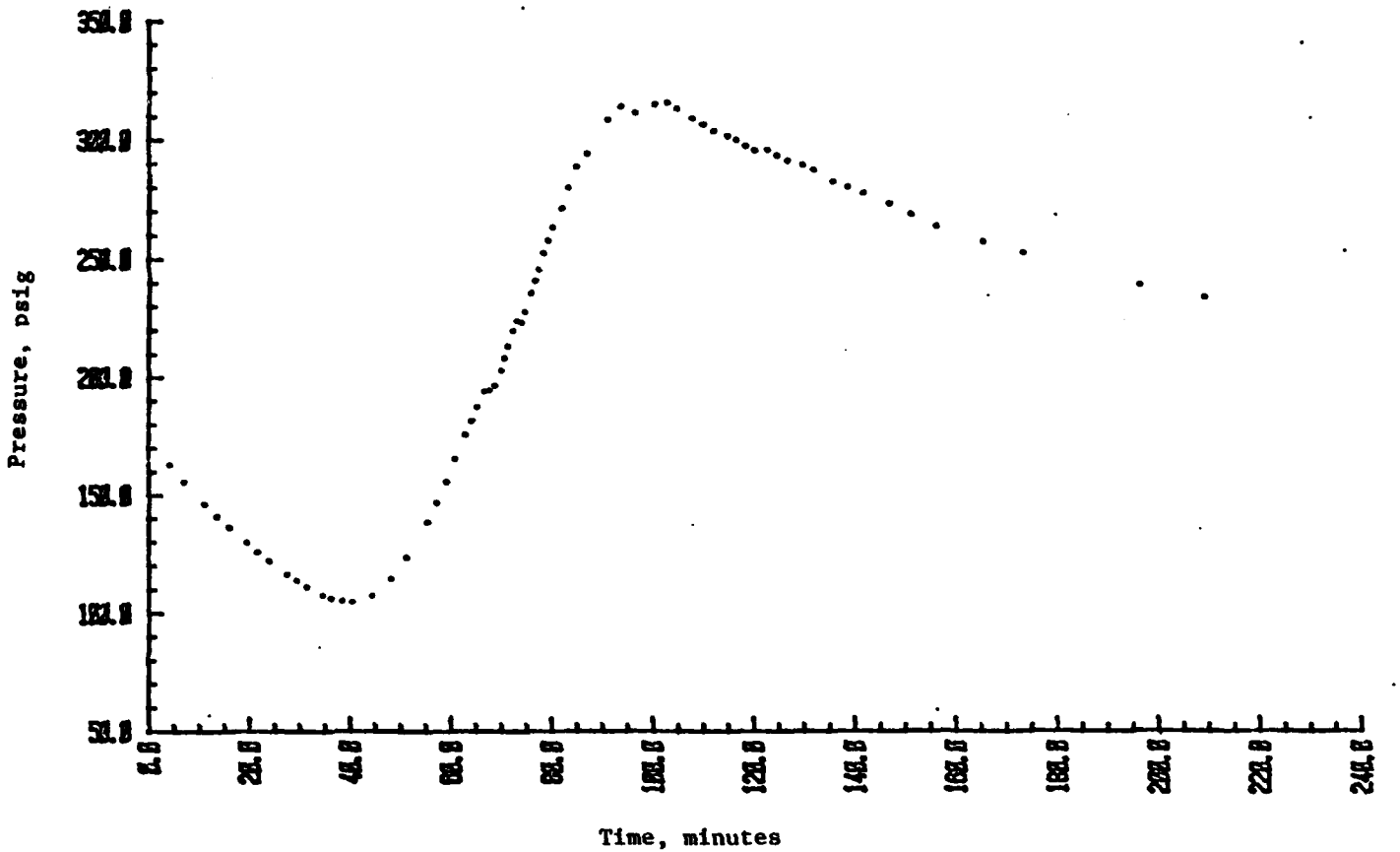

Figure 45. Pressure Versus Time for the Third Elevated Temperature Exotherm Detected During the ARC Analysis of Cell No. I-3 (Lithium Limited)

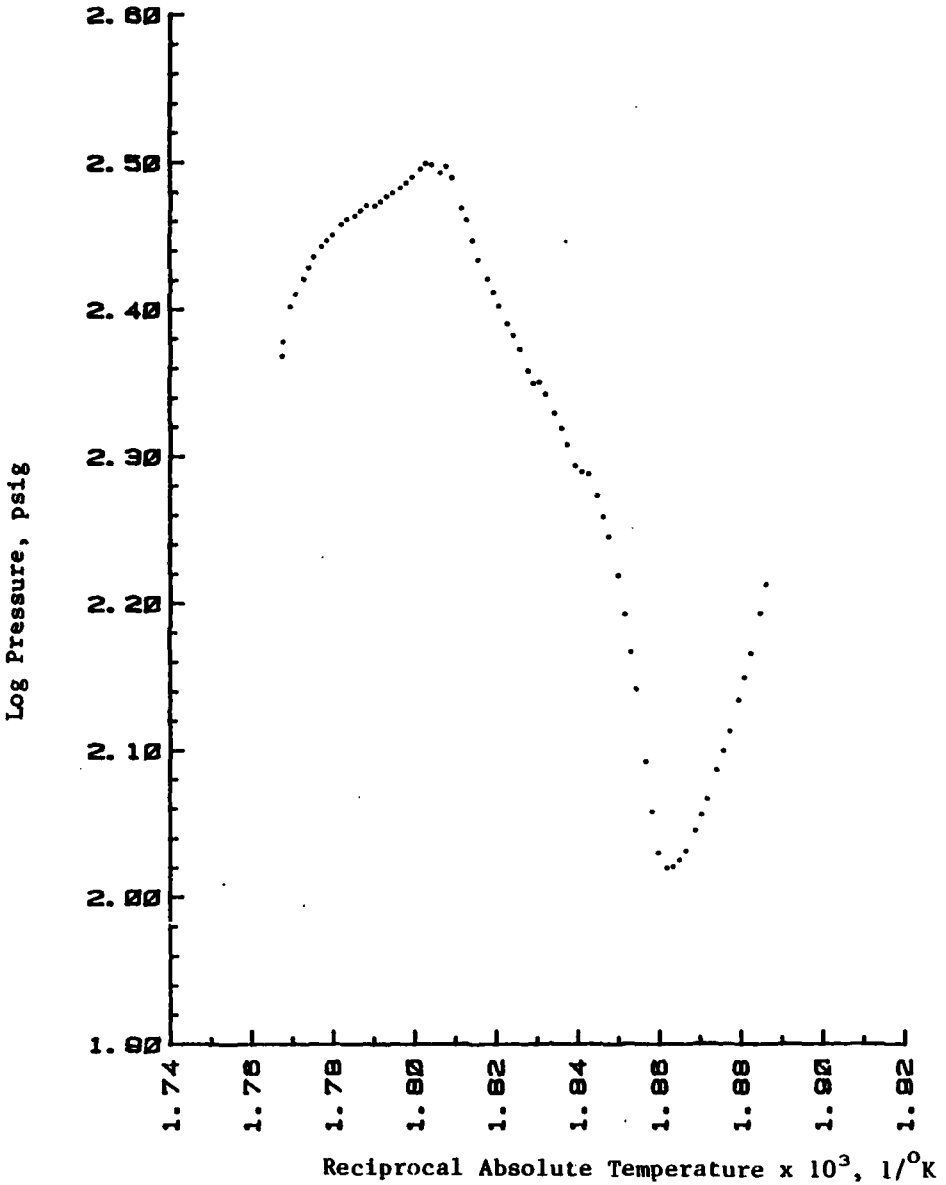

Figure 46. Log Pressure Versus 1/T Plot for the Third Elevated Temperature Exotherm Detected During the ARC Analysis of Cell No. I-3 (Lithium Limited)

Table 35. Summary of the Three Peaks Observed in the Third Elevated Temperature Exotherm of Cell No. I-3 (Lithium Limited)

	Peak Number		
	1	2	3
Initial Temperature, °C	256.6	265.1	280.6
Initial Pressure, psig	174.9	114.3	310.7
Initial Temp. Rate, °C/min	0.133	0.110	0.149
Final Temperature, °C	265.1	279.7	292.8
Final Pressure, psig	114.3	308.1	233.2
Max. Temperature Rate, °C/min	0.236	0.629	0.253
Max. Pressure Rate, psig/min	1.9	7.1	1.0
Adiabatic Temperature Rise, °C	8.5	14.6	12.2
ΔH, cal	102	174	146
Pressure Change, psig	-60.6	193.8	-77.5
Activation Energy, kcal/mole	39.9	290.0	118.4
Reaction Order	0.1	2.0	1.4
Projected Temperature Rise for Li/SO_2 "D" Cell, °C	17.2	29.6	24.7

Cell No. II-3 (Coulombically Balanced)

This cell gave no exotherms during the electrical phase of testing. During the final heat and search operation, the cell leaked at about 165°C. The leakage led to instrumentation problems which made further testing of this cell impossible. The two small exotherms detected below 165°C are summarized in Table 36. Because these exotherms are so small, no data plots have been made.

Cell No. III-3 (Excess Carbon)

This cell gave no exotherms during the electrical phase of testing. During the final heat and search operation, a total of three exotherms were detected, as summarized in Table 37. The first two exotherms were small, but the third was significant. The data plots for the third exotherm are given in Figures 47 through 50. The log temperature rate versus 1/T plot (Figure 48) shows that this exotherm is composed of five individual reactions (peaks) as summarized in Table 38.

Table 36. Summary of Exotherms Detected During the Final Heat and Search Operation of Cell No. II-3 (Coulombically Balanced)

	Exotherm No. 1	Exotherm No. 2
Initial Temperature, °C	84.37	102.26
Initial Pressure, psig	40.1	50.7
Initial Temperature Rate, °C/min	0.025	0.196
Final Temperature, °C	84.44	106.42
Final Pressure, psig	40.4	60.1
Maximum Temperature Rate, °C/min	0.025	0.196
Temperature Rise, °C	0.07	4.16
Pressure Change, psig	0.3	9.4
Time Duration of Exotherm, min	13.1	50.4
ΔH, cal	0.9	52.0
Projected Final Temperature for Li/SO_2 "D" Cell, °C	84.5	110.1
Projected Temperature Rise for Li/SO_2 "D" Cell, °C	0.13	7.9

Table 37. Summary of Exotherms Detected During the Final Heat and Search Operation of Cell No. III-3 (Excess Carbon)

	Exotherm Number		
	1	2	3
Initial Temperature, °C	52.14	118.04	156.29
Initial Pressure, psig	43.9	88.4	124.3
Initial Temp. Rate, °C/min	0.038	0.058	0.322
Final Temperature, °C	57.40	123.46	338.87
Final Pressure, psig	48.70	90.2	464.8
Max. Temperature Rate, °C/min	0.038	0.058	2.13
Max. Pressure Rate, psig/min	-	-	5.9
Temperature Rise, °C	5.26	5.42	182.58
Pressure Change, psig	4.8	1.8	350.5
Time Duration of Exotherm, min	218	213	646
ΔH, cal	56.8	58.5	1971
Projected Final Temperature for Li/SO_2 "D" Cell, °C	65.0	131.3	602.4
Projected Temperature Rise for for Li/SO_2 "D" Cell, °C	12.8	13.2	446.1

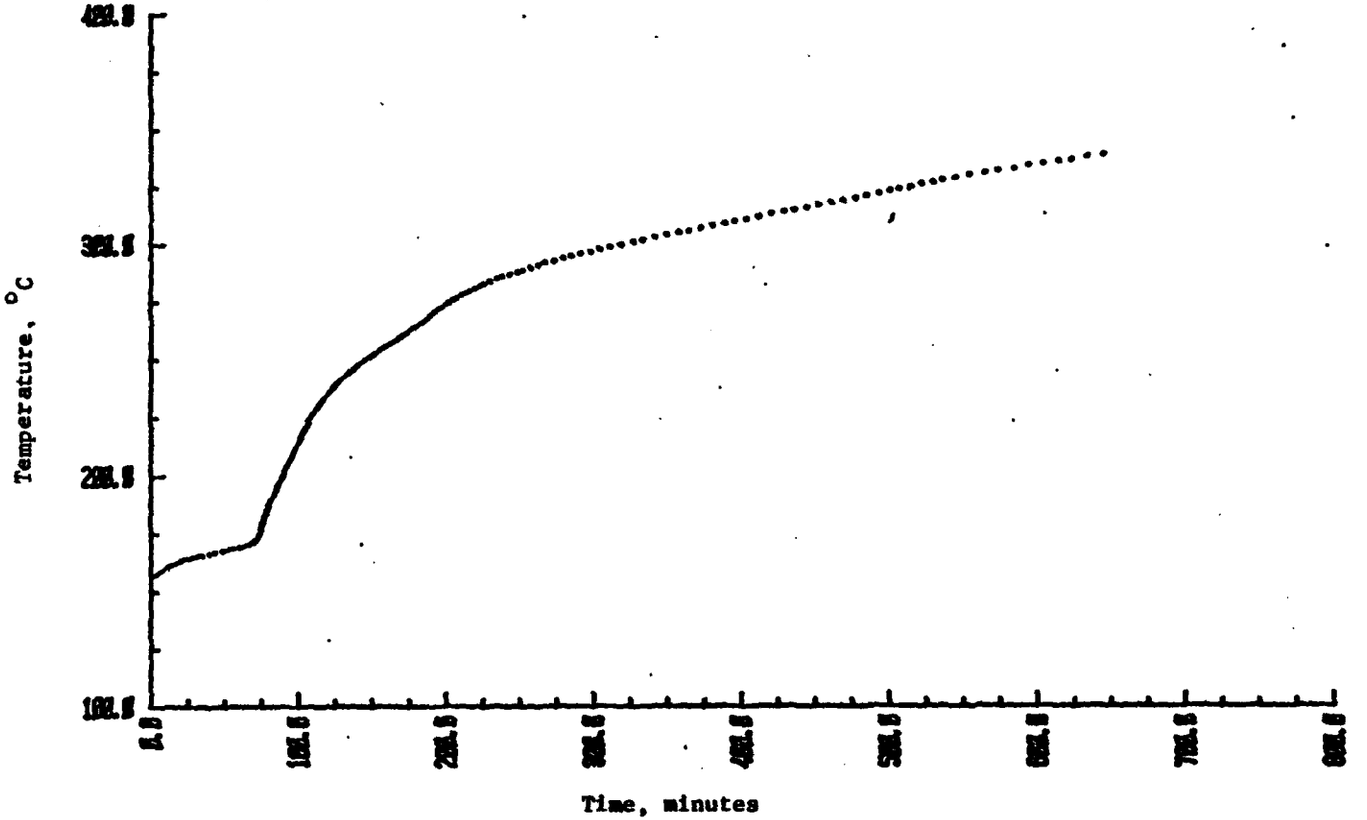

Figure 47. Temperature Versus Time Plot for the Third Elevated Temperature Exotherm Detected During the ARC Analysis of Cell No. III-3 (Excess Carbon)

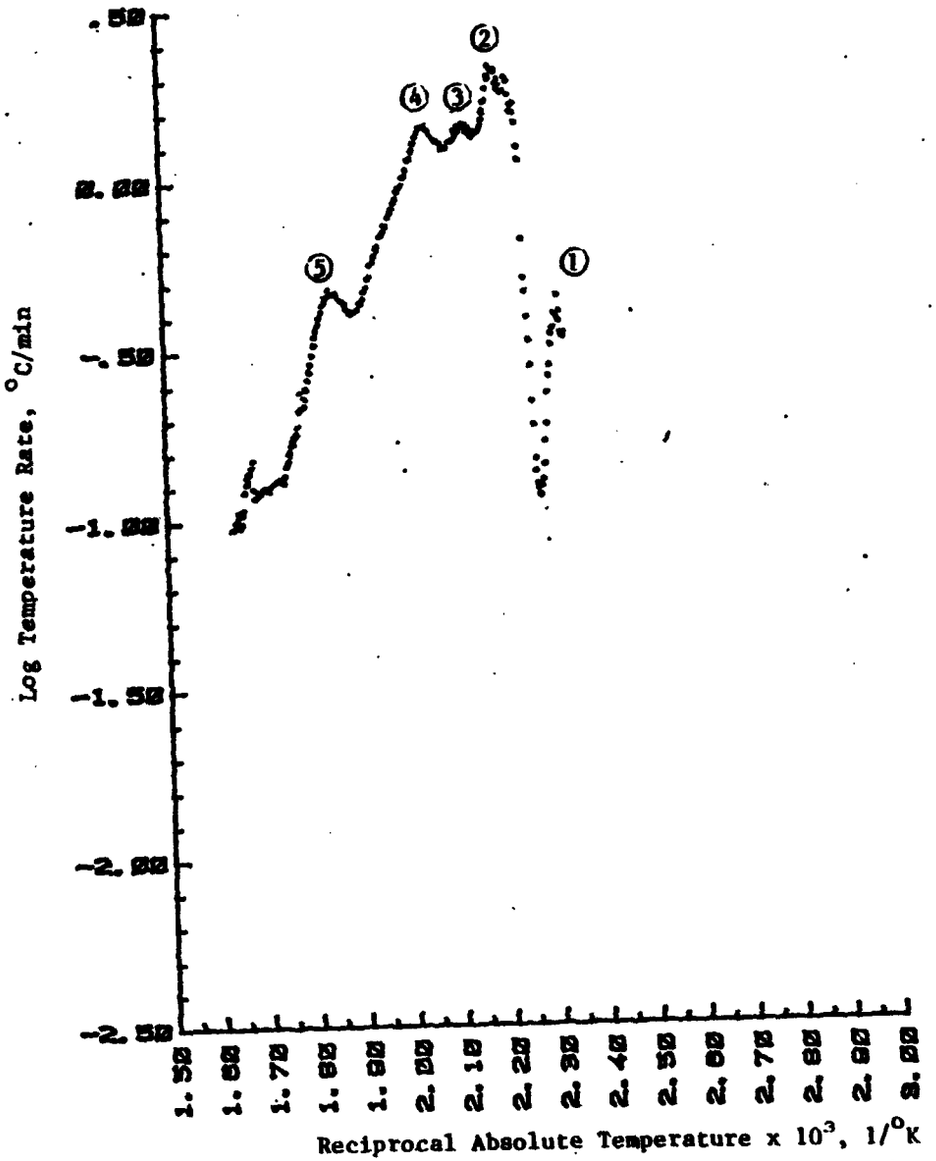

Figure 48. Log Temperature Rate Versus 1/T Plot for the Third Elevated Temperature Exotherm Detected During the ARC Analysis of Cell No. III-3 (Excess Carbon)

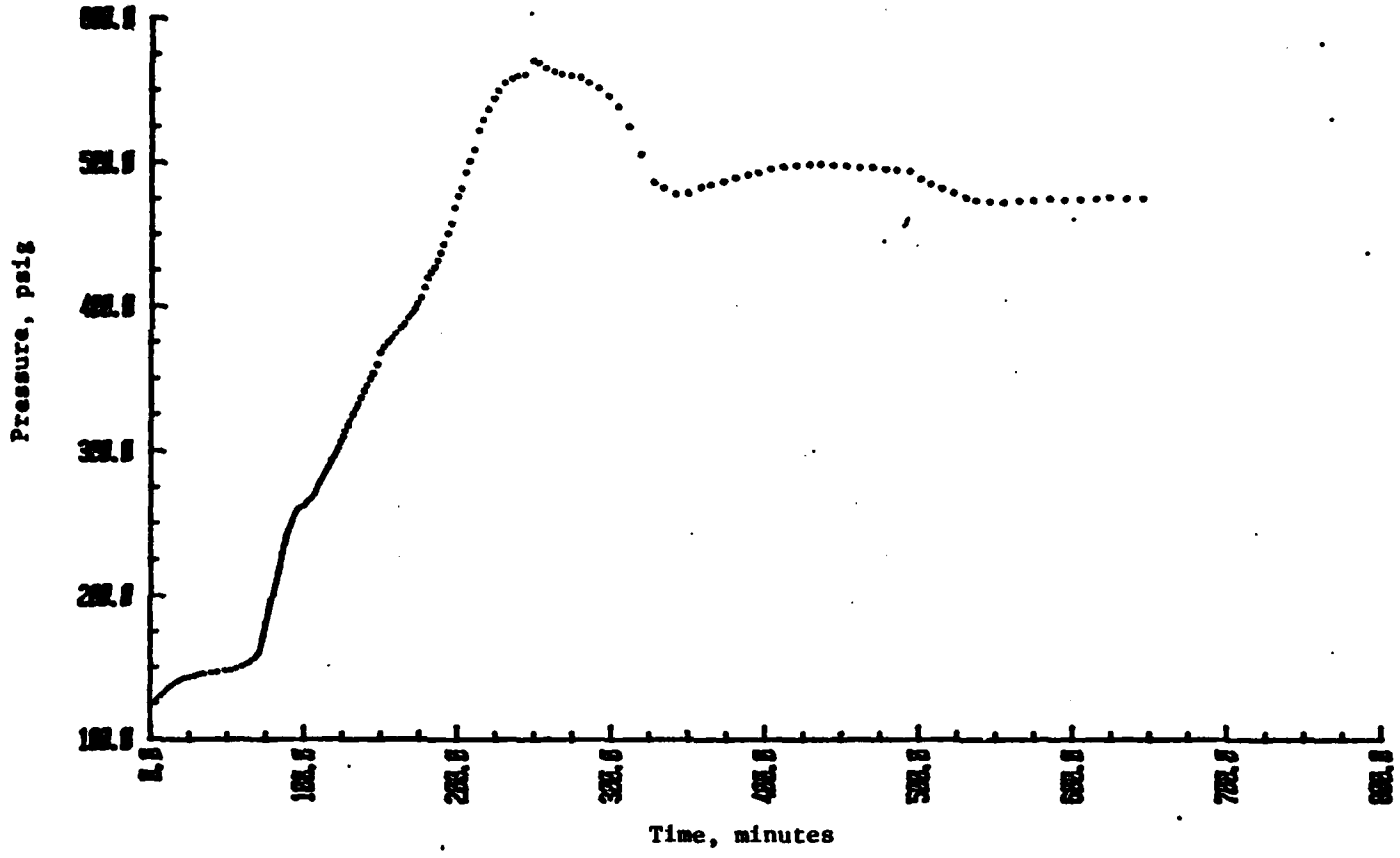

Figure 49. Pressure Versus Time Plot for the Third Elevated Temperature Exotherm Detected During the ARC Analysis of Cell No. III-3 (Excess Carbon)

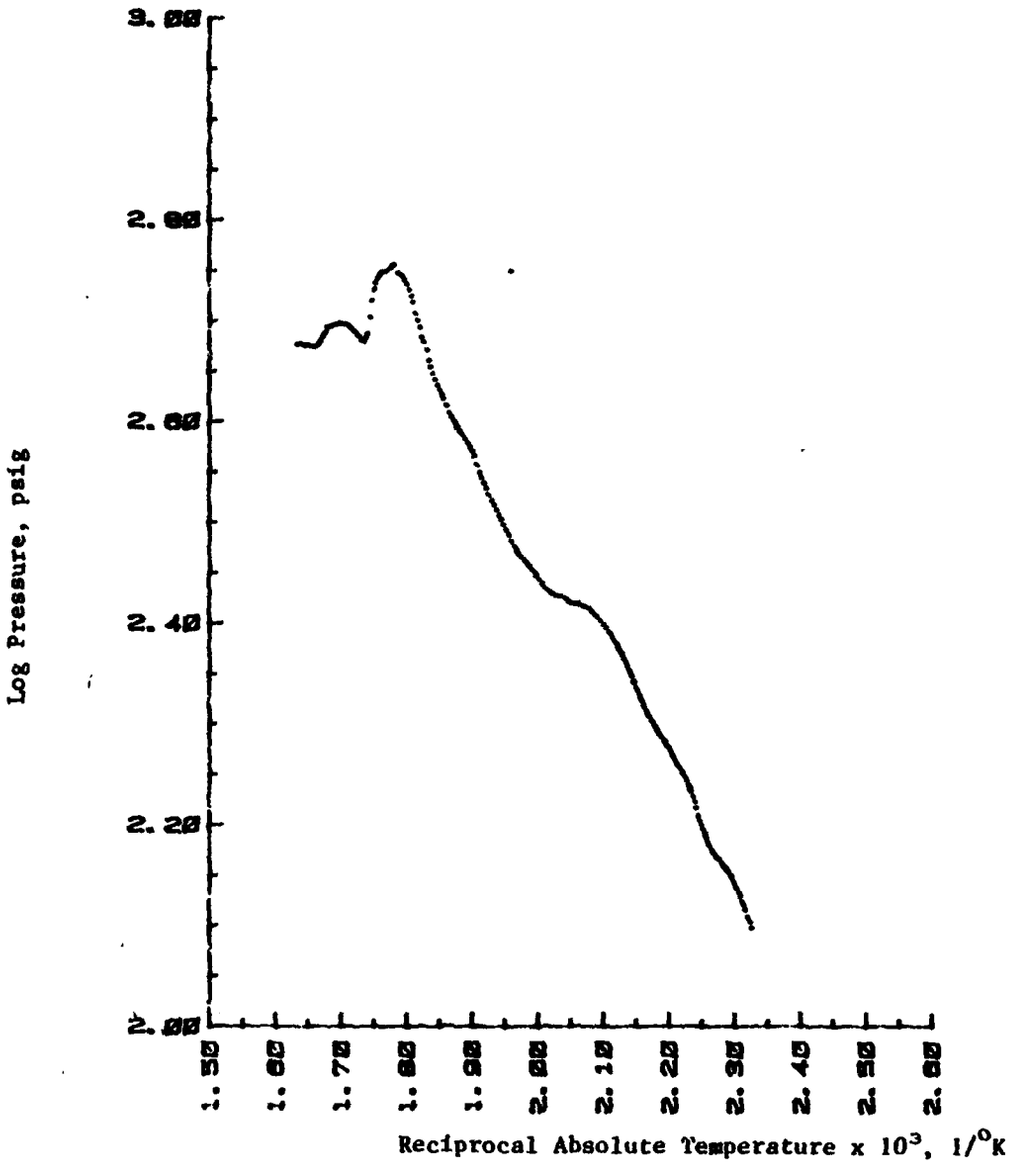

Figure 50. Log Pressure Versus 1/T Plot for the Third Elevated Temperature Exotherm Detected During the ARC Analysis of Cell No. III-3 (Excess Carbon)

Table 38. Summary of the Five Peaks Detected During Elevated Temperature Testing of Cell No. III-3 (Excess Carbon)

	1	2	3	4	5
Initial Temperature, °C	156.3	166.8	189.7	206.6	254.7
Initial Pressure, psig	124.3	147.3	210.2	257.7	378.1
Initial Temp. Rate, °C/min	0.322	0.115	1.376	1.223	0.407
Final Temperature, °C	166.8	189.7	206.6	254.7	300.9
Final Pressure, psig	147.3	210.2	257.7	378.1	485.7
Max. Temp. Rate, °C/min	0.446	2.135	1.453	1.418	0.467
Max. Pressure Rate, psig/min	1.4	5.9	5.3	2.7	3.8
Adiabatic Temp. Rise, °C	10.5	22.9	16.9	48.1	46.2
ΔH, cal	113	247	182	519	499
Pressure Change, psig	23.0	62.9	47.5	120.4	107.6
Activation Energy, kcal/mole	45.7	200.0	9.5	9.0	17.3
Reaction Order	0.9	1.6	0.2	0.7	1.0
Projected Temperatur Rise for Li/SO_2 "D" Cell, °C	25.6	56.0	41.3	118	113

Cell No. IV-3 (Excess Lithium)

This was the only cell in the group to give an exotherm during resistive overdischarge. This exotherm, however, was very significant, as shown in Table 39, causing the cell temperature to rise to 328°C, at which point the cell leaked.

Figures 51 through 54 show the data plots for this exotherm. The log temperature rate versus 1/T plot (Figure 52) clearly shows that this exotherm is actually composed of seven individual reactions (peaks) as summarized in Table 40.

Table 39. Summary of Exotherm Detected During Resistive Overdischarge Testing of Cell No. IV-3 (Excess Lithium)

Initial Temperature, ^{o}C	29.24
Initial Pressure, psig	13.3
Initial Temperature Rate, $^{o}C/min$	0.078
Final Temperature, ^{o}C	327.81
Final Pressure, psig	233.2
Maximum Temperature Rate, $^{o}C/min$	0.545
Maximum Pressure Rate, psig/min	3.66
Temperature Rise, ^{o}C	298.6
Pressure Change, psig	219.9
Time Duration of Exotherm, min	1948
ΔH, cal	3559
Projected Final Temperature for Li/SO_2 "D" Cell, ^{o}C	613
Projected Temperature Rise for Li/SO_2 "D" Cell, ^{o}C	584

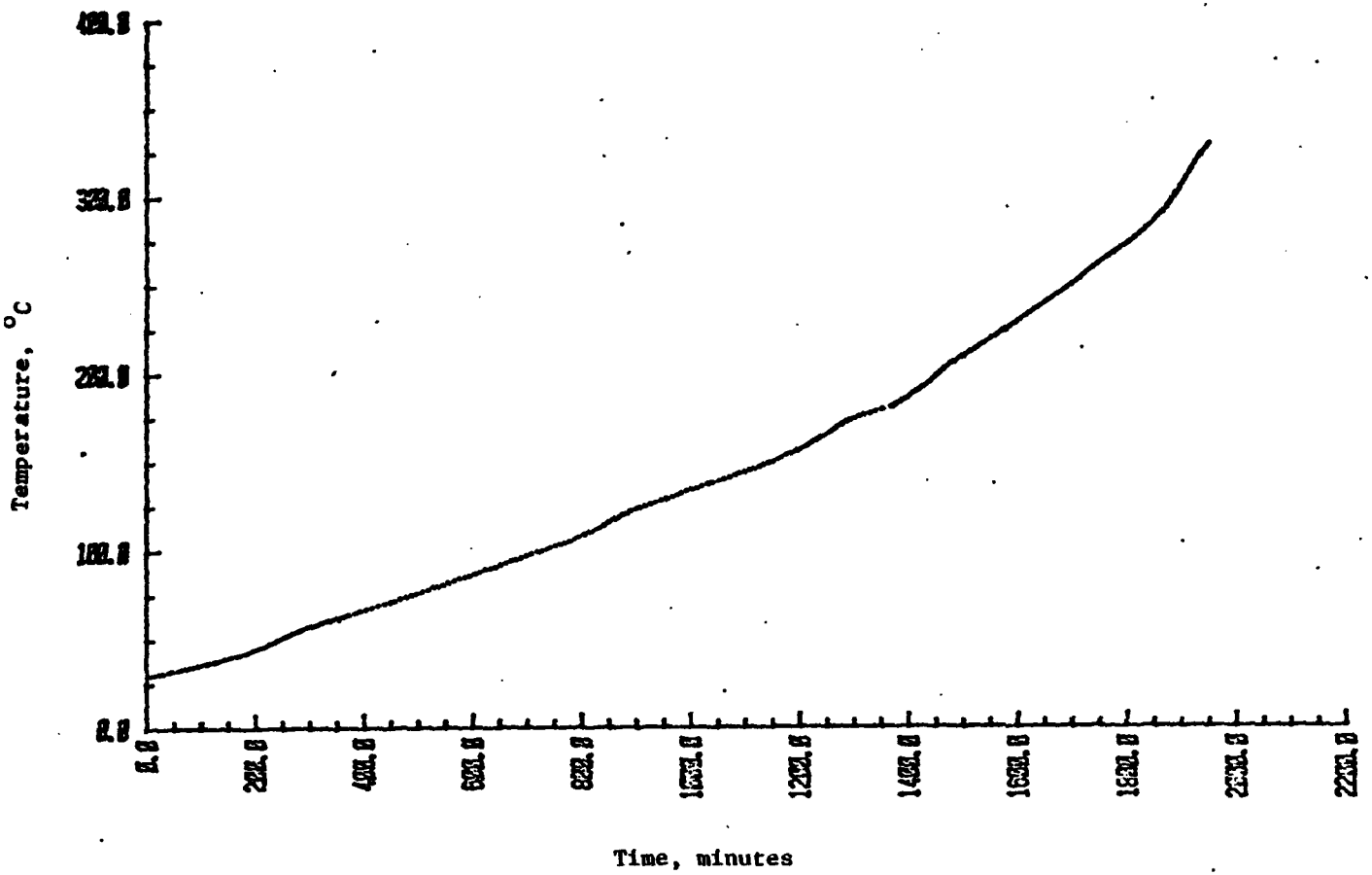

Figure 51. Temperature Versus Time Plot for the Exotherm Detected During Resistive Overdischarge Testing of Cell No. IV-3 (Excess Lithium)

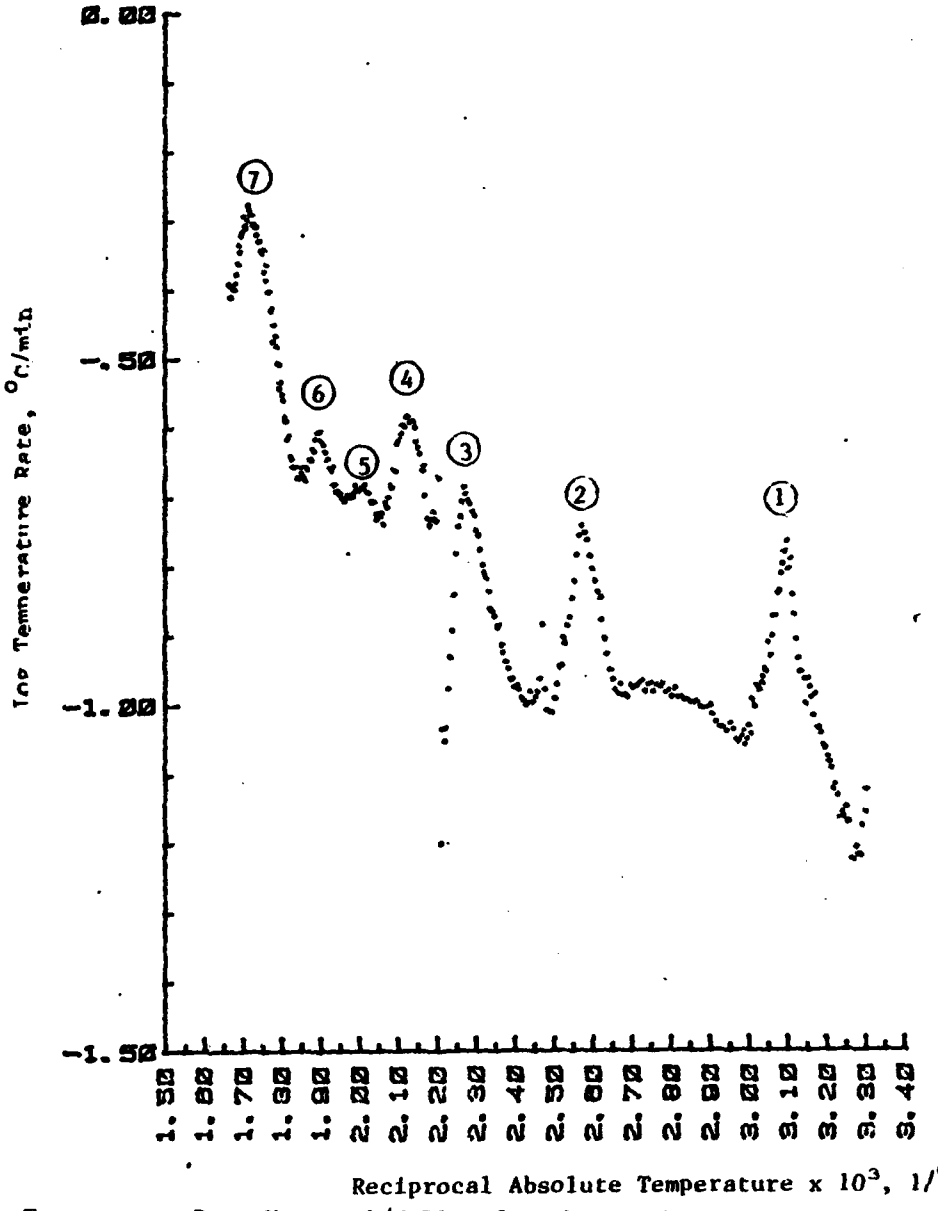

Figure 52. Log Temperature Rate Versus 1/T Plot for the Exotherm Detected During Resistive Overdischarge Testing of Cell No. IV-3 (Excess Lithium)

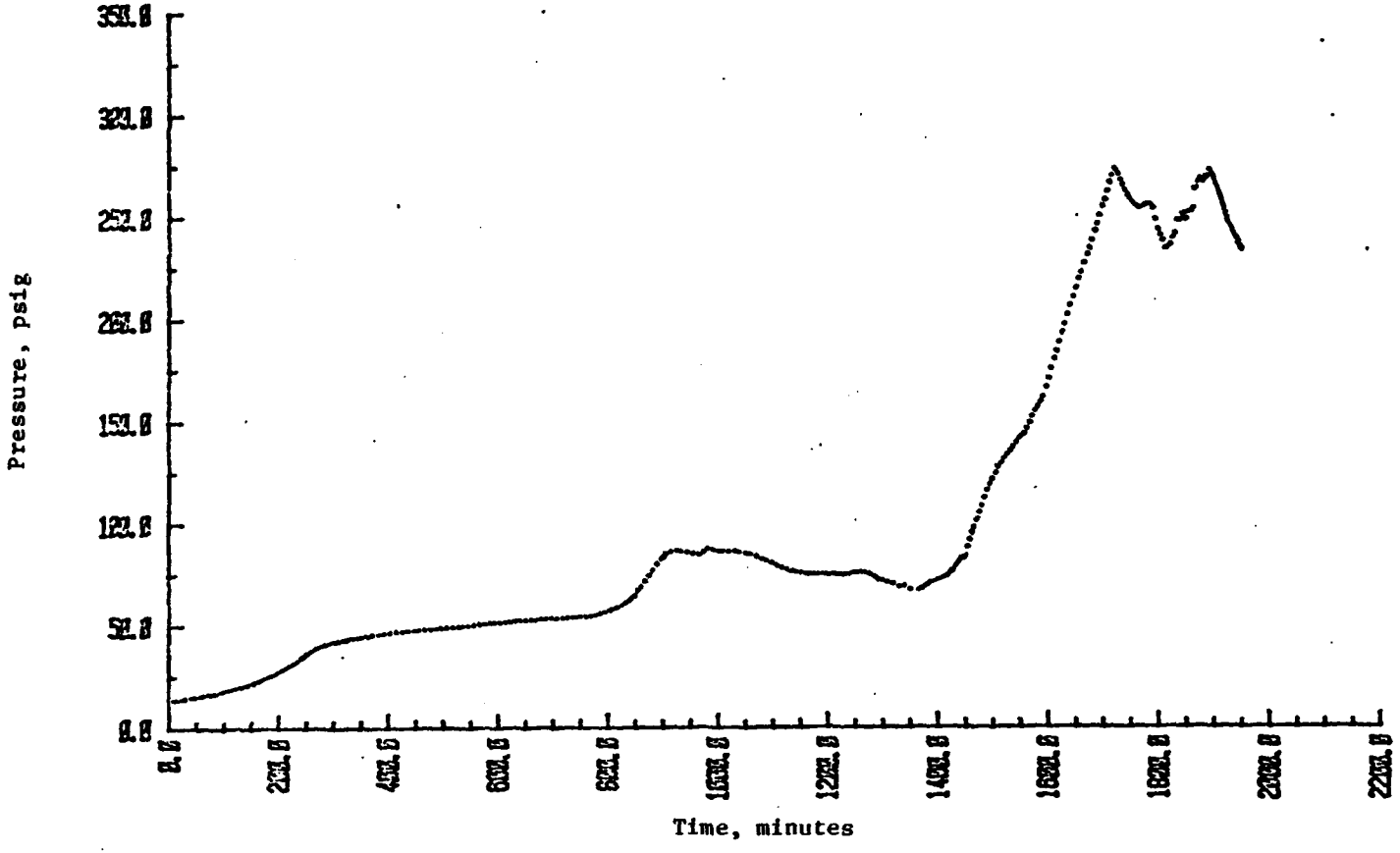

Figure 53. Pressure Versus Time Plot for the Exotherm Detected During Resistive Overdischarge of Cell No. IV-3 (Excess Lithium)

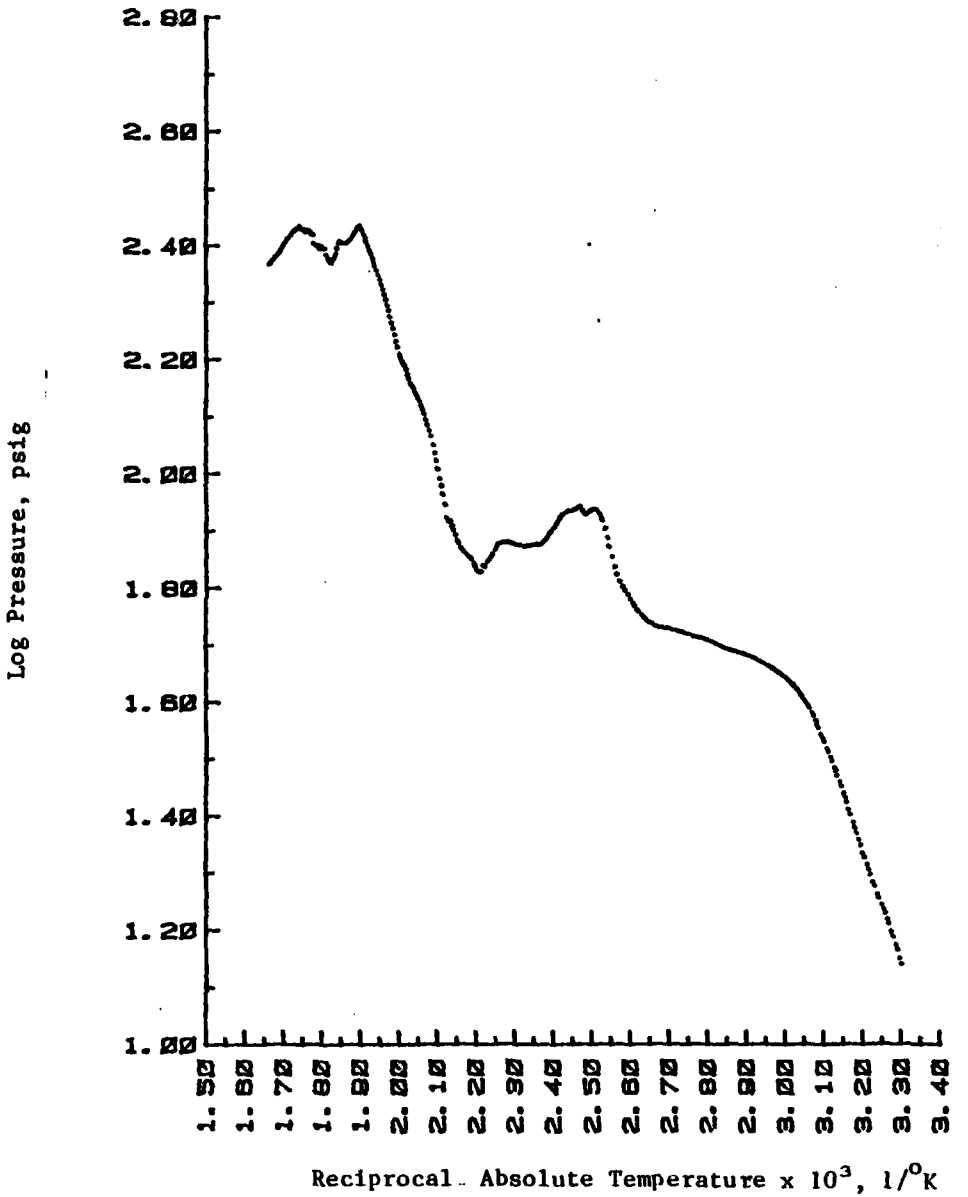

Figure 54. Log Pressure Versus 1/T Plot for the Exotherm Detected During Resistive Overdischarge of Cell No. IV-3 (Excess Lithium)

Table 40. Summary of the Seven Peaks Observed in the Exotherm Detected During the Resistive Overdischarge Testing of Cell No. IV-3 (Excess Lithium)

	Peak Numbers						
	1	2	3	4	5	6	7
Initial Temperature, °C	33.2	102.5	139.2	185.5	216.3	238.1	270.5
Initial Pressure, psig	16.5	54.1	85.0	71.8	138.1	212.6	250.3
Initial Temp. Rate, °C/min	0.060	0.104	0.100	0.182	0.186	0.198	0.213
Final Temperature, °C	61.44	128.2	179.8	216.3	238.1	270.5	327.0
Final Pressure, psig	44.4	85.5	67.1	138.1	212.6	250.3	233.8
Max. Temp. Rate, °C/min	0.172	0.180	0.206	0.260	0.206	0.248	0.528
Max. Pressure Rate,psig/min	0.23	0.41	0.05	1.42	0.97	0.98	3.6
Adiabatic Temp.Rise, °C	28.2	25.7	40.6	30.8	21.8	32.4	56.5
ΔH, cal	336	306	484	367	260	386	673
Pressure Change, psig	27.9	31.4	-17.9	66.3	74.5	37.7	-16.5
Activation Energy,kcal/mole	26.0 ±	14.5	10.2	20.2	8.4	23.0	20.2
Reaction Order	1.4	0.6	0.2	0.8	0.2	0.2	0.5
Projected Temp. Rise for Li/SO_2 "D" Cell, °C	55.2	50.3	79.4	60.3	42.6	63.4	110

Group D Tests

Low Temperature Testing

Group D Tests

Objective

The objective of the Group D tests was to evaluate the thermal behavior of Li/SO_2 cells when discharged and reverse discharged at low temperatures.

Experimental

These tests were conducted galvanostatically at $-35^{\circ}C$ employing a current density of 3 mA/cm^2. These conditions were selected so as to simulate the tests conducted at NASA Langley[1] on Mallory L026HS cells where explosions were observed when the cells were allowed to warm up to room temperature following reverse discharge at low temperatures.

Because the ARC instrument does not have subambient capabilities, the electrical testing (i.e., discharge and reverse testing) was carried out in an environmental chamber. The cells were first connected to the calorimeter in the normal manner and the entire calorimeter lid assembly placed in the environmental chamber. The cells were allowed to equilibrate at the test temperature several hours before the testing was started. During the tests, the cell potentials were continuously recorded on a strip chart recorder.

The construction features of the two Group D cells are summarized in Table 41. Both cells tested were of the coulombically balanced design.

Discharge Performance

The discharge performance of the two Group D cells is summarized in Table 42 while Table 43 summarizes the component ratios present at the 2.0 volt cutoff. The reverse discharge testing that was conducted on Cell No. II-6 is summarized in Table 44.

Thermal Behavior

Both Group D cells gave exotherms during the final heat and search operation. These exotherms were significantly greater than those observed in the previous cells, both with respect to temperature rates, pressure rates, and final pressure values.

Table 41. Construction Features of the Group D Cells

Cell No.	Li/SO_2 Ratio	SO_2/C Ratio	Li/C Ratio	Electrolyte Quantity, gm	Cathode Surface Area, cm^2	Thermal Inertia Value, ϕ
II-5	1.00	1.13	1.13	6.28	68.64	2.25
II-6	0.98	1.13	1.12	6.31	68.64	2.14

Table 42. Discharge Performance to 2.0 Volts for Group D Cells

Cell No.	Current, mA	Run Time, hr	Capacity Delivered, Ah	Average Voltage, V	Discharge Efficiency, %		
					Anode	Carbon	SO_2
II-5	206	2.11	0.434	2.24	24.3	27.5	24.3
II-6	206	2.93	0.604	2.29	34.2	38.1	33.6

Table 43. Cell Status at End of Discharge to 2.0 Volt Cutoff

Cell No.	Cell Design	SO_2/Li	SO_2/Li Area, mg/cm^2
II-5	Coulombically Balanced	1.004	47.11
II-6	Coulombically Balanced	1.024	41.49

Table 44. Summary of Reverse Discharge Testing Performed on Cell No. II-6 (Coulombically Balanced)

Time in Reverse, hr	19.2
Current, mA	206
[1] Degree of Reverse Discharge, %	220

(1) Based on original SO_2 capacity

Cell No. II-5 (Coulombically Balanced)

This cell was discharged to 2.0 volts at -35°C at a rate of 3 mA/cm^2 and then subjected to an ARC analysis. This, therefore, represents the first cell evaluated in an ARC analysis with no prior overdischarge testing. Because of the significant quantities of lithium remaining at the start of the ARC testing and the absence of any overdischarge products, the results obtained with this cell can be more easily interpreted, at least in terms of postulating reactions than other cells subjected to a more complex test schedule.

During the ARC testing, a significant exotherm was detected at 112°C which caused the cell temperature to rise to 337°C, at which point the cell leaked. Table 45 summarizes the characteristics of this exotherm while the data plots are shown in Figures 55 through 58. The high heating rates, pressure rates, and pressure rise show that this exotherm constitutes a substantial hazard.

The log temperature rate versus 1/T plot (Figure 56) shows that this exotherm is composed of several individual reactions. The complexity of the data makes it difficult to resolve the individual peaks but for the purpose of analysis, four peaks have been identified, as labeled in Figure 56. The characteristics of these peaks are summarized in Table 46. To aid in the interpretation of these peaks, a summary of the cell open circuit voltage behavior as a function of temperature during the ARC analysis is given in Table 47.

The stable open circuit voltage indicates that the sharp peak initiating at 159°C does not involve the anode. Because there are no overdischarge products present, this peak is postulated to be the thermal decomposition of dithionite. The sharp voltage transitions to zero volts observed between 209 and 218°C most likely represent momentary short circuits caused by melting of the polypropylene separator material. It is quite possible that the region between 159°C and 238°C (i.e., peaks 2 and 3) represents a single reaction where the observed inflections are caused by disruptions in the cell brought about by degradation of the separator material. The peak initiating at 238°C appears to involve the anode as evidenced by the continuously declining open circuit potential. This is, therefore, postuated to be the reaction between lithium metal and the electrolyte solution.

Table 45. Summary of Exotherm Detected During the Heat and Search Testing of Cell No. II-5 (Coulombically Balanced)

Initial Temperature, °C	93.74
Initial Pressure, psig	115.1
Initial Temperature Rate, °C/min	0.022
Final Temperature, °C	336.78
Final Pressure, psig	1550.8
Maximum Temperature Rate, °C/min	17.7
Maximum Pressure Rate, psig/min	245
Temperature Rise, °C	243.0
ΔH, cal	3006
Pressure Change, psig	1435.7
Projected Final Temperature for Li/SO_2 "D" Cell, °C	569
Projected Temperature Rise Li/SO_2 "D" Cell, °C	475

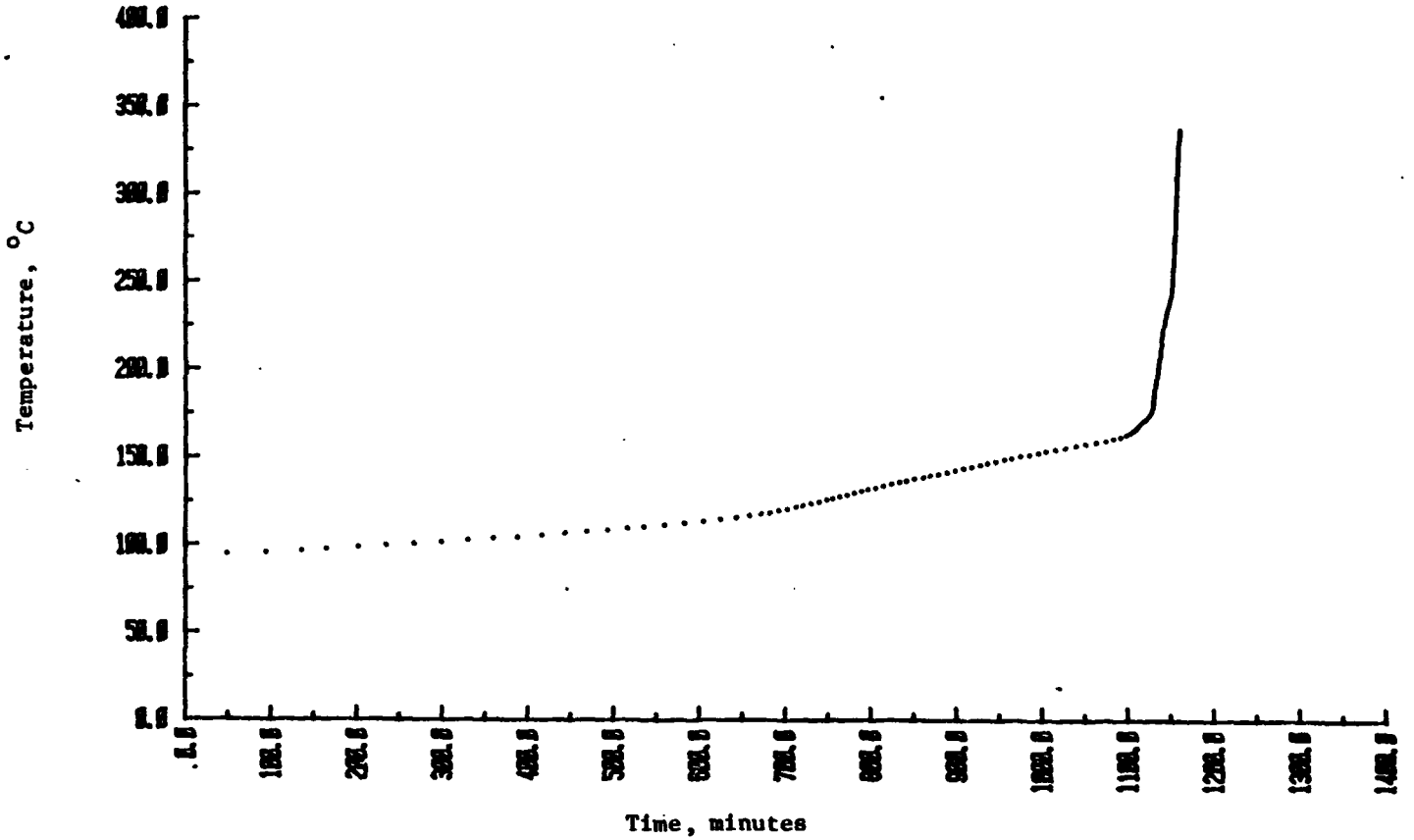

Figure 55. Temperature Versus Time Plot for the Exotherm Detected During the ARC Analysis of Cell No. 11-5 (Coulombically Balanced)

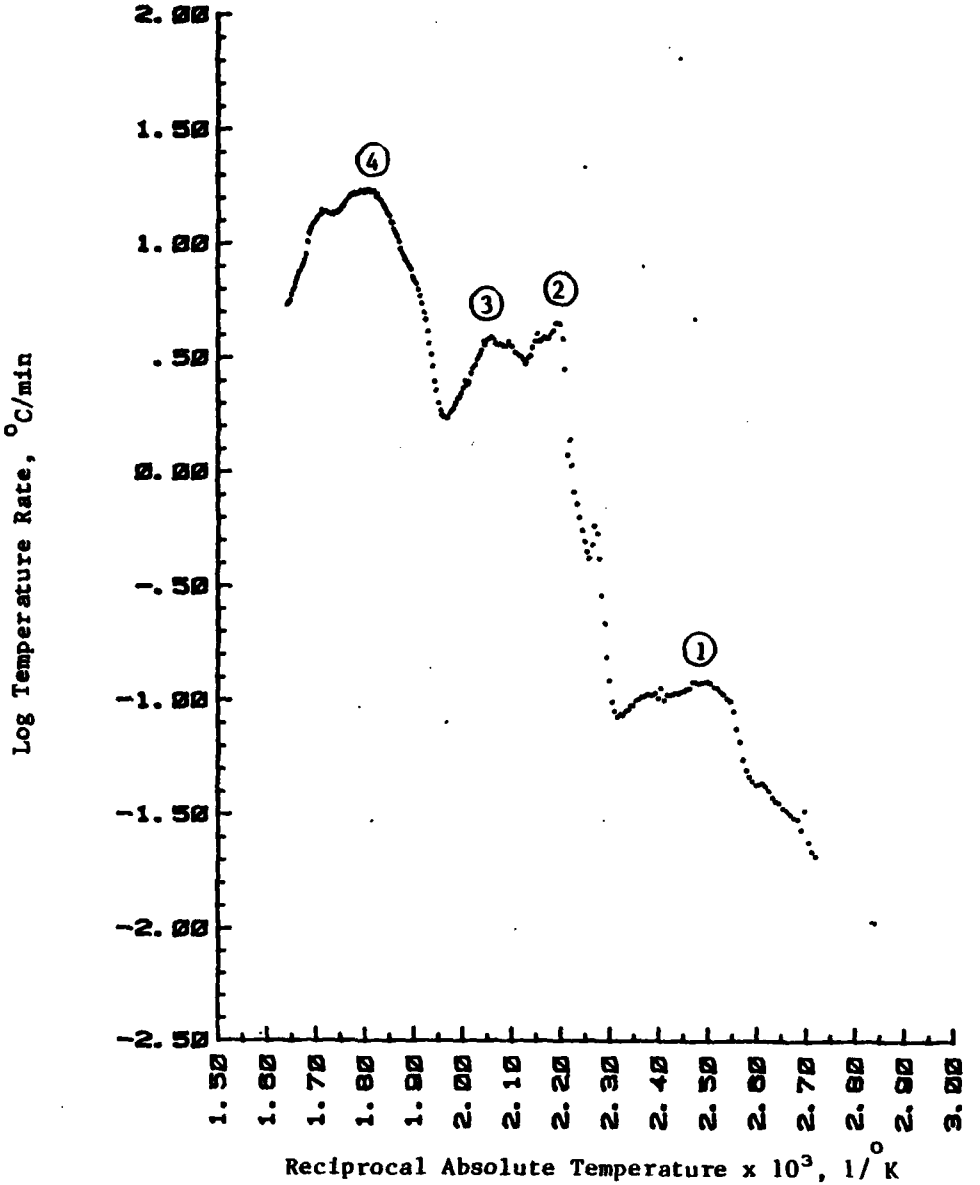

Figure 56. Log Temperature Rate Versus 1/T for the Exotherm Detected During the ARC Analysis of Cell No. II-5 (Coulombically Balanced)

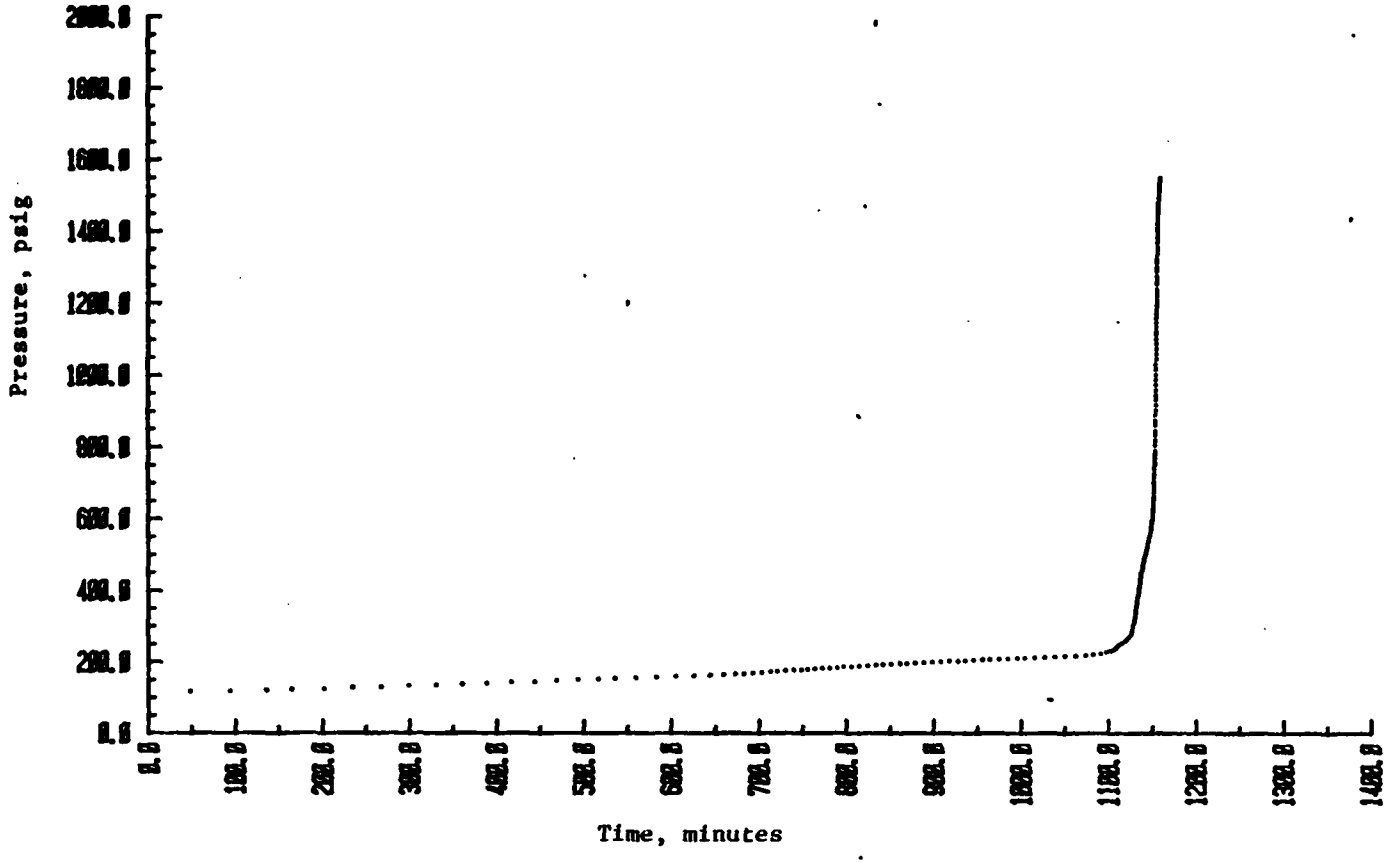

Figure 57. Pressure Versus Time Plot for the Exotherm Detected During the ARC Analysis of Cell No. II-5 (Coulombically Balanced)

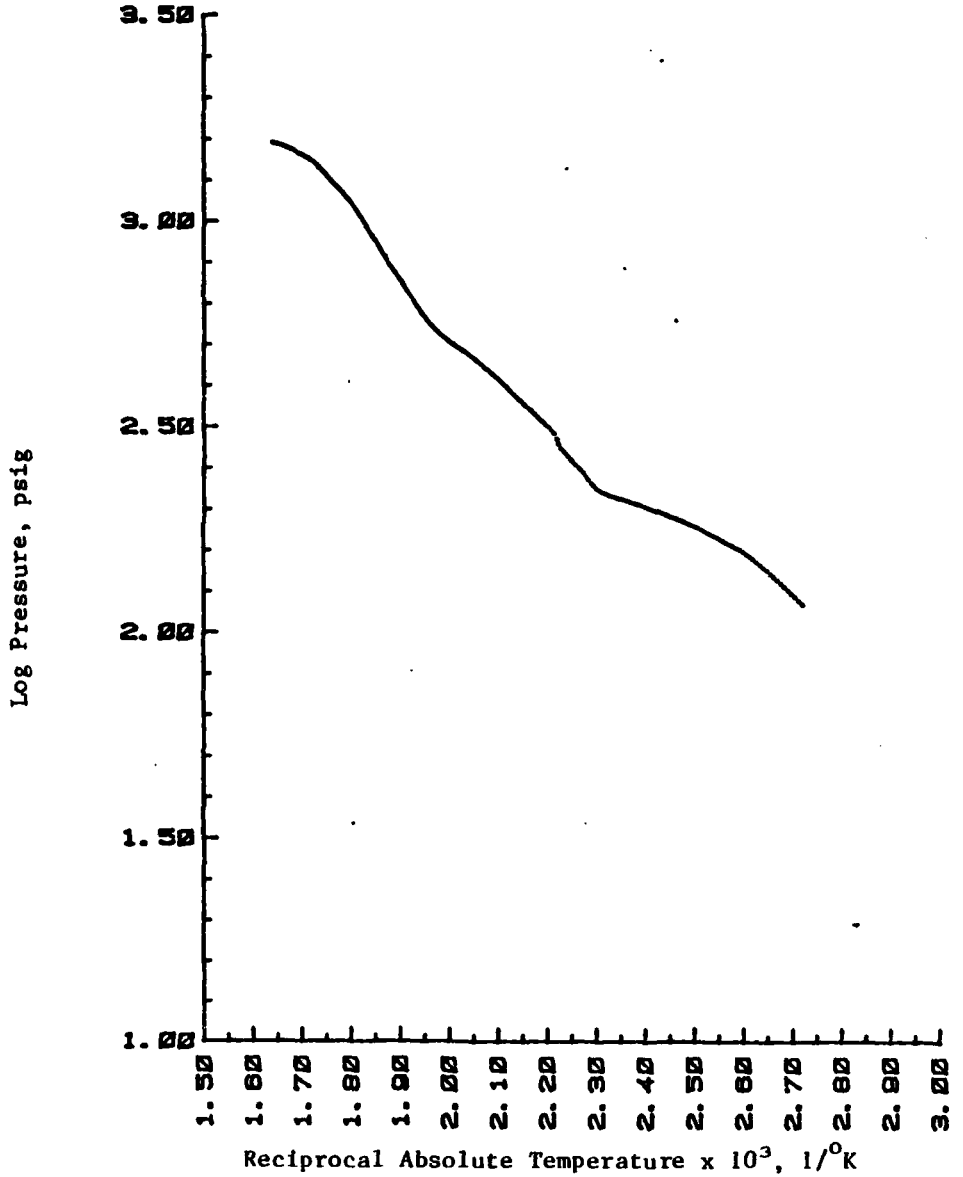

Figure 58. Log Pressure Versus 1/T Plot for the Exotherm Detected During the ARC Analysis of Cell No. II-5 (Coulombically Balanced)

Table 46. Summary of the Four Peaks Detected During the ARC Analysis of Cell No. II-5 (Coulombically Balanced)

	Peak Number			
	1	2	3	4
Initial Temperature, °C	111.8	159.1	197.0	237.6
Initial Pressure, psig	156.9	218.6	384.6	567.0
Initial Temperature Rate, °C/min	0.043	0.086	2.992	1.775
Final Temperature, °C	132.7	197.0	237.6	336.8
Final Pressure, psig	188.4	384.6	567.0	1550.8
Maximum Temperature Rate, °C/min	0.119	4.465	3.969	17.721
Maximum Pressure Rate, psig/min	0.18	19.6	18.3	245.0
Adiabatic Temperature Rise, °C	20.9	37.9	40.6	99.2
ΔH, cal	258	469	502	1227
Pressure Change, psig	31.5	166.0	182.4	983.8
Activation Energy, kcal/mole	46.4	117.4	12.0	64.1
Reaction Order	1.0	1.5	0.6	1.0
Projected Temperature Rise for Li/SO_2 "D" Cell, °C	40.9	74.2	79.4	194.1

Table 47. Summary of Cell Open Circuit Voltage Behavior During Final ARC Testing of Cell No. II-5 (Coulombically Balanced)

Temperature Interval, °C From	To	Cell Voltage Behavior
Start of Test	159	Voltage stable - slowly dropping from 2.96V to 2.92V
159	166	Voltage noisy (0.05 volt transients) - voltage slowly dropping from 2.92v to 2.85V
166	178	Voltage stable - slowly dropping from 2.85V to 2.78V
178	181	Voltage rapidly oscillating between 2.75V and 2.92V
181	209	Voltage stable - slowly dropping to 2.66V
209	213	Voltage drops sharply to zero volts and remains there for approximately 1.2 minutes. Recovers to 2.38V
216	218	Voltage drops sharply to zero volts and remains there for approximately 0.1 minutes. Recovers to 2.35V
218	241	Voltage stable - slowly drops to 2.07V
241	297	Voltage dropping steadily to zero volts (requires approx. 6 minutes to reach zero volts)
297	337	Negative voltage transients of up to -1.5 volts
337	-	Cell leaks

Cell No. II-6 (Coulombically Balanced)

The testing of this cell involved discharge and reverse discharge at -35°C at a rate of 3 mA/cm^2. The subsequent ARC testing yielded some extremely interesting results which give perspective to the results obtained with the cells from Groups A, B, and C.

Exothermic behavior was initially detected at 77.5°C leading to a 213°C temperature rise. The cell finally leaked at 291°C. Table 48 summarizes the characteristics of this exotherm while the data plots are shown in Figures 59 through 62. At approximately 108°C, a very violent reaction occurred. Fortunately, the cell hardware remained intact, thus allowing temperature and pressure data to be obtained. The magnitude of this reaction can be more fully appreciated from the maximum temperature and pressure rates observed; 200°C/min and 1730 psig/min., respectively. These results clearly demonstrate that low temperature reverse discharge of Li/SO_2 cells represents a significant explosion hazard.

The overall exotherm for this cell has been broken into four individual reactions, as labeled in Figure 60. The characteristics of these reactions are summarized in Table 49. Because the reaction initiating at 108°C was too fast for the instrument to accurately follow, meaningful kinetic parameters could not be determined for this reaction.

Table 48 Summary of Exotherm Detected During the Heat and Search Testing of Cell No. II-6 (Coulombically Balanced)

Initial Temperature, °C	77.48
Initial Pressure, psig	41.1
Initial Temperature Rate, °C/min	0.804
Final Temperature, °C	290.54
Final Pressure, psig	880.6
Maximum Temperature Rate, °C/min	199.5
Maximum Pressure Rate, psig/min	1730
Temperature Rise, °C	213.1
ΔH, cal	2518
Pressure Change, psig	839.5
Projected Final Temperature for Li/SO_2 "D" Cell, °C	474.0
Projected Temperature Rise for Li/SO_2 "D" Cell, °C	396.6

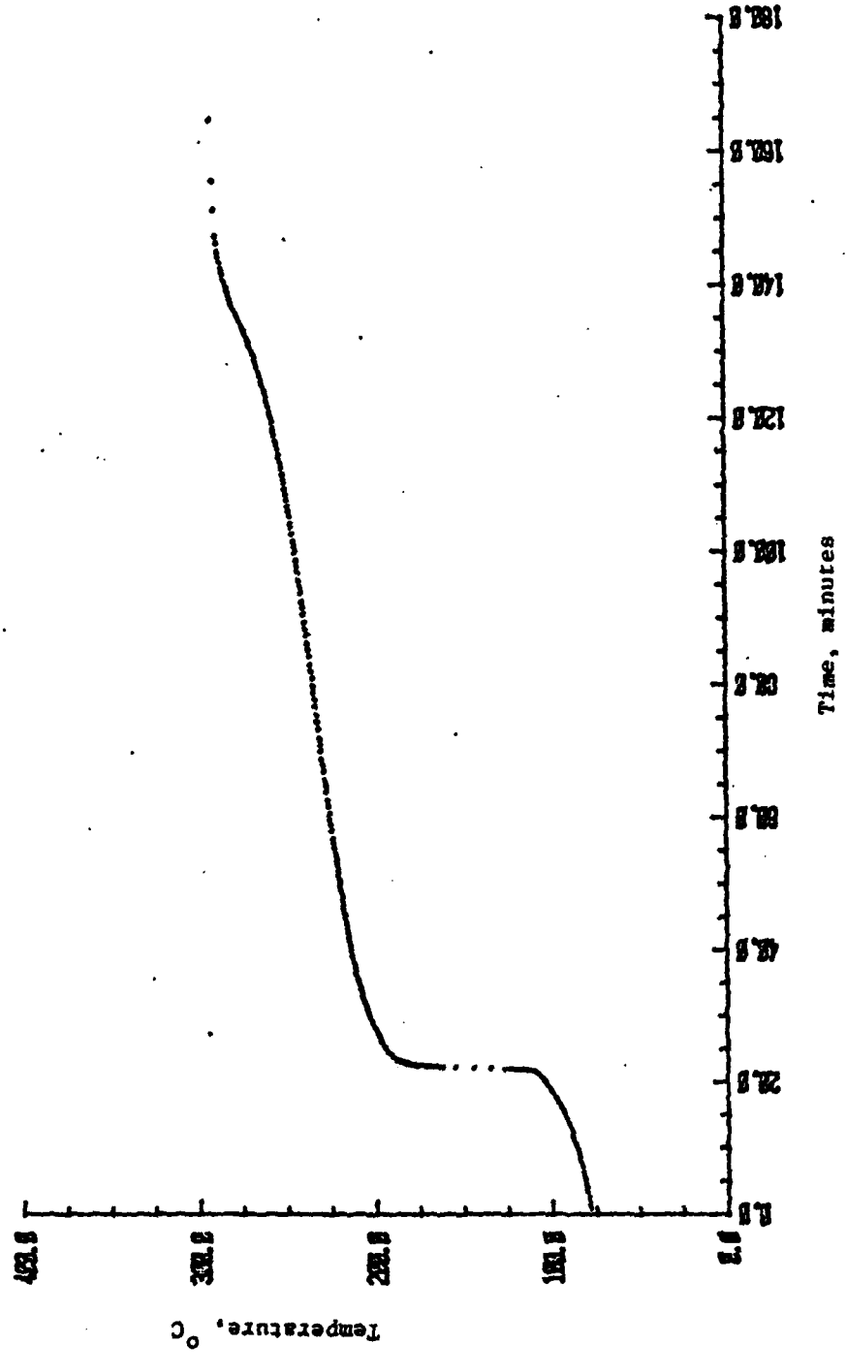

Figure 59. Temperature Versus Time Plot for the Exotherm Detected During the ARC Analysis of Cell No. 11-6 (Coulombically Balanced)

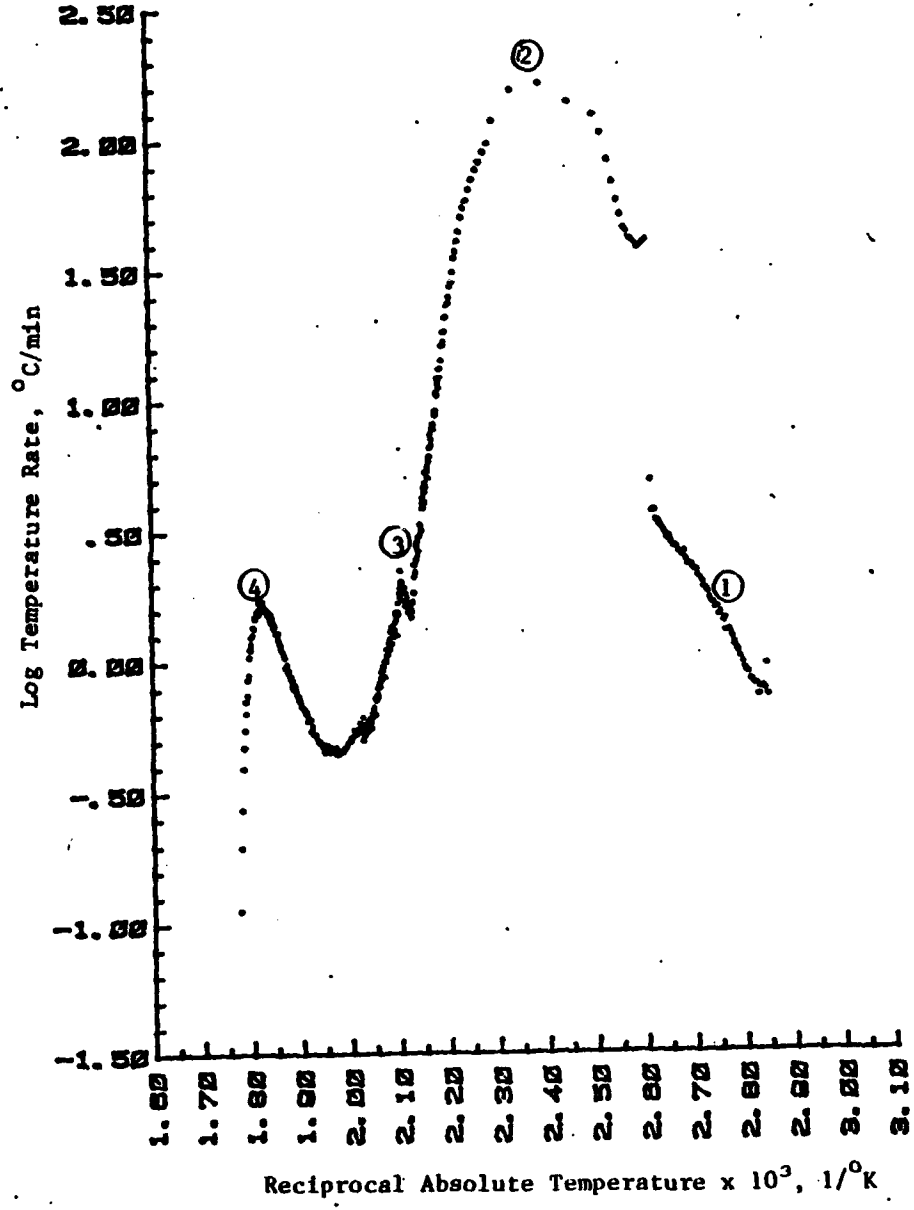

Figure 60. Log Temperature Rate Versus 1/T Plot for the Exotherm Detected During the ARC Analysis of Cell No. II-6 (Coulombically Balanced)

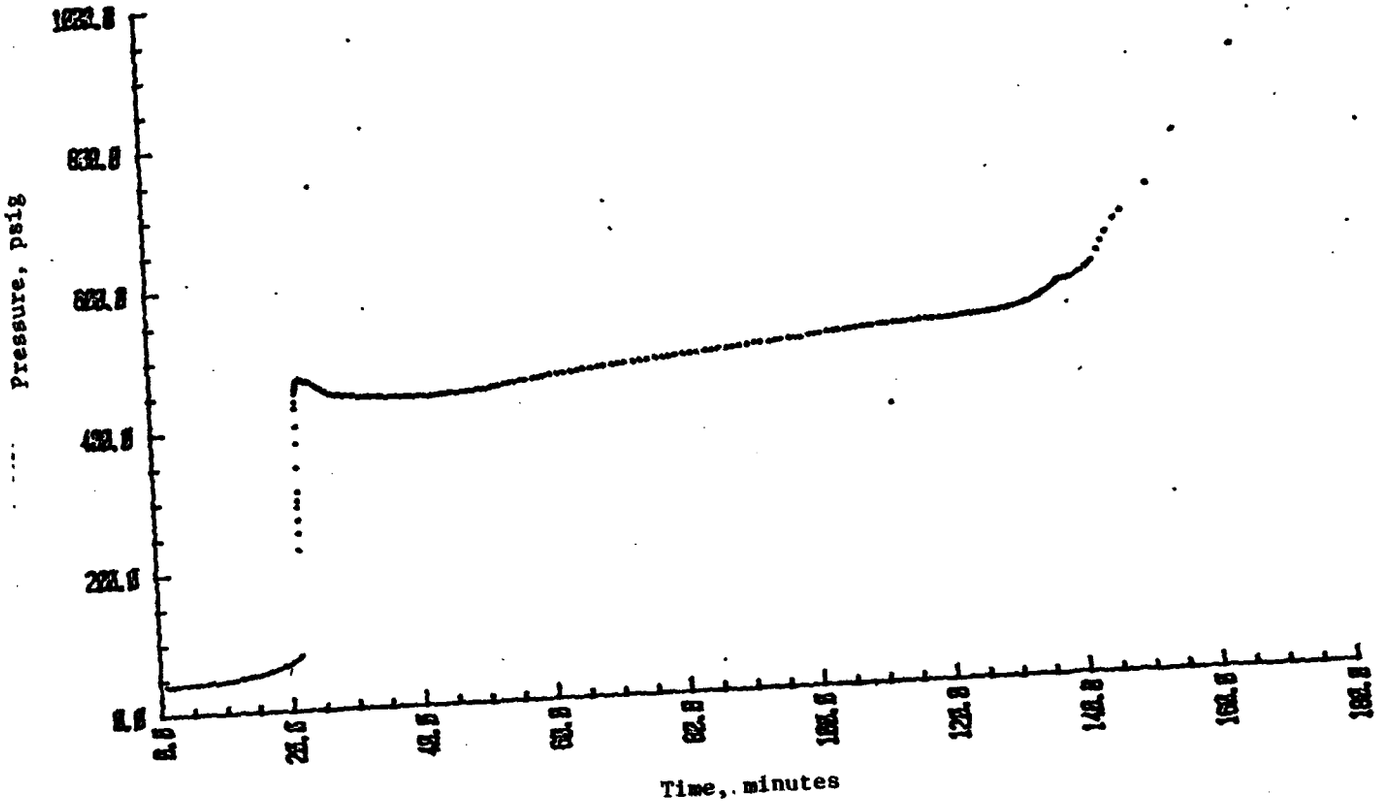

Figure 61. Pressure Versus Time Plot for the Exotherm Detected During the ARC Analysis of Cell No. II-6 (Coulombically Balanced)

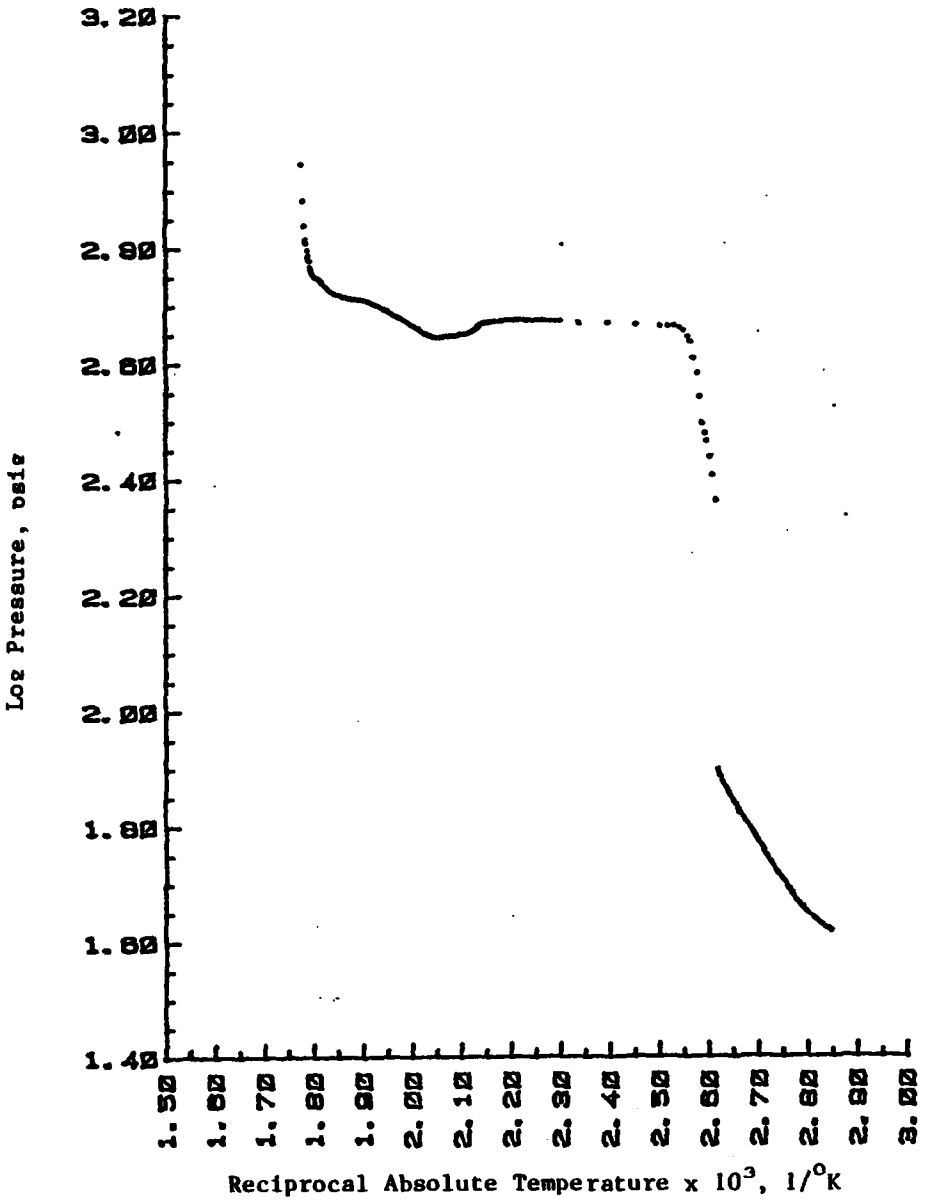

Figure 62. Log Pressure Versus 1/T Plot for the Exotherm Detected During the ARC Analysis of Cell No. II-6 (Coulombically Balanced)

Table 49. Summary of the Four Peaks Detected During the ARC Analysis of Cell No. II-6 (Coulombically Balanced)

	Peak Number			
	1	2	3	4
Initial Temperature, °C	77.5	108.0	197.0	243.8
Initial Pressure, psig	41.1	76.6	454.0	496.5
Initial Temperature Rate, °C/min	0.804	3.353	1.461	0.497
Final Temperature, °C	108.0	197.0	216.0	290.4
Final Pressure, psig	76.6	454.0	440.3	880.6
Maximum Temperature Rate, °C/min	3.353	199.5	2.208	1.704
Maximum Pressure Rate, psig/min	7.5	1730	< 0	17.9
Adiabatic Temperature Rise, °C	30.5	89.5	19.0	46.6
ΔH, cal	360	1052	224	551
Pressure Change, psig	35.5	377.4	-13.7	384.1
Activation Energy, kcal/mole	22.5	(1)	41.3	52.0
Reaction Order	0.5	(1)	1.3	1.0
Projected Temperature Rise for Li/SO_2 "D" Cell, °C	56.8	165.6	35.4	86.7

(1) The rate of this reaction was too fast for a kinetic analysis to be made.

Interpretation of ARC Results

Interpretation of Results

In this section, interpretation of the results will be conducted in terms of quantitatively assessing the hazards associated with the different test conditions evaluated and postulating reaction schemes to account for the exotherms observed. Hazards will be evaluated with respect to the observed heating rates, pressure rates, and overall pressure and temperature increases. Reaction schemes will be proposed based on the published results of DTA studies of cell components.

Hazard Analysis

The hazard associated with a particular test mode is primarily a function of the rate of pressure generation and overall pressure rise. Temperature effects are only important inasmuch as they influence the pressure behavior. In order to quantify the hazards, an arbitrary scale has been established, as shown in Table 50. This scale is based on the premise that a cell will incorporate a vent that opens at 400 to 500 psig. Also, these evaluations are based only on the thermal behavior of the chemical reactions taking place. Ohmic heating effects can be significant, particularly during forced overdischarge, and can greatly add to the hazards associated with a given test mode.

Table 51 summarizes the thermal and pressure behavior of all 14 cells tested in this program and gives each cell a hazard rating. For the purpose of this evaluation, it has been assumed that all exotherms observed in a cell (including those detected during electrical testing) are thermally linked leading to one continuous temperature spiral. Although this was not the case in most instances, this provides for a worst-case condition from which to evaluate the hazards.

In general, forced overdischarge and resistive overdischarge at ambient temperature led only to venting hazards. Although significant temperature increases occurred, the temperature and pressure rates were low enough so that the pressure relief vent should function properly and eliminate explosion hazards. Even considering the lower ϕ-values and possible reduced void volumes of Li/SO_2 hardware cells, these results indicate that there is no significant explosion hazard. Again, however, these conclusions are based only on the effects of the chemical reactions

Table 50. Arbitrary Scale Used to Quantify Hazards Associated with Li/SO_2 Cells.

Total Pressure Rise, psig	Maximum Pressure Rate, psig/min	Hazards
<100	<1	Safe
100-2000	1 - 10	Venting
100-2000	10 - 100	Violent Venting
100 - 2000	>100	Exposion

Table 51. Hazard Analysis Summary of the Fourteen Test Cells[1]

Cell Group	Cell No.	Cell Design	Test Conditions	Current Density, mA/cm²	Test Temp., °C	Temp. Rise, °C	Max. Temp. Rate, °C/min	Pressure Rise, psig	Max. Pressure Rate, psig/min	Hazard Rating
A	I-1	Lithium Limited	Forced Overdischarge	1.0	25	-	-	-	-	-
"	II-1	Coulombically Balanced	" "	"	"	-	-	-	-	-
"	III-1	Excess Carbon	" "	"	"	-	-	-	-	-
"	IV-1	Excess Lithium	" "	"	"	302	0.34	490	1.4	Venting
B	I-2	Lithium Limited	Forced Overdischarge	5.0	25	182	0.33	(2)	(2)	(2)
"	II-2	Coulombically Balanced	" "	"	"	210	0.12	169	0.24	Venting
"	III-2	Excess Carbon	" "	"	"	273	0.56	129	0.54	Venting
"	IV-2	Excess Lithium	" "	"	"	306	4.0	171	0.17	Venting
C	I-3	Lithium Limited	Resistive Overdischarge	5 ohm load	25	212	0.63	168	7.1	Venting
"	II-3	Coulombically Balanced	" "	"	"	(2)	(2)	(2)	(2)	(2)
"	III-3	Excess Carbon	" "	"	"	287	2.1	421	5.9	Venting
"	IV-3	Excess Lithium	" "	"	"	299	0.54	220	3.7	Venting
D	II-5	Coulombically Balanced	Discharge to 2V	3.0	-35	243	17.7	1436	245	Explosion
"	II-6	" "	Forced Overdischarge	"	"	213	199.5	840	1730	Explosion

Notes: (1) The temperature and pressure increases reported in this table represent the increases observed from the start of the first exotherm detected to the end of the last exotherm observed even though these exotherms may not have occurred continuously during the experiment.

(2) Because of cell leakage problems, the data are incomplete.

and ohmic heating effects, especially during forced overdischarge, could substantially increase the hazards involved.

The results tend to indicate that cells undergoing resistive overdischarge yield higher pressure rates, and overall pressure increases. In particular, the pressure rates are significantly greater. There appear to be no significant trends related to cell design other than the obvious one, of course, that cells containing excess lithium can undergo the Li/AN reaction and become exothermic at relatively low temperatures.

In contrast to the room temperature tests, the low temperature tests were very dramatic with both cells being rated as an explosion hazard. Previously, it had been assumed that the problems associated with low temperature forced overdischarge were the result of the Li/AN reaction. During the electrical testing, the SO_2 would be depleted but the Li/AN reaction would be inhibited by the low temperature. Upon warming up, the Li/AN reaction would begin, generating heat and methane gas until the pressure rose to the point where the cell vented. The results obtained with Cell No. II-6, however, clearly show that something else is happening. Apparently, the low temperatures allow the accumulation of an unstable product(s) which then reacts explosively when the cell warms up.

Cell No. II-5 gives the hazards associated with the thermal behavior of a normally discharged Li/SO_2 cell that has not been subjected to abusive conditions. Because this cell was discharged at low temperatures, it probably represents worst-case conditions. The results show that this cell represents an explosion hazard but not nearly as severe as that indicated for Cell No. II-6.

Reaction Schemes

Exotherms Detected During Electrical Testing

The exotherms detected during electrical testing are postulated to be due to the Li/AN reaction. Because the quantities of active materials were accurately known, these cells offer an opportunity to better understand the conditions necessary for the initiation of this reaction. This is beneficial to both the battery user and the battery manufacturer.

Table 52 lists the component ratios present in the 12 room-temperature test cells at the completion of discharge to a two volt cutoff and indicates which cells demonstrated exothermic behavior during overdischarge. The SO_2/Li and SO_2/Li area ratios provide two measures of the materials balance present at the end of discharge. It is interesting to note that no exothermic behavior was observed in any of the cells at the 2.0 volt cutoff, even at low SO_2 concentrations. Therefore, some degree of overdischarge is required to trigger the Li/AN reaction and, as expected, forced overdischarge appears to be much more effective in initiating the reaction. DeMasi[3] has postulated that an SO_2/Li area ratio of 10 mg/cm^2 is sufficient to inhibit the Li/AN reaction but these results show that the reaction can occur at values as high as 25.5 under conditions of forced overdischarge at 5.0 mA/cm^2. The SO_2/Li ratio appears to be a better indicator with stability occurring at values greater than 2.0 during forced overdischarge and greater than 0.8 for resistive overdischarge.

Table 53 summarizes the characteristics of the exotherms detected during overdischarge. The exotherms detected for cells force discharged into reversal were all found to be first order reactions with activation energies ranging from 4.5 to 8.0 kcal/mole. These results are consistent with those reported by Dey[2] where activation energies for the Li/AN reaction were found to range from 5.9 to 13.1 kcal/mole, depending on the solution composition. The initial peak detected in Cell No. IV-3 during resistive overdischarge, however, is different from the others as evidenced by the significantly higher activation energy. These results indicate that a different reaction or reaction mechanism may be occurring in this cell.

Table 52. Cell Status at End of Discharge to 2.0 Volt Cutoff Versus Exothermic Behavior During Overdischarge for the Cells Tested at Ambient Temperature.

Cell No.	Discharge Current Density, mA/cm²	SO_2/Li	SO_2/Li Area, mg/cm²	Overdischarge Test Mode	Exotherms During Overdischarge
I-1	1.0	11.3	31.3	Constant Current	No
II-1	1.0	3.0	13.8	"	No
III-1	1.0	2.0	17.4	"	No
IV-1	1.0	0.19	6.4	"	Yes
I-2	5.0	7.0	41.5	Constant Current	No
II-2	5.0	1.1	23.0	"	Yes
III-2	5.0	1.7	25.5	"	Yes
IV-2	5.0	0.44	25.2	"	Yes
I-3	4.6	8.5	30.9	Resistive (5 ohms)	No
II-3	5.3	0.87	22.8	"	No
III-3	4.4	1.3	24.3	"	No
IV-3	5.5	0.43	22.8	"	Yes

Table 53. Summary of Exotherms Detected During Overdischarge Testing at Ambient Temperature.

	Cell Number				
	IV-1	II-2	III-2	IV-2	IV-3
Initial Temperature, °C	40.5	45.7	77.3	44.0	33.2
Initial Pressure, psig	33.8	19.2	59.4	15.4	16.5
Initial Temperature Rate, °C/min	0.100	0.082	0.103	0.246	0.078
Final Temperature, °C	86.5	102.2	116.4	64.9	61.4
Final Pressure, psig	115.6	79.5	68.1	23.3	44.4
Maximum Temperature Rate, °C/min	0.116	0.121	0.124	0.246	0.172
Maximum Pressure Rate, psig/min	0.25	0.24	0.07	0.08	0.23
Temperature Rise, °C	46.0	56.5	39.1	20.8	28.2
Pressure Change, psig	81.8	60.3	8.7	7.9	27.9
Time Duration of Exotherm, min.	1228	1610	554	220	280
ΔH, cal	541	704	431	254	336
Activation Energy, kcal/mole	5.9	4.5	8.0	8.0	26.0
Reaction Order	1.0	1.0	0.9	1.0	1.4

All of the overdischarge exotherms were found to lead to a pressure rise but over a long time interval, thus producing low pressure rates. Also, these exotherms were all characterized by low rates of temperature rise indicating slow kinetics in spite of the low activation energies.

Exotherms Initiating Over 100°C

Table 54 summarizes the peaks with initiation temperatures over 100°C observed in the exotherms produced by the various test cells and groups them according to their thermal and pressure characteristics. As can be seen, in many instances, good correlation is obtained between the peaks of different cells. The groupings given in Table 54 indicate the following general trends in the data:

- o Room Temperature - Overdischarged cells (either ohmic or constant current) give one of the following two types of reactions in the 135-160°C temperature range.
  - Slight pressure producing; E ≈ 50 KCal/mole.
  - Pressure reducing: E ≈ 10 kcal/mole
- o Discharged and overdischarged cells give an exothermic reaction between 160 and 170°C; moderately pressure producing with wide variation in activation energies.
  - This reaction is often not observed if the pressure reducing reaction at 135 - 160°C is present.
- o Low rate forced overdischarged and resistive overdischarged cells give an exothermic reaction between 180 and 190°C; moderately pressure producing; E ≈ 18 kcal/mole.
- o Discharged and overdischarged cells exhibit a moderate to large exothermic reaction between 195 and 210°C; moderately pressure producing; E ≈ 10 kcal/mole.
- o Discharged and overdischarged cells give one or more moderate-to-large exothermic reactions between 235 and 260°C.
  - Low temperature cells - highly pressure producing; E ≈ 50 kcal/mole.

Table 54. Summary of Exotherm Peaks Initiating Above 100°C

	Cell Number							
	IV-1	III-2	IV-2	I-3	III-3	IV-3	II-5	II-6
Initiation Temp, °C							112	108
E, kcal/mole							46.4	-
ΔH, cal							258	1052
ΔP, psig							32	377
Initiation Temp, °C		117				103		
E, kcal/mole		18.0				14.5		
ΔH, cal		85				306		
ΔP, psig		-12				31		
Initiation Temp, °C		125						
E, kcal/mole		196.2						
ΔH, cal		177						
ΔP, psig		-12						
Initiation Temp, °C	135				156			
E, kcal/mole	60.0				45.7			
ΔH, cal	328				113			
ΔP, psig	21				23			
Initiation Temp, °C		147		145		139		
E, kcal/mole		8.3		12.0		10.2		
ΔH, cal		105		236		484		
ΔP, psig		1		-78		-18		
Initiation Temp, °C	163	160			167		159	
E, kcal/mole	18.3	87.2			200.0		117.4	
ΔH, cal	188	428			247		469	
ΔP, psig	15	61			63		166	

Table 54. continued

	Cell Number							
	IV-1	III-2	IV-2	I-3	III-3	IV-3	II-5	II-6
Initiation Temp, °C	180				190	186		
E, kcal/mole	25.5				9.5	20.2		
ΔH, cal	233				182	367		
ΔP, psig	48				48	66		
Initiation Temp, °C								197
E, kcal/mole								41.3
ΔH, cal								224
ΔP, psig								-14
Initiation Temp, °C	208	206			207	216	197	
E, kcal/mole	10.1	16.2			9.0	8.4	12.0	
ΔH, cal	256	1057			519	260	502	
ΔP, psig	104	-			120	75	182	
Initiation Temp, °C							238	244
E, kcal/mole							64.1	52.0
ΔH, cal							1227	551
ΔP, psig							984	384
Initiation Temp, °C			242	257				
E, kcal/mole			8.0	39.9				
ΔH, cal			421	102				
ΔP, psig			-7.4	-61				
Initiation Temp, °C	255				255	238		
E, kcal/mole	21.8				17.3	23.0		
ΔH, cal	105				499	386		
ΔP, psig	61				108	38		
Initiation Temp, °C				265				
E, kcal/mole				290.0				
ΔH, cal				174				
ΔP, psig				194				

Table 54. continued

	Cell Number							
	IV-1	III-2	IV-2	I-3	III-3	IV-3	II-5	II-6
Initiation Temp, °C	264					270		
E, kcal/mole	28.7					20.2		
ΔH, cal	437					673		
ΔP, psig	52					-17		
Initiation Temp, °C		322		281				
E, kcal/mole		236.9		118.4				
ΔH, cal		110		146				
ΔP, psig		-		-78				
Initiation Temp, °C								
E, kcal/mole								
ΔH, cal								
ΔP, psig								
Initiation Temp, °C								
E, kcal/mole								
ΔH, cal								
ΔP, psig								
Initiation Temp, °C								
E, kcal/mole								
ΔH, cal								
ΔP, psig								
Initiation Temp, °C								
E, kcal/mole								
ΔH, cal								
ΔP, psig								
Initiation Temp, °C								
E, kcal/mole								
ΔH, cal								
ΔP, psig								

- Room temperature cells - can be either pressure reducing or moderately pressure producing reactions; E ≈ 22 kcal/mole.

- Cells containing excess lithium either resistive overdischarged or force overdischarged at low rates give large exothermic reactions between 260 and 270°C. E = 25 kcal/mole; pressure behavior not clear.

- Overdischarged lithium-limited cells give a moderate exothermic reaction between 260 and 270°C; moderately pressure producing; E = 290 kcal/mole.

Because of the complexity of the sample mixture present in an actual Li/SO_2 cell, assigning reactions to the peaks observed is difficult. Some speculations can be made, however, based on the published DTA results for various cell components and possible reaction products. Table 55 provides a summary of the published DTA results. In addition to these reactions, DiMasi et al[4], have proposed that the exothermic reaction between sulfur dioxide and methane could also be involved. This reaction is given by the following equation

$$3CH_4 + 4\ SO_2 \longrightarrow 4\ H_2S + 3\ CO_2 + 2\ H_2O$$

Table 55. Summary of Published DTA Results on Li/SO_2 Cell Components and Possible Reaction Products

Reactants	Initiation Temperature, °C	Relative Magnitude of Exotherms	Reference
Li + Celgard Separator	- No exotherms detected -		2
Li + LiBr/AN-SO_2 Electrolyte	156	Moderate	5
	180, 182	Large	5,2
	211	Large	2
Li + LiBr	142,124	Moderate	5,2
Li + AN	89	Large	2
	149	Large	2
Li + SO_2	- No exotherms detected -		2
$Na_2S_2O_4$	91	Small	2
	125	Small	2
	211, 190	Large	5,2
	284	Moderate	6
Cathode from discharged cell	179	Moderate	2
$Na_2S_2O_4$ + Br_2	143	Large	2
	204	Not Specified	2
Li + $Na_2S_2O_4$	190	Moderate	5
	256	Large	
Li + C + $Na_2S_2O_4$	198	Moderate	2
	292	Large	2
Li + Teflon	279	Large	2
Li + Al	180	Large	2
LiAl + AN	154	Large	2
LiAl Alloy + S	204	Large	2
	298	Large	2
LiAl Alloy + AN/SO_2 (75/25)	424	Large	2
Li + S	127, 160	Large	5,2
Li + S + $Na_2S_2O_4$	164	Large	2
Li + Li_2SO_3 (anhydrous)	- No exotherms detected -		5,2

Table 55 (continued)

Reactants	Initiation Temperature, °C	Relative Magnitude of Exotherms	Reference
Li + Li_2SO_3 (as received)	126	Moderate	2
	151	Large	2
	190	Moderate	2
Cathode from a cell forced overdischarged	58	Small	2
	177	Moderate	2
	237	Large	2
Li + CH_4	- No exotherms detected -		2
Li + S_2Br_2	362	Large	2
	386	Not specified	2
	400	Not specified	2
CH_4 + Br_2	324	Not specified	2

Using this information as a guide, the reactions occurring between 135°C and 170°C in the cells tested at room temperature are postulated to involve the thermal decomposition of $Li_2S_2O_4$. The reactions observed between 180 and 190°C are believed to be due to the reaction of the electrolyte solution with lithium metal, either that remaining at the anode or deposited in the cathode. The reactions occurring between 195 and 220°C are believed to represent reactions involving the decomposition products of dithonite, probably involving deposited lithium metal.

With respect to the cells tested at -35°C, the violent reaction observed at 108°C in cell No. II-6 (forced overdischarged) apparently results from the formation of a reaction product that is unstable at elevated temperatures. This indicates that either an alternate discharge/overdischarge mechanism is operative at low temperatures or that the normal discharge/overdischarge products are formed in a much more reactive state due to temperature induced changes in particle size, surface films, etc. More work is required to elucidate the mechanism of this reaction. The decline of the open circuit potential of cell No. II-5 (discharge to 2.0V) accompanying the peak at 238°C indicates that this reaction involves the reaction of molten lithium with the electrolye solution. A similar reaction is observed in cell No. II-6 indicating that this cell also contains significant quantities of lithium metal, probably present in the cathode.

Conclusions and Recommendations

These studies have demonstrated the unique capabilities of the ARC instrument in studying the hazards associated with lithium cells. Its sensitivity allows detailed information to be obtained on the reactions occurring in actual cells, including determination of the kinetic parameters. The pressure data are particularly important in accurately assessing the hazards associated with these cells and are readily obtained with this instrument. Our cell design has been shown to be capable of remaining hermetic up to approximately 290°C, thus allowing cells to be evaluated over a wide temperature range. The cell container is rugged enough to withstand high pressures and, for the first time, thermal and pressure data have been collected during and following an internal explosion in a Li/SO_2 cell.

The results have shown that a significant explosion hazard exists with cells force overdischarged at low temperatures and we recommend that future efforts concentrate on this critical area. These efforts should strive to define the threshold temperature below which the explosion hazard exists, the degree of overdischarge required to initiate the explosion hazard, whether or not resistive overdischarge can lead to an explosion hazard, and most importantly, the reactions responsible for the explosions including identification of any unstable species produced during overdischarge. It is important to include characterization of the conditions leading to an explosion hazard in this investigation in order to provide the lithium battery user with the information needed to ensure safe operation until the problem can be resolved.

Although the low temperature explosion hazard should certainly receive the highest priority in any future effort, this work has also identified other areas where additional effort would be beneficial, as discussed below.

Our results have shown that only in a severely lithium-limited cell can the lithium/acetonitrile reaction be prevented during forced overdischarge. This, however, imposes a severe capacity penalty on overall cell performance, and is, therefore, not a practical solution. Because this reaction can lead to cell venting, a solution to this problem is desirable. Here we recommend that work continue and be supported to look for alternate solvents to replace acetonitrile and for additives able to inhibit the Li/AN reaction.

Although this work has shown that exothermic reactions initiated during and following forced overdischarge and resistive overdischarge at ambient temperature do not constitute an explosion hazard, the effects of ohmic heating are not clearly defined. This is an area where more information is certainly needed and we recommend that studies be continued to define the magnitude of ohmic heating during discharge and forced overdischarge as a function of cell design, current density, and temperature.

Finally, we feel that it is important that effort be continued to better understand the elevated temperature reactions occurring in the Li/SO_2 system following discharge, forced overdischarge, and resistive overdischarge. Although they may not constitute an explosion hazard by themselves, they could contribute to an explosion when coupled with ohmic heating effects. Although much work has already been done in this area employing DTA, more information is needed. Pressure data would be very useful for assessing the hazards associated with a given reaction and also for helping to interpret the data obtained in cell analyses, such as were done in this program. Gas phase reactions, such as the postulated SO_2 and CH_4 reaction, need to be studied and more information is needed on the effects of acetonitrile and/or the standard electrolyte solution on known reactions such as the thermal decomposition of $Li_2S_2O_4$, the Li/S reaction, etc.

We believe that the ARC technique possesses unique capabilities well suited for safety studies of lithium systems which can be effectively applied in all of the recommended areas of investigation. We hope that the ARC can continue to be an integral part of the Navy's overall strategy for effecting solutions to the safety problems associated with both the Li/SO_2 and the $Li/SOCl_2$ systems.

TASK II

MICRO-CALORIMETER STUDIES

DR. KWANG Y. KIM
CORPORATE TECHNOLOGY CENTER
BLOOMINGTON, MN

Task II: Micro-Calorimeter Studies

The overall objective of this task was to provide support to the ARC work in the area of reaction thermodynamics. The specific objectives were:

- to determine the heat of reaction of lithium metal with acetonitrile at 25°C
- to determine the heat of reaction of lithium/aluminum alloy with acetonitrile at 25°C.

Instrument Design and Operation

The micro-calorimeter was designed and built in-house by Honeywell's Dr. Kwang Y. Kim. The instrument is compatible with the corrosive components of both the Li/SO_2 and $Li/SOCl_2$ system while, at the same time, it has a high sensitivity and rapid response time.

The calorimeter assembly, shown schematically in Figure 63, consists of three main parts; the cell, the thermopiles, and the aluminum heat sinks. The calorimeter cell consists of two identical glass chambers. One chamber is empty while the other contains an electric heater used for calibration. By making the heater an integral part of the calorimeter, calibration can be performed during each analysis. Once assembled, the cell is placed in the calorimeter so that both sides are in contact with thermopiles. The thermopiles, in turn, are in contact with two large aluminum heat sinks maintained at constant temperature.

During operation, the liquid reactant (electrolyte solution or pure solvent) is placed in the compartment with the electric heater. The electrochemical cell or solid reactant is placed in the empty compartment. If an electrochemical cell is being tested, leads are brought through the compartment lid to provide external electrical connection. In this way, the cell can be discharged while in the calorimetric chamber. The calorimetric cell is then assembled, placed in the

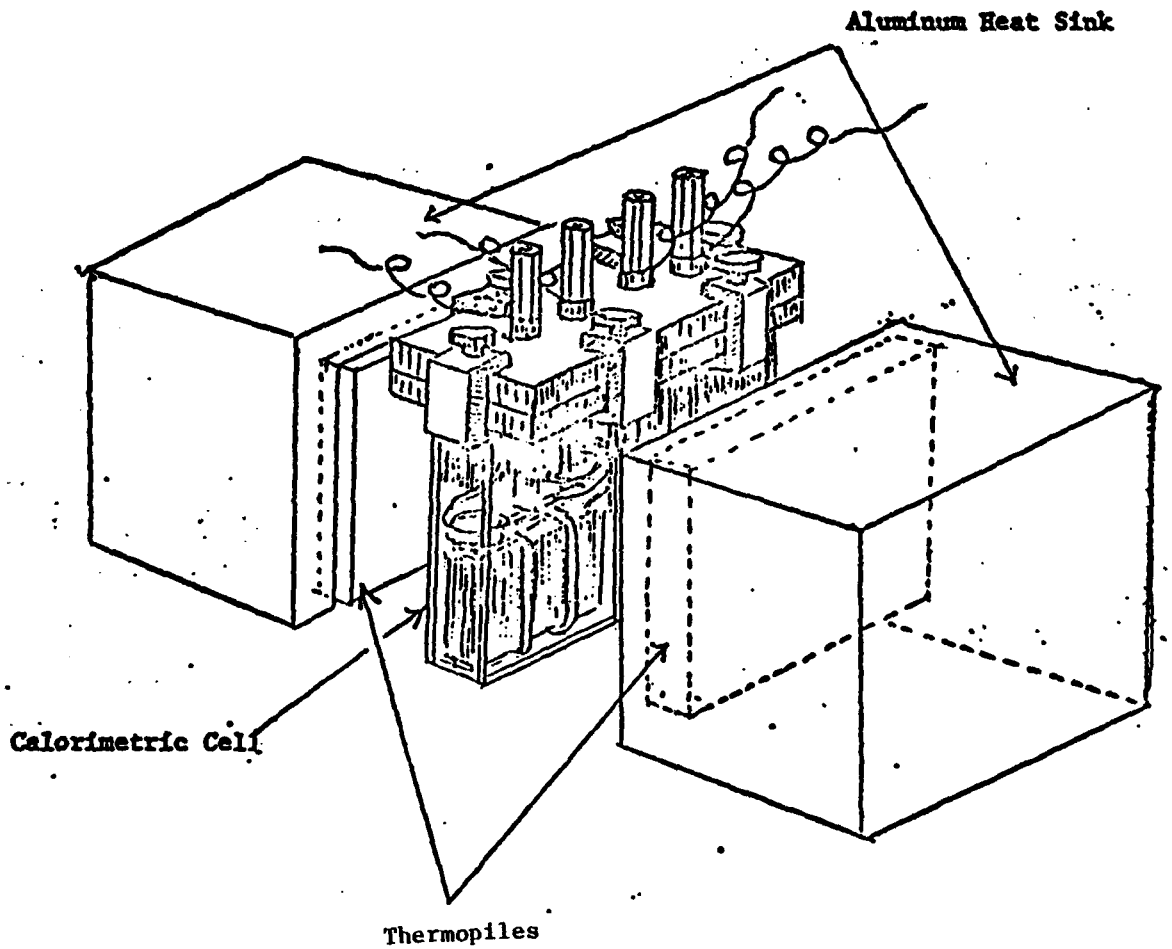

Figure 63. Schematic of Modified Micro-Calorimeter

calorimeter, and allowed to come to thermal equilibrium with the aluminum blocks. Once thermal equilibrium has been obtained, the instrument is calibrated by passing a known amount of electric current through the heater and measuring the temperature response. The liquid is then transferred to the other compartment and the temperature measured as a function of time.

During a reaction, heat is transferred between the calorimetric cell and the heat sinks through the thermopiles. The temperature difference (ΔT) between the cell and the heat sinks is reflected as a potential difference by the thermopiles. The temperature difference is the driving force for heat flow which, in turn, is proportional to heat generation. The rate of heat flow ($\dot{q}$) at time (t) can be shown to be

$$\dot{q} = \frac{\partial q}{\partial t} = \frac{KA\Delta T(t)}{d} \tag{12}$$

where:

$\dot{q}$ = rate of heat flow, cal/sec
K = thermal conductivity, cal/cm-sec-^{o}C
A = cross-sectional area, cm^2
d = conduction distance, cm
$\Delta T(t)$ = temperature difference at time (t), ^{o}C

Since T(t) is proportional to the thermopile potential, V(t), the above equation can be simplified to

$$q = \alpha \int_{o}^{t} V(t)dt \tag{13}$$

where α is a constant which can be determined from the calibration data. The integration of this equation can be carried out either geometrically from a chart recording or by an electronic integrator.

Thermodynamics of the Lithium-acetonitrile Reaction -

Lithium metal was obtained from Foote Mineral Company and used without further purification. Acetonitrile was purchased from Burdick & Jackson Lab Inc., and was further purified by distillation employing a Perkin-Elmer spinning band column. The purified solvent had a water content of 40 ppm as determined by the Karl Fischer method.

The micro-calorimetric experiments were conducted by reacting 12 to 22 mg of lithium metal with 2.0 ml of acetonitrile at 25°C. Acetonitrile was in excess to ensure complete reaction of the lithium metal. It was observed that the lithium-acetonitrile reaction was relatively slow at this temperature, requiring over four hours for completion. A typical calorimetric output is shown in Figure 64 where the total generated heat is proportional to the area under the curve.

The reaction product was observed to be a yellow solid insoluble in acetonitrile but readily soluble in water. The absence of gas evolution when a drop of water was added to the post-reaction system confirmed that the lithium metal was totally consumed.

Table 56 shows the results of four experiments. A mean value of -54.6 ± 1.0 kcal/mole-Li was obtained for the exothermic heat of reaction and, as can be seen from the results, good reproducibility was obtained between experiments. For comparison, some calculated heats of reaction reported in the literature are listed in Table 57. As can be seen, our experimental value falls midway between the two calculated values demonstrating that our results are consistent with those expected from thermodynamic considerations.

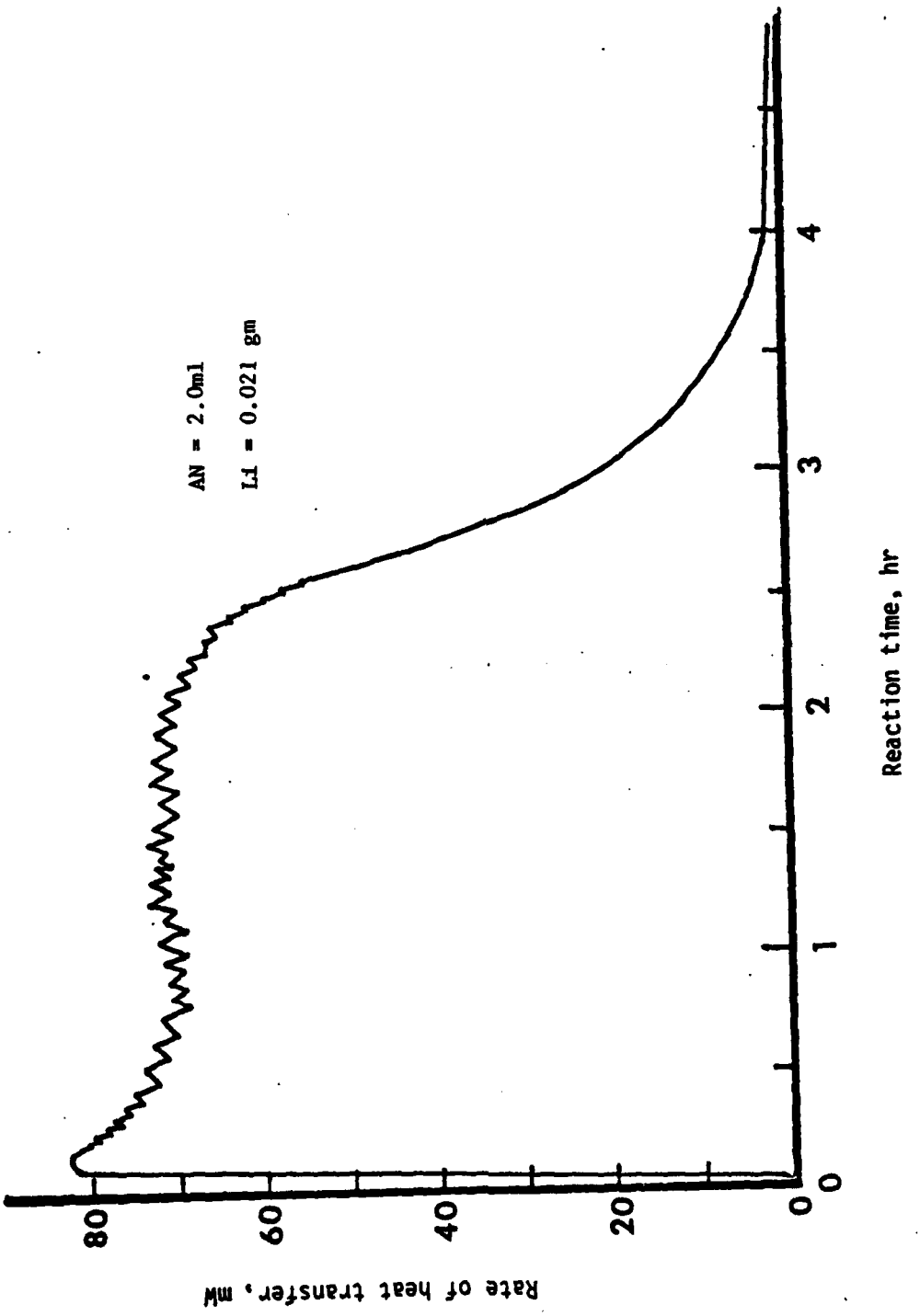

Figure 64. Typical Calorimetric Output for the Lithium-Acetonitrile Reaction at 25°C

Table 56. Micro-Calorimetric Results for Lithium-Acetonitrile Reaction at 25°C

Experiment No.	Lithium Sample Size, gm	AN/Li Molar Ratio	Measured Heat of Reaction		ΔHr	
			Joules	Calories	KJ/mole-Li	KCal/mole-Li
1	0.0222	12.0	-729.8	-174.3	-228.1	-54.48
2	0.0200	13.3	-654.4	-156.3	-227.0	-54.23
3	0.0116	22.9	-401.0	- 95.8	-239.9	-57.31
4	0.0212	12.5	-671.9	-160.5	-219.9	-52.53

Average Values

$\overline{\Delta Hr} = -228.7 \pm 4.1$ kJ/mole-Li

$\overline{\Delta Hr} = -54.6 \pm 1.0$ kcal/mole-Li

Notes:

1) The atomic weight of lithium is taken to be 6.939.

The reported uncertainty is the standard deviation of the mean.

Table 57. Summary of Calculated Values Reported for the Heat of Reaction of Lithium with Acetonitrile

Postulated Reaction	Heat of Reaction, kcal	ΔHr, kcal/mole-Li	Reference
$4Li + 4CH_3CN \rightarrow 4LiCN + 2CH_4 + C_2H_4$	-150	-37.5	6
$2Li + 3CH_3CN \rightarrow LiCN + CH_4 + (CH_3CNCH_2CN)^- + Li^+$	-160	-80.0	4

Thermodynamics of the Lithium/Aluminum Alloy - Acetonitrile Reaction -

Two grades of Li/Al alloy were employed in this work; one obtained from Foote Mineral Company manufactured by a thermal process and the other manufactured in-house electrochemically. The thermal grade represented material of high purity manufactured under well controlled conditions. It had a specified lithium content of 19.93 percent by weight (1:1 atomic ratio of lithium to aluminum). The electrochemical grade, on the other hand, simulated the method of formation in an actual cell except that a more inert electrolyte solution was employed to prevent premature reaction.

More specifically, the electrochemical alloy grade was prepared following the procedure described by Dey[7]. A three-plate cell was made by sandwiching an aluminum foil cathode between two lithium anodes with glass mat separators between the electrodes. The resulting cell stack was placed between glass plates and the entire assembly secured by tying with Teflon-coated nickel wire. The cell was placed in a glass jar and activated with a 1.0M $LiClO_4$/PC electrolyte solution. The electrodes were externally shorted and the cell allowed to stand overnight. The Li/Al alloy, which was recovered as a dark gray powder, was washed with tetrahydrofuran and dried in vacuum.

Both grades of Li/Al alloy were analyzed by X-ray diffraction to determine their bulk composition and by Auger spectroscopy to characterize their surface states. The x-ray diffraction analyses were made employing a Debye-Scherrer camera (114mm dia.) using filtered cobalt radiation. The resulting data, comprising of "d" values (interplanar spacing) and line intensities, were processed through the JCPDS (Joint Committee on Powder Diffraction Standards) library file.

Both grades of alloy gave essentially the same spectra and the only lithium/aluminum compound identified in the library file matching their diffraction pattern was the intermetallic compound LiAl (JCPDS Card No. 3-1215). The X-ray diffraction data for the two samples are shown in Table 58 along with the data for aluminum metal, LiAl (from Card No. 3-1215), and CoKβ radiation. Table 59 shows a comparison of the average intensities for the two grades of alloy with the data from JCPDS Card No. 3-1215 for LiAl. The primary difference between the two grades of

Table 58. Comparative Analysis of Diffraction Data for Li/Al Alloy Samples

LiAl[a]		LiAl[b]		Al		LiAl Card No. 3-1215		CoKβ
d	I	d	I	d	I	d	I	d
4.0	10	4.0	10			3.65	60	3.65
3.65	90	3.65	100					
2.74	10							
2.47	10	2.47	10					
2.34	50			2.34	100			
2.245	100	2.25	100			2.26	80	2.25
2.02	30			2.024	50			
1.91	70	1.92	70			1.92	60	
1.585	50	1.59	50			1.58	50	
1.46	50	1.46	50			1.46	50	
1.43	40			1.43	20			
1.295	80	1.297	80			1.30	80	
1.22	50	1.222	50	1.22	20	1.22	60	
1.17	20			1.169	10			
1.122	50	1.123	50			1.12	60	
1.075	50	1.074	50			1.07	60	
1.003	60	1.006	60	1.01	10	1.01	70	
.969	40	.970	40			0.969	40	
.927	30			.929	10			
.917	30	.918	40			0.918	40	
.905	10			.905	10			

a. Electrochemically synthesized in this lab.

b. Thermally synthesized by Foote Mineral Company.

Table 59. Comparison of the Experimental X-ray Data to That of LiAl

Alloy Samples Examined[a]		LiAl Card No. 3-1215	
d	I[b]	d	I
3.65	100	3.65	60
2.25	100	2.26	80
1.92	70	1.92	60
1.59	50	1.58	50
1.46	50	1.46	50
1.297	80	1.30	80
1.222	50	1.22	60
1.123	50	1.12	60
1.074	50	1.07	60
1.006	60	1.01	70
0.970	40	.969	40
0.918[c]	40	.918	40

a. Average of experimental Li/Al alloy data from electrochemically and thermally prepared samples.

b. Normalized to 100.

c. Data limit with cobalt radiation.

material is tha :he electrochemical grade appears to contain some free aluminum metal. Also, the electrochemical grade has an unidentified line at 2.74 Å which may be indicative of an aluminum or lithium oxide. From these results, it may be concluded that both grades of alloy represent the intermetallic compound LiAl consistent with the results of Dey[7] although, as expected, the thermal grade appears to be of higher purity.

The Auger spectra for the two grades of alloy are presented in Figures 65 and 66 while Table 60 summarizes the results. Both samples were found to be practically identical in terms of their lithium/aluminum ratios and concentrations of other major components/contaminants. The high oxygen content indicates that the surface of both samples was covered by an oxide film.

Micro-calorimetric experiments were conducted by reacting 50-100 mg samples of the Li/Al alloy with 2.0 ml of acetonitrile at 25°C. Again, acetonitrile was maintained in excess to ensure complete reaction of the solid reactants. Unexpectedly, no appreciable heat was given off with either grade of alloy, even after several hours of contact. These results, therefore, indicate that LiAl is not reactive with acetonitrile at 25°C.

To supplement the micro-calorimetric work, a second type of experiment was performed in which 32.0 mg of the electrochemical grade alloy were introduced into 3.0 ml of acetonitrile and the resulting mixture allowed to stand for 15 hours at room temperature. The acetonitrile was then evaporated under a stream of argon gas and the unreacted alloy recovered and dried. No physical changes in the alloy could be detected and a gravimetric anlysis showed that, within experimetal limits, no weight change had occurred. An Auger analysis was performed on the recovered material. The resulting spectrum is shown in Figure 67 while the results are summarized in Table 61. It was found that the lithium/aluminum ratio and oxygen content were similar to the as-manufactured material. It is also important to note that no nitrogen was detected in the surface analysis. Since LiCN is one of the products of the lithium-actonitrile reaction, nitrogen should be detectable if the reaction has occurred to any appreciable extent. These results, therefore, substantiate those obtained in the micro-calorimetric studies and demonstrate that LiAl is not reactive with acetonitrile at 25°C.

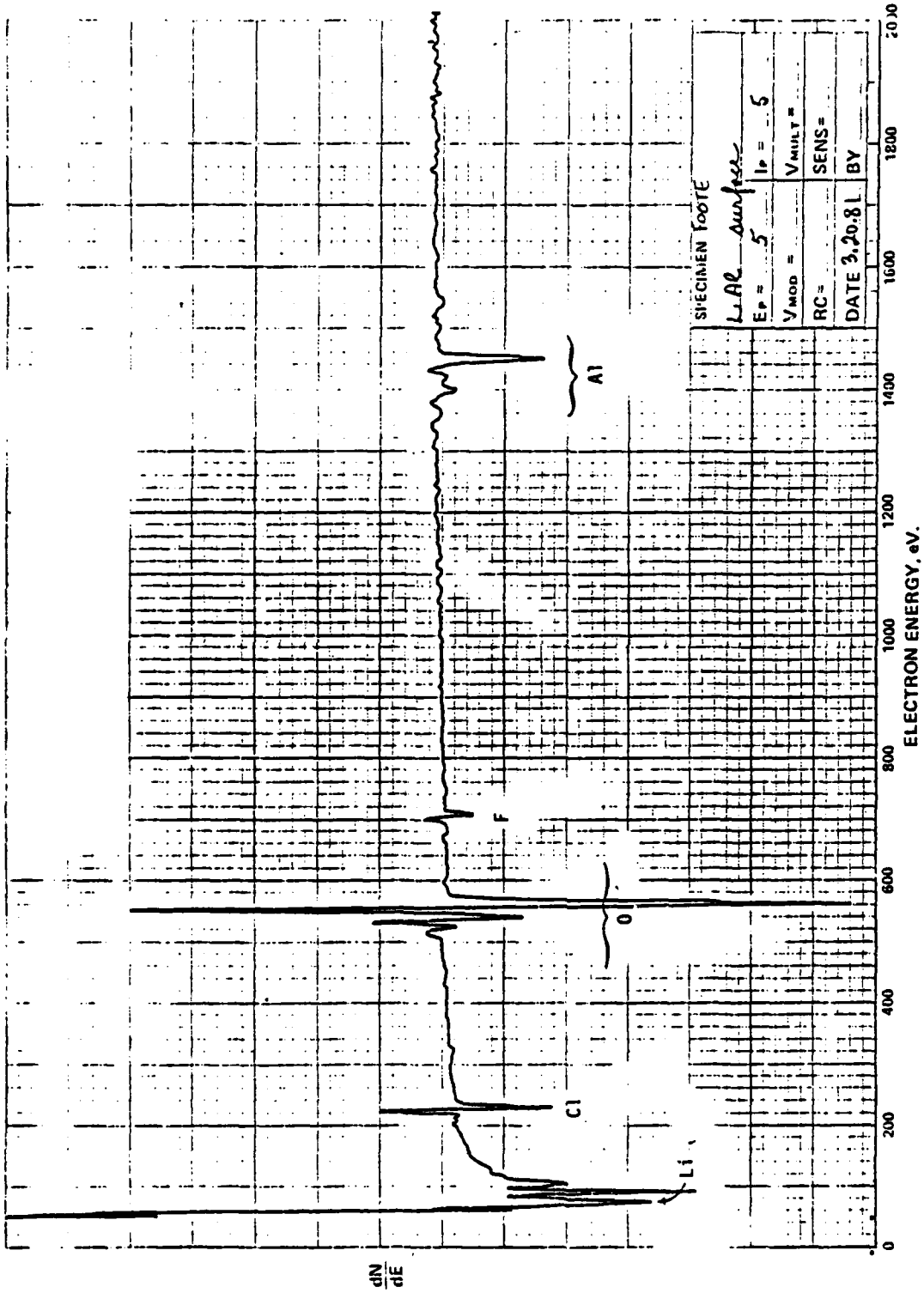

Figure 65. Auger Spectrum of Thermally Prepared Li/Al Alloy from Foote Mineral Company

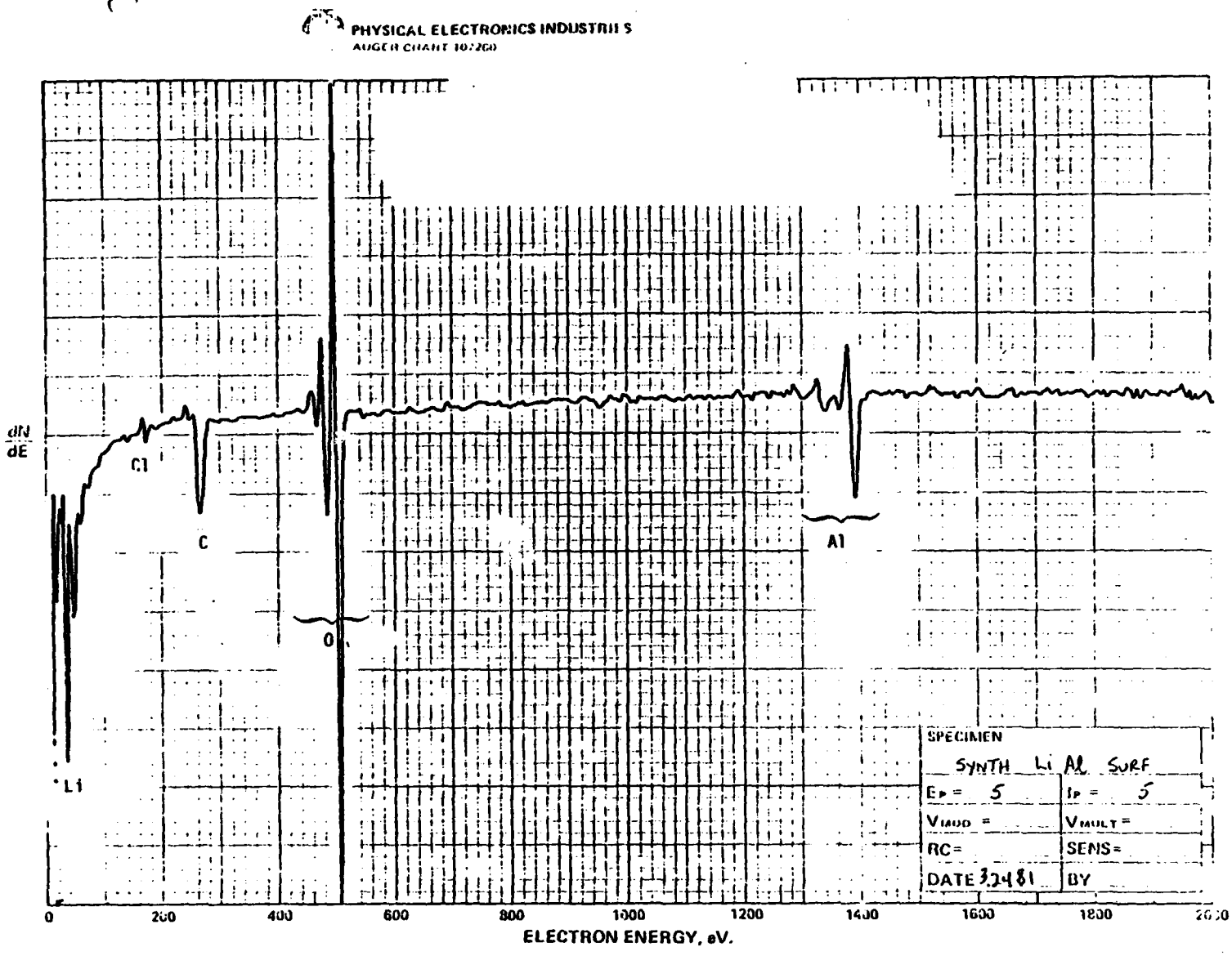

Figure 66. Auger Spectrum of Electrochemically Prepared Li/Al Alloy

Table 60. Results of Auger Analysis of Li/Al Alloys

Element	Electrochemical Grade	Thermal Grade
Li	31	33
Al	16	15
O	39	47
C	13	N.D.
Cl	<1	4
F	N.D.	1

Notes: 1) The above values represent atomic percent

2) N.D. = not detected

AD-A119 381 HONEYWELL POWER SOURCES CENTER HORSHAM PA F/G 10/3
LITHIUM-SULFUR DIOXIDE (LI/SO2) BATTERY SAFETY HAZARDS - THERMA--ETC(U)
MAR 82 W B EBNER, K Y KIM, H V VENKATASETTY N60921-81-C-0085
UNCLASSIFIED NL

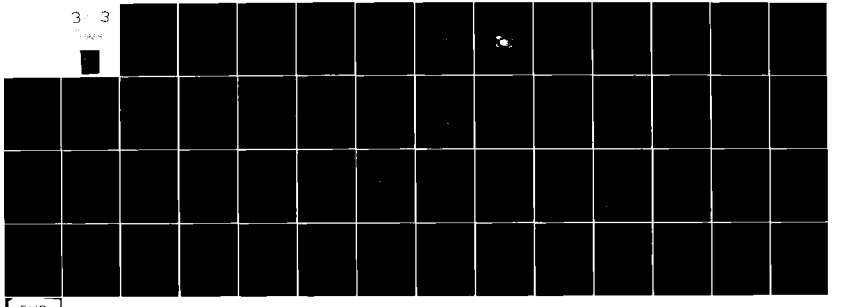

END
DATE FILMED
10 82
DTIC

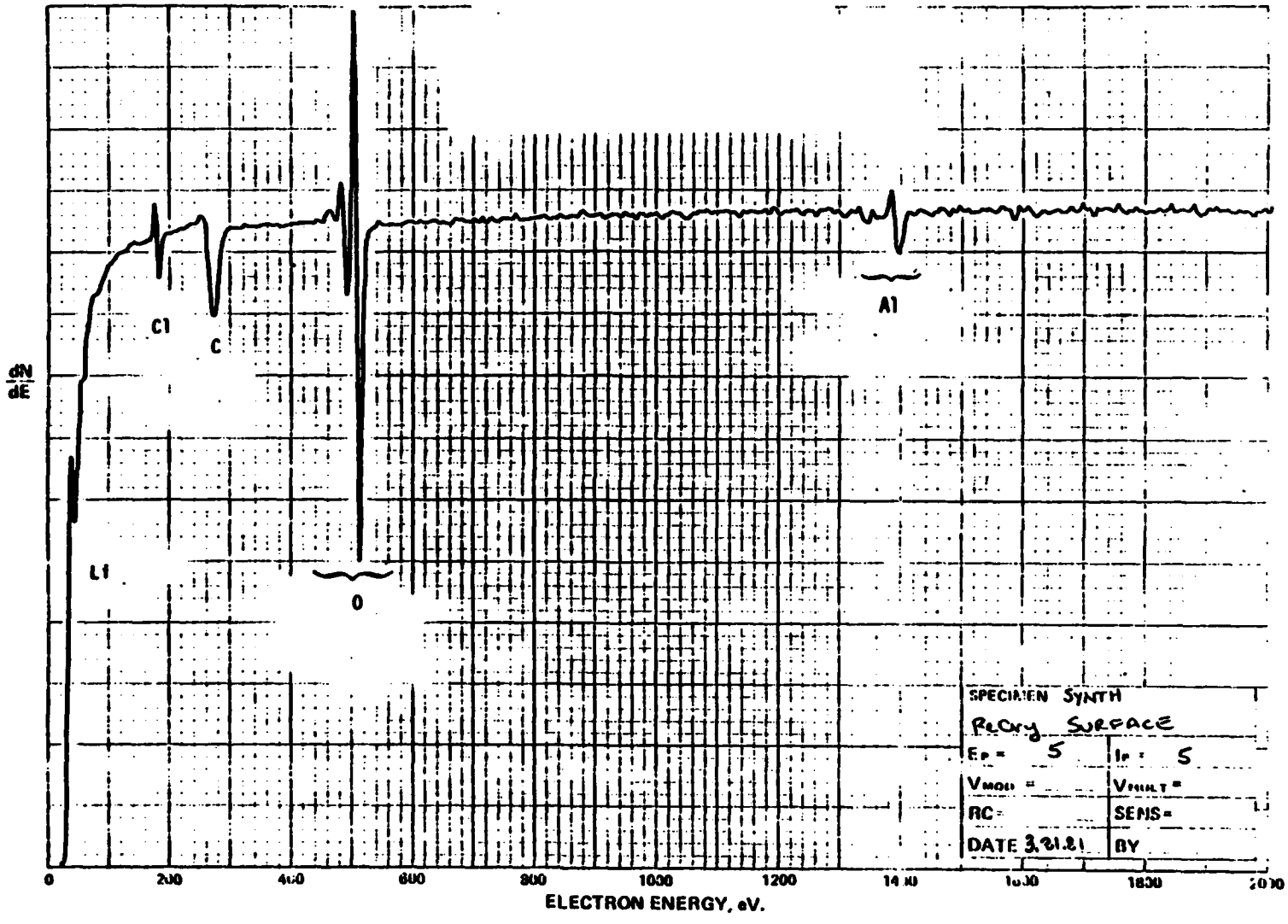

Figure 67. Auger Spectrum of Electrochemically Prepared Li/Al Alloy after 15 Hours of Contact with Acetonitrile at 25°C.

Table 61. Results of Auger Analysis of Electrochemically Prepared Li/Al Alloy After 15 Hours of Contact with Acetonitrile at 25°C

Element	Concentration, Atomic Percent
Li	15
Al	6
O	50
C	26
Cl	3
N	N.D.

Note: N.D. = not detected

These findings are consistent with Dey's DTA studies[2] where it was shown that thermally prepared Li/Al alloys are unreactive with acetonitrile up to a temperature of about 154°C. Taylor[8] on the other hand, has reported that Li/Al alloys prepared electrochemically in LiBr/AN-SO_2 solutions at ambient temperature undergo vigorous reaction, even with large amounts of SO_2 present. This difference in reactivity could be the result of oxide films that form on atmospheric contact. Another possibility is that an alloy of different composition and higher reactivity is electrochemically formed in acetonitrile solutions. Finally, the difference in reactivity could be a time dependent phenomenon where reactivity decreases as the lithium diffuses into the bulk material away from the surface. Further studies, therefore, are required to understand these differences in observed reactivity so that the impact of Li/Al alloys on Li/SO_2 cell safety can be better defined.

TASK III

FTIR SPECTROSCOPY STUDIES

DR. H. V. VENKATASETTY
CORPORATE TECHNOLOGY CENTER
BLOOMINGTON, MN

Task III: Fourier Transform Infrared Spectroscopy Studies

The overall objective of this task was to provide support to the ARC work in the area of reaction product identification. The specific objective was:

- To identify reaction products of electrolyte oxidation on nickel and stainless steel electrodes.

Instrumentation and Methodology

This work was conducted employing an electrochemical infrared cell in which the reaction products to be identified are generated in situ. The spectroelectrochemical cell, shown in Figures 68 and 69, incorporates a laminated structure consisting of two KBr windows and a polyethylene spacer containing the electrodes. The working electrode, either a nickel or stainless steel wire grid, is located in the center of the cell, in the direct path of the electromagnetic radiation. The counter electrode, Shawinigan black with Teflon pressed onto a nickel grid, is located on one side of the working electrode while a lithium reference electrode is located on the other side. To prevent leakage, the KBr windows are sealed to the polyethylene spacer with epoxy and the entire cell assembly secured in a mounting fixture (See Figure 68). The thickness of the polyethylene spacer was chosen such that the path length for infrared absorption was less than 1.0 mm.

The spectra were obtained over the region of 4000 - 400 cm^{-1} using a Digilab Fourier transform spectrometer (Model FTIR-14) equipped with a KBr beam splitter. The resolution with this instrument is 8 cm^{-1} in this spectral region. The electrolysis experiments were carried out employing a Princeton Applied Research Model 173 potentiostat/galvanostat with a Model 179 digital coulometer. Electrode potentials were recorded on a Hewlett-Packard X-Y recorder. A schematic of the experimental setup is shown in Figure 70. Electrolyte manufacture and assembly of the spectroelectrochemical cell were carried out in a dry box.

Results and Discussion

Spectra of Pure Acetonitrile

For reference, Table 62 summarizes the absorption bands of pure acetonitrile. The very strong band appearing at 2250 cm^{-1} is due to symmetrical C≡N stretching (V_2)

I.R. CELL

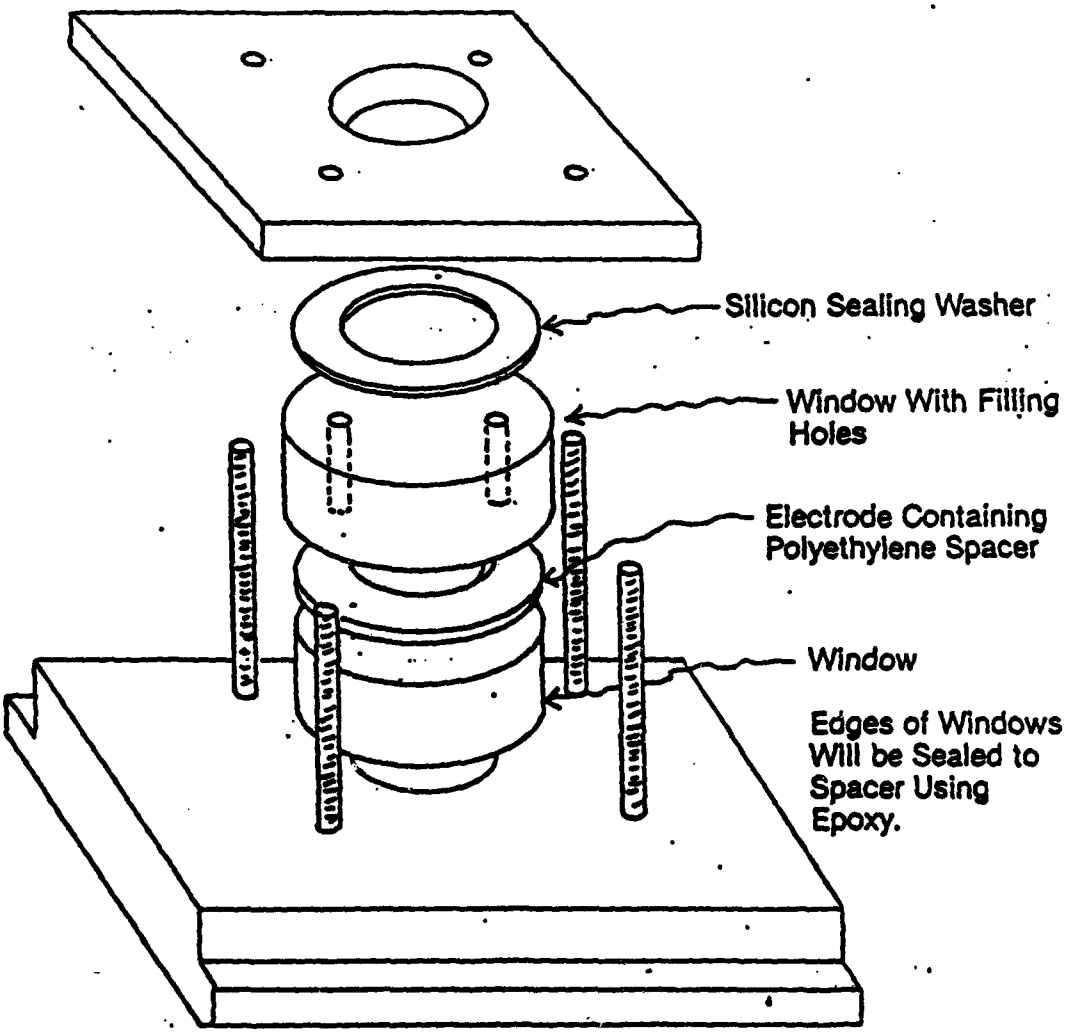

Figure 68. Spectroelectrochemical Cell Assembly

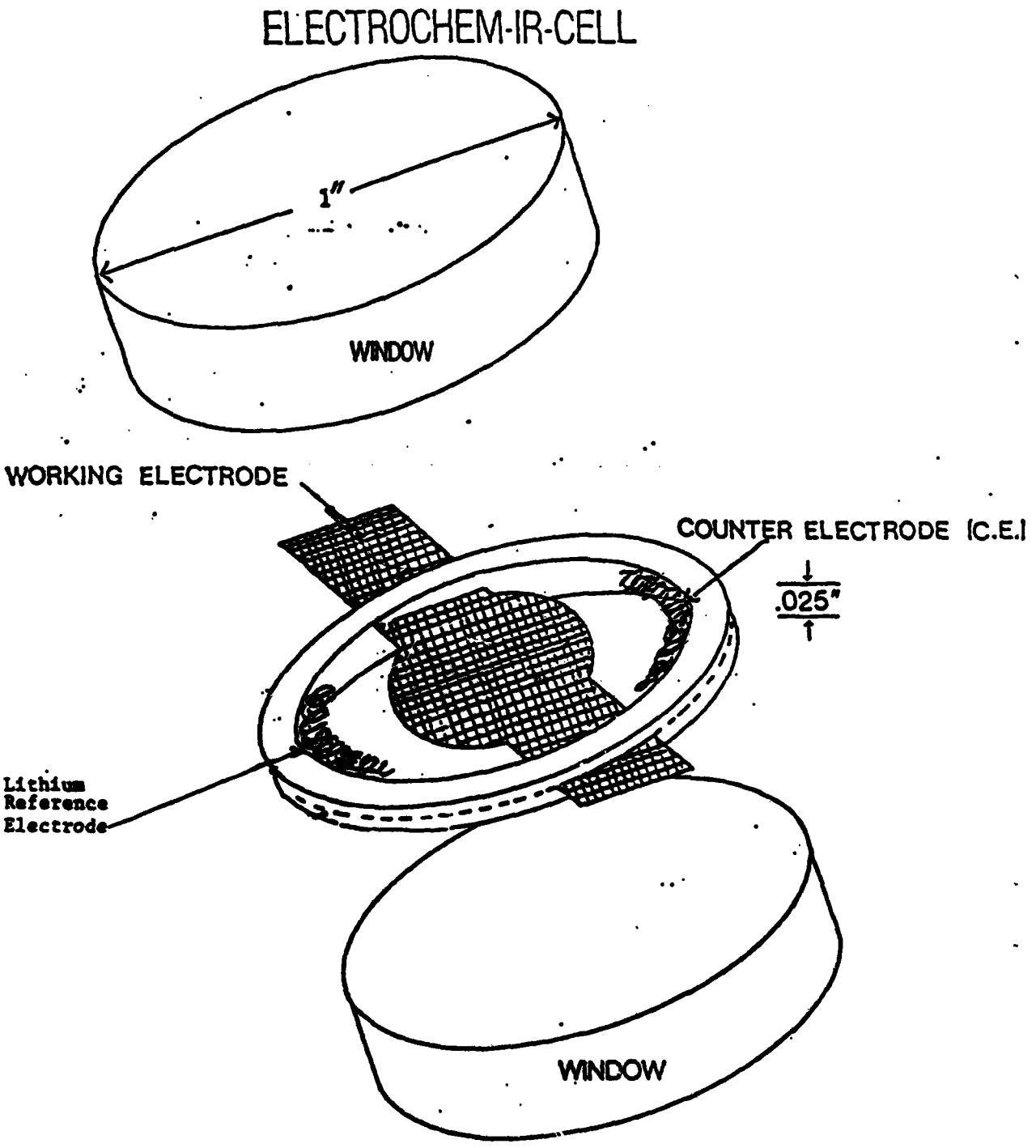

Figure 69. Electrode Configuration Used in the Spectroelectrochemical Cell

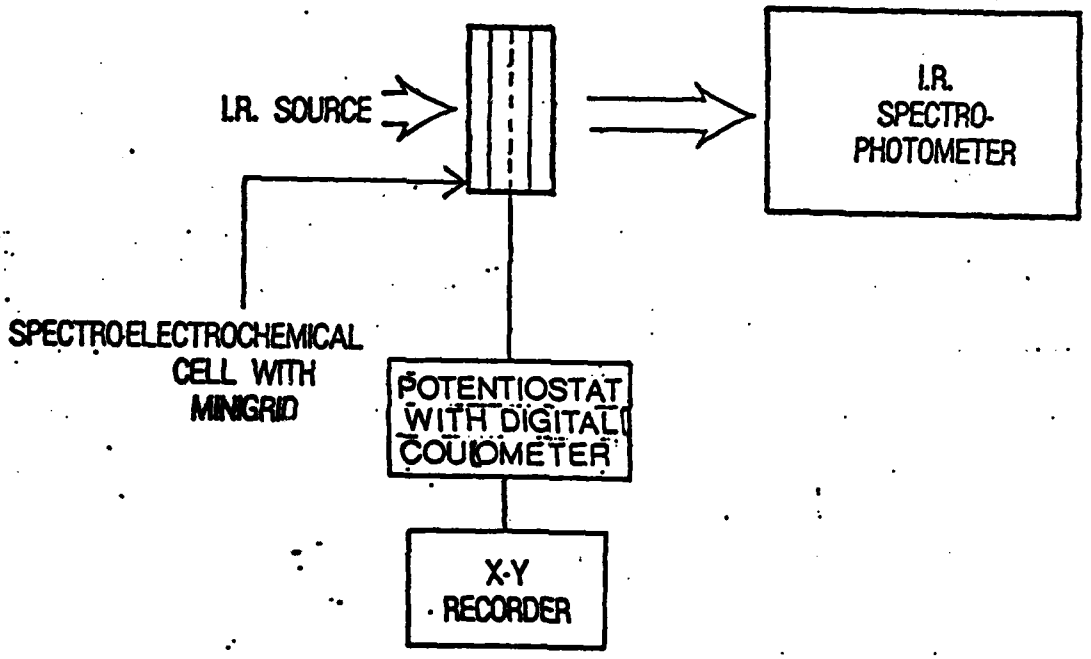

Figure 70. Schematic of Spectroelectrochemical System

Table 62. Summary of IR Absorption Bands for Pure Acetonitrile

Absorption Bands Frequencies (cm^{-1})	Intensity	Assignments
3600	VW & B	Water, OH group
3200	W	$2\nu_4 + \nu_3$
3160	S	$\nu_1 + \nu_4$ combination
3005	S	ν_5 degenerate C-H stretch
2940	S	ν_1 symm C-H stretch
2625	M	$\nu_2 + \nu_8$ combination
2410	M	
2295	S	$\nu_3 + \nu_4$ combination
2250	VS	ν_2 sym. C≡N stretch
2200	W	
1920	W & B	
1690	W	
1440	VS & B	ν_6 degenerate CH_3 deformation
1370	VS	ν_3 sym. CH_3 deformation
1200	W & B	
1040	VS	ν_7 degenerate CH_3 rocking mode
920	S	ν_4 sym. C-C stretch
378	VS	ν_8 degenerate C-C≡N bending

W = weak
M = medium
S = strong
VS = very strong
B = broad
Sh = shoulder

mode and the strong band at 2295 cm^{-1} is due to combination modes of $V_3 + V_4$. Another strong band appears at 920 cm^{-1} due to symmetrical (V_4) C-C stretch.

Nickel Electrode Results

The electrolyte solution employed in these studies had the following composition.

CH_3CN - 46 weight percent
SO_2 - 46 weight percent
LiBr - 8 weight percent

Electrolysis was carried out at a constant current of 10 mA with the nickel working electrode connected as the anode. Figure 71 shows the cathode (i.e., carbon electrode) versus lithium reference potential as a function of time. After dropping below -2 volts versus lithium, the cathode potential began to decline very rapidly. As a result, the electrolysis current was reduced to 7.5 mA during the latter part of the experiment.

Figure 72 shows the spectrum of the starting electrolyte solution while Figures 73 and 74 show the spectra of the solution during different stages of the electrolysis. The absorption peaks observed in these spectra are summarized in Tables 63 through 65. The spectra show that electrolysis reduces the intensity of all the bands characteristic of acetonitrile and SO_2. Other changes occurring in the spectra as a result of electrolysis are summarized as follows:

- The band at 930 cm^{-1} becomes split.
- A new band of medium intensity appears at 800 cm^{-1}.
- The band at 660 cm^{-1} increases in intensity.
- The band at 530 cm^{-1} increases in intensity.

In addition to the above changes in the IR spectra, it was observed that following electrolysis, the solution had developed a greenish blue color.

Stainless Steel Electrode Results

The composition of the electrolyte solution employed in these studies was as follows:

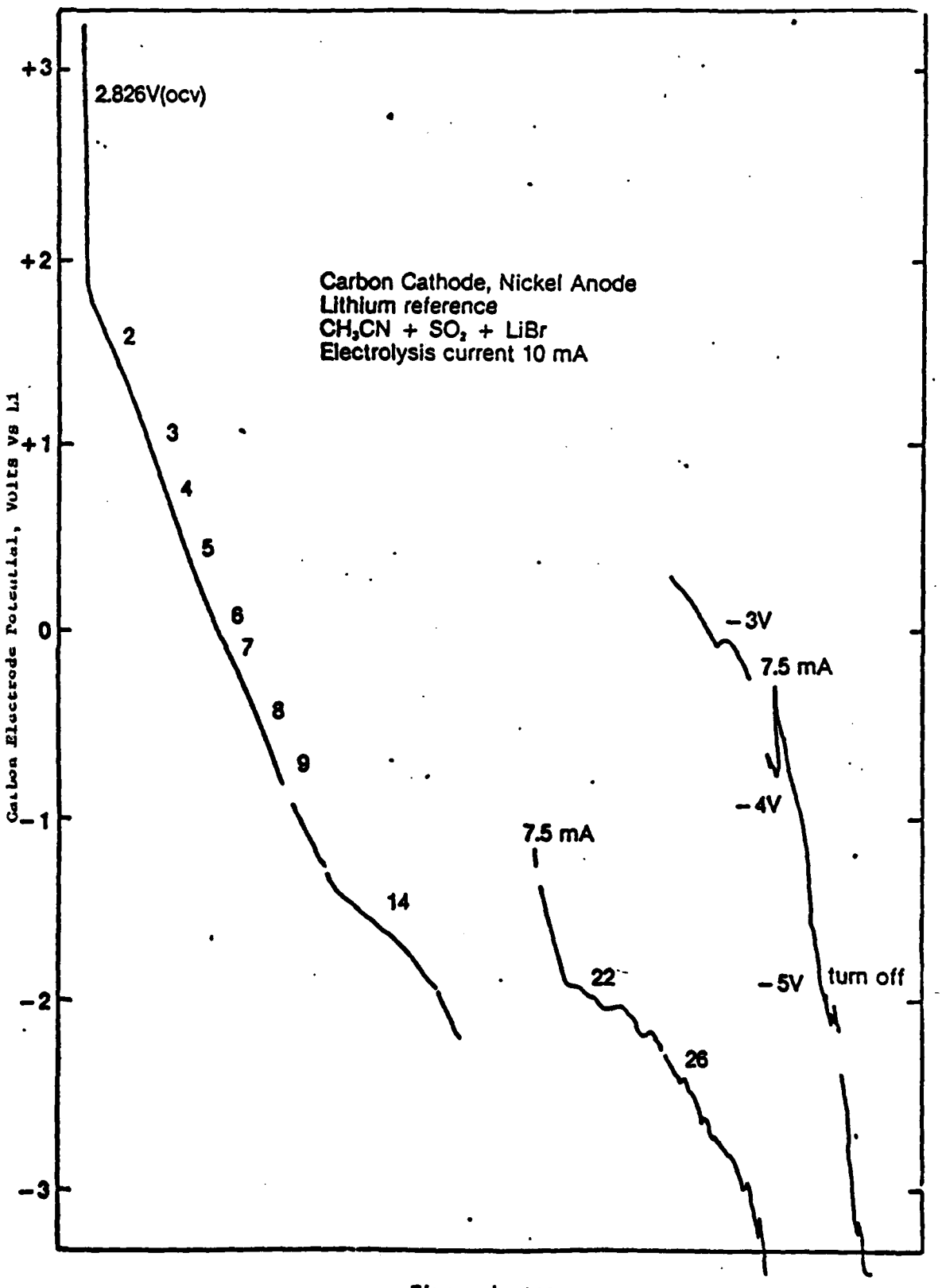

Figure 71. Carbon Electrode Potential Versus Time During the Electrolysis Experiment with a Nickel Anode

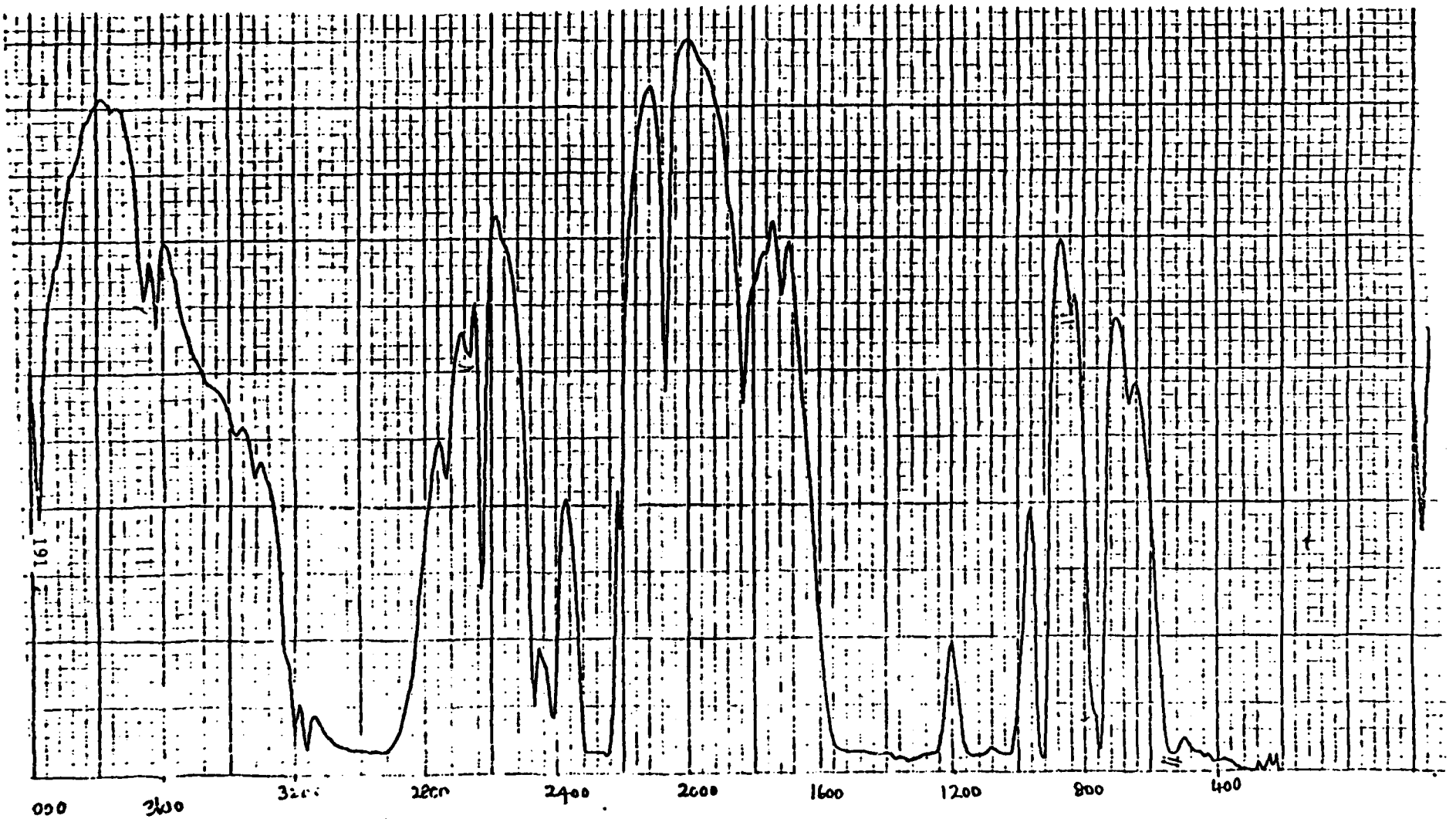

Figure 72. IR Spectrum of LiBr/AN/SO_2Electrolyte Solution Prior to Electrolysis with a Nickel Working Electrode

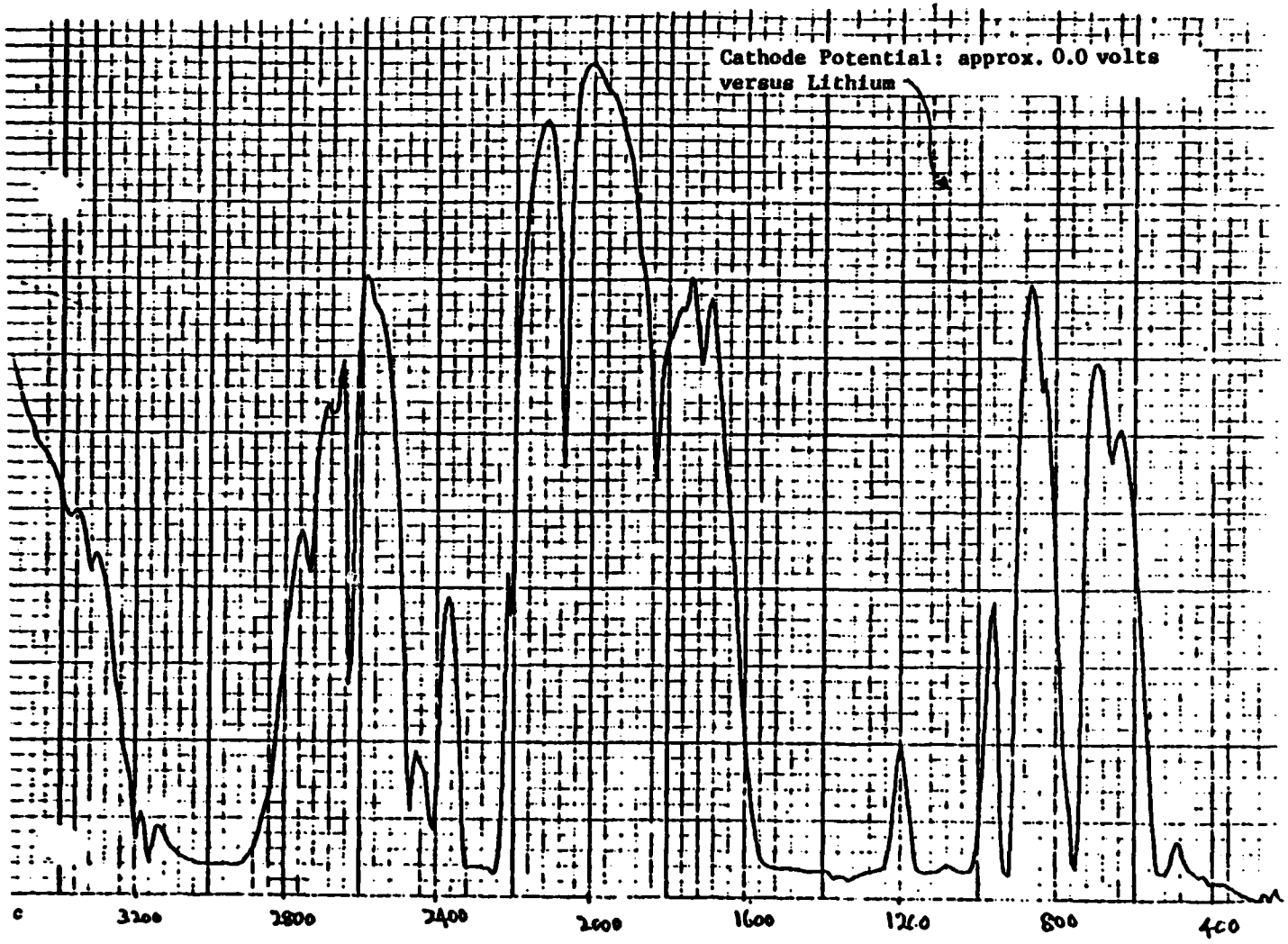

Figure 73. IR Spectrum of LiBr/AN-SO_2 Electrolyte Solution Following Approximately 6 Minutes of Electrolysis with a Nickel Working Electrode.

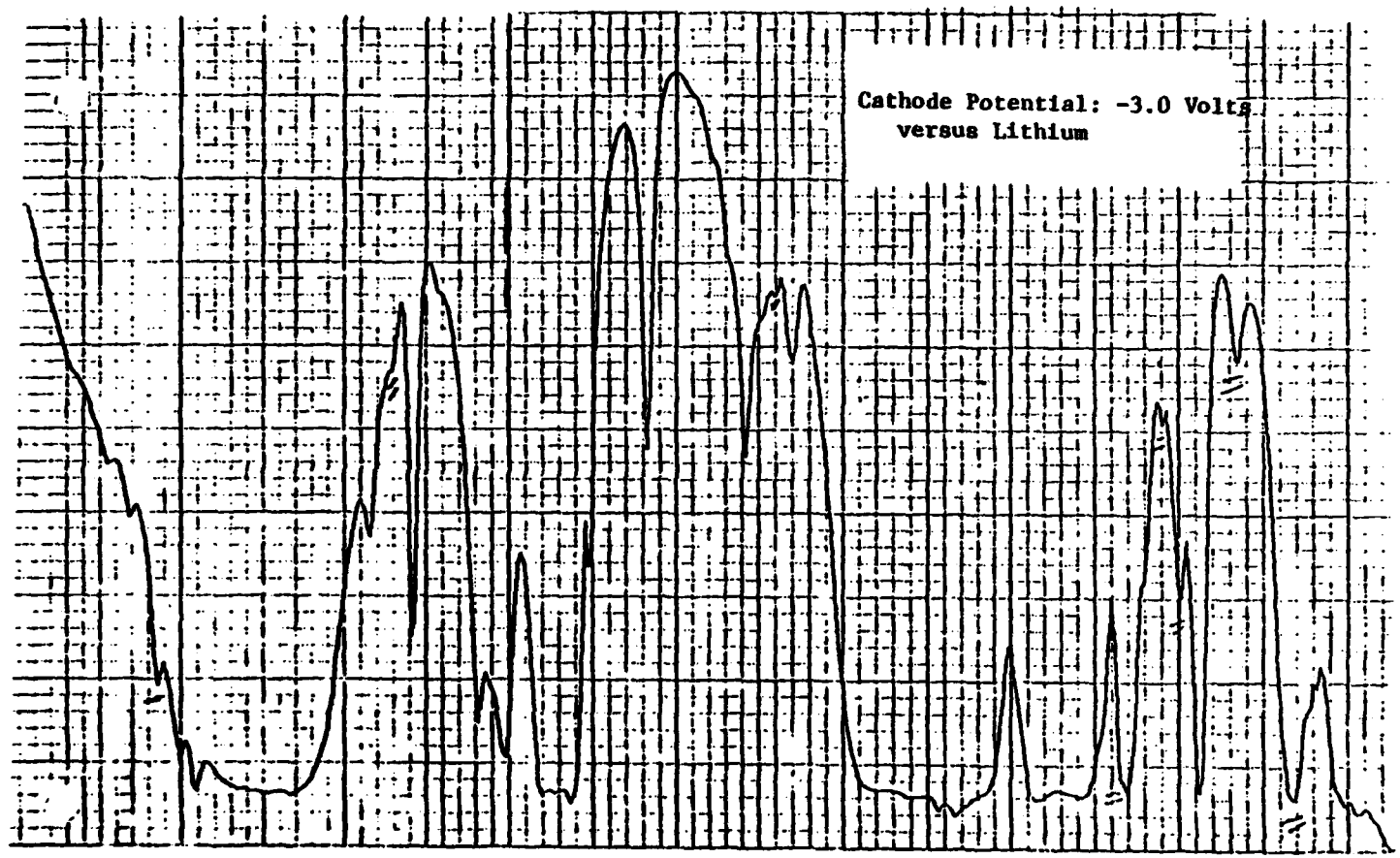

Figure 74. IR Spectrum of Li/Br/AN-SO_2 Electrolyte Solution Following Approximately 30 Minutes of Electrolysis with a Nickel Working Electrode

Table 63. Summary of IR Absorption Bands Observed for LiBr/AN-SO_2 Electrolyte Solution Prior to Electrolysis with a Nickel Anode

FREQUENCY (cm^{-1})	INTENSITY	ASSIGNMENTS
3975	M	OH gp Vib of water attached to L
3660	W	OH gp Vib of water
3625	W	
3230	sh	$2V_4+V_3$
3200	W	
3160	W	V_1+V_4 of CH_3CN
2880-3120	VS &Vb	V_1+V_5 of CH Str
2730	W	2 V_3 of CH_3 in CH_3CN
2665	W	
2630	S	V_2+V_8 of CH_3CN
2470	W	
2410	M	V_1+V_3 of SO_2
2240-2320	S&b	V_2 Sym Str of C ≡ N + $2V_2$ of SO_2
2210	W	
2070	M	
1830	M	V_2+V_3 of SO_2
1720	W	
1240-1560	S&Vb	V_3 asym S-O Str of SO_2; V_6 degenerate CH_3 def; V_3 sym CH_3 def
1020-1160	S&b	V_1 Sym S-O Str of SO_2
930	S	V_4 Sym C-C Str
840	W	
770 750	sh S	2 V_8 of CH_3CN
540	W	ν_2 of SO_2

Table 64. Summary of IR Absorption Bands Observed for LiBr/AN-SO_2 Electrolyte Solution Following Approximately 6 Minutes of Electrolysis with a Nickel Anode (Cathode Potential = 0.0 volts versus Li)

FREQUENCY (cm^{-1})	INTENSITY	ASSIGNMENT
3975	M	OH gp Vib of water attached to L.
3660	W	OH gp Vibr of water
3620	W	
3230	Sh	$2V_4+V_3$
3200	W	
3160	W	V_1+V_4 of CH_3CN
2880-3120	VS & Vb	V_1+V_5 of CH Str
2730	W	
2665 (2670)	V.W.	
2630	S	V_2+V_8 of CH_3CN
2470	W	
2410	M	V_1+V_3 of SO_2
2240-2320	S&b	V_2 Sym. Str of C≡N gp
2210	W	
2070	M	
1830	M	
1720	W	
1240-1560	S &Vb	V_3 asym S-O str of SO_2 V_6 degc. CH_3 def. V_3 Sym. CH_3 def.
1020-1160	S&b	V_1 Sym S-O str of SO_2
930	S	V_4 Sym C-C Str.
840	V.W.	
···0	sh	
750	S	2 V_8 of CH_3CN
660	W	
530 (535)	W	ν_2 of SO_2

Table 65. Summary of IR Absorption Bands Observed for LiBr/AN-SO_2 Electrolyte Solution Following Approximately 30 Minutes of Electrolysis with a Nickel Anode (Cathode Potential = -3.0 Volts Versus Li)

FREQUENCY (cm^{-1})	INTENSITY	ASSIGNMENT
3975	M	OH Vibr of Water solvated to Li
3680	VW	OH Vib of water
3665	W	
3625	W	
3250		
	W	$2\ V_4+V_3$
3200	W	
3160	W	V_1+V_4 of CH_3CN
2880-3120	VS &Vb	V_1+V_5 of CH in CH_3CN
2730	W	
2680	Sh	
2630	S	V_2+V_8 of CH_3CN
2470	W	
2405	M	V_1+V_3 of SO_2
2240-2320	S&b	V_2 Sym Str of C ≡ N gp
2210	W	
2070	M	
1830	M	
1720	W to M	
1240-1560	S&Vb	V_3asym S-O Str of SO_2
		V_6 deg CH_3 def +V_3SymCH_3def
1020-1160	S&b	V_1 sym S-O Str of SO_2
920	S	V_4 sym C-C Str.
880	Sh	$S_2O_4^=$
840	W	
800	M	$S_2O_4^=$
660	W	
530	S	$S_2O_4^=$

CH_3CN - 53.6 weight percent
SO_2 - 40.0 weight percent
LiBr - 6.4 weight percent

As with the nickel electrode tests, electrolysis was carried out at a constant current of 10 mA with the working electrode connected as an anode. Figure 75 shows the cathode potential as a function of time.

Figure 76 shows the spectrum of the starting solution while Figures 77 and 78 show the spectra of the solution during different stages of the electrolysis. The absorption peaks observed are summarized in Tables 66 through 69. Again, it was observed that electrolysis reduces the intensity of the bands characteristic of SO_2 and acetonitrile. Other changes in the spectra as a result of electrolysis are summarized as follows:

- The band at 2470 cm^{-1} increases in intensity.
- The broad band appearing at 1020 - 1130 cm^{-1} becomes split.
- The band at 530 cm^{-1} increases in intensity.

Following electrolysis, the solution was reddish brown in color.

Interpretation of Results

Under the present contract, only a limited investigation was possible to study the products formed from oxidation of the electrolyte solution at nickel and stainless steel electrodes. This preliminary study, however, has demonstrated the feasibility of using FTIR spectrometry to study electrochemical reactions involving the Li/SO_2 technology. The spectroelectrochemical cell developed in this program allows continuous monitoring of the products of an electrochemical reaction, is sufficiently leak-proof for use with SO_2 containing solutions, is inexpensive to fabricate, and readily allows the use of different electrode materials.

The initial experiments carried out with nickel and stainless steel electrodes have shown that distinctive changes in the electrolyte spectra occur as the result

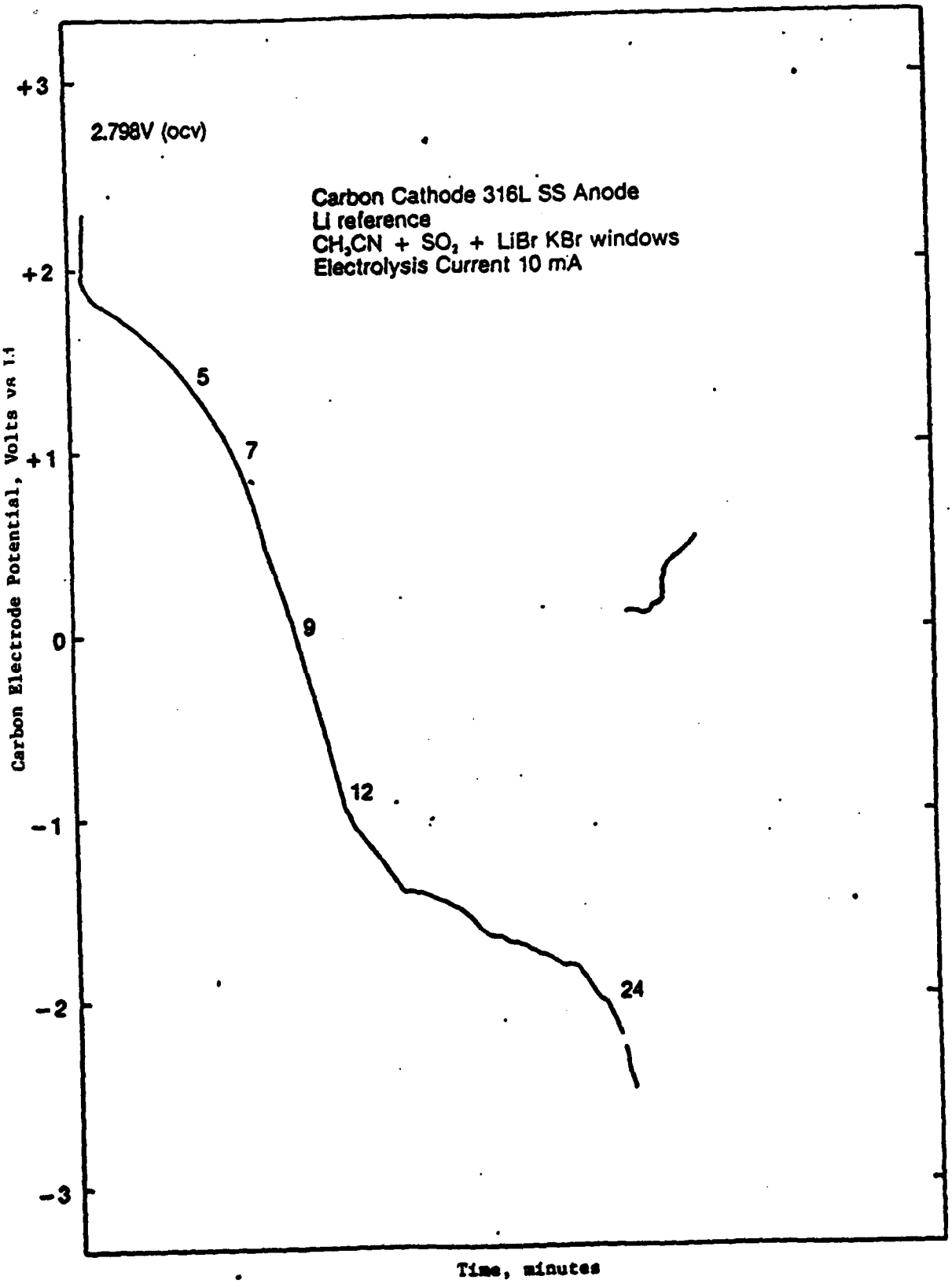

Figure 75. Carbon Electrode Potential Versus Time During the Electrolysis Experiment with a Stainless Steel Anode

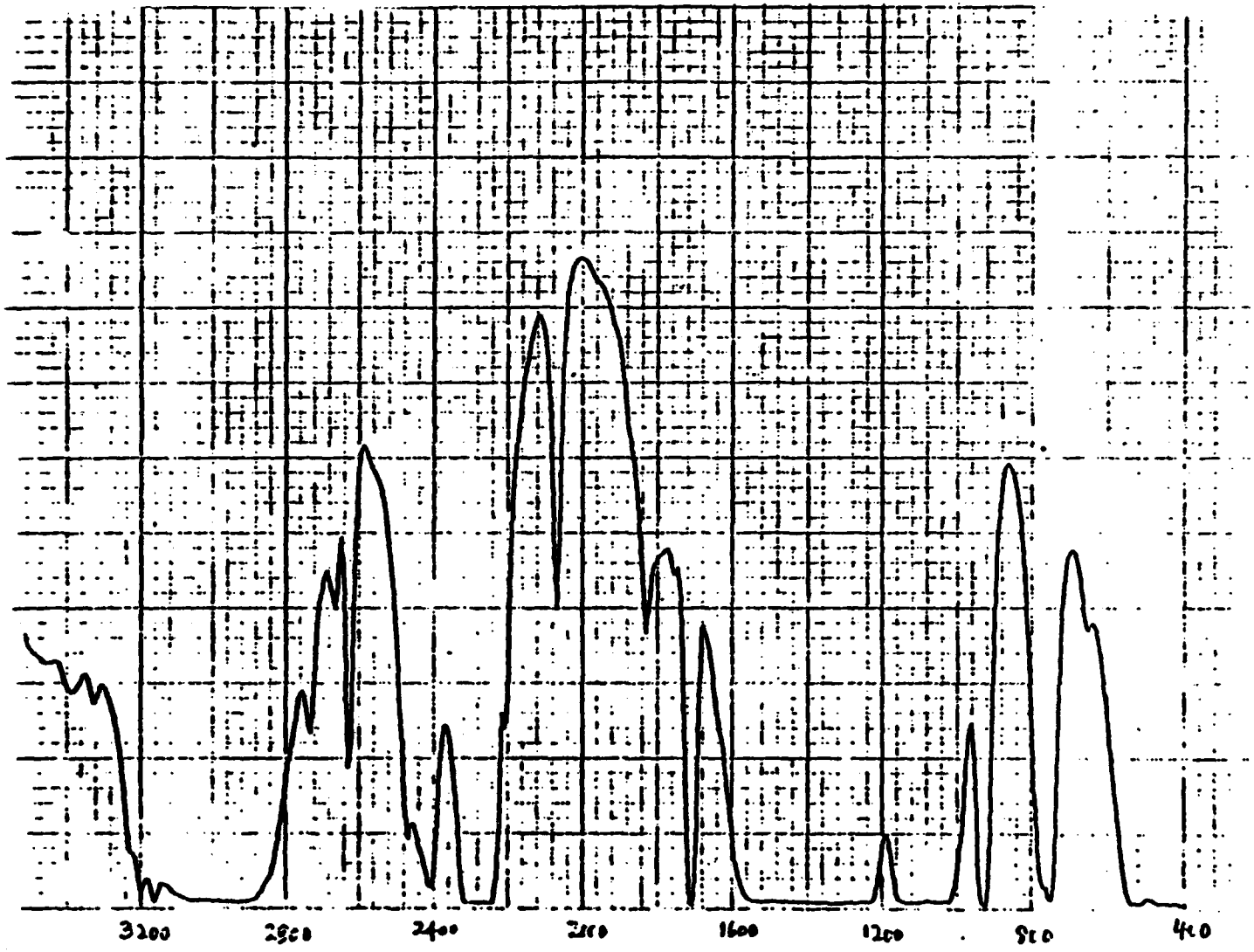

Figure 76. IR Spectrum of LiBr/AN-SO_2 Electrolyte Solution Prior to Electrolysis with a 316L Stainless Steel Anode.

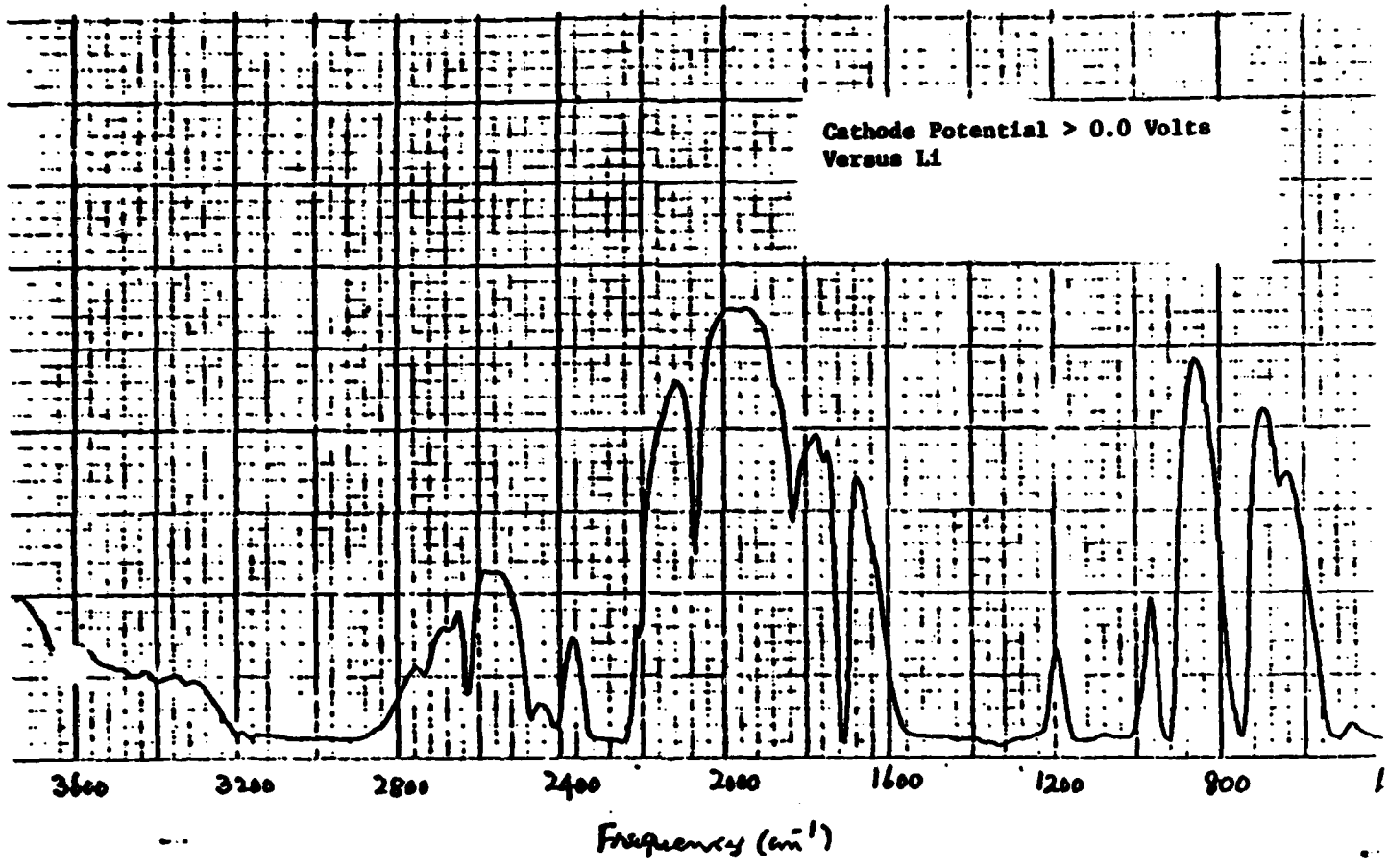

Figure 77. IR Spectrum of LiBr/AN-SO_2 Electrolyte Solution Following Short Period of Electrolysis with a 316L Stainless Steel Anode

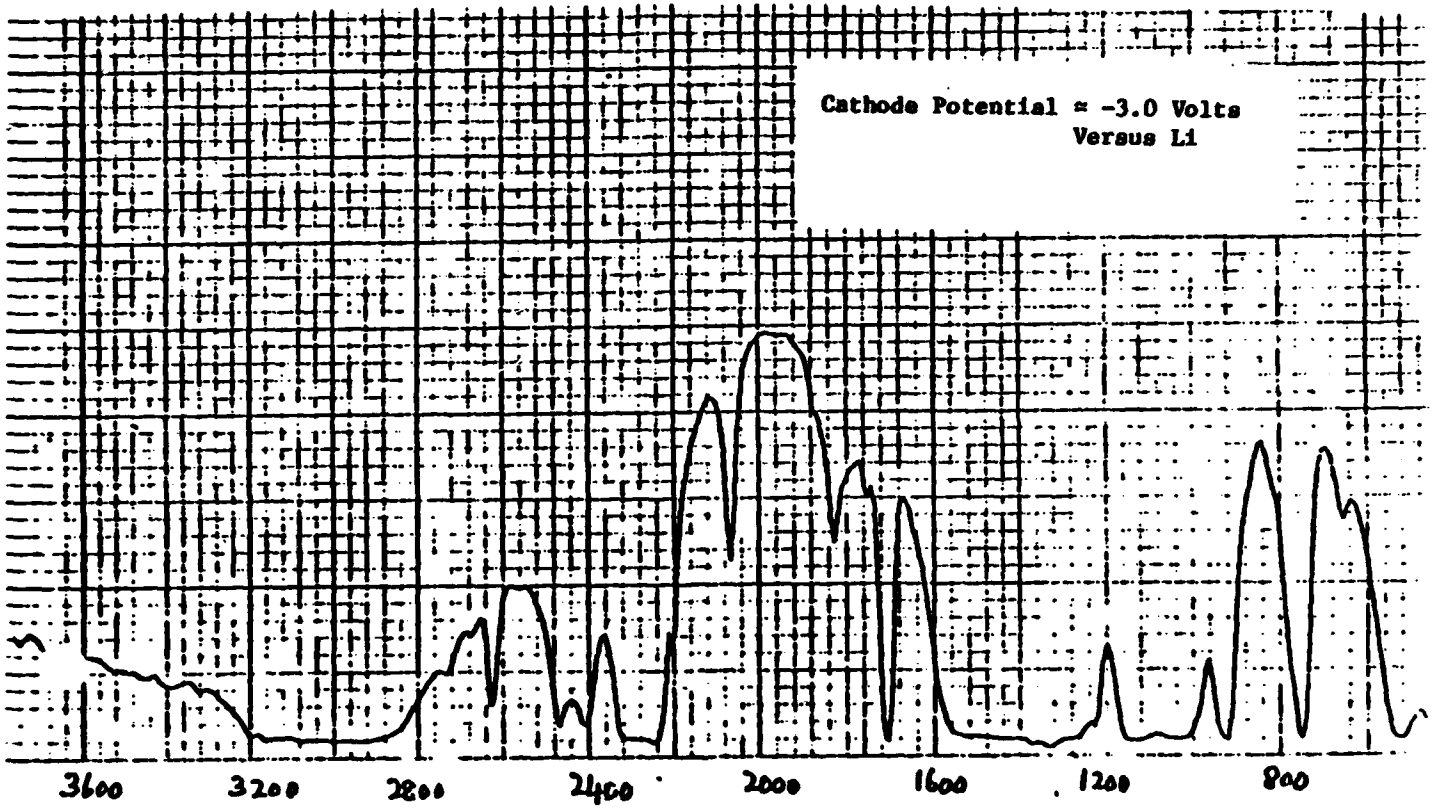

Figure 78. IR Spectrum of LiBr/AN-SO_2 Electrolyte Solution Following Approximately 30 Minutes of Electrolysis with a 316L Stainless Steel Anode

Table 66. Summary of IR Absorption Bands Observed for LiBr/AN-SO_2 Electrolyte Solution Prior to Electrolysis with a 316L Stainless Steel Anode.

FREQUENCY (cm^{-1})	INTENSITY	ASSIGNMENTS
3975	M	OH Vib of Water solvated to Li
3660	W	OH Vib of Water
3625	W	
3385	W	
3320	W	
3200	W	$2V_4+V_3$
3160	W	V_1+V_4 Combination
2840-3120	S&Vb	V_1 C-H Sym. Str of CH_3CN + $\sqrt{5}$
2730	W	$2V_3$ of CH_3 in CH_3CN
2665	W	
530	S	V_2+V_8 Combination
2470	W	
2410	M	V_1+V_3 of SO_2
2240-2320	S&b	V_2 Sym Str C≡N of CH_3CN $2V_1$ of SO_2
2070	S	
1830	M	V_2+V_3 of So_2
1710	S	
1220-1560	S&Vb	V_3&V_6 Sym CH_3 def $+V_3$ of SO_2
1020-1160	S&b	$V_7$of CH_3 rock made of CH_3CN+V_1 o SO_2
930	S	V_4 Sym C-C Stretch or CH_3CN
775	sh	
745	S	
655	W	
540	W	$V_2$of So_2

Table 67. Summary of IR Absorption Bands Observed for LiBr/AN-SO_2 Electrolyte Solution Following Short Period of Electrolysis with a 316L Stainless Steel Anode (Cathode Potential > 0.0 Volts versus Li)

FREQUENCY (cm^{-1})	INTENSITY	ASSIGNMENTS
3975	M	OH Vibration of water bonded to Li
3660	W	OH Vibration of water
3625	W	
3400	W	
3325		
3200	W	$2V_4$+V_3 of CH_3CN
3160	W	V_1+V_4 of CH_3CN
2840-3120	S&V-b	V_1 C-H Sym Sh of CH_3CN
2730	W	$2V_3$ of CH_3 in CH_3CN
2665	W	
2630	S	V_2+V_8 of CH_3CN
2470	W	
2415	M	V_1+V_3 of So_2
2240-2320	S&b	V_2 Sym Str of CEN gp of CH_3CN 2 V_1 of So_2
2070	S	
1830	M	V_2 V_3 of So_2
1710	S	
1220-1560	S&Vb	V_3 and V_6 Sym CH_3 def & V_3 of So_2
1020 1160	S&b	V_1 of So_2 and V_7 of CH_3 rock made of CH_3CN
930	S	V_4 Sym C-C Stsch of CH_3CN
770	sh	
750	S	
540	W	V_2 of So_2

Table 68. Summary of IR Absorption Bands Observed for LiBr/AN-SO_2 Electrolyte Solution Following Electrolysis for Approximately 12 Minutes with a 316L Stainless Steel Anode (Cathode Potential = -1.0 Volt versus Li)

FREQUENCY (cm^{-1})	INTENSITY	ASSIGNMENT
3975	W	OH Vibr of water bonded to Li
3660	VW	
3620	W	OH Vibration of water
2840-3200	m&b	V_1 of C-H Sym Sh of CH_3CN
2730	sh	
2670	sh	
2630	M	V_2+V_8
2470	W/m	
2410	W/m	V_1+V_3 of So_2
2240-2320	m + b	V_2 Sym Sh of C N gp
2070	m	2 V_1 of So_2
1830	m	$V_2+V_3$of So_2
1710	S	
1220-1560	S&Vb	V_3&V_6 Sym CH_3 def of CH_3CN V_3 of So_2
1020-1160	S&b	$V_7$of CH_3 rock and V_1 of So_2
930	m/s	V_4Sym C-C Sh of CH_3CN
770	Sh	
660	W	
530	m	S_2O_4

Table 69. Summary of IR Absorption Bands Observed for LiBr/AN-SO_2 Electrolyte Solution Following Electrolysis for Approximately 24 Minutes with a 316L Stainless Steel Electrode (Cathode Potential ≈ -2.0 Volts versus Li)

FREQUENCY (cm^{-1})	INTENSITY	ASSIGNMENTS
3975	W	OH Vib of water bonded to Li
3660	V-W	OH Vibrations of water
3620	W	
2880-3200	m & b	V_1 C-H Sym Stry CH_3CN
2730	Sh	
2670	Sh	
2630	m	V_2+V_8
2470	W	
2410	W	V_1+V_3 of So_2
2240-2320	m&b (S&b)	V_2 Sym Str of C N gp
2070	M	
1830	M	V_2+V_3 of So_2
1/10	S	
1220-1560	S&Vb	V_3 alym S-O Str of So_2
		V_3 Sym & V_6 of CH_3 gp
1020-1160	S&b	V_1 of S-O of So_2 & V_7 of CH_3
930	m/s	V_4 Sym C-C Sketch of CH_3CN
750	S	
530	m	$S_2O_4^=$

of electrolysis. More work is required before a detailed interpretation can be made. Tentatively, the splitting of the band at 1130 cm^{-1} and 1020 cm^{-1} and the increase in intensity of the 530 cm^{-1} band are attributed to the presence of $S_2O_4^{=}$, actually a cathodic reduction product. More definitive conclusions can be arrived at by conducting additional analyses in the far infrared region (600 - 50 cm^{-1}) where interference by acetonitrile and $S_2O_4^{=}$ bands are minimal.

The solution color changes observed, greenish blue for the nickel electrode and red for the stainless steel electrode, strongly suggest that dissolution of the electrode materials is occurring as part of the oxidation process. In addition, some color changes may be the result of charge-transfer complexes with cathodic reduction products such as have been reported in the literature[9,10]. Future studies, therefore, should also include investigations of the color changes occurring as they could provide much information on the reactions taking place.

References

1. SAF-ALERT LaRC-5-77-02

2. Dey, A.N. and Holmes, R. W., "Analysis of Pressure Producing Reactions in Lithium-Sulfur Dioxide Cells," Final Report DELET-TR-77-0472-F, Contract DAAB07-77-C-0472 (ERADCOM), P. R. Mallory & Co., Inc., November 1979.

3. DiMasi, G. J. and Christopoulos, J. A., "Performance, Storage, Safety and Disposal of Li/SO_2 Cells," Proceedings of the 1980 Goddard Space Flight Center Battery Workshop, NASA Conference Publication 2177, 61 (1980).

4. DiMasi, G. J. and Christopulos, J. A., "The Effects of the Electrochemical Design Upon the Safety and Performance of the Lithium-Sulfur Dioxide Cells," 28th Power Sources Symposium, 179 (1978).

5. Dallek, S., James, S. D., and Kilroy, W. P., "Exothermic Reactions among Components of Lithium-Sulfur Dioxide and Lithium-Thionyl Chloride Cells," J. Electrochem. Soc., 128, 508 (1981).

6. Bro, P., "Heat Generation in Li/SO_2 Cells During Low Rate Discharge", Proceedings of the Symposia on Power Sources for Biomedical Implatable Applications and Ambient Temperature Lithium Batteries, 80-4, 570 (1980).

7. Dey, A. N., "Electrochemical Alloying of Lithium in Organic Electrolytes", J. Electrochem. Soc., 118, 1547 (1971).

8. Taylor, H. and Bowden, W., "Li/SO_2 Cells of Improved Stability", 28th Power Sources Symposium, 183 (1978).

9. Fouchard, O. T., Gardner, C. L., Adams, W. A., and Laman, F. C., "Raman and ESR Spectroscopic Studies of the Electroreduction of Sulfur Dioxide," Proceedings of the Symposium on Lithium Batteries, 81-4, 98 (1981).

10. Baddiel, C. B., Taik, M. J., and Janz, G. J., "Nonaqueous Silver Nitrate Solutions. Spectral Studies in Acetonitrile," J. Phys. Chem., 69, 3634 (1965).

11. Dull, R. W. and Dull, R., "Mathematics for Engineers," McGraw-Hill Book Company, Inc., New York, 679 (1951).

12. Bois, G. P., "Tables of Indefinite Integrals," Dover Publications, Inc., New York, 44 (1961).

Appendices

APPENDIX I

DESIGN AND OPERATING PRINCIPLES OF THE ACCELERATING RATE CALORIMETER

The Accelerating Rate Calorimeter is a microprocessor-controlled adiabatic calorimeter. Because it was designed specifically for the purpose of thermal hazard evaluation, this instrument has significant inherent advantages over conventional techniques such as DTA and DSC. Essentially, these advantages are as follows:

- The tests are conducted adiabatically so that the self-heating rate can be determined.
- Sample pressure can be continuously monitored.
- The experiments are easily designed to closely simulate end-use conditions.
- The instrument is rugged enough to withstand explosions.
- Reaction products can be easily recovered for analysis.

The primary objectives of thermal hazard evaluations are:

1) To define the stability of a system (i.e., chemical mixture, battery, etc.) over a specified temperature region.

2) To characterize the thermodynamics and kinetics of any reactions observed within the specified temperature region.

3) To characterize the pressure of the system over the specified temperature region.

In principle, objectives (1) and (2) can be readily met employing conventional techniques such as DTA and DSC. The difficulty arises when attempting to make predictions about the thermal behavior of a large scale process based on the results of these methods. In order to make accurate predictions, the thermal properties of all components of the system and its surroundings must be known and the dynamic thermal behavior of the system defined, including the effects of self-heating. Normally, the problem becomes so complex that only crude approximations can be made. Since DTA and DSC cannot provide pressure data, additional tests must be conducted to meet objective (3). Usually, the techniques employed measure the pressure-time responses at different isothermal temperatures and the data obtained are qualitative in nature and mainly used for screening purposes.

The Accelerating Rate Calorimeter was designed to overcome these problems by simulating the actual operating environment of the system as closely as possible so that little or no extrapolation is required from the experimental test conditions to those in the actual end-use application. In addition, the design of the Accelerating Rate Calorimeter allows pressure data to be continuously obtained so that the magnitude of the safety problem can be readily assessed for any state of the system over the temperature range evaluated.

An analysis is conducted by first loading the sample into a metallic "bomb" which is then connected to the pressure transducer and placed in the calorimeter. The sample bombs come in a variety of materials and types to allow wide flexibility in experimental design. Figure I-1 shows a schematic of the calorimeter. For safety, the calorimeter is sealed inside a steel containment vessel during an analysis.

The microprocessor is programmed to search for a reaction exotherm by elevating the sample temperature by a fixed increment (step heat) and then checking for a self-heating rate exceeding a preselected threshold. Once an exotherm is detected, the bomb is maintained adiabatic until the completion of the reaction. Adiabatic conditions are achieved by maintaining the bomb and jacket temperatures exactly equal. To ensure temperature uniformity throughout the calorimeter, the jacket is composed of three zones, top, side, and base, which are individually heated and controlled. Automatic collection of time, temperature, and pressure data

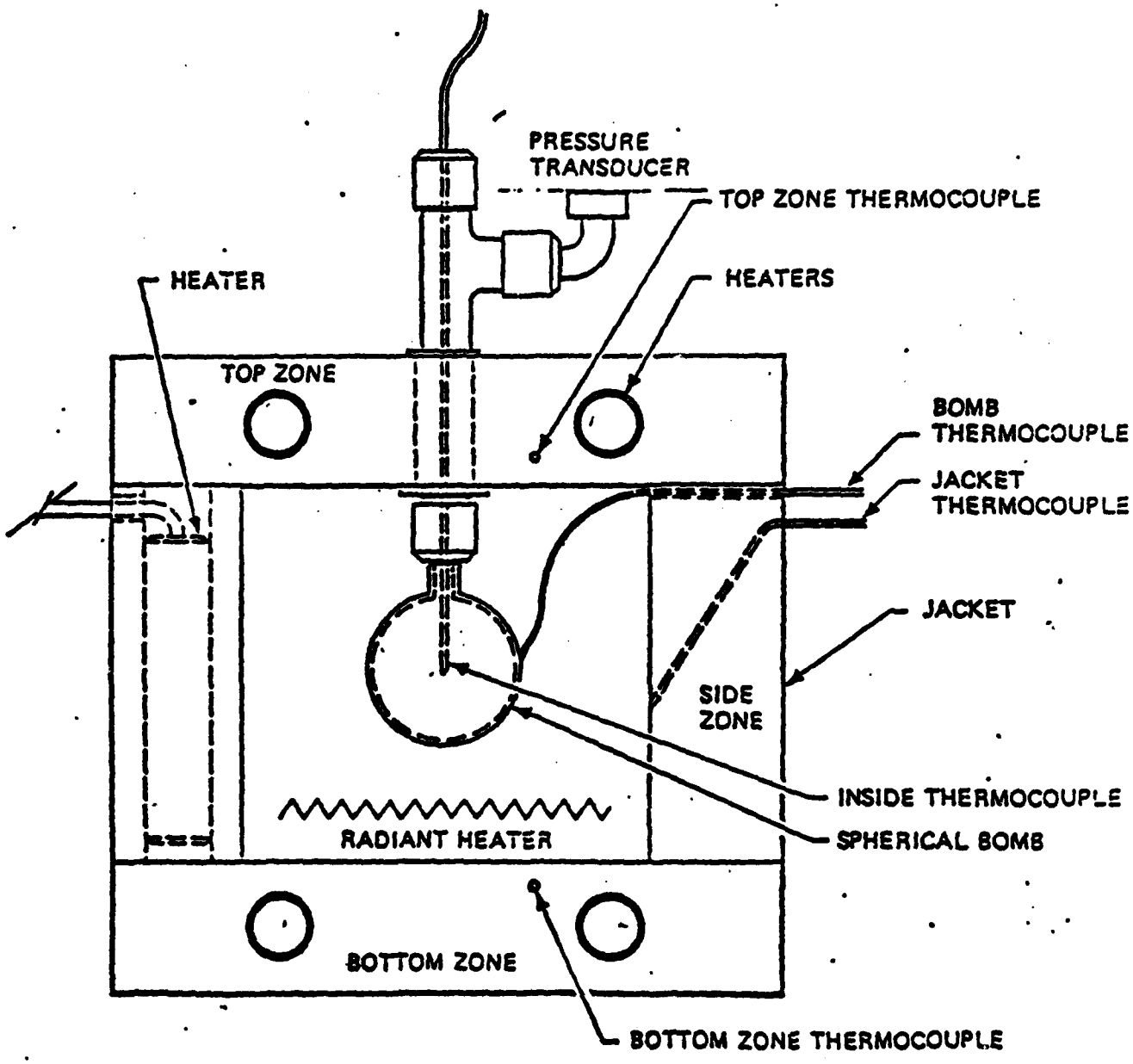

Figure I-1. Schematic of Accelerating Rate Calorimeter

is carried out until the reaction has finished and the self-heat rate has dropped below the threshold value.

Figure I-2 illustrates the operational sequence for detecting and following an exothermic runaway reaction. The maximum temperature capability of the instrument is 450°C and it is able to detect self-heating rates of less than 0.01°C/min. A self-accelerating, or thermal runaway reaction is one in which the exothermic heat of reaction is available to continuously heat the reactants to higher temperatures and thereby increase the reaction rate. Such reactions occur when the rate of heat generation exceeds the rate of heat dissipation to the surroundings and are characterized by exponential time-temperature profiles as illustrated in Figure I-2.

The ARC provides the time-temperature profile of a system under adiabatic conditions. Here, the system refers to the sample plus the bomb. In these experiments, the bomb absorbs a fraction of the heat generated thus serving to thermally dilute the sample. By controlling the sample mass, the bomb mass, and bomb material, the experiment can be made to closely simulate end-use conditions. By this means, accurate predictions can be made for systems where complex reactions occur whose kinetics and thermodynamics are not well understood and/or whose thermal properties are not well defined. The key factor in experimental design, therefore, is thermal inertia which is defined as follows:

$$\phi = 1 + \frac{Mb\ \bar{C}vb}{Ms\ \bar{C}vs}$$

where:

ϕ = Thermal inertia
Mb = Mass of bomb, gm
Ms = Mass of sample, gm
$\bar{C}vb$ = Average heat capacity of bomb, cal/gm - °K
$\bar{C}vs$ = Average heat capacity of sample, cal/gm - °K

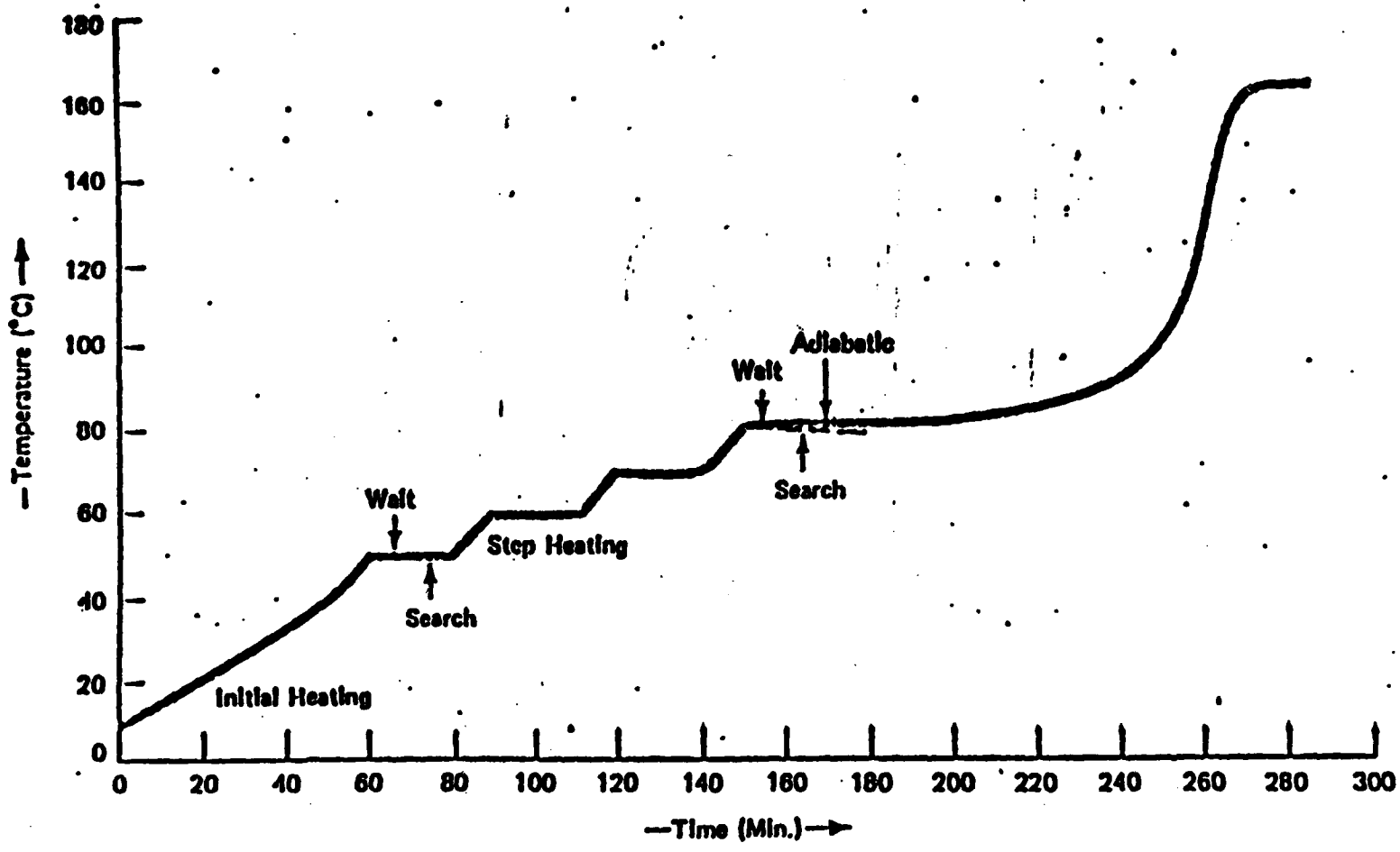

Figure I-2.The Heat-Wait-Search Operation Mode of an Accelerating Rate Calorimeter

As can be seen from the above equation, a pure chemical (i.e., Mb = 0) would have thermal inertia of 1.0. Also, the inverse of thermal inertia, $1/\phi$, is commonly understood to be the degree of adiabaticity. By matching the thermal inertia of the experiment to the thermal inertia of the end-use application, an accurate evaluation of the thermal hazard can be made without having to have any knowledge of the kinetics or thermodynamics of the reactions involved.

For exotherms consisting of a single reaction, the interpretation of the ARC data is usually made by determining the time-to-maximum rate as a function of temperature. The time-of-maximum-rate is also often referred to as the time-of-explosion since this is the outcome of many thermal runaway reactions. By extrapolating the linear portion of the time-to-maximum-rate versus temperature curve to lower temperatures, one can accurately predict the hazard at any given temperature.

A typical time-to-maximum-rate curve is shown in Figure I-3. This curve represents the thermal decomposition of Di (tert-Butyl) peroxide which is believed to be a simple first-order reaction occurring by the following mechanism.

$$(CH_3)_3C\text{-}O\text{-}O\text{-}C(CH_3)_3 \rightarrow 2CH_3\text{-}\overset{\overset{O}{\|}}{C}\text{-}CH_3 + CH_3\text{-}CH_3$$

Di (tert-Butyl) Peroxide Acetone Ethane

The two curves shown in Figure I-3 clearly show the significant effect of thermal inertia on the behavior of the system. At low temperature, the rate of reaction is low and the reactant concentration is relatively constant. In this region, the reaction can be well approximated by zero order kinetics and the zero-order curve is normally that which is used to extrapolate to lower temperatures. The zero-order curve for Di (t-Butyl) perioxide (ϕ = 7.42) is shown in Figure I-4.

The safety of a given system, therefore, is characterized by the zero-order time-to-maximum-rate curve and the time line for the system. The latter is the rate at which the system can dissipate heat to its surroundings and is defined as follows:

$$T_L = \frac{M_s \bar{C}_{vs}}{\mu a}$$

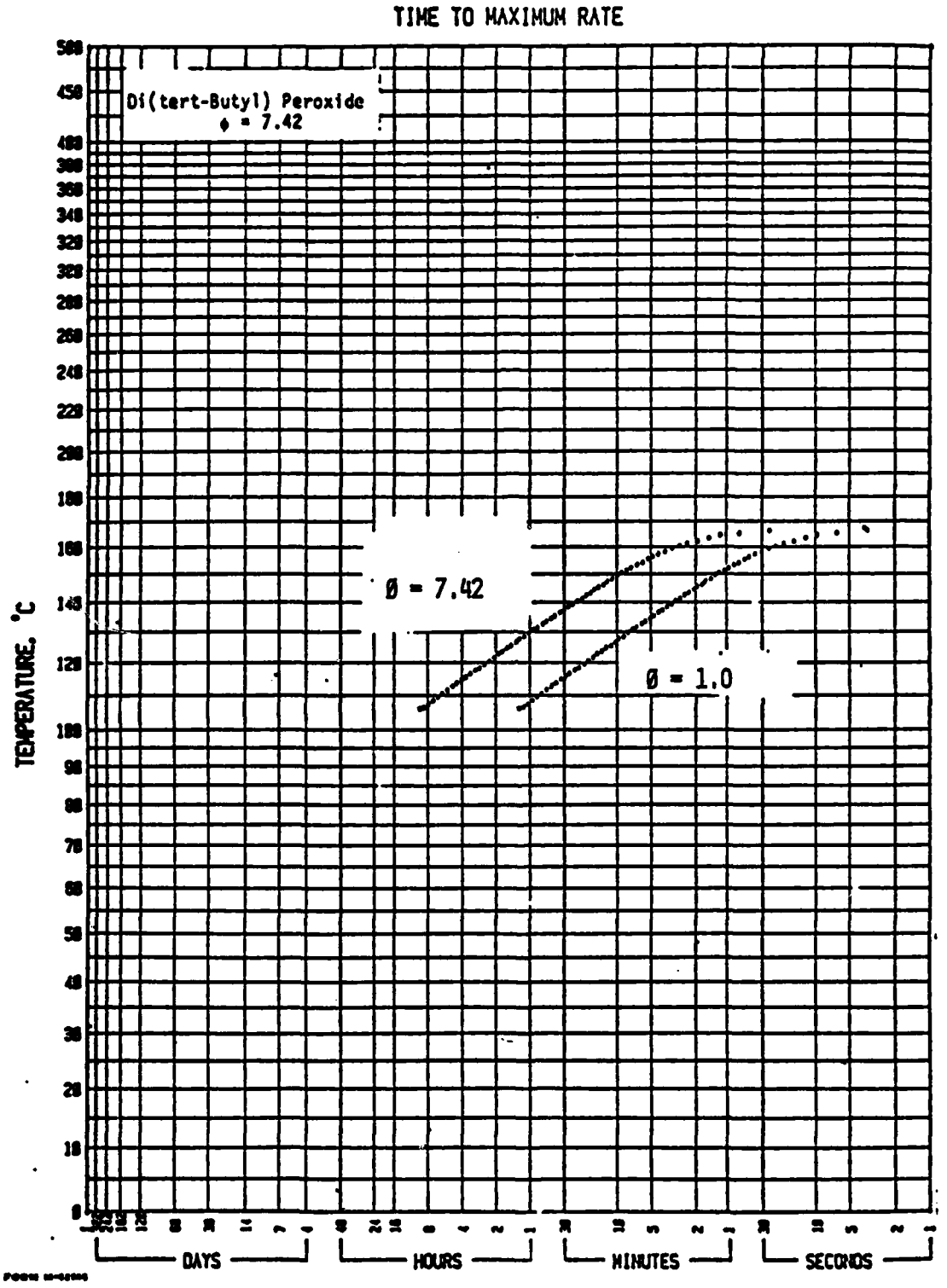

Figure I-3. Time-To-Maximum-Rate Versus Temperature Curve for Di (tert-Butyl) Peroxide.

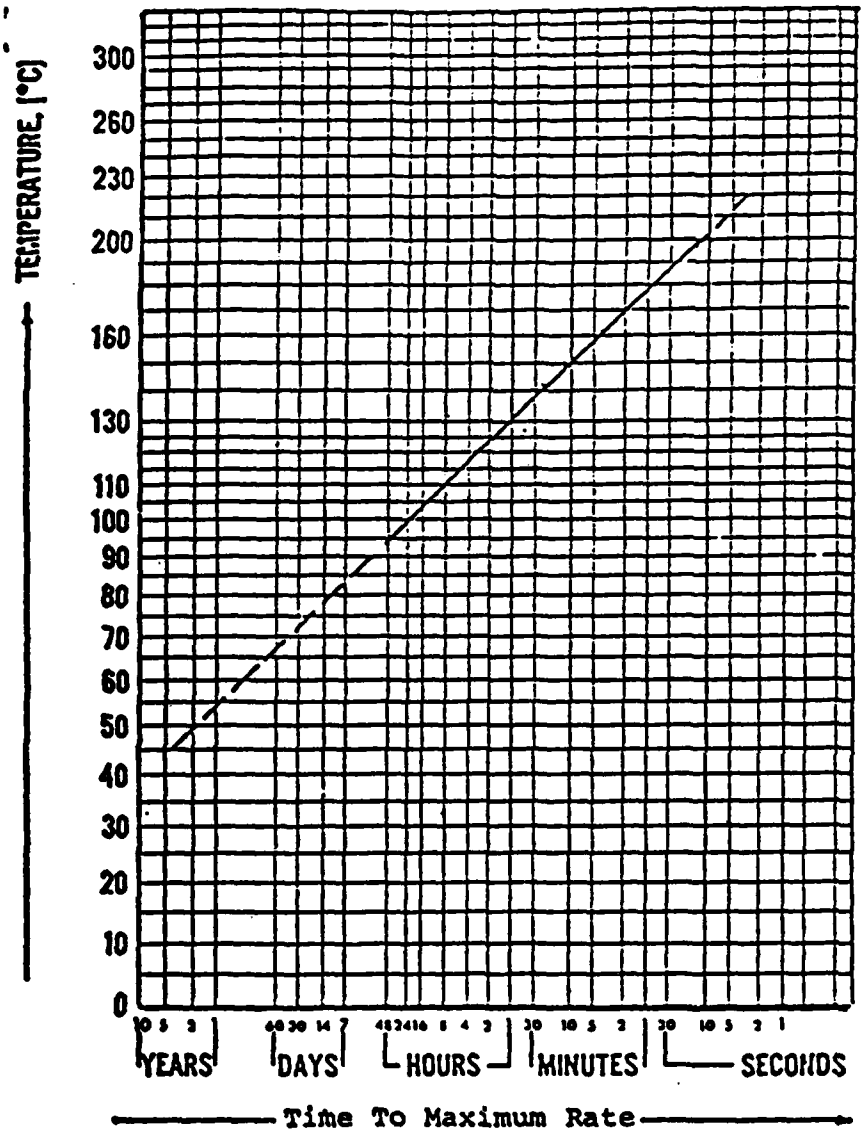

Figure I-4. Zero-Order Time to Maximum Rate of Decomposition for Di-T-Butyl Peroxide.

where:

T_L = Time line of system, sec.
μ = Heat transfer coefficient of system, cal/cm^2 - sec - ^oC
a = Effective heat transfer area, cm^2
M_s = Sample mass, gm
$\bar{C}_{vs}$ = Average heat capacity of sample, cal/gm - ^oK

This parameter can be readily calculated from thermal properties of the system or determined empirically for those systems whose thermal properties are not known. The relationship between the zero-order curve and the time line is shown in Figure I-5. Once the system reaches the temperature of no return, it will go into a thermal runaway mode since the rate of heat generation will exceed the rate of heat dissipation. At temperatures much above the temperature of no return, the system becomes essentially adiabatic and the time to maximum rate (or explosion) is given by the zero order line.

Although the principal function of the Accelerating Rate Calorimeter is to perform thermal hazard analyses in the manner described above, it can also provide kinetic data for some simple reactions. To date, the mathematics have been worked out only for simple reactions and for autocatalytic reactions. For these reaction types, the following kinetic parameters can be readily obtained.

- Activation energy
- Frequency factor
- Reaction order
- Rate constant
- Molar heat of reaction

The specific heat of reaction, however, can be obtained for any reaction type since this parameter does not require knowledge of the reaction mechanism.

The microprocessor is programmed to make nine different plots of the data. The raw data include:

1) Temperature versus time
2) Rate of temperature rise versus time
3) Pressure versus time

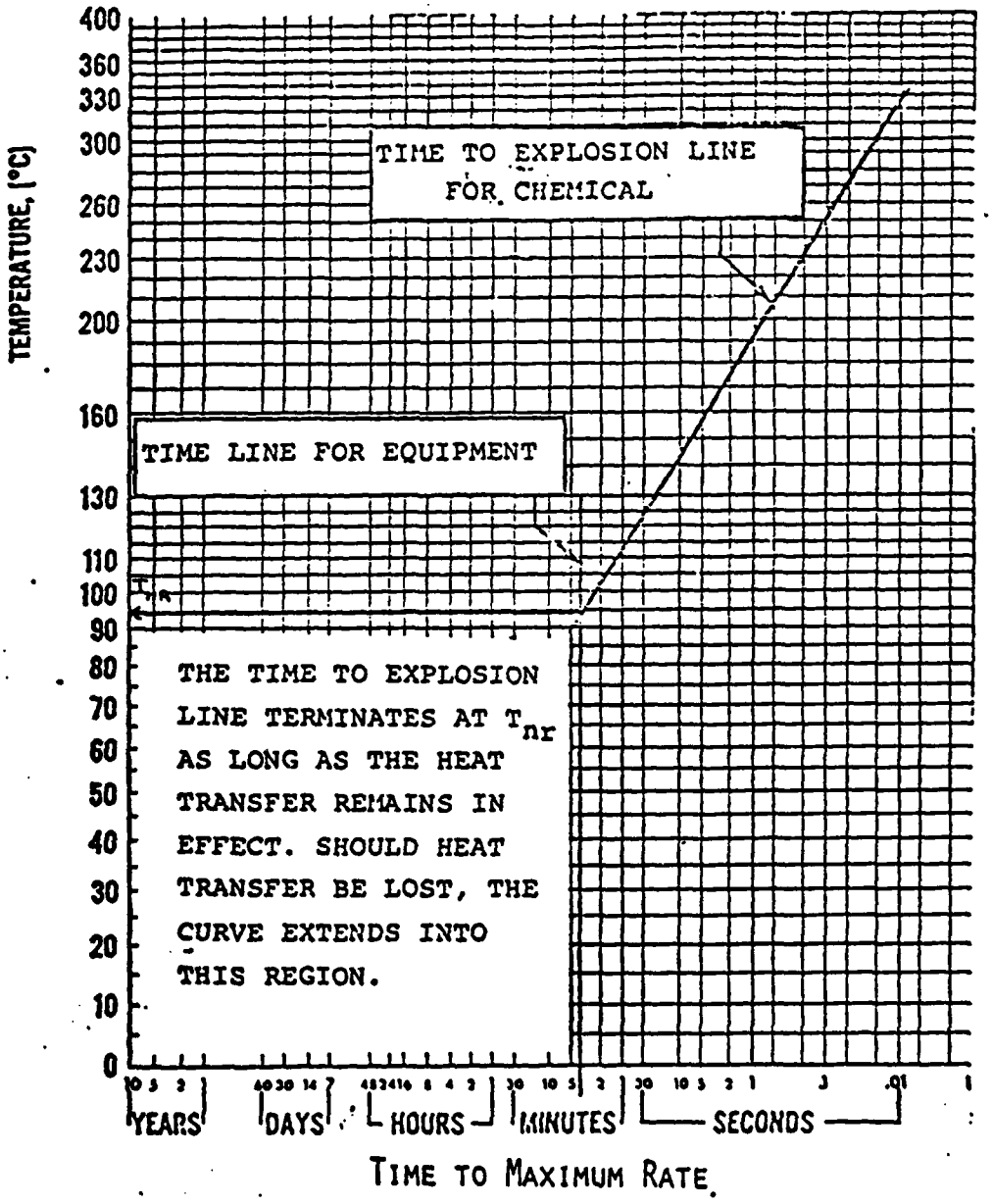

Figure I-5. Graphical Determination of the Temperature of No Return for a System.

The plots are:

1) Temperature versus time
2) Log of self-heat rate versus the reciprocal of temperature
3) Pressure versus temperature
4) Log of pressure versus the reciprocal of temperature
5) Log of pressure rate versus the reciprocal of temperature
6) Log of pressure rate versus log of temperature rate
7) Reciprocal of temperature versus log of time to maximum rate
8) Log of pseudo rate constant versus the reciprocal of temperature
9) Activation energy versus temperature

From these plots, one can measure:

- Adiabatic temperature rise
- Temperature of maximum rate
- Time to maximum rate
- Self-heat rate at any temperature
- Pressure at any temperature
- Pressure rate at any temperature

These plots are also of diagnostic value to determine the type of reaction taking place. If the reaction is found to be a simple nth order reaction or an auto-catalytic reaction, the kinetic parameters can then be easily obtained.

APPENDIX II

DERIVATION OF MATERIALS BALANCE EQUATIONS

1) Derivation of Equation (7)

$$\text{Cathode Capacity (Ah)} = Cc\left(\frac{Ah}{cm^3}\right) \times Vc\left(\frac{cm^3}{l}\right) =$$

$$Cc\left(\frac{Ah}{cm^3}\right) \times Ac\left(\frac{cm^2}{l}\right) \times Tc\left(\frac{cm}{l}\right) \qquad \text{(II-1)}$$

$$\text{Anode Capacity (Ah)} = Ca\left(\frac{Ah}{cm^3}\right) \times Va\left(\frac{cm^3}{l}\right) =$$

$$Ca\left(\frac{Ah}{cm^3}\right) \times Aa\left(\frac{cm^2}{l}\right) \times Ta\left(\frac{cm}{l}\right) \qquad \text{(II-2)}$$

Equating under the condition that Ac = Aa = A gives:

$$Ca \times A \times Ta = Cc \times A \times Tc \qquad \text{(II-3)}$$

Solving for Ta yields

$$Ta = \frac{Cc \times A \times Tc}{Ca \times A} = \frac{CcTc}{Ca} \qquad \text{(II-4)}$$

Multiplying this result by the Li/C ratio gives the anode thickness for the specified materials balance; i.e.,

$$Ta = \frac{CcTcR_3}{Ca} \qquad \text{(II-5)}$$

The specific capacity of lithium metal is:

$$Cc = \frac{1}{6.94}\left(\frac{eq}{gm}\right) \times 96{,}500\left(\frac{A\text{-}sec}{eq}\right) \times \frac{1}{3600}\left(\frac{hr}{sec}\right) \times 0.534\left(\frac{gm}{cm^3}\right) =$$

$$2.062\ Ah/cm^3$$

Substituting this value into the above equation yields equation (7).

$$Ta = \frac{(Tc)(Cc)(R_3)}{2.062} \qquad \text{(II-6)}$$

Notation:

Aa = Geometric anode area, cm^2
Cc = Geometric cathode area, cm^2
Ca = Specific anode capacity, Ah/cc
Cc = Specific cathode capacity, Ah/cc
R_3 = Li/C ratio
Ta = Anode thickness, cm
Tc = Cathode thickness, cm
Va = Anode volume, cm^3
Vc = Cathode volume, cm^3

2) Derivation of Equation (12)

The electrolyte solution is 68 weight percent SO_2.

Therefore:

$$\text{Moles } SO_2 = \frac{1}{64} \left(\frac{\text{mole}}{\text{gm}}\right) \times El \left(\frac{\text{gm}}{l}\right) \times 0.68 \qquad \text{(II-7)}$$

and

$$El = \frac{(\text{moles } SO_2)(64)}{0.68} = 94.1\ (\text{moles } SO_2) \qquad \text{(II-8)}$$

From the specified component ratios

$$R_1 = \frac{Li}{SO_2} = \frac{\text{moles Li}}{\text{moles } SO_2} \qquad \text{(II-9)}$$

and

$$\text{Moles } SO_2 = \frac{\text{moles Li}}{R_1} = \frac{1}{R_1} \left(\frac{W}{6.94 \text{ gm/mole}}\right) \qquad \text{(II-10)}$$

Therefore,

$$El = \frac{64W}{(6.94)(0.68)(R_1)} = \frac{13.56W}{R_1} \qquad \text{(II-11)}$$

As can be seen, the use of this equation requires a knowledge of the anode weight. This parameter can be readily estimated using the anode dimensions given in Table 4 and a value of 0.534 g/cc for the density of lithium metal. Once the cell assembly has been completed, the actual measured lithium weight is used to make the final calculation on the electrolyte quantity required.

Notation:

El = Required quantity of electrolyte solution, gm
R_1 = Li/SO_2 ratio
W = Lithium weight, gm

APPENDIX III

DERIVATION OF EQUATIONS USED TO CALCULATE COMPONENT LENGTHS OF SPIRAL-WRAP CELLS*

The method used to calculate the component lengths of a wound electrode cell configuration was developed at Honeywell by Mr. Matt Faust. This technique employs the spiral of Archimedes as the geometric model. The basic characteristic of this spiral is a constant gain in the distance of a point on the spiral from the origin of the spiral with each completed revolution. Mathematically, in polar coordinates, the spiral of Archimedes can be represented as follows:

$$p = \frac{K\theta}{2\pi} \tag{III-1}$$

In terms of the number of revolutions, the equation becomes

$$p = Kn \tag{III-2}$$

where $n = \theta/2\pi$.

The length of the spiral at any given point is calculated using the following general equation for determining the distance along the length of a plane curve in polar coordinates (11).

$$S = \int_{\theta_1}^{\theta_2} \left[p^2 + \left(\frac{dp}{d\theta}\right)^2 \right]^{1/2} d\theta \tag{III-3}$$

Differentiating Equation (III-1) gives:

$$\frac{dp}{d\theta} = \frac{K}{2\pi} \tag{III-4}$$

Substituting this result, along with Equation (III-1), into Equation (III-3) yields

$$S = \int_{\theta_1}^{\theta_2} \left[\left(\frac{K\theta}{2\pi}\right)^2 + \left(\frac{K}{2\pi}\right)^2 \right]^{1/2} d\theta \tag{III-5}$$

---

* The notation used in this discussion is given on Page 229.

which can now be further reduced to:

$$S = \int_{\theta_1}^{\theta_2} \frac{K}{2\pi} \sqrt{\theta^2 + 1}\ d\theta \qquad \text{(III-6)}$$

From a table of integrals, (12),the solution is found to be

$$S = \frac{K}{2\pi} \left[\frac{\theta}{2}\sqrt{\theta^2 + 1} + \frac{1}{2} \ln \left(\theta + \sqrt{\theta^2 + 1}\right)\right] \Bigg|_{\theta_1}^{\theta_2} \qquad \text{(III-7)}$$

Expressing in terms of the number of revolutions, the equation becomes:

$$S = K \left[\frac{n}{2} \sqrt{4\pi^2 n^2 + 1} + \frac{1}{2\pi} \ln \left(2\pi n + \sqrt{4\pi^2 n^2 + 1}\right)\right]_{n_1}^{n_2} \qquad \text{(III-8)}$$

In a spiral-electrode configuration, the winding of the electrodes begins on a round mandrel of radius (r). The cell stack consists of the anode, cathode, bottom and top separators. The location of a component within the cell stack is given by its edge distance, the latter being defined as the thickness of the particular component plus the sum of the thicknesses of all components on top of it in the cell stack. Here, the top component is defined as the one closest to the mandrel at the start of the wrap.

For a final wrap diameter (d), the spiral equation becomes

$$p = \frac{d}{2} = tn \qquad \text{(III-9)}$$

where the increase in distance from the origin with each completed turn is now given by the thickness of the cell stack (t). The length of a given component can now be determined by evaluating Equation (III-8) between the two limits of integration. The upper limit (n_2) is the number of revolutions required, beginning at the origin, for the cell wrap to just equal its final diameter (d). When this occurs, the edge of the component in question will be removed from the outside surface of the wrap by the thickness of the components below it in the cell stack; i.e., by the amount (t-E). Equation (III-9) now

becomes

$$\frac{d}{2} - (t - E) = tn_2 \qquad \text{(III-10)}$$

Empirically, it has been found that better results can be obtained by adding another term to this equation as follows:

$$\frac{d}{2} - (t - E) = tn_2 + \frac{t}{4} \qquad \text{(III-11)}$$

Solving for n_2 now yields

$$n_2 = \frac{1}{t}\left[\frac{d}{2} + E - 0.75t\right] \qquad \text{(III-12)}$$

The lower limit of integration (n_1) is the number of revolutions, again starting at the origin, for the component in question to reach its starting point on the wrap mandrel. In this position, the component will be separated from the mandrel by its edge distance so that the effective radius involved in determining the number of revolutions is (r + E). This is now substituted into Equation (III-2) giving

$$r + E = tn_1 \qquad \text{(III-13)}$$

Solving for n_1 yields

$$n_1 = \frac{r + E}{t} \qquad \text{(III-14)}$$

To summarize, the length of a component (electrode or separator) in a wrap cell having an overall diameter (d) can be determined by evaluating Equation (III-8) between the limits of n_1 and n_2. For easy reference, the three working equations are listed below.

$$S = t\left[\frac{n}{2}\sqrt{4\pi^2n^2 + 1} + \frac{1}{2\pi}\ln\left(2\pi n + \sqrt{4\pi^2n^2 + 1}\right)\right]\Bigg|_{n_1}^{n_2} \qquad \text{(III-8)}$$

$$n_2 = \frac{1}{t}\left[\frac{d}{2} + E - 0.75t\right] \qquad \text{(III-12)}$$

$$n_1 = \frac{r + E}{t} \qquad \text{(III-14)}$$

To illustrate the use of this technique, consider the following example.

Final wrap diameter (d) =	0.486 in.
Radius of wrap mandrel (r) =	0.062 in.
Anode thickness =	0.010 in.
Cathode thickness =	0.026 in.
Separator thickness =	0.0015 in.
Total cell stack thickness =	0.039 in.
Top component =	Cathode (normal wrap)

To determine the cathode length, first determine its edge distance. Since the cathode is the top component, its edge distance is merely its own thickness, 0.026 in. Next, determine the upper and lower limits of integration as follows:

Upper limit

$$n_2 = \frac{1}{0.039}\left[\frac{0.486}{2} + 0.026 - (0.75)(0.039)\right] = 6.15 \text{ revolutions}$$

Lower limit

$$n_1 = \frac{0.061 + 0.026}{0.039} = 2.23 \text{ revolutions}$$

Evaluating Equation (III-8) with respect to n_2 gives

$$S_2 = 0.039\left[\frac{6.15}{2}\sqrt{(4)(\pi)^2(6.15)^2 + 1} + \frac{1}{2}\ln\left((2)(\pi)(6.15) + \sqrt{(4)(\pi)^2(6.15)^2 + 1}\right)\right] = 4.66 \text{ in.}$$

Evaluation with respect to n_1 yields

$$S_1 = 0.039 \left[\frac{2.23}{2} \sqrt{(4)(\pi)^2(2.23)^2 + 1} + \frac{1}{2\pi} \ln \left((2)(\pi)(2.23) + \sqrt{(4)(\pi)^2(2.23)^2 + 1} \right) \right] = 0.632 \text{ in.}$$

The cathode length is given by the difference between these two values, i.e.,

$$S = S_2 - S_1 = 4.66 - 0.632 = 4.03 \text{ in.}$$

In like manner, the length of the anode or separators can be readily determined. The results for the anode are as follows:

Edge distance (E) =	0.038 in.
n_2 =	6.44 resolutions
n_1 =	2.53 revolutions
Length (S) =	4.31 in.

List of Symbols

d = Final diameter of cell wrap

E = Edge distance of component whose length is being determined.

K = The increase in distance from the origin to a point on the spiral with each completed turn.

n = Number of revolutions of spiral

p = Distance from origin to point on spiral

r = Radius of wrap mandrel

S = Length of cell component

t = Total cell stack thickness

θ = Total angle (in radians) through which the spiral has revolved

DISTRIBUTION

Defense Technical Information Center
Cameron Station
Alexandria, VA 22314 12

Naval Material Command
Attn: Code 08T223
Washington, DC 20360 1

Office of Naval Technology
Code MAT-0716
Attn: A. J. Faulstich
800 N. Quincy Street
Arlington, VA 22217 1

Office of Naval Research
Attn: G. Neece (Code ONR 413)
800 N. Quincy Street
Arlington, VA 22217 2

Naval Research Laboratory
Attn: Dr. Fred Saalfield
(Code NRL 6100) 1
A. Simon (Code NRL 6130) 1
4555 Overlook Avenue, S.W.
Chemistry Division
Washington, DC 20375

Naval Air Systems Command
Attn: Dr. H. Rosenwasser
(Code NAVAIR 301C) 1
E. Nebux
(Code NAVAIR 5332) 1
Washington, DC 20361

Naval Electronic Systems Comm.
Attn: A. H. Sobel
(Code PME 124-31) 1
Washington, DC 20360

Naval Sea Systems Command
Attn: F. Romano (Code 63R3) 1
A. Himy (Code 5433) 1
E. Daugherty (Code 04He) 1
Washington, DC 20362

Strategic Systems Project Office
Attn: K. N. Boley (Code NSP 2721) 1
M. Meserole (Code NSP 2722) 1
Department of the Navy
Washington, DC 20360

Naval Air Development Center
Attn: J. Segrest (Code 6012) 1
R. Schwartz (Code 30412) 1
Warminister, PA 18974

Naval Civil Engineering Laboratory
Attn: Dr. W.S. Hayes (Code L-52) 1
F. Rosell 1
Port Hueneme, CA 93040

Naval Intelligence Support Center
Attn: Dr. H. Ruskie (Code 362) 1
Washington, DC 20390

Naval Ocean Systems Center
Attn: Dr. S.Szpak (Code 6343) 1
San Diego, CA 92152

Naval Surface Weapons Center
Attn: Dr.Wm.P. Kilroy (Code R33) 5
Dr. D.W. Ernst (Code R33) 4
Dr. Stanley James
(Code R33) 1
Dr. R.Frank Bis (Code R33) 2
Dr.Carl Mueller (Code R33) 1
D. Warburton (Code R33) 1
Dr.Gerald Hoff (Code R33) 1
White Oak Laboratory
Silver Spring, MD 20910

U.S. Army Electronics Command
Attn: A.J. Legath
(Code DRSEL-TL-P) 1
E. Brooks
(Code DRSEL-TL-PD) 1
G. DiMasi 1
Dr. W. K. Behl 1
Dr. Sol Gilman
(Code DELET-PR) 1
Fort Monmouth, NJ 07703

Army Material and Mechanical
Research Center
Attn: J. J. DeMarco 1
Watertown, MA 02172

USA Mobility Equipment
R and D Command
Attn: J.Sullivan (Code DRXFB) 1
Electrochemical Division
Fort Belvoir, VA 22060

Edgewood Arsenal
Attn: Library
Aberdeen Proving Ground 1
Aberdeen, MD 21010

Picatinny Arsenal
Attn: Dr. B. Werbel
(Code SARPA-FR-E-L-C) 1
A. E. Magistro
(Code SARPA-ND-D-B) 1
U. S. Army
Dover, NJ 07801

Harry Diamond Laboratory
Attn: J. T. Nelson
(Code DELHD-DE-OP) 1
Department of Army Material
Chief, Power Supply Branch
2800 Powder Mill Road
Adelphi, MD 20783

Headquarters, Department of
Transportation
Attn: R. Potter
(Code GEOE-3/61) 1
U. S. Coast Guard, Ocean
Engineering Division
Washington, DC 20590

NASA headquarters
Attn: Dr. J. H. Ambrus 1
Washington, DC 20546

NASA Goddard Space Flight Center
Attn: G.Halpert (Code 711) 1
Greenbelt, MD 20771

NASA Lewis Research Center
Attn: J. S. Fordyce
(Code MS 309-1) 1
2100 Brookpark Road
Cleveland, OH 44135

Naval Electronic Systems Command
Attn: T. Sliwa
(Code NAVELEX-01K) 1
Washington, DC 20360

Naval Weapons Center
Attn: Dr. E. Royce (Code 38) 1
China Lake, CA 93555

Naval Weapons Support Center
Attn: D. G. Miley (Code 305) 1
Electrochemical Power Sources
Division
Crane, IN 47522

Naval Underwater Systems Center
Attn: J. Moden (Code SB332) 1
Newport, RI 02840

Air Force of Scientific Research
Attn: Library 1
Directorate of Chemical Science
1400 Wilson Boulevard
Arlington, VA 22209

Frank J. Seiler Research
Laboratory, AFSC
USAF Academy, CO 80840 1

Air Force Aero Propulsion
Laboratory
Attn: W. S. Bishop
(Code AFAPL/POE-1) 1
R. Marsh
(Code AFWAL/POOC-1) 1
Wright-Patterson AFB, OH 45433

Office of Chief of Research and
Development
Department of the Army
Attn: Dr. S. J. Magram 1
Energy Conversion Branch
Room 410, Highland Building
Washington, DC 20315

U. S. Army Research Office
Attn: B. F. Spielvogel 1
P.O. Box 12211
Research Triangle Park, NC 27709

NASA Scientific and Technical
Information Facility
Attn: Library 1
P.O. Box 33
College Park, MD 20740

Bell Laboratories
Attn: Dr. J. J. Auborn 1
600 Mountain Avenue
Murray Hill, NJ 07974

Brookhaven National Laboratory
Attn: J. Sutherland
Building 815
Upton, NY 11973 1

California Institute of Technology
Attn: Library 1
Jet Propulsion Laboratory
4800 Oak Grove Drive
Pasadena, CA 91103

Argonne National Laboratory
Attn: Dr. E. C. Gay 1
9700 South Cass Avenue
Argonne, IL 60439

John Hopkins University Applied Physics Laboratory
Attn: Library 1
Howard County
Johns Hopkins Road
Laurel, MD 20707

Oak Ridge National Laboratory
Attn: K. Braunstein 1
Oak Ridge, TN 37830

Sandia Laboratories
Attn: Sam Levy (Mail Services Section 3154-3) 1
P.O. Box 5800
Albuquerque, NM 87715

University of Tennessee
Attn: G. Mamantov 1
Department of Chemistry
Knoxville, TN 37916

Applied Research Laboratory
Attn: Library 1
Penn State University
University Park, PA 16802

Catalyst Research Corporation
Attn: G. Bowser 1
1421 Clarkview Road
Baltimore, MD 21209

ESB Research Center
Attn: Library 1
19 W. College Avenue
Yardley, PA 19067

EIC Corporation
Attn: S. B. Brummer 1
55 Chapel Street
Newton, MA 02158

Eagle-Picher Industries, Inc.
Attn: Robert L. Higgins 1
Electronics Division, Couples Department
P.O. Box 47
Jopkin, MO 64801

Foote Mineral Company
Attn: H. R. Grady 1
Exton, PA 19341

Gould, Inc.
Attn: S. S. Nielsen 1
40 Gould Center
Rolling Meadows, IL 60008

GT & E Laboratory
Attn: Dr. Keitch Kleindinst 1
520 Winter Street
Waltham, MA 02154

GTE Product Corp.
Attn: Dr. R.MacDonald 1
520 Winter Street
Waltham, MA 02254

Hughes Aircraft Company
Attn: Dr. L. H. Fentnor 1
Aerospace Groups
Missile Systems Group
Tucson Engineering Laboratory
Tucson, AZ 85734

Lockheed Missiles and Space Co.Inc.
Attn: R. H. Kinsey 62-52,
Bldg 156A, Fac 1 1
P.O. Box 504
Sunnyvale, CA 94086

Duracell Int., Inc.
Attn: D. Linden 1
Battery Division
South Broadway
Tarrytown, NY 10591

Duracell Int., Inc.
Attn: Richard Dupont 1
Dr. A.N. Dey 1
Laboratory for Physical Science
Burlington, MA 01803

Union Carbide Battery Products Div.
Attn: R. A. Powers 1
P.O. Box 6116
Cleveland, OH 44101

Wilson Greatbatch LTD.
Attn: Library 1
1000 Wehrle Drive
Clarence, NY 14030

Yardney Electric Corporation
Attn: Library 1
82 Mechanic Street
Pawcatuck, CT 02891

Rockwell International
Attn: Dr. Samuel J. Yosim 1
Atomics International Div.
8900 DeSoto Avenue
Canoga Park, CA 91304

Stanford University
Attn: C. John Wen 1
Center for Materials Research
Room 249, McCullough Bldg.
Stanford, CA 94305

EDO Corporation
Attn: E.P. DiGiannantonio 1
Government Products Div.
2001 Jefferson Davis Highway
Arlington, VA 22202

RAI Research Corp.
Attn: Dr. Carl Perini 1
225 Marcus Blvd.
Hauppauge, NY 11787

Battery Engineering
Attn: Dr. N. Marincic 1
80 Oak St.
Newton, MA 02164

RAY-O-VAC
Attn: R. Foster Udell 1
101 East Washington Ave.
Madison, WI 53703

Lawrence Berkeley Laboratory
Attn: F. McLamore 1
University of California
Berkeley, CA 94720

TRW Systems
Attn: Ed Moon, Rm.2251, Blgd. 0-1 1
One Space Park
Redondo Beach, CA 90278

ALTUS Corporation
Attn: Dr. Adrian E. Zolla 1
1610 Crane Court
San Jose, CA 95112

PCI
70 McQuesten Parkway South
Mount Vernon, NY 10550
Attn: Thomas Reddy 1

Dr. P. Bro
Hyde Park Estates
Santa Fe, NM 87501 1

Old Dominion University
Dept. of Chemical Sciences
Norfold, VA 23508
Attn: R. L. Ake 1

Corporate Technology Center
10701 Lyndale Ave. So.,
Bloomington, MN 55420
Attn: H.V.Venkatasetty 1
Steven Schafer 1

Honeywell Inc.
Mat & Process Eng.
Attn: Dr. K. Y. Kim MN11-1812 1
600 2nd St. N.E.
Hopkins, MN 55343

The Aerospace Corporation
Attn: Harlan Bittner 1
P.O. Box 92957
Los Angeles, CA 90009